DEVELOPMENT AND USE OF NON-INVASIVE TECHNIQUES TO STUDY THE MECHANISM OF AN ANTI-TUBERCULOSIS DRUG IN LIVE MYCOBACTERIA

Suzanna Helen Harrison

Doctor of Philosophy

University of York

Department of Chemistry

September 2024

ABSTRACT

Tuberculosis, caused by *Mycobacterium tuberculosis*, is responsible for over 1 million deaths per year. Bedaquiline is a key antibiotic in the treatment of drug-resistant tuberculosis and its discovery stirred an interest in developing therapies targeting mycobacterial bioenergetics. Despite bedaquiline's importance, several incompatible models for its mode of action have developed: that it acts as a direct inhibitor of mycobacterial ATP synthase or that it disrupts the proton motive force through protonophore or H^+/K^+ ionophore action.

Non-invasive techniques applied to living cells offer the potential of monitoring real-time changes in bioenergetic systems. To this end, visible-wavelength remission spectroscopy and ^{31}P NMR are applied here to better understand mycobacterial bioenergetics and unravel bedaquiline's mode of action.

Visible-wavelength remission spectroscopy was used to examine the effects of bedaquiline on the mycobacterial oxidative phosphorylation system in *Mycobacterium smegmatis* and *Mycobacterium tuberculosis.* Comparison between these effects and those of established bioenergetic inhibitors and protonophores/ionophores show bedaquiline acts as a direct inhibitor of ATP synthase. Experiments with cytochrome *bd* oxidase knockout strains demonstrate the oxygen consumption increase observed on bedaquiline addition is due to an increase in activity of cytochrome *bd* oxidase.

The use of ^{31}P NMR to study metabolism in live cells was explored: experiments on unoxygenated *Mycobacterium smegmatis* cultures demonstrate that this method can be used to monitor levels of phosphorylated metabolites. A system for oxygenating and mixing bacterial cultures during NMR experiments was developed for future use.

Establishing that bedaquiline acts as a direct inhibitor of ATP synthase allows rationalisation of its synergy with other compounds and for its role in future combination regimes to be evaluated. The NMR data sets the scene for others to measure the effect bedaquiline has on the ATP/ADP ratio in live mycobacteria to further understand how inhibition of ATP synthase eventually leads to cell death.

AUTHOR'S DECLARATION

I declare that this thesis is a presentation of original work and I am the sole author. This work has not previously been presented for a degree or other qualification at this University or elsewhere. All sources are acknowledged as references.

Where data collection has been performed in collaboration with or by colleagues is disclosed in the text. Work on the mechanism of bedaquiline in *Mycobacterium smegmatis* and *Mycobacterium tuberculosis* as determined by visible-wavelength remission spectroscopy is currently being prepared for publication, but has not been submitted prior to the writing of this thesis.

ACKNOWLEDGEMENTS

I would like to thank Dr Jamie Blaza for his support and encouragement over the past four years, along with all the other members of the Blaza group. I feel very grateful to have been a part of such a supportive and bright group of people. Particular thanks need to be extended to Rowan Walters for all of her help with the bioenergetic chamber, Dr Pooja Gupta for teaching me the skills needed to start culturing bacteria and Dr Morwan Osman for helping me to get started with culturing BSL-2 organisms. I also want to express my gratitude towards the technicians in YSBL for ensuring smooth operation of our lab space.

I need to thank Dr Aneurin Kennerly and everyone at CHyM, especially Dr Victoria Annis, for all of their support on the NMR side of my project. A massive thanks also needs to go to Dr Roger Springett for kindly donating the bioenergetic chamber to the lab and for continuing to provide support for it, as well as Professor Gregory Cook and his lab group for providing our mycobacteria mutant strains.

Lastly, I want to extend personal thanks to my parents for their unending support and willingness to sit through numerous practise presentations and meal-time lectures on mycobacteria.

ABBREVIATIONS

3NP	3-nitropropionate
ADP	Adenosine-5'-disphosphate
AMP	Adenosine-5'-monophosphate
ATP	Adenosine-5'-triphosphate
AU	Arbitrary units
BAM15	N^5,N^6-Bis(2-fluorophenyl)[2,1,3]oxadiazolo[4,5-*b*]pyrazine-5,6-diamine
BDQ	Bedaquiline
CAD	Computer Aided Design
CCCP	Carbonyl cyanide *m*-chlorophenyl hydrazine
CFZ	Clofazimine
CHQAD	N-(4,4-difluorocyclohexyl)-2-((4-oxo-3,4-dihydroquinazolin-2-yl)thio)acetamide
DARQs	Diarylquinolines
DCCD	*N*,*N*-dicyclohexylcarboiimide
DEPMPH	Diethyl(2-methylpyrrolidin-2-yl)phosphonate
FDA	United States Food and Drug Administration
FCCP	Carbonyl cyanide-p-trifluoromethoxyphenylhydrazone
GAPDH	Glyceraldehyde 3-phosphate dehydrogenase
GCP	Glycerol phosphorylcholine
HEPES	4-(2-hydroxyethyl)piperazine-1-ethanesulfonic acid

HQNO	2-heptyl-4-quinolinol 1-oxide
HSQC	Heteronuclear Single Quantum Correlation
IC_{50}	Half-maximal inhibitory concentration
IMV	Inverted membrane vesicle
LPM	Litres per minute
LSPN	List of Prokaryotic Names with Standing in Nomenclature
MAC	*Mycobacterium avium* complex
MBC	Minimum bactericidal concentration
MTBC	*Mycobacterium tuberculosis* complex
MDP	Methylene diphosphonate
MeP	Methyl phosphonate
MIC	Minimum inhibitory concentration
MK	Menaquinone
MKH_2	Menaquinol
MOPS	3-morpholinopropane-1-sulfonic acid
MRI	Magnetic resonance imaging
Msm	*Mycobacterium smegmatis*
MT	Magnetisation transfer
Mtb	*Mycobacterium tuberculosis*
NAD^+	Nicotinamide adenine dinucleotide
NADH	Dihydronicotinamide adenine dinucleotide

NDH-1	Type I NADH:MK oxidoreductase
NDH-2	Type II NADH:MK oxidoreductase
NMR	Nuclear Magnetic Resonance
NTM	Non-tuberculosis mycobacteria
OCR	Oxygen consumption rate
OD	Optical density
PCr	Phosphocreatine
PDE	Phosphodiester
PEEK	Polyether ether ketone
PGK	Phosphoglycerate kinase
PheP	Phenyl phosphonate
P_i	Inorganic phosphate
P_{iec}	Extracellular inorganic phosphate
P_{iic}	Intracellular inorganic phosphate
PME	Phosphomonoester
PMF	Proton motive force
ppm	Parts per million
RD1	Region of difference 1
RF	Radiofrequency
RGM	Rapidly growing mycobacteria
rRNA	Ribosomal ribonucleic acid

SDH	Succinate dehydrogenase
SGM	Slow growing mycobacteria
SNR	Signal-to-noise ratio
SOD	Superoxide dismutase
ST	Saturation transfer
TB	Tuberculosis
tBuMeP	Diethyl(1-(tert-butylamino)-eth-1-yl)phosphonate
TFPZ	Trifluoperazine
TR	Repetition time
Tris	Tris(hydroxymethyl)aminomethane
TRZ	Thioridazine
UQ	Ubiquinone
UQH_2	Ubiquinol
UV-vis	Ultra-violet visible
WT	Wild type
δ	Chemical shift
ΔpH	pH gradient
ΔΨ	Electrochemical gradient

TABLE OF CONTENTS

1. INTRODUCTION

1.1. AN INTRODUCTION TO MYCOBACTERIA

1.1.1. Characteristics of mycobacterial cells

The genus name *Mycobacterium* was established in 1896, with the prefix myco- coming from the Greek word for fungus and referring to the tendency of bacteria in this genus to grow colonies that appear to be mould-like on liquid media (Lehmann and Neumann, 1896). At the time of writing, the List of Prokaryotic Names with Standing in Nomenclature (LSPN) recognises 197 species as belonging to the genus and having been validly published (Parte et al., 2020; Parte, 2024). This list features both obligate pathogens and environmental bacteria, with some acting as opportunistic pathogens while others remain unlinked to disease.

Despite the variation in environmental niches, there are several key features that unite the members of this genus. All *Mycobacterium* species possess a characteristic cell wall comprised of a layer of peptidoglycan closest to the cell membrane, followed by an arabinogalactan layer which is itself covalently joined to mycolic acids; β-hydroxy fatty acids containing around 60-90 carbon atoms (figure 1.1) (Greenwood et al., 2007). An additional layer of free polysaccharides, proteins and lipids forms a capsule around the cell wall, with the exact composition of this layer depending on the species (Daffé and Draper, 1998; Pereira et al., 2020).

The mycolic acids in mycobacterial cell walls make them acid-fast, meaning after the bacteria have been stained, they do not readily decolourise on treatment with acids used in classic staining procedures. This property means that in Gram stain tests mycobacteria appear only faintly Gram-positive or Gram-neutral (Trifiro et al., 1990; Fisher et al., 1990), despite the fact they do not possess an outer-membrane and have a thick peptidoglycan layer like Gram-positive bacteria. The lack of a clear Gram stain test result has led to mycobacteria being ascribed the Gram-positive label based on these traits alone in literature (Cook et al., 2009; Forbes et al., 2018), however this is somewhat controversial. The hydrophobic nature of the mycolic acid layer means it

has some similarities to the outer-membranes of Gram-negative bacteria (Greenwood et al., 2007), and so mycobacteria do not neatly fall into either the Gram-positive or Gram-negative category.

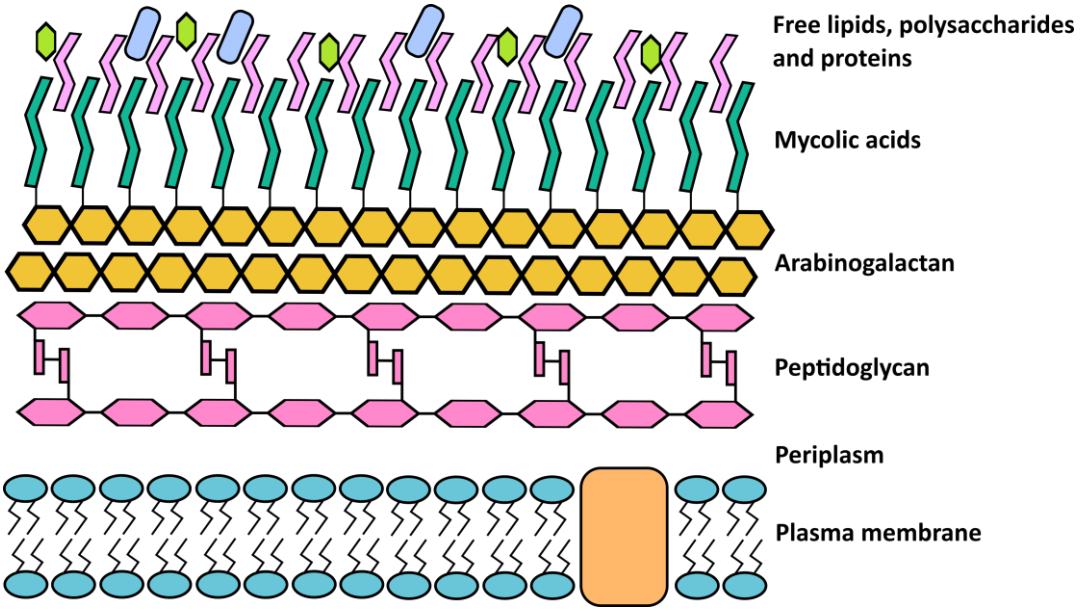

***Figure 1.1**: The structure of mycobacterial cell walls. The exact composition of the mycolic acid layer as well as the capsule of free lipids, polysaccharides and proteins depends upon the individual species.*

Some other notable traits of mycobacteria are that they are obligate aerobes, have rod-shaped cells and do not sporulate (Cook et al., 2009; Traag et al., 2010). They are also generally considered to be non-motile, although *Mycobacterium marinum* (*M. marinum*) has been observed to display actin-based motility under intracellular conditions; a strategy employed by bacteria across multiple genera that involves stimulating polymerisation of actin in host cells (Stamm et al., 2003). Sliding motility has also been reported in some mycobacterial species (Martínez, Torello and Kolter, 1999), with sliding being defined as a type of movement across a surface reliant on the materials that make up a cell's exterior providing reduced friction between the cell and the surface (Henrichren, 1972).

Mycobacteria can be categorised by growth rate. Species that form visible colonies on solid media in under 7 days are referred to as rapidly growing mycobacteria (Kim et al., 2013). Species that take over 7 days to form colonies are described as slow growing

mycobacteria. Slow growing mycobacteria can be further categorised into one of three groups depending on their pigmentation using a system devised by Runyon (Runyon, 1959). Group I is made up of species that produce a pigment on exposure to light, otherwise known as photochromogens, while group II species are scotochromogens, meaning they produce a pigment under light and dark conditions. The remaining nonchromogens, species that do not produce pigment, are sorted into group III. Rapidly growing mycobacteria are also described by the Runyon classification system, with all of them being placed into a single group (group IV).

Recently there has been some debate over whether the *Mycobacterium* genus should be split into five separate genera (*Mycobacterium*, *Mycolicibacterium*, *Mycolicibacter*, *Mycolicibacillus* and *Mycobacteriodes*). Previously, assortment of species into the *Mycobacterium* genus was mostly based upon 16S rRNA analysis along with the physical characteristics of cells (Rogall et al., 1990; Stahl and Urbance et al., 1990), with comparison of housekeeping gene sequences being used to further define the phylogenetic relationships between species (Guillemin, Cambau and Jarlier, 1995; Kim et al., 2005; Tortoli et al., 2012). In 2018, Gupta et al. examined the whole genome sequences of 150 mycobacterial species and found these species could be sorted into one of five distinct clades (Gupta, Lo and Son, 2018).

The result of this study was the proposal that the *Mycobacterium* genus should be reclassified to include only members of one clade, with other mycobacteria being sorted into one of the other four genera listed above. As pathogenic mycobacteria are split across these new genera, there has been some reluctance to adopt the new nomenclature over concerns it may result in confusion in a clinical setting (Tortoli et al., 2019; Armstrong and Parrish, 2021). Additionally, a later study which considered the percentage of conserved proteins along with the alignment fraction and average nucleotide identity of 146 mycobacterial species and 214 other bacterial species in the *Corynebacteriaceae* family, found this approach did not support the proposed split (Meehan et al., 2021).

Currently, *Mycobacterium* is considered to be synonymous with the newly introduced genera. To limit confusion, and based on the new evidence provided, this report will

use only the genus name *Mycobacterium* to refer to the bacteria in all five of the newer genera.

1.1.2. An overview of the range of diseases caused by mycobacteria

The most common human disease resulting from infection with mycobacteria is tuberculosis (TB), caused by members of the *Mycobacterium tuberculosis* complex (MTBC). The MTBC is comprised of several species known to cause tuberculosis in humans and/or animals, with the validly published members being *Mycobacterium tuberculosis (M. tuberculosis), Mycobacterium africanum (M. africanum), Mycobacterium bovis (M. bovis), Mycobacterium caprae (M. caprae), Mycobacterium pinnipedii (M. pinnipedii) and Mycobacterium microti (M. microti)* (Gagneux, 2018; Parte et al., 2020; Parte, 2024).

TB is currently the leading cause of death due to a single infectious agent/complex worldwide (World Health Organisation, 2024a). Each year there are over 1 million TB-related deaths, with an estimated 1.25 million occurring in 2023, accompanied by 10.8 million new cases in the same year. As well as causing active infections, MTBC members are able to persist in hosts without causing symptoms and this is referred to as latent TB (Kiazyk and Ball, 2017). Around one quarter of the global population is thought to be infected with MTBC bacilli, and it is estimated 5-10% of these latent infections will go on to develop into the active form of the disease (World Health Organisation, 2024a). This reactivation is complex and not fully understood, however it is known that comorbidities, such as HIV coinfection and diabetes, greatly increase the risk of reactivation of a latent TB infection, likely due to their impacts on the immune system (Kiazyk and Ball, 2017; Ngo, Bartlett and Ronacher, 2021).

TB most commonly affects the lungs (pulmonary TB), with TB infection in any other organ being referred to as extrapulmonary TB. Extrapulmonary TB cases account for around one in five diagnosed TB cases and extrapulmonary TB is more common in immunosuppressed individuals (Golden and Vikram, 2005; Gambhir et al., 2017), although it should be noted the definition of extrapulmonary TB varies depending on region. In the UK, infection of the pleura with TB is labelled as pulmonary TB, whereas

in the USA it is regarded as extrapulmonary TB (Chaisson and Nachega, 2010). Symptoms of pulmonary TB include a persistent but initially non-productive cough, that may progress to production of blood-stained sputum, along with fever, malaise and night sweats. It is also common for pulmonary TB infection to result in a loss of appetite and weight loss, with the impact of these symptoms on patients resulting in the disease being historically referred to as Phthisis, the Greek word for consumption (Moonan, 2018). In the case of extrapulmonary TB, the exact form the disease takes is dependent on where the infection is located (Chaisson and Nachega, 2010).

Some species show a high host specificity for humans, namely *M. tuberculosis* and *M. africanum* (Brites and Gagneux, 2015). Cases of animal infection with *M. tuberculosis* have been reported but these are usually believed to be due to human-to-animal transmission (O'Reilly and Daborn, 1995; Ocepek et al., 2005; Schmidt et al., 2008). Other members of the MTBC are also known to cause TB in humans, with the majority of these cases arising from infection with *M. bovis* and *M. caprae*. *M. bovis* has the largest known host range of all members of the MTBC, with domestic cattle acting as the primary source of human infection (O'Reilly and Daborn, 1995), while caprids act as the main animal reservoir of *M. caprae* (Rodríguez et al., 2011). Together *M. bovis* and *M. caprae* account for approximately 1-3% of human cases, with almost all of these cases being a result of zoonotic transmission (Müller et al., 2013).

While studies have shown it is possible for members of the MTBC to persist in the environment for a number of months (Fine et al., 2011; Velayati et al., 2015), the main sources of exposure are from animal and human reservoirs, with bacteria being transmitted from host-to-host. Human-to-human transmission mainly occurs via respiratory droplets (Riley et al., 1959; Yates et al., 2016), while consumption of unpasteurised dairy products is a major driver of zoonotic transmission (Cosivi et al., 1998; Collins et al., 2022).

Leprosy is the second most common mycobacterial disease in humans, although it is significantly less prevalent than TB, with around 174,000 new cases reported in 2022 (World Health Organisation, 2023a). The disease is caused by the intracellular pathogens *Mycobacterium leprae (M. leprae)* and *Mycobacterium lepromatosis (M.*

lepromatosis), with neither able to be cultured *in vitro*. In addition to infecting humans, *M. leprae* is also known to infect armadillos, some non-human primates and, more recently, has been found in red squirrel populations in the UK (Meyers et al., 1991; Hamiliton et al., 2008; Avanzi et al., 2016). Samples of *M. leprae* have also been found in the environment but host-to-host transmission via respiratory droplets is believed to be the major driver of new infections (Ploemacher et al., 2020).

Leprosy mainly affects the peripheral nervous system and skin, with symptoms often including numbness in affected areas and skin lesions (Lockwood, 2010). The severity of disease depends upon the immune response of the host, with leprosy infections existing on a scale between two extremes. A strong cell-mediated immune response reduces the ability of the bacteria to replicate resulting in a less severe infection referred to as tuberculoid leprosy. Lepromatous leprosy describes cases where there is no effective cell-mediated immune response and thus a greater bacterial load.

M. leprae was thought to be the only causative agent of leprosy until *M. lepromatosis* was first isolated from a leprosy patient in 2008 (Han et al., 2008), with subsequent and retrospective diagnoses linking the species to other leprosy cases in humans (Deps and Collin, 2021). Like *M. leprae*, *M. lepromatosis* has been detected in red squirrel populations (Avanzi et al., 2016), but thus far does not have any other known natural hosts besides humans. Given the relatively recent discovery of the species, it is possible further natural hosts may be found in future studies.

All other mycobacterial species are grouped together under the term non-tuberculosis mycobacteria (NTM) and are environmental organisms. A number of these species, particularly slow growing mycobacteria, are capable of causing disease in humans, often in immunosuppressed individuals (Collins, 1989). These infections can manifest in a number of ways depending on the species responsible and the site of infection. The four main manifestations are chronic pulmonary disease, especially where there is already damage to lung tissue, swelling of the lymph nodes (lymphadenitis), post-inoculation skin-lesions or abscesses and disseminated disease (Grange and Davies, 2010). Only two infections resulting from NTM bacteria are recognised as their own distinct and named diseases, with these being Buruli ulcer, caused by *Mycobacterium*

ulcerans (*M. ulcerans*) and aquarium granuloma (also known as swimming pool/fish tank granuloma), caused by *M. marinum*.

There were slightly under 2000 suspected cases of Buruli ulcer in 2023 (World Health Organisation, 2024b). The disease usually first presents as a painless subcutaneous skin nodule which proceeds to ulcerate 1 to 3 months after infection (Meyers and Portaels, 2010). The size of the resulting ulcer is variable, especially as it is possible for the bacteria to disseminate and spread outwards from the affected area. In addition to the disfiguring, and sometimes debilitating, effect of the disease, there is also a risk of secondary infection at the site of the ulcer (Kpeli and Yeboah-Manu, 2019). Currently, the mode of transmission is poorly understood. Infections are believed to arise from skin being inoculated with *M. ulcerans* via coming into contact with infected water, however insect vectors have also been proposed to contribute to disease spread (Merritt et al., 2010).

Aquarium granuloma presents as lesions in the skin which often resemble warts (Grange and Davies, 2010). Due to the relative rarity of the infection, it is less well-documented compared to the other three named mycobacterial diseases. In the USA the annual incidence rate is estimated to be between 0.05-0.27 cases per 100,000 adults per year (Aubry et al., 2017). As the name implies, the disease is acquired from breaks in the skin barrier being in contact with water infected with *M. marinum* (Grange and Davies, 2010).

Other species of mycobacteria responsible for NTM infections include the rapidly growing *Mycobacterium abscessus* (*M. abscessus*), *Mycobacterium chelonae* (*M. chelonae*) and *Mycobacterium fortuitium* (*M. fortuitium*) (Grange and Davies, 2010). All three of these species are capable of causing pulmonary, cutaneous or soft tissue infections depending on the route of infection. The most common cause of pulmonary infection with rapidly growing mycobacteria is *M. abscessus* (Griffith, Girard and Wallace, 1993; Esther et al., 2010), which is also notable for having intrinsic resistance to several antibiotics used against other mycobacterial infections, making it difficult to treat (Luthra, Rominski and Sander, 2018).

The most common slow growing mycobacteria known to cause pulmonary disease include the members of the *Mycobacterium avium* (*M. avium*) complex (MAC) along with *Mycobacterium kansasii* (*M. kansasii*), *Mycobacterium gordonae* (*M. gordonae*) and *Mycobacterium xenopi* (*M. xenopi*) (Hoefsloot et al., 2013). Transmission routes are currently not well understood, however as mycobacteria are known to exist in various water sources, including inside household plumbing (Honda et al., 2016), it is believed exposure to contaminated water, particularly aerosols, is the main source of infection (Falkinham, 2013; Morimoto et al., 2018). There is also evidence for host-to-host transmission of *M. abscessus* (Bryant et al., 2016).

Cutaneous and soft tissue infections caused by the rapidly growing mycobacteria listed above along with the slow growing *Mycobacterium haemophilum* (*M. haemophilum*) and MAC are usually linked to some form of inoculation via trauma or invasive procedures (Lindeboom et al., 2011; Wi, 2019). Examples of where such transmission has occurred include surgeries, with a number being cosmetic procedures (Meyers et al., 2002; Sax et al., 2015; Shen et al., 2024), tattooing (Drage et al., 2010; Giulieri et al., 2011), and acupuncture (Koh et al., 2010). Much like with pulmonary infections, the contamination is thought to come from mycobacteria in water supplies, either through direct contact or via contaminated water being used to clean instruments followed by improper sterilisation.

Overall, mycobacterial infections (summarised in table 1.1) represent a significant global health burden, with the majority of this being due to TB. Other mycobacterial diseases, although less prevalent, still have a dramatic effect on the quality of life of infected individuals, from both a health and social perspective in the case of disfiguring infections like leprosy and Buruli ulcer. To develop and best exploit treatment options for mycobacterial diseases, it is of vital importance that we have a thorough understanding of the biology of these organisms.

***Table 1.1**: Most common mycobacteria associated with human infection. For NTM infections, the most common forms of disease for each species are listed. The abbreviations RGM and SGM are used in place of rapidly growing mycobacteria and slow growing mycobacteria respectively.*

Species	**Associated complex**	**RGM or SGM**	**Associated disease**	**Main (suspected) transmission route**
M. tuberculosis	MTBC	SGM	Tuberculosis	Person-to-person, respiratory droplets
M. africanum	MTBC	SGM	Tuberculosis	Person-to-person, respiratory droplets
M. caprae	MTBC	SGM	Tuberculosis	Animal-to-person, respiratory droplets
M. bovis	MTBC	SGM	Tuberculosis	Animal-to-person, respiratory droplets and contaminated dairy
M. leprae	*M. leprae* complex	SGM	Leprosy	Person-to-person and animal-to-person, respiratory droplets
M. lepromatosis	*M. leprae* complex	SGM	Leprosy	Person-to-person, respiratory droplets
M. ulcerans	n/a	SGM	Buruli Ulcer	Skin injury in contact with contaminated water

M. marinum	n/a	SGM	Aquarium granuloma	Skin injury in contact with contaminated water
M. abscessus	*M. abscessus* complex	RGM	NTM infection (pulmonary, cutaneous and soft tissue)	Contaminated water/surface (person-to-person recorded) (aerosols, injury/surgery)
M. chelonae	n/a	RGM	NTM infection (pulmonary, cutaneous and soft tissue)	Contaminated water or surface (aerosols, injury/surgery)
M. fortuitum	n/a	RGM	NTM infection (pulmonary, cutaneous and soft tissue)	Contaminated water or surface (aerosols, injury/surgery)
M. avium	MAC	SGM	NTM infection (pulmonary, lymphadenitis and disseminated)	Contaminated water or surface (aerosols, injury/surgery)
M. intracelluare	MAC	SGM	NTM infection (pulmonary, lymphadenitis and disseminated)	Contaminated water or surface (aerosols, injury/surgery)

M. chimera	MAC	SGM	NTM infection (pulmonary, cutaneous and soft tissue)	Contaminated water or surface (aerosols, injury/surgery)
M. haemophilum	n/a	SGM	NTM infection (cutaneous and soft tissue)	Contaminated water or surface (injury/surgery)
M. kansasii	n/a	SGM	NTM infection (pulmonary)	Contaminated water (aerosols)
M. xenopi	n/a	SGM	NTM infection (pulmonary)	Contaminated water (aerosols)
M. gordonae	n/a	SGM	NTM infection (pulmonary)	Contaminated water (aerosols)

1.2. EVOLUTION OF MYCOBACTERIA

1.2.1. The divergence of rapidly growing and slow growing mycobacteria

Genetic evidence points towards one of the early major divergences in the course of mycobacterial evolution being the split of slow growing and rapidly growing mycobacteria from a rapidly growing common ancestor (Devulder, de Montclos and Flandrois, 2005). Comparison of the genomes of 157 mycobacterial species revealed distinct differences between the genomes of slow growing and rapidly growing mycobacteria, with a couple of exceptions where species display a slow or intermediate growth phenotype but genetically resemble rapidly growing mycobacteria and one example where the reverse is true (Bachmann et al., 2019). These outliers appear to be descended from the slow growing and rapidly growing

mycobacteria common ancestors respectively and later evolved to have different growth rates.

Slow growing mycobacteria only possess one 16S rRNA cistron compared to the two 16S rRNA cistrons found in nearly all rapidly growing mycobacteria and this difference has been proposed to contribute to the growth rate difference between the two (Primm, Lucero and Falkinham, 2004). It should be noted however that *M. abscessus* and *M. chelonae*, two rapidly growing mycobacteria, also possess only one 16S rRNA cistron, demonstrating the growth rate of mycobacteria is determined by a number of factors (Prammananan et al., 1998). Another genetic difference between slow growing mycobacteria and rapidly growing mycobacteria that may also affect growth rate are that rapidly growing mycobacteria possess a larger number of genes related to amino acid transport, metabolism and transcription compared to slow growing mycobacteria (Bachmann et al., 2019).

Comparison of genomes from 187 mycobacterial species demonstrated slow growing mycobacteria genomes are overall smaller and contain fewer genes than rapidly growing mycobacteria genomes (Zhang et al., 2023). The genes found to be enriched in slow growing mycobacteria are associated with cellular defence and virulence (Bachmann et al., 2019). These include the ESX-5 Type II section system, which plays a key role in transporting PPE proteins, another set of genes enriched in slow growing mycobacteria which have been implicated to have a role in immune evasion (Forrellad et al., 2013; Saini et al., 2016).

1.2.2. The emergence of pathogenic mycobacteria

There are two groups of mycobacterial species which display a pathogenic rather than a mainly environmental lifestyle, with these being the MTBC and the *M. leprae* complex. The current theory on how this lifestyle change occurred is that an environmental *Mycobacterium* ancestor was taken up and then adapted to survive inside free-living protozoa (Gagneux, 2018). As the bacterium accumulated intracellular survival strategies, with these allowing evasion of digestion by the protozoa, it gained the ability to survive inside mammalian macrophages, and later, the ability to be transmitted from host-to-host.

Evidence for this theory comes in the fact that environmental mycobacteria today are found in the same environments as amoeba (soil and water). Survival of mycobacteria inside amoeba has been demonstrated *in vitro* and acid-fast staining has been used to visualise mycobacteria inside of amoeba acquired from environmental samples (Adékambi et al., 2006; Lahiri and Krahenbuhl, 2008; Delafont et al., 2014). The question of when this change from environmental bacteria to pathogen occurred in the course of the evolution of mycobacteria remains. The ability of numerous mycobacteria to cause human and animal infection suggests traits allowing mycobacteria to survive in intracellular environments have been acquired throughout the evolution of members of the genus, with the MTBC and *M. leprae* complex representing unique events of acquired host-to-host transmission ability at the expense of environmental survival.

The MTBC and *M. leprae* complex are both groups of slow growing mycobacteria, indicating adoption of the pathogenic lifestyle must have occurred after the divergence of rapidly growing and slow growing mycobacteria. Several phylogenetic trees for the *Mycobacterium* genus have been assembled based on sequence similarity of select proteins or rRNA (Kim et al., 2005; Han et all., 2009; Pin et al., 2014). The relationships drawn between different mycobacterial species vary depending on the method of analysis, however *M. leprae* has been identified as being more closely related to the environmental *M. haemophilum* than to *M. tuberculosis* (Tufariello et al., 2015). This indicates the separation of the common ancestors of the *M. leprae* complex and the MTBC occurred before the conversion to a pathogenic lifestyle. Therefore, two mycobacterial ancestor species made the jump from environmental organisms to surviving inside and relying on transmission between mammalian hosts.

1.2.3. Evolution of the MTBC

There is some debate over when the divergence of the MTBC occurred, with different estimates placing the most recent common ancestor of the complex as having existed 70,000 years ago or less than 6,000 years ago (Comas et al., 2013; Bos et al., 2014). This latter estimate does not match ancient MTBC DNA findings recovered from 9,000-11,000-year-old human remains from the Eastern Mediterranean region (Hershkovitz

et al., 2008; Baker et al., 2015). Aside from ancient DNA, evidence for the presence of human-adapted TB in ancient civilisations exists in the form of human remains with spinal deformities characteristic of TB infection of the spine known as Pott's lesions and written records. One of the oldest known examples of the former is a skeleton discovered in Italy, with radiocarbon dating placing these remains as being from somewhere between 4000-3500 BC (Formicola, Milanesi and Scarsini, 1987), while the oldest known written record comes from India and is thought to be from 1500-1000 BC (Barberis et al., 2017). These ancient skeletal remains indicate the presence of human-adapted TB around 5,500-6,000 years ago, however without genetic/molecular evidence, it is impossible to draw conclusions about the strain responsible for the observed lesions.

It was originally theorised that TB was passed from domestic animals to humans, with *M. bovis* being the most likely candidate for this infection that later evolved into *M. tuberculosis* and *M. africanum* (Manchester, 1984; Stead et al., 1995). This theory arose due to the human specificity of *M. tuberculosis* relative to the broader host range of *M. bovis*, with animal-to-human transmission deemed more likely than the possibility of the frequent human-to-human spread required to sustain *M. tuberculosis* in ancient human populations. Genetic analysis has since revealed the *M. bovis* genome is smaller than that of *M. tuberculosis*, making it much more likely *M. bovis* evolved from *M. tuberculosis* (Brosch et al., 2002). Mapping deletions across *M. bovis, M. africanum* and *M. microti*, a rodent-adapted member of the MTBC, genomes relative to *M. tuberculosis* reveals these three species likely belong to the same lineage, with *M. africanum* being the most similar to *M. tuberculosis*.

The place of origin of *M. tuberculosis*, as well as where *M. africanum* diverged, is thought to be Africa. Modern *M. tuberculosis* and *M. africanum* strains can be divided across nine distinct lineages (table 1.2). Two of these, L2 and L4, show a global spread, while others are more region-specific, with five lineages being restricted to specific areas in Africa, the only continent where all lineages are present (Ngabonziza et al., 2020; Coscolla et al., 2021; Netikul et al., 2021; Phyu et al., 2022). These lineages also correspond to differences in disease outlook. For example, L1 has a higher case fatality

rate and is associated with infections in older patients while L2 strains are more likely to be multidrug-resistant.

***Table 1.2**: The different lineages of the human specific species of MTBC and their distribution.*

Lineage	Species	Geographical distribution
L1	*M. tuberculosis*	East Africa, South and Southeast Asia
L2	*M. tuberculosis*	Africa, Asia and Europe
L3	*M. tuberculosis*	South Asia, North and East Africa
L4	*M. tuberculosis*	Global
L5	*M. africanum*	West Africa
L6	*M. africanum*	West Africa
L7	*M. tuberculosis*	Horn of Africa
L8	*M. tuberculosis*	African Great Lakes region
L9	*M. africanum*	East Africa

1.3. PATHOLOGY

1.3.1. Granulomas in mycobacterial infections

Exposure to mycobacteria does not always result in active or latent infections. Approximately half of those exposed to members of the MTBC test negative for mycobacterial infection, demonstrating the ability of the immune system to eliminate mycobacteria (Lerner, Borel and Gutierrez, 2015). In cases where the immune system

is unable to fully clear the *Mycobacterium* bacilli, they can be contained within a granuloma. Granulomas are aggregates of immune cells that form around sites of infection and are a key aspect of mycobacterial infection, as while they effectively contain the mycobacterial cells, they also serve as an environment where these cells can persist and then potentially reemerge from.

The process of granuloma formation is as follows: upon *Mycobacterium* bacilli gaining entry into the host, the innate immune system identifies them as foreign and they are engulfed by macrophages. The usual progression of immune defence would see fusion of the phagosome containing the bacilli with a lysosome and subsequent destruction of the invading pathogen. Mycobacteria, however, are able to avert this process (Armstrong and Hart, 1971), with several mycobacterial cell wall lipids having been found to effectively block phagosome/lysosome fusion (Goren et al., 1976; Indrigo, Hunter and Actor, 2003; Hmama et al., 2004). The infected macrophages release cytokines to recruit to further macrophages and other immune cells to the site of infection (Ehlers and Schaible, 2012). The result is a granuloma; a structure comprised of a layer of lymphocytes surrounding a core of healthy and infected macrophages. At this point the bacilli are effectively contained, and, in TB, this is what constitutes a latent infection, where the infected individual is asymptomatic and non-infectious. Inside the granuloma, the bacilli have limited access to oxygen and nutrients, however mycobacteria are able to alter their metabolic state, allowing them to survive under these conditions with little to no replication (Rustad et al., 2009).

Over time the cells in the centre of the granuloma may undergo necrosis, with the resulting debris being referred to as caseum. This type of granuloma is known as a caseous necrotic granuloma and in these structures the *Mycobacterium* bacilli will move into the caseum (Alsayed and Gunosewoyo, 2023). It is also possible for fibroblasts, collagen-producing cells that can be recruited into granulomas, to form a fibrous layer around the granuloma, forming a fibrotic granuloma (McCaffrey et al., 2022). The outer layer of fibrotic granulomas can then be mineralised, forming a fibro-calcified granuloma, with this form typically being associated with latent infections (Mattila, et al., 2013).

Under select circumstances, such as HIV infection or other forms of immunosuppression, the contained *Mycobacterium* bacilli can become reactivated. Once this occurs, the bacilli will multiply inside the granuloma until the structure of the granuloma fails and they are released, with the potential to then be transmitted to a new host in the case of host-to-host transmissible infections, i.e. TB and leprosy (Alsayed and Gunosewoyo, 2023).

1.3.2. Mycolactones in mycobacterial pathology

Mycolactones are a group of compounds comprised of a 12-membered macrolactone ring, with one side-chain branching from C11 and a second variable polyunsaturated side-chain branching from C5. They are produced by few mycobacterial species, with *M. ulcerans* and *M. marinum* currently being the only known mycolactone-producing mycobacteria to infect humans (Hong et al., 2008). Only select strains of *M. marinum* produce mycolactones, whereas all known strains of *M. ulcerans* produce at least one form of these compounds, with the exact structure depending on the strain.

The ability of select mycobacteria to produce mycolactones is related to the acquisition of a plasmid (pMUM), likely by a common ancestor which then diverged into the different species found today (Yip, et al., 2007). The exact role of these compounds in the survival of *M. ulcerans* in the environment is unknown, however they do play a key role in the pathology of Buruli ulcer. Mycolactones are cytotoxic and analgesic, with these properties being responsible for the key symptom of *M. ulcerans* infection: a painless ulcer (Yotsu et al., 2018). These compounds also have immunosuppressive effects, and this, combined with their cytotoxicity, means that after an initial period of incubation inside host cells, *M. ulcerans* is a mainly extracellular pathogen, which is in contrast to other mycobacteria (Huber et al., 2008).

1.4. CURRENT TREATMENT OPTIONS FOR MYCOBACTERIAL INFECTIONS

1.4.1. First-line TB treatments

Mycobacteria are intrinsically resistant to many common antibiotics including β-lactams due to their unique cell wall (Jarlier and Nikaido, 1994). Additionally, finding

treatments that are able to penetrate granulomas and kill dormant mycobacteria as well as those that are actively replicating presents another challenge in curing mycobacterial infections. As TB is the most common mycobacterial disease, a significant number of drugs developed to treat mycobacteria have first been investigated for activity against the MTBC.

The current recommended treatment for drug-susceptible TB is a two-month course of rifampicin, isoniazid, ethambutol and pyrazinamide, followed by a four-month course of just rifampicin and isoniazid (World Health Organisation, 2023b). Isoniazid was found to be effective against TB in patients in the early 1950s and has been used as part of standard TB therapy in the decades since (Selikoff and Robitzek, 1952). Its mechanism, however, was only determined in the late 1990s, with the use of isoniazid resistance mutants demonstrating isoniazid forms a radical species following activation with a mycobacterial catalase peroxidase (Chakraborty and Rhee, 2015). This radical reacts with NAD^+ and the resulting product inhibits the InhA enzyme which is required for biosynthesis of mycolic acids.

Ethambutol was shown to have activity as an anti-TB drug and was first used to treat patients in the 1960s alongside isoniazid, with it later being incorporated into standard TB treatment (Ferebee, Doster and Murray, 1966). Despite over sixty years having passed since its discovery, the mode of action of ethambutol is still not entirely understood, but is believed to involve inhibition of arabinosyltransferases which are used by mycobacteria in the formation of their cell walls (Zhang et al., 2020). Rifampicin was also first used to treat TB in the 1960s, becoming part of the standard treatment for pulmonary TB in the 1970s alongside isoniazid and ethambutol (British Thoracic and Tuberculosis Association, 1976; Sensi, 1983). Rifampicin acts via inhibiting DNA-dependent RNA polymerase and therefore preventing transcription in mycobacteria (Campbell et al., 2001). Despite being one of the most potent treatment options against TB, bacteria can develop a high level of resistance against rifampicin through one-step mutations, thus the need for co-administration with other antibiotics (Goldstein, 2014).

Studies showing the activity of pyrazinamide against the MTBC in human patients took place in the 1950s, however there was a high rate of hepatitis when pyrazinamide was administered to patients alongside isoniazid (McDermott et al., 1954). This was later found to be an issue with dosage, and in the 1980s trials in which pyrazinamide was added to TB treatment regimens featuring isoniazid, rifampicin and ethambutol demonstrated its inclusion was able to decrease the required treatment time, leading to the current recommended treatment protocol (Muschenheim et al., 1955; Somner and Angel, 1981). In mycobacterial cells, pyrazinamide is converted to pyrazinoic acid via the action of an amidase (Chakraborty and Rhee, 2015). The bactericidal effects of pyrazinamide are associated with accumulation of this pyrazinoic acid inside cells, however the exact mechanism behind this observation remains unclear.

Although the rifampicin, isoniazid, ethambutol and pyrazinamide treatment regimen is effective, as these drugs have been in use for decades, it is perhaps not surprising that issues have arisen regarding drug resistance. An estimated 410,000 TB cases in 2022 were caused by drug-resistant strains (World Health Organisation, 2023b). Both isoniazid-resistant and rifampicin-resistant strains occur, with multidrug-resistant TB being resistant to both rifampicin and isoniazid.

1.4.2. Second-line TB treatments

A push for newer anti-TB drugs resulted in development of the BPaL regimen, which involves treatment with bedaquiline (BDQ), pretomanid and linezolid over a period of six to eighteen months depending on the individual case. It is currently employed in the treatment of drug-resistant, multidrug-resistant and pre-extensively drug-resistant TB (World Health Organisation, 2023b). Pre-extensively drug-resistant TB is defined as resistance to rifampicin and any fluoroquinolone, while extensively drug-resistant TB harbours the same resistances as the above along with resistance to BDQ or linezolid. Moxifloxacin, a fluoroquinolone, is included in treatment of drug-resistant cases, with this being known as the BPaLM regimen. Use of these regimens in clinical trials has resulted in around 90% treatment success rates (Ali et al., 2024).

Linezolid and moxifloxacin were both initially used in the treatment of other bacterial infections and were later found to also be active against mycobacteria (Guay, 2006;

Leach et al., 2011). Linezolid prevents protein synthesis through binding to bacterial ribosomes, while moxifloxacin inhibits DNA gyrase and topoisomerase IV. BDQ and pretomanid were both developed in the 2000s specifically to treat TB (Stover et al., 2000; Andries et al., 2005). When BDQ was approved for use by the FDA in 2012, it was the first new TB treatment to be approved in over 40 years (Jones, 2013). This alone has made it notable in the history of TB treatment, however it is BDQ's mechanism of action that has had an especially important impact in the mycobacterial field. BDQ targets bioenergetics in mycobacteria, a previously neglected target in drug development that has since been the subject of increasing interest, with this being detailed in sections 1.5 and 1.6. Pretomanid later gained FDA approval in 2019, and although its mechanism has yet to be fully studied, it is known to act as a prodrug, with the active form believed to target an enzyme used in cell wall synthesis (FDA, 2019; Abrahams et al., 2023).

1.4.3. Treatment of leprosy and NTM infections

The current recommended treatment for leprosy is a six-to-twelve-month course of rifampicin, clofazimine (CFZ) and dapsone, with minocycline, ofloxacin and clarithromycin being used as second-line treatments (Chen et al., 2022). CFZ was originally developed as a potential anti-TB agent in the 1950s, however it was shelved after it was found to deliver inconsistent results in *in vivo* models (Xu, Koval and Katanaev, 2023). In the 1960s, CFZ was repurposed towards leprosy treatment, becoming part of the recommended regimen in 1977. The mechanism of CFZ is described in detail in section 1.5 as it pertains to bioenergetics. Dapsone is a sulfone that had been used in leprosy treatment since 1946 and acts by inhibiting folate biosynthesis (Kar and Gupta, 2015).

M. ulcerans infections are treated using a course of rifampicin and clarithromycin, a broad spectrum antibiotic that inhibits protein synthesis in bacteria (Peters and Clissold, 1992; Van Der Werf et al., 2020). Treatment of other NTM infections is complicated by different mycobacterial species having different drug susceptibility profiles (Pennington et al., 2021). To date, no antibiotics have been developed specifically to treat NTM diseases, with anti-TB drugs or other antibiotics being used

on a case-by-case basis. In some cases, usually where there has been a poor response to drug therapies, this is combined with surgical excision of infected material (Tseng et al., 2020; Wang, Jia and Li, 2023).

1.5. MYCOBACTERIAL BIOENERGETICS

1.5.1. Mycobacterial metabolism

The topic of metabolism covers all of the processes used by cells to supply themselves with the energy and materials required for survival and growth (Mashabela, de Wet and Warner, 2019). An understanding of metabolism, and regulation of metabolic processes in response to changing external conditions, is of great importance in the study of pathogens. By understanding which of these processes are vital for pathogen survival during infection, metabolism opens up as a potential drug target (Murima, McKinney and Pethe, 2014). By definition, the subject of mycobacterial metabolism includes bioenergetic processes, which are the focus of the rest of this report. This section will focus on mycobacterial central carbon metabolism, as it is these reactions that ultimately supply electrons to the electron transport chain (ETC) where the final stage of aerobic respiration occurs (Rhee et al., 2011).

Central carbon metabolism in mycobacteria involves several interlinked pathways which allow catabolism of multiple carbon sources. In terms of key pathways there are glycolysis, gluconeogenesis, the pentose phosphate shunt and the TCA cycle (Cumming and Steyn, 2015). In glycolysis, glucose is converted to pyruvate with net generation of ATP and NADH, while gluconeogenesis involves the synthesis of glucose from noncarbohydrates. The pentose phosphate shunt acts as an alternative pathway to part of glycolysis and generates ribose sugars, which are important for DNA and RNA synthesis (Stincone et al., 2014). The TCA cycle is a series of reactions that generate reduced coenzymes, which can deliver electrons to the ETC, along with ATP and carbon dioxide. There is also the glycoxylate shunt, which bypasses part of the TCA cycle, namely the stages where carbon dioxide is generated (Ahn et al., 2016).

When growing mycobacteria *in vitro*, carbohydrates such as glucose or succinate are frequently used as carbon sources, however under infection conditions, mycobacteria

have limited access to nutrients and will primarily metabolise host lipids (Gago, Diacovich and Gramajo, 2018). Fatty acids undergo β-oxidation and can either enter the TCA cycle as acetyl coenzyme A, or through the methyl malonate pathway or methylcitrate cycle (Rhee et al., 2011). The side chain of cholesterol is also broken down by β-oxidation, with the products of this also entering the TCA cycle as acetyl coenzyme A and via the methyl malonate pathway or methylcitrate cycle (Rhee et al., 2011; Abuhammad, 2017). However the stages involved in the catabolism of the sterol ring are not yet fully understood (Abuhammad, 2017). Mycobacteria metabolise lipids while in a non-replicating state during infection, with the glyoxylate shunt being utilised to reduce loss of carbon as carbon dioxide under these conditions (de Carvalho et al., 2010).

M. tuberculosis is able to co-catabolise several carbon sources simultaneously (de Carvalho et al., 2010). This is unusual as many bacteria exhibit diauxic growth, i.e. where one carbon source is preferentially metabolised first, followed by a switch to a second carbon source. It has been theorised this co-catabolism is linked to the pathogenic nature of *M. tuberculosis* and it may be advantageous for survival during infection. Whether mycobacteria that act as opportunistic pathogens share this ability has not yet been demonstrated, but co-catabolism of carbon sources has been observed in *M. bovis* (Davis et al., 2024).

1.5.2. An introduction to bioenergetics

Bioenergetics is the study of the transformation of energy by living organisms. Energy, either from light or a chemical energy source is converted into chemical potentials such as ATP/ADP or NADH/NAD^+ that can be used by cells to power energy-requiring processes. A significant portion of bioenergetic research as it pertains to respiration has been focused on mitochondria and, as a result, our understanding of this area in eukaryotes exceeds that in prokaryotes. Therefore, before discussing bioenergetics in mycobacteria, it is important to first outline the systems found in mitochondria, as these have influenced how similar processes are thought to function in bacterial systems.

Chemiosmotic theory is a core part of bioenergetics and describes a system where ions are transported across a membrane, resulting in charge and concentration gradients (Nicholls and Ferguson, 2002). Movement of ions back down these gradients is then used to drive endergonic reactions. Oxidative phosphorylation in respiration relies upon this principle, with a proton, or sodium ion in the case of some bacteria (Mulkidjanian, Dibrov and Galperin, 2008), gradient across a membrane being coupled to ATP synthesis. ATP is then hydrolysed elsewhere in the cell to enable energy-requiring cellular processes to occur.

In mitochondria, a series of membrane proteins, collectively referred to as the ETC, use energy from the transfer of electrons to pump protons from the mitochondrial matrix into the intermembrane space (figure 1.2) (Nicholls and Ferguson, 2002). The ETC consists of four complexes; first is NADH-ubiquinone (UQ) oxidoreductase which oxidases NADH produced in earlier stages of respiration and reduces UQ, forming ubiquinol (UQH_2). During this process, the enzyme also pumps four protons across the membrane for every pair of electrons transferred. Succinate dehydrogenase (SDH), complex II in the mitochondrial ETC, acts as part of the TCA cycle converting succinate to fumarate and also reducing UQ but without proton-pumping.

UQH_2 is oxidised back to UQ by complex III, UQH_2-cytochrome *c* oxidoreductase, which transfers electrons from UQH_2 to cytochrome *c*, a protein located on the inter-membrane space side of the inner membrane. These electrons are finally transferred to complex IV, cytochrome *c* oxidase, where oxygen is used as a terminal electron acceptor and combines with protons to form water. Both complex III and complex IV translocate protons as this electron transfer occurs, further contributing to the build-up of a proton gradient across membrane. This gradient can be spilt into two components, an electrochemical gradient ($\Delta\Psi$) and a pH gradient, (ΔpH), with the combination of the two being referred to as the proton motive force (PMF). The PMF drives protons back across the membrane through the enzyme ATP synthase, which utilises the energy from this proton movement to drive the synthesis of ATP from ADP and inorganic phosphate (P_i). ATP synthase is also sometimes dubbed complex V, although as it is not involved in electron transfer, it is not part of the ETC.

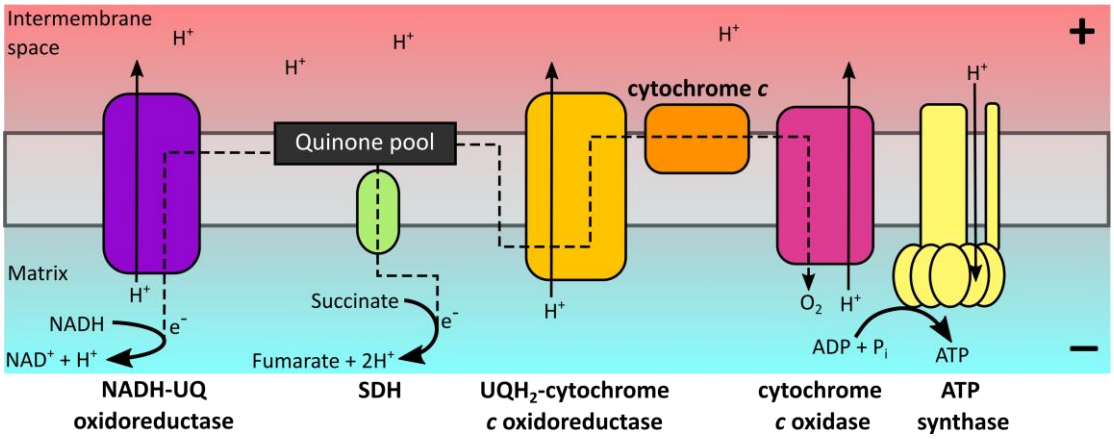

***Figure 1.2**: The oxidative phosphorylation system in mitochondria, located at the inner membrane.*

1.5.3. Oxidative phosphorylation in mycobacteria

The oxidative phosphorylation system in mycobacteria is located at the cell membrane and has several key differences compared to the mitochondrial system. Firstly, mycobacteria utilise menaquinone (MK) in place of UQ, with the significance of this from a bioenergetics perspective being that MK has a more negative midpoint potential than UQ and is therefore less readily reduced (Kishi et al., 2017). Mitochondrial ATP synthase, as well as a number of bacterial ATP synthases, will run in reverse, catalysing ATP hydrolysis and transporting protons into the inter-membrane space or periplasm. ATP synthase in mycobacteria does not display this same hydrolysis activity (Haagsma et al., 2010).

The composition of the ETC is also different in mitochondria versus mycobacteria (figure 1.3), with there being some variation between species, as summarised in figure 1.4. Type I NADH:MK oxidoreductase (NDH-1), encoded by the *nuo* operon, acts as an equivalent to complex I in mycobacteria, oxidising NADH while reducing MK to menaquinol (MKH_2) and pumping protons into the periplasm (Weinstein et al., 2005). Mycobacteria also harbour a type II NADH:MK oxidoreductase (NDH-2), with *M. tuberculosis* containing two versions of the NDH-2 gene, *ndh* and *ndhA*. NDH-2 fulfils the same function as NDH-1 but without the accompanying proton movement, making it less energy efficient. In spite of this, NDH-2 is responsible for a majority of NDH activity in mycobacteria, with NDH-1 activity being 95% lower than NDH-2 activity in

M. smegmatis and 75% lower in *M. bovis* BCG (Vilchèze et al., 2005). Additionally, the genes coding NDH-1 are not essential for growth in *M. tuberculosis* (Sassetti, Boyd and Rubin, 2003) and are lacking altogether in members of the *M. leprae* complex. One theory as to why NDH-2 activity is so much greater than that of NDH-1 is that, as NDH-1 is a proton pumping complex, a high PMF could limit its activity and therefore electron flux through the ETC, which is not the case for NDH-2 (Cook et al., 2014).

Mycobacteria possess two versions of SDH (SDH1 and SDH2), with the *M. tuberculosis* ETC also containing a fumarate reductase (FRD), encoded by *frdABCD*, which catalyses the reverse reaction to SDH (Cook et al., 2014). SDH1 is anchored to the membrane by a single hydrophobic subunit whereas SDH2 has two anchoring subunits (Gong et al., 2020; Zhou et al., 2021). SDH2 has been observed to be essential in *M. smegmatis* when grown on solid LB medium under aerobic conditions, with a knockout of the SDH2 operon proving lethal (Pecsi et al., 2014). In comparison, a knockout of SDH1 displayed similar growth to the WT, indicating increased SDH2 activity is able to compensate for a lack of SDH1 but not vice versa.

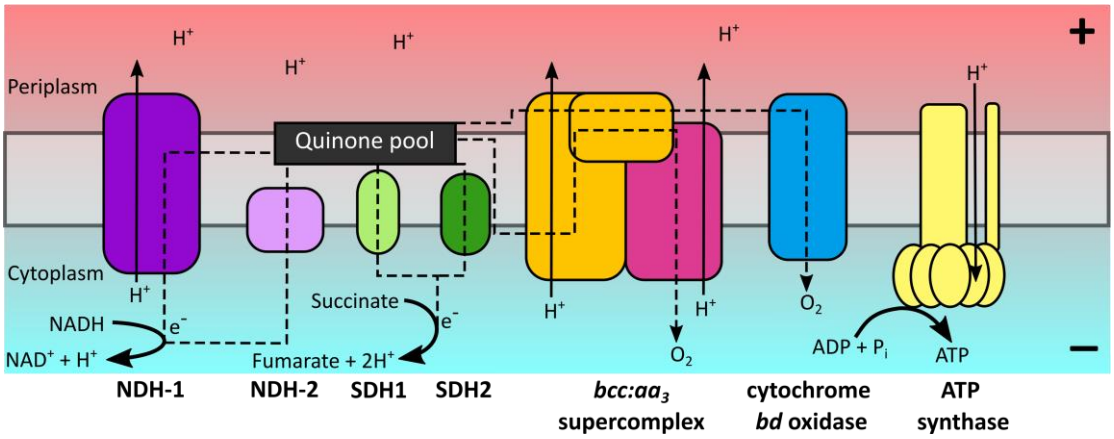

Figure 1.3: *Composition of the oxidative phosphorylation system in M. smegmatis, a model organism frequently used to study mycobacterial systems. Most mycobacteria possess a similar ETC, with differences being highlighted in figure 1.4.*

MK-cytochrome *c* oxidoreductase *bcc* (encoded by *qcrCAB*) is the mycobacterial equivalent of complex III and contains a cytochrome *cc* domain from which electrons are transferred to cytochrome *c* oxidase aa_3 (encoded by *ctaBCDE*) (Wiseman et al., 2018). These two enzymes, along with a superoxide dismutase (SOD), form a structure

termed the *bcc:aa₃* supercomplex. The supercomplex exists as a dimer, with two *aa₃* subunits positioned on either side of a pair of adjacent *bcc* subunits and two SOD subunits on the periplasm side of the complex.

As with complex III and complex IV in mitochondria, the supercomplex translocates protons across the membrane, with a total of six protons being moved per pair of electrons passed through the complex (Cook et al., 2014). SOD is able to convert superoxide into hydrogen peroxide and molecular oxygen, and is therefore able to prevent damage from superoxide produced either by mycobacteria themselves during respiration or as part of a host immune response (Lundgren et al., 2018). It has been theorised that as a part of the supercomplex, SOD may funnel electrons to the cytochrome *cc* domain in the *bcc* subunit instead of forming hydrogen peroxide (Wiseman et al., 2018).

Unlike mitochondria, almost all mycobacteria possess a second terminal oxidase: cytochrome *bd* oxidase (encoded by *cydAB*). In contrast to the supercomplex, cytochrome *bd* oxidase is non-proton pumping and therefore only contributes to PMF generation via transmembrane charge separation (Jasaitis et al., 2000). Under aerobic conditions, the supercomplex acts as the dominant pathway for electrons and cytochrome *bd* oxidase is not essential for growth (Matsoso et al., 2005; Lu et al., 2019). Cytochrome *bd* oxidase does however play an important role in enabling mycobacteria to survive hypoxic conditions, like those found in granulomas, and other stressors including antibiotic treatment due to the enzyme's high oxygen affinity (Kana et al., 2001; Boot et al., 2017).

Species	NDH-1	NDH-2	SDH1	SDH2	FRD	supercomplex	cytochrome *bd* oxidase
M. smegmatis	■	■	■	■		■	■
M. tuberculosis	■	■	■	■	■	■	■
M. bovis	■	■	■	■	■	■	■
M. leprae		■		■		■	
M. ulcerans	■	■	■	■		■	
M. marinum	■	■	■	■		■	■
M. avium	■	■	■	■		■	■
M. absecssus	■	■	■	■		■	■

Figure 1.4: *The composition of the ETC across several species of mycobacteria, with shaded boxes representing the enzymes present in a species, while unshaded boxes are absent (Kanehisa, 2019; Kanehisa and Goto, 2000; Kanehisa et al., 2023; Kanehisa Laboratories, 2024). This list of mycobacteria includes the model non-pathogenic organism M. smegmatis and several important human pathogens.*

1.5.4. Drugs targeting oxidative phosphorylation in mycobacteria

The differences between the oxidative phosphorylation systems in mitochondria and mycobacteria can be exploited as potential drug targets. Already, BDQ and CFZ have been approved for treatment of TB and leprosy respectively. CFZ appears to act via a redox cycling mechanism, competing with MK for reduction by NDH-2 and then undergoing non-enzymatic oxidation by oxygen, releasing reactive oxygen species in the process (Yano et al., 2011). NDH-2 is an attractive target due to the lack of an equivalent enzyme in mitochondria and has been the subject of some focus (Dunn et al., 2014; Murugesan et al., 2018; Dam et al., 2022). Several potential NDH-2 inhibitors or redox cycling compounds like CFZ have been synthesised and displayed activity

against *M. tuberculosis*, but have yet to be taken further in terms of clinical development (Warman et al., 2013; Dunn et al., 2014; Murugesan et al., 2018; Dam et al., 2022).

Another anti-mycobacterial drug targeting the oxidative phosphorylation system is Q203 or telacebec. Q203 is currently in the phase II clinical trial stage for treatment of Buruli ulcer, with a phase IIa trial for treatment of TB having already been completed (TB Alliance, 2024; de Jager et al., 2020). The drug acts via inhibiting MK-cytochrome *c* oxidoreductase *bcc* and therefore preventing electron transfer through the supercomplex (Pethe et al., 2013). As most mycobacteria possess a second terminal oxidase, Q203 is only bacteriostatic against the likes of *M. tuberculosis*, making co-administration with a cytochrome *bd* oxidase inhibitor highly desirable. A potential *bd* oxidase inhibitor, ND-011992, has been identified and shown to be bactericidal against *M. tuberculosis* and *M. bovis* BCG in combination with Q203, but has yet to be developed further (Lee et al., 2021).

1.6. BEDAQUILINE (BDQ)

1.6.1. Discovery of BDQ and current uses

Development of BDQ as an anti-TB drug began with a screening of drug prototypes for growth inhibition activity against the model organism *M. smegmatis* (Andries et al., 2005). The lead compound was optimised to generate a set of diarylquinolines (DARQs) and their activity against *M. tuberculosis* H37Rv was evaluated (Van Gestel et al., 2004). BDQ was identified as the compound with the greatest activity, having an MIC of 0.030 µg/mL (Andries et al., 2005).

A series of further experiments found that BDQ has similarly low MICs (0.030-0.120 µg/mL) for several *M. tuberculosis* clinical isolates resistant to current anti-TB drugs, including rifampicin and, most notably from a mechanistic standpoint, moxifloxacin (Andries et al., 2005). Moxifloxacin is a quinoline, and the fact cross-resistance was not observed with BDQ, along with BDQ displaying no activity against purified DNA gyrase, demonstrates DARQs have a different target to quinolines. BDQ's activity is

specific to mycobacteria, with the drug having much higher MICs (≥4 μg/mL) in bacterial species belonging to different families (Andries et al., 2005).

Identification of BDQ's actual target was achieved through *in vitro* isolation and genomic sequencing of BDQ-resistant mycobacteria (Andries et al., 2005). In both BDQ-resistant *M. tuberculosis* and *M. smegmatis*, the only commonly mutated gene was atpE, which codes for the c-subunit of F_0F_1-ATP synthase. This provided early evidence that BDQ binds to ATP synthase, as well as explaining the selectivity of BDQ for mycobacteria, given the structural differences in ATP synthases from bacteria of other genera.

Since BDQ's discovery, it has undergone clinical trials for the treatment of TB and been approved for use by the FDA (Jones, 2013). BDQ has seen much success as part of the BPaL and BPaLM regimens, and has also been used in the treatment of infections caused by NTM (Ali et al., 2024; Omar et al., 2024). Prior to clinical trials with BDQ being initiated, its activity against members of the MAC, *M. abscessus, M. ulcerans, M. kansasii, M. marinum* and *M. fortuitum* was evaluated (Andries et al., 2005). BDQ displayed potent activity against all mycobacterial species tested, with MIC values between 0.003-0.010 μg/mL for all strains tested, save for *M. abscessus* and *M. ulcerans* where BDQ MIC values were between 0.25-0.5 μg/mL. It has since been shown that while BDQ can inhibit growth in *M. avium*, considerably higher concentrations are required for bactericidal activity compared with *M. tuberculosis* (Lounis et al., 2009). Despite this, in one case study, treatment of a disseminated *M. avium* infection with BDQ in combination with other antibiotics resulted in culture conversion (Gil et al., 2021).

BDQ has been used to treat pulmonary infections caused by members of the MAC and *M. abscessus*, with six out of ten patients showing a microbiologic response following six months of treatment (Philley et al., 2015). Additionally, BDQ-containing treatment regimens have been able to cure extrapulmonary *M. abscessus* and *M. fortuitum* infections (Omar et al., 2024).

1.6.2. BDQ's binding site

BDQ possesses two chiral centres and its enantiomer displays a much lower potency, which is indicative of specific binding occurring between BDQ and ATP synthase (figure 1.5) (Andries et al., 2005). Identification of two specific point mutations in the c-ring, Asp32 → Val (D32V) and Ala63 → Pro (A63P), in BDQ resistant *M. smegmatis* and *M. tuberculosis* strains provided the first evidence for the location of the drug's binding site. From the time of these experiments, however, it would be another fifteen years before the structure of BDQ bound to a complete mycobacterial ATP synthase enzyme was solved.

Initial modelling of the interaction between the F_0-region of F_0F_1-ATP synthase and BDQ was conducted using a homology model based on ATP synthase from *Escherichia coli* (*E. coli*) with 37% of the amino acids replaced to match the common sequence in *M. tuberculosis* strains (Jonge et al., 2007). Following optimisation of this structure, it was hypothesised that BDQ's binding site was located between the a- and c-subunits, i.e. close in proximity to the two commonly mutated residues in BDQ-resistant strains. Docking simulations showed BDQ mimicking an arginine residue on the a-subunit (Arg186) and interacting with Glu61, effectively blocking a space required for rotation of the c-ring and thereby preventing proton transfer.

A later series of biochemical assays demonstrated that BDQ's activity is independent of the PMF, suggesting it does not compete with protons for its binding site (Haagsma et al., 2011). Dose-dependent inhibition of ATP synthesis by BDQ was fitted to a one-site binding hyperbola with R^2>0.99, indicating BDQ's mechanism involves single-site binding, which is consistent with the hypothesis based on the *E. coli* homology model.

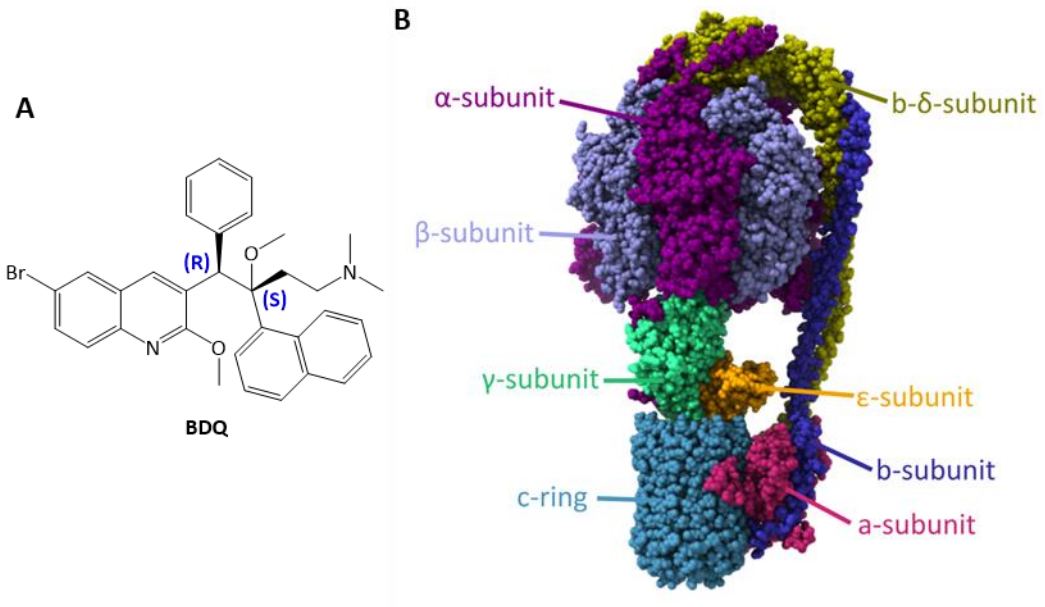

Figure 1.5: *Structures of (**A**) BDQ with its two chiral centres labelled and (**B**) M. tuberculosis ATP synthase, obtained using cryo-electron microscopy (Zhang et al., 2024).*

A second homology model based on the crystal structure of the c-ring of *Spirulina platensis* (*S. platensis*) ATP synthase, a structure that shares 30% of its sequence with the *M. tuberculosis* c-ring, was produced by Segala et al. (Segala et al., 2012). BDQ docking simulations with this model, along with observations that no mutations in the ATP synthase a-subunit had been linked to BDQ-resistance (Huitric et al., 2010), led the group to propose that BDQ does not bind at a site between the a- and c-subunits, but rather in a pocket formed by adjacent c-subunits.

Biukovic et al. (2013), however, theorised that BDQ may be binding to the ε-subunit, the N-terminal domain of which interacts with the c-ring (Biukovic et al., 2013). HSQC NMR spectra of the isolated ε-subunit do show peak distortions indicative of binding during titration experiments with BDQ at a 1:2 molar ratio and this is also supported by results from intrinsic tryptophan fluorescence spectroscopy. From this, a model in which two molecules of BDQ interact with the ε- and c-subunits of ATP synthase was generated by modifying an *E. coli* structure. The idea of BDQ having a second binding site runs counter to the results from the dose dependent inhibition experiment and is further undermined by the lack of association between mutations in the ε-subunit and

BDQ-resistance (Andries et al., 2005; Haagsma et al., 2011). Therefore, it may be BDQ can form interactions with the ε-subunit but evidence suggests these are not key to its activity.

The first non-homology based model showing BDQ bound to part of a mycobacterial ATP synthase was produced using x-ray crystallography to solve the structure of the c-ring from *Mycobacterium phlei* (*M. phlei*) the sequence of which has over 80% similarity with the *M. tuberculosis* c-ring (Preiss et al., 2015). Co-crystallisation of the protein with BDQ yielded a structure where the drug is shown to bind identically to all nine c-subunits in the ring, interacting with nine residues (Gly62, Leu63, Glu65, Ala66, Ala67, Tyr68, Phe69, Ile70 and Leu72), several of which match those highlighted in the *S. platensis* homology model (Leu59, Glu61, Ala63, Tyr64 and Ile66) (Segala et al., 2012). These residues are located in and around the ion-binding site situated between adjacent c-subunits and are generally conserved across mycobacterial species.

Comparison of this structure with the isolated c-ring revealed a change in conformation of Phe69 occurs upon BDQ binding to avoid a steric clash (Preiss et al., 2015). The hydroxyl and dimethylamino groups of the drug form hydrogen bonds with the carboxylate groups of Glu65, forming a structure that resembles a transition state involved in ion translocation. Preiss et al. (2015) propose that binding of a single BDQ molecule locks the c-ring in this state, therefore preventing rotation and ATP generation.

The complete structure of ATP synthase from *M. smegmatis* was solved using cryo-electron microscopy on the enzyme both with and without BDQ (Guo et al., 2021). No binding of BDQ to the ε-subunit can be seen, further invalidating this subunit as being involved in the drug's mechanism. Each c-subunit can be observed to bind one molecule of BDQ, excluding the two c-subunits blocked by the a-subunit. Five BDQ molecules occupy the binding site seen in the *M. phlei* structure but two are bound in novel sites involving the a-subunit, which provides a deeper pocket for BDQ to bind in.

One of these sites, dubbed the leading site, is located on the c-subunit that would have just been in contact with the a-subunit and bound a proton from the periplasmic

space following normal rotation of the c-ring (Guo et al., 2021). Binding of BDQ in this location involves the same residues as the other site along with Phe213, Pro214, Val217, Trp218 and Phe221 on the a-subunit, with the side chain of Phe221 moving to prevent a clash with the drug. Guo et al. (2021) suggest that the leading site may be the most crucial to BDQ's activity as it presents the deepest binding cavity. The second novel site, the lagging site, involves the c-subunit that will next interact with the a-subunit and release a proton into the cytoplasm. In addition to the c-subunit only site residues, this site is formed from Leu70, Pro172, Ile173, and Val176 on the a-subunit.

Density maps obtained from experiments in which isolated mycobacterial ATP synthase was treated with BDQ and then washed show BDQ remains in the leading and lagging sites while the c-subunit only sides have reduced occupancy (Guo et al., 2021). This indicates that interaction with the a-subunit enhances the binding of BDQ, and lends further credence to the leading-site being the most important from an activity standpoint. The lack of a-subunit mutations associated with BDQ resistance, however, suggests binding in the c-subunit only sites is still sufficient for BDQ to display bactericidal effects.

These cryo-electron microscopy structures also provide evidence that the hook-like projections (α-extensions) attached to each of the three α-subunits are responsible for the lack of ATP hydrolysis activity observed with mycobacterial ATP synthases. A single one of these α-extensions is in contact with the γ-subunit in any given rotational state and Guo et al. (2021) propose that the interaction between the two prevents rotation of the γ-subunit in the reverse direction. Lending further proof to this theory, an enzyme modified such that the α-extensions were truncated showed ATP hydrolysis activity.

A structure for BDQ bound to *M. tuberculosis* ATP synthase was acquired more recently using cryo-electron microscopy (figure 1.6) (Zhang et al., 2024). BDQ was found to occupy similar sites as with ATP synthase from *M. smegmatis*, although Ala24 on the c-subunits was newly identified as making up part of the BDQ binding site, while Gly58 was not. Additionally, in the *M. tuberculosis* structure there is loss of π-π

interactions between BDQ and Phe213 on the a-subunit in the leading site, as in *M. tuberculosis* the phenylalanine residue is replaced by alanine.

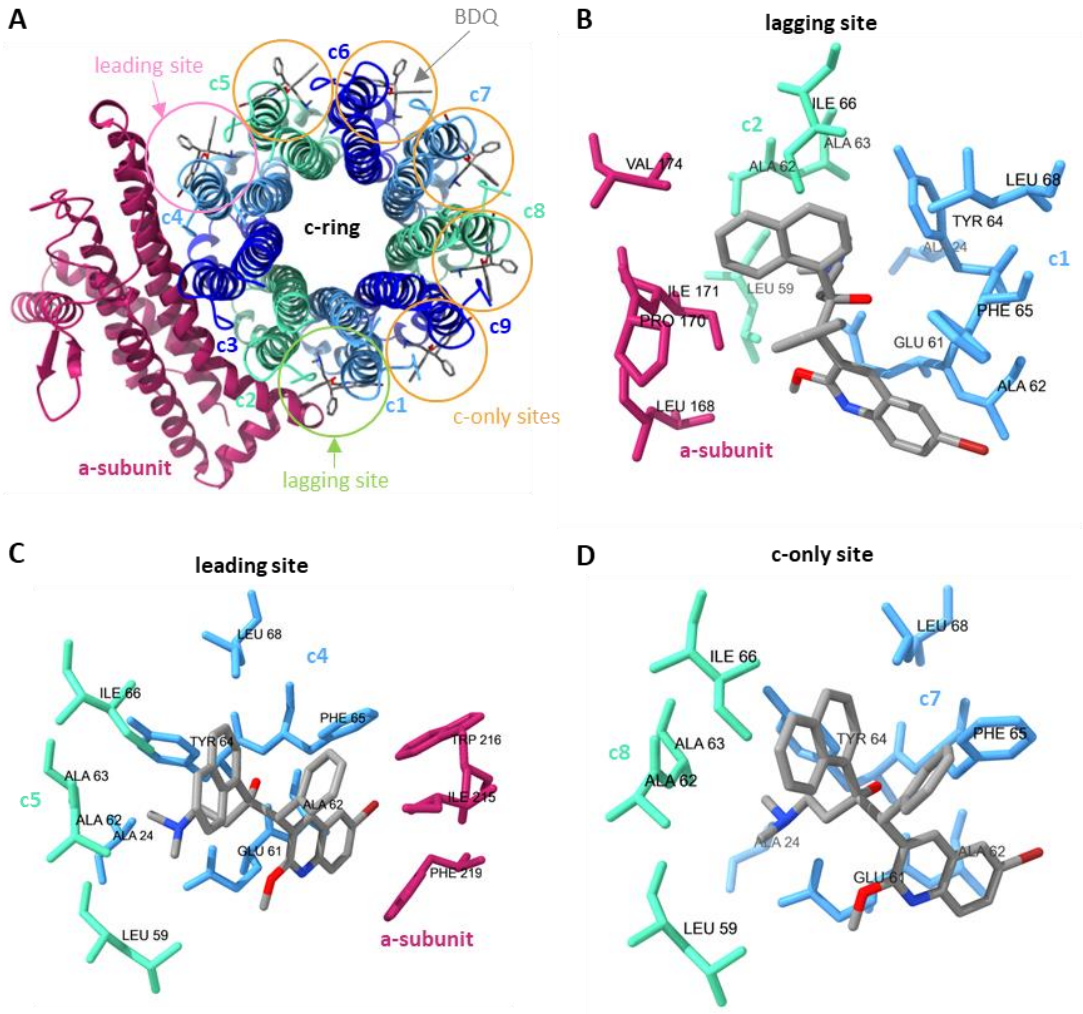

Figure 1.6: *Structure of (**A**) BDQ bound to the a- and c-subunits of ATP synthase from M. tuberculosis with the lagging, leading and c-only binding sites highlighted along with the (**B**) lagging, (**C**) leading and (**D**) c-only site binding pockets with the key residues labelled. The structures were acquired using cryo-electron microscopy (Zhang et al., 2024).*

1.6.3. The mode of action of BDQ

The importance of ATP synthase in BDQ's mechanism along with the drug's ability to bind to it are by now well-established, but the effects of this binding are still much debated. The most long-standing and overall favoured theory is that initially put forward by Andries et al. (2005), that BDQ acts as a direct inhibitor of ATP synthase,

blocking the proton channel and preventing ATP synthesis. This hypothesis is supported by findings that treatment of aerobic and non-replicating *M. tuberculosis* with BDQ results in an appreciable drop in ATP levels within 24 hours (Lamprecht et al., 2016; Koul et al., 2008).

In this mechanism, the bactericidal effects of BDQ may be due to bacteria being unable to sustain enough ATP production for growth and/or due to disruption of the $NADH/NAD^+$ ratio (Tran and Cook, 2005). BDQ has a time-dependent killing effect, with significant rates of cell death in *M. tuberculosis* cultures only being observed post day-four following treatment with sufficient concentrations of BDQ (Koul et al., 2014). This observation supports BDQ's bactericidal effects being related to insufficient production of ATP. ATP levels in mycobacteria drop five-fold when these bacteria enter a non-replicating state, and it has been demonstrated *M. tuberculosis* cells can survive up to a ten-fold decrease in ATP (Gengenbacher et al., 2010; Koul et al., 2008). It follows that mycobacteria are able to survive treatment with BDQ in an ATP-depleted state for the first few days post exposure, generating small amounts of ATP through substrate-level phosphorylation, before ATP levels drop below those needed to maintain cell viability.

A study in which the oxygen consumption rate (OCR) of *M. smegmatis* cells following treatment with BDQ was monitored using a Clark electrode showed an immediate increase in OCR occurs upon addition of the drug (Hards et al., 2015). This finding was later replicated in *M. tuberculosis* using a Seahorse XF Analyser, although the rate of OCR increase was slower (Lamprecht et al., 2016). These observations run counter to expectations of BDQ acting as a direct ATP synthase inhibitor, as prevention of protons moving through the enzyme should result in a build-up of protons on one side of the membrane. This increases the PMF which in turn places backpressure on the system, reducing the rate at which electrons flow down the chain and thus also reducing the OCR (Ripple, Kim and Springett, 2013).

The OCR increase observed with BDQ led to the hypothesis it may be acting as an uncoupler (Hards et al., 2015). Classical uncouplers or protonophores are able to transport protons across a membrane, allowing them to move down $\Delta pH/\Delta\Psi$ without

passing through ATP synthase. In response to dissipation of the PMF, cells increase the rate of electron flow down the chain, and therefore their OCR, in an effort to compensate. The result is a system where are protons are cycled across the membrane without this movement contributing to ATP generation, i.e. the system is uncoupled. As BDQ activity is dependent on the drug being able to bind to ATP synthase, it was proposed BDQ acts via disrupting the interactions between the a- and c- subunits in F_0F_1-ATP synthase and thus allows uncoupled proton movement across the membrane (Hards et al., 2015).

In support of this theory, high doses of BDQ (300x MIC) have been shown to reduce ΔpH in *M. tuberculosis* inverted membrane vesicles (IMVs), although no corresponding drop in ΔΨ is observed (Lamprecht et al., 2016). Additionally, BDQ does not increase the proton conductance of the membrane, unlike the known protonophore CCCP. Lamprecht et al. (2016) propose that these observations are due to BDQ acting as a direct ATP synthase inhibitor, with the increase in OCR being a result of mycobacteria having some mechanism by which they are able to limit the effects of backpressure.

An alternative hypothesis to explain these findings is that, rather than acting similarly to a protonophore, the disturbance of the a- and c-subunit interface by BDQ results in protons being allowed to move into the cytoplasm, while another cation, most likely potassium, moves into the periplasm (Hards et al., 2015; Hards et al., 2018). This would dissipate ΔpH, thus leading to an increase in OCR, but not ΔΨ. BDQ has been observed to acidify the inside of liposomes if a potassium ion gradient exists in the opposite direction (Hards et al., 2018), although this does not fit with ATP synthase binding being required for BDQ to display bacteriostatic/bactericidal effects.

BDQ shows bacteriostatic effects at nanomolar concentrations in *M. tuberculosis* and is bactericidal at micromolar concentrations (Koul et al., 2014). This has led to the proposal that BDQ acts predominantly as a direct ATP synthase inhibitor at low concentrations, with its uncoupling activity becoming more relevant as the concentration increases (Hards et al., 2018; Guo et al., 2021). In this theory, the downstream effects of disruption to the PMF eventually lead to bacterial cell death,

thus why BDQ is only bactericidal at micromolar concentrations. Another observation that lends credence to this theory is that the ATP hydrolysis activity of purified mycobacterial ATP synthase with truncated α-subunits is inhibited with nanomolar concentrations of BDQ (Courbon et al., 2023). When the concentration of BDQ is increased to micromolar amounts, this hydrolysis activity is restored, however this effect is restricted to isolated protein and could not be replicated in IMVs.

At present, BDQ's mode of action, as in whether it acts predominantly as a direct inhibitor of ATP synthase or disrupts the PMF through uncoupled proton movement, is still being debated. There is also the question of how this activity eventually leads to the death of mycobacterial cells. This is a subject of debate for antibiotics in general, with there being some evidence for a unified mechanism wherein antibiotic killing is a result of downstream oxidative damage (Kohanski, Dwyer and Collins, 2010). A recent study on *M. smegmatis* demonstrates cell death following antibiotic exposure correlates with high ATP levels rather than production of reactive oxygen species, implicating this as being part of a common mechanism for mycobacterial killing by antibiotics (Lodhiya et al., 2024). It is unlikely, however, that BDQ also kills via this method, as all the proposed modes of action prevent rapid production of ATP. If killing of mycobacteria by other antibiotics is reliant on a burst of ATP, this has serious implications for the use of BDQ in combination therapies. In order to inform future work on effective combination therapies and guide the development of second-generation compounds, it is important both BDQ's mode of action and how this results in cell death are understood.

1.6.4. Consequences for the cell

Examination of the *M. tuberculosis* transcriptome following BDQ treatment reveals upregulation of the ATP synthase operon and the mycobacterial dormancy regulon for at least 3 hours following BDQ addition (Koul et al., 2014). The dormancy regulon contains 48 genes involved in the adaption of mycobacteria from an aerobic to a hypoxic environment and vice versa, allowing cells to maintain their NAD^+/NADH ratios and sustain low levels of ATP while in a nonreplicating state (Leistikow et al., 2010). These effects likely help to mitigate the impact of ATP synthase inhibition by

BDQ (whether via preventing movement through the proton channel or an uncoupling mechanism). Following 6 hours of exposure to BDQ, there is some upregulation of isocitrate lyase, an enzyme involved in the glyoxylate cycle, and cytochrome *bd* oxidase, both of which are associated with bacterial survival under stress conditions (Koul et al., 2014; Schnappinger et al., 2003; Boot et al., 2017).

Metabolic downstream effects of BDQ on mycobacteria include an increased reliance on substrate-level phosphorylation through glycolysis to maintain ATP levels, a reduction in the rate of gluconeogenesis and activation of the glyoxylate shunt and methylcitrate cycle (Mackenzie et al., 2020). The extent of these effects varies depending on the available carbon source. Following BDQ treatment there is a correlation between changes in cellular ATP levels and a number of metabolites involved in ADP/ATP dependent pathways, with the correlation between ATP and glutamine being the strongest (Wang et al., 2019). Co-administration of BDQ and a glutamine synthase inhibitor results in an increase in BDQ's potency against *M. tuberculosis* along with a shortened killing time. These findings highlight glycolysis and glutamine synthesis as potential targets in the development of future antibiotics that will synergise with BDQ.

1.6.5. Compatibility of BDQ with other antibiotics

The BPaL regimen has a high rate of success, indicating the killing effects of pretomanid and linezolid are not compromised by inhibition of ATP synthesis or potential disruption to the PMF (Ali et al., 2024). However, in pairwise studies, linezolid and pretomanid do not appear to be synergistic with BDQ (Cokol et al., 2017). The efficacy of these combinations was studied in mouse models of TB, and pretomanid and BDQ together were shown to be less effective than BDQ alone during the first month of treatment (Tasneen et al., 2016). When pretomanid and BDQ are coadministered with linezolid, the combination of the three shows a much greater efficacy at two-months compared to any two of the antibiotics being used without the third (Tasneen et al., 2016). This demonstrates there is some synergy when the three are administered together, although there is the potential for combination therapies with BDQ to be further optimised.

BDQ displays antagonism with rifampicin, likely due protein synthesis being downregulated in response to BDQ binding to ATP synthase (Cokol et al., 2017). Additionally, co-administration of the two results in more rapid clearance of BDQ from the body in humans due to rifampicin inducing the CYP3A4 enzyme in the liver, meaning the two cannot be used together effectively (Svensson et al., 2015). Despite the success of the BPaLM regimen, BDQ and moxifloxacin also show antagonism in a pairwise study looking at their activity against *M. tuberculosis* (Cokol et al., 2017).

BDQ is synergistic with CFZ against *M. tuberculosis* and members of the *M. abscessus* complex (Cokol et al., 2017; Ruth et al., 2019). Both BDQ and CFZ resistance can arise through upregulation of the MmpL5 efflux pump, meaning there is greater chance of cross-resistance (Hartkoorn, Uplekar and Cole, 2014). BDQ also displays synergy with pyrazinamide, with TB-infected mice displaying 100% culture conversion following two months of treatment with both drugs, which BDQ or pyrazinamide alone were unable to achieve (Ibrahim et al., 2006). As questions remain around pyrazinamide and BDQs' modes of action, the reasoning behind this synergy is currently unclear.

While there are several established anti-mycobacterial drugs that can be used effectively with BDQ detailed here, a better understanding of the effects of BDQ binding to ATP synthase would enable more strategic formulation of combination therapies. Additionally, it may highlight possible future targets in mycobacteria that may be exploited through use of BDQ.

1.7. MYCOBACTERIAL BIOENERGETIC METHODOLOGY

1.7.1. Techniques for studying bioenergetics

There are several ways one may gain insight into the bioenergetic processes that occur inside cells and the responses to changes in internal or external conditions. There are three main methods that have thus far been applied to mycobacteria, with these being metabolomics, oximetry and working with model/simplified systems such as IMVs.

Metabolomics refers to the quantitative analysis of metabolites in a biological system. The usual workflow involves growth of cells, sometimes with labelling of substrates, followed by lysis, sample processing, separation and detection. Separation is often

achieved through liquid or gas chromatography, while mass spectrometry and NMR act as the most common detection techniques (Lenz and Wilson, 2007). The power of metabolomics comes from the ability to profile compounds from, and therefore study, a vast number of cellular processes, meaning of the three methods listed above, it is able to provide the most detailed information (Johnson, Ivanisevic and Siuzdak et al., 2016). In the case of bioenergetics, the lysis requirement for this style of analysis presents an issue in that, with the fast time scale on which these processes occur, it is possible there may be some disruption to metabolite concentrations during cell breakage procedure. Additionally, it is not possible to monitor real-time changes in cells as they occur, with different batches of cells being used to examine the effects of different conditions.

In comparison, oximetry, i.e. OCR measurements, can provide real-time information on changes in metabolic flux but does not provide significant insight into the exact processes occurring, as demonstrated with alternate explanations being presented for the OCR increase observed with BDQ (Hards et al., 2015; Lamprecht et al., 2016). These measurements can be made with a Clark electrode, which only provides information on oxygen consumption is discussed further in section 3.1.2, or a Seahorse XF Analyser. The latter uses solid-state sensors containing oxygen and proton sensitive fluorophores to measure the concentrations of these compounds (Ferrick, Neilson and Beeson, 2008; Chacko et al., 2013). Over the course of an experiment, the sensor is lowered for a set period to create a microchamber and the changes in oxygen and proton concentration are measured and used to calculate rates for OCR and proton efflux.

Use of IMVs allows specific probing of the oxidative phosphorylation system. The ETC must be energised by addition of an electron donor, namely NADH or succinate, and the proton-pumping activity can be monitored through quenching of pH sensitive fluorophores contained inside the vesicle (Harden et al., 2024). Alternatively, ATP concentrations can be monitored via luciferase assay or quench and measure procedures. The disadvantages of this method include finding preparation methods to ensure a high level of inverted versus non-inverted vesicles and, due to the need for external electron donors, it is not suited for experiments exploring long-term

effects (Futai, 1974; Hards et al., 2018). Data obtained using IMVs also contains no information about the potential downstream effects of factors that impact the oxidative phosphorylation system.

Use of the above techniques in combination can allow for a detailed picture of the bioenergetic processes in cells, however there are still gaps in current knowledge, as the controversy over BDQ's mode of action shows. The focus of this thesis, therefore, is to develop methods that can add to our present understanding of mycobacteria and be applied to the study of BDQ. The use of live cell techniques, namely visible wavelength remission spectroscopy and ^{31}P NMR is explored. These have the benefit of allowing real-time analysis like oximetry, but can provide further information on cellular processes without the caveats that come with using a simplified system like IMVs.

1.7.2. Use of model organisms

Virulent strains of *M. tuberculosis* are classed as BSL-3 organisms, meaning specialist equipment and training are required in order to work with these strains (Asai et al., 2020). This, along with *M. tuberculosis* being a slow-growing organism and difficult to culture, can act as barrier to research. Therefore, model organisms are frequently used in place of virulent *M. tuberculosis* to circumvent one or multiple of these potential issues (Sparks et al., 2023).

The ideal model organism is one that closely matches the pathogen one wishes to study, while being more accessible. *M. smegmatis* is a rapidly growing *Mycobacterium* species, with a doubling time of 3-4 hours, and is classed as BSL-1 organism (Klann et al., 1998; Sparks et al., 2023). These properties mean *M. smegmatis* is considerably easier to work with than virulent mycobacteria, although there has been some debate over its suitability as a model organism (Reyrat and Kahn, 2001). The genome of *M. smegmatis* is over 1.5x greater than that of *M. tuberculosis*, demonstrating that there are clear genetic differences between the two species. However, almost two thirds of the protein-coding genes in *M. tuberculosis* are orthologous with *M. smegmatis* genes, with around 1150 of these sharing greater than 50% amino acid identity with each other as well as with other pathogenic mycobacteria including *M. abscessus*, *M. avium*

and *M. leprae* (Sparks et al., 2023). Of the 41 *M. tuberculosis* virulence factors discussed in an extensive review by Smith (2003), 17 of these have orthologs in *M. smegmatis*, with these including genes involved in amino acid and purine biosynthesis (*leuD*, *trpD*, *proC* and *purC*), regulation of transcription (*phoP*, *prrA*, *mprA* and *hspR*) and the oxidative stress response (*katG*, *ahpC* and *sodC*) (Kanehisa, 2019; Kanehisa and Goto, 2000; Kanehisa et al., 2023; Kanehisa Laboratories, 2024).

The use of *M. smegmatis* as a model organism was somewhat validated through the development of BDQ, as it was via screening with *M. smegmatis* that DARQs were identified as potential anti-TB compounds (Andries et al., 2005). *M. smegmatis* has also been employed in the study of mycobacterial genetics, the mycobacterial cell envelope and the modes of action of anti-TB drugs, including isoniazid and ethambutol (Sparks et al., 2023). Due to the non-pathogenic nature of *M. smegmatis*, it is unsuitable for macrophage infection studies.

Alternatives to *M. smegmatis* include BSL-2 compatible strains of *M. tuberculosis* and *M. bovis*, with *M. bovis* BCG and *M. tuberculosis* H37Ra being two commonly used strains (Zheng et al., 2008; Liang et al., 2022). While these strains are genetically more similar to *M. tuberculosis*, they share the caveats of being slow-growing and difficult to culture, as well as requiring a BSL-2 laboratory space. Therefore, in situations where BSL-2/BSL-3 facilities are unavailable or a fast supply of culture is required, although not a perfect reflection of the systems founds in *M. tuberculosis*, *M. smegmatis* is the most suitable model organism.

1.8. THESIS AIMS AND OBJECTIVES

Aims: To develop and apply ^{31}P NMR and visible-wavelength remission spectroscopy to understand mycobacterial bioenergetics as it powers a living cell. Use these methods to understand the action of the important antibiotic BDQ in *M. smegmatis* and *M. tuberculosis.*

Objectives:

1) Develop appropriate microbiological techniques in order to secure a ready supply of *M. smegmatis* and *M. tuberculosis*, grown in set and understood conditions, for later experiments.

2) Establish visible-wavelength remission spectroscopy as a technique to measure the electron-occupancy of cytochromes within living mycobacteria.

3) Perform initial experiments using visible-wavelength remission spectroscopy alongside OCR measurements to examine the effects of classical bioenergetic inhibitors and uncouplers. Interpret these results to understand how the mycobacterial bioenergetic system responds compared to mitochondria and establish a library of compounds that are effective for studying the impact of other compounds on the oxidative phosphorylation system.

4) Resolve the mechanism of BDQ in living mycobacteria. Find that BDQ acts as a direct inhibitor of ATP synthase, with its activity resembling that of the known ATP synthase inhibitor DCCD. The idiosyncratic increase in OCR stems from an increase in the activity of cytochrome *bd* oxidase on BDQ addition rather than from uncoupling activity.

5) Explore the potential and pitfalls of ^{31}P NMR to measure phosphorylated metabolites in living cells. Construct a system that can be used to mix and supply cultures with oxygen inside an NMR machine without compromising the quality of spectra while conducting initial experiments on unoxygenated cultures.

2. MATERIALS AND METHODS

2.1. GROWTH CONDITIONS

2.1.1. Bacterial strains

All bacterial strains used are listed in table 2.1. *M smegmatis* JR128 was provided by the Luisi laboratory, University of Cambridge. *M smegmatis* mc^{2}155, AtpE^{D32V}, Δ*cydAB,* Δ*qcrCAB* and *M. tuberculosis* mc^{2}6230 and Δ*cydAB* were supplied by the Cook laboratory, University of Otago.

Table 2.1*: Bacterial strains used in experiments with the bioenergetic chamber and NMR studies.*

Species	Strain	Genotype	Reference
M. smegmatis	JR128	mc^{2}4157 with *groELΔC* P_{acet}-*T7 RNA polymerase::L5(Kan)*	Rock et al., 2015
M. smegmatis	mc^{2}155	WT	Snapper et al., 1990
M. smegmatis	AtpE^{D32V}	mc^{2}155 with point mutation in *atpE* (D32V)	Koul et al., 2007
M. smegmatis	Δ*cydAB*	mc^{2}155 with deletion of *cydAB*	Lu et al., 2019
M. smegmatis	Δ*qcrCAB*	mc^{2}155 with deletion of *qcrCAB*	Chong et al., 2020
M. tuberculosis	mc^{2}6206	H37Rv with deletion of *leuD* and *panCD*	Samspon et al., 2004
M. tuberculosis	mc^{2}6230	H37Rv with deletion of *panCD* and the RD1 region	Sambandamurthy et al., 2006

M. tuberculosis	Δ*cydAB*	$mc^2$6230 with deletion of *cydAB*	Berney laboratory, Albert Einstein College of Medicine, strain not published
Bacillus subtilis (*B. subtilis*)	168	In-frame 3 base pair deletion in *trpC* (I110del)	Burkholder and Giles, 1947

2.1.2. Growth conditions for bioenergetic chamber experiments

M. smegmatis strains were grown in Middlebrook 7H9 media (Sigma-Aldrich) supplemented with Tween 80 (0.05% v/v) and glycerol (50 mM), with kanamycin (30 µg/mL) added to starter cultures of JR128 and D-(-)-arabinose (5 mM) added to $AtpE^{D32V}$ cultures. 7H9 media, Tween 80 and glycerol were combined prior to autoclaving with other supplements being filter-sterilised and added afterwards.

7H10 agar plates ($mc^2$155, $AtpE^{D32V}$, Δ*cydAB* and Δ*qcrCAB*) or kanamycin LB agar plates (JR128) were inoculated with -70 °C glycerol stock and incubated at 37 °C for 48-72 hours. Once single colonies were visible, plates were stored at 4 °C and single colonies were used to inoculate 50 mL of media in 250 mL conical flasks to prepare starter cultures. These cultures were incubated (37 °C, 200 rpm) until an OD_{600} of 2.5-5 was reached (ca. 72 hours).

JR128 cultures were grown in 500 mL of media in 1L plastic conical flasks with samples for bioenergetic chamber experiments taken throughout a 7-hour period (OD_{600} = 0.9-2.9). All other *M. smegmatis* strains were grown in 50 mL of media in 250 mL conical flasks, with multiple cultures being inoculated at the same time using different volumes of starter culture to achieve an OD_{600} suitable for bioenergetic chamber experiments (OD_{600} ~ 1-2) at staggered times.

M. tuberculosis strains were grown in Middlebrook 7H9 media (Sigma-Aldrich) supplemented with Tween 80 (0.05% v/v), glycerol (55 mM), Middlebrook OADC

(bovine albumin fraction V (50 mg/mL), D-glucose (20 mg/mL), catalase (0.04 mg/mL), oleic acid (0.5 mg/mL), sodium chloride (8.5 mg/mL)) (10% v/v) and pantothenate (48 µg/mL). Leucine (0.5 mg/mL) was added to $mc^2$6206 cultures. Starter cultures were prepared by inoculating 10 mL of growth media with 10 µL glycerol stock in T25 cell culture flasks. These were incubated without shaking (37 °C) until an OD_{600} > 1 was reached (ca. 14 days).

Cultures for bioenergetic chamber experiments were prepared using 120 mL media in T225 cell culture flasks ($mc^2$6206) or 40 mL media in T75 cell culture flasks ($mc^2$6230 and *cydAB*) and were incubated without shaking (37 °C) until an OD_{600} of 0.7-1.3 was reached (ca. 5-7 days).

2.1.3. NMR chamber growth measurements

B. subtilis 168 spores (2 µL) were added to LB broth (39 mL) in the NMR airlift chamber and a 250 mL conical flask, both of which were then incubated at 37 °C. The conical flask was shaken and the NMR chamber culture was mixed and oxygenated using a flow of filtered compressed air.

M. smegmatis $mc^2$155 was grown in Middlebrook 7H9 media (Sigma-Aldrich) supplemented with Tween 80 (0.05% v/v), antifoam C emulsion (0.05% v/v) and a carbon source (succinate or glycerol, 50 mM). Two conical flasks, each containing 39 mL of media, were inoculated and incubated overnight (37 °C, 200 rpm) until an OD_{600} of 0.4-0.6 was reached. One culture was then transferred to the NMR chamber, incubated in a water bath (37 °C) and a filtered flow of approx. 80% oxygen at a rate of 0.05 LPM was bubbled through. OD_{600} readings were taken roughly every two hours, with fresh media being used to top up the NMR chamber if there was a noticeable drop in volume.

2.2. BIOENERGETIC CHAMBER CONDITIONS

2.2.1. Metabolic inhibitor/ionophore stock preparation

Stock solutions of metabolic inhibitors/ionophores were prepared as outlined in table 2.2. Dilutions were prepared as needed for experiments with the bioenergetic

chamber using the same solvent as the stock solution. All BDQ experiments used the ethanol stock solution except for those that required the addition of 10 µM BDQ to the bioenergetic chamber.

***Table 2.2**: List of inhibitor stock solutions.*

Inhibitor/ionophore/ uncoupler	Supplier	Concentration of stock solution/ mM	Solvent
CCCP	Alfa Aesar	50	Ethanol
FCCP	MedChemExpress (MCE)	50	Ethanol
BAM15	Sigma-Aldrich	2	Ethanol
Rotenone	Santa Cruz Biotechnology	1	Ethanol
Piericidin A	Apexbio	12	Ethanol
TRZ	Sigma-Aldrich	75	Ethanol
TFPZ	Cayman Chemical Company	80	Water
HQNO	Cambridge Bioscience	10	Ethanol
CFZ	Thermo Scientific Chemicals	0.5	Ethanol
CHQAD	Drug Discovery Unit, University of Dundee	10	Ethanol
3NP	Fluorochem	50	Water

Antimycin A	Sigma-Aldrich	2.5	Ethanol
Oligomycin A	Selleck Chemicals	6.3	Ethanol
DCCD	Sigma-Aldrich	100	Ethanol
Nigericin	Cayman Chemical Company	5	Ethanol
Valinomycin	Cayman Chemical Company	10	Ethanol
BDQ	AdooQ Bioscience	0.3	Ethanol
		10	DMSO

2.2.2. Bioenergetic chamber measurements

For *M. smegmatis* experiments, 5 mL of culture were removed and cells from this extract were then pelleted in a centrifuge tube (tabletop swing bucket centrifuge, 4500 rpm, 5 mins, 37 ^{o}C), washed once and resuspended in a buffer solution (20 mM HEPES, 150 mM NaCl or KCl) or growth media excluding Tween 80.

For *M. tuberculosis* experiments, 30 mL (mc^{2}6206) or 35 mL (mc^{2}6230 and Δ*cydAB*) of culture were removed and cells from this extract were then pelleted in a centrifuge tube (tabletop swing bucket centrifuge, 4500 rpm, 5 mins, 37 ^{o}C), washed once and resuspended in 5 mL of media excluding Tween 80 and Middlebrook OADC.

These cell suspensions were transferred to the bioenergetic chamber: a quartz crucible contained in an aluminium block with a stainless-steel lid and glass stirrer bar (Ripple, Kim and Springett 2013). The temperature in the chamber was maintained at 37 ^{o}C. For all experiments unless specified, the oxygen concentration was kept at 100 µM/min. Oxygen was delivered via a flow of oxygen/nitrogen gas through platinum-cured silicon tubing, with the mixture being adjusted using oxygen concentration

measurements made via the fluorescence lifetime of a phosphorescent membrane fitted to the inside of the chamber. The OCR of cell suspensions was determined by comparing the rate of oxygen delivery through the silicon tubing with the measured oxygen concentration inside the chamber. The tubing was replaced after each experiment.

Cytochrome attenuation spectra were recorded as outlined by Rocha and Springett (Rocha and Springett, 2019). In experiments that used fitting, cytochrome spectra were fitted to model spectra obtained from cytochromes in mitochondria. Where cells were suspended in buffer solution, glycerol (10 µL, 70 %) was added shortly after the start of data collection. Small volumes (2-50 µL) of metabolic inhibitors/ionophores were added to achieve the total concentration specified for each experiment.

2.3. NMR EXPERIMENTS

2.3.1. Sample preparation

To determine the reference power required for a 90^{o} radiofrequency pulse, a 0.2 M solution of P_i was prepared by dissolving NaH_2PO_4 (780 mg, 5 mmol) in deionised water (25 mL).

For the wide-bore NMR spectrum of *M. smegmatis*, the sample was prepared by Rowan Walters. Briefly, *M. smegmatis* JR128 was grown using the same conditions as for bioenergetic chamber experiments. Once cells reached mid-exponential phase they were spun down (tabletop swing bucket centrifuge, 4500 rpm, 5 mins, 37 ^{o}C), and resuspended in Tris-SO_4 buffer solution (25 mM, pH 7.2) at approximately 10x their original concentration. A 25 mL sample was transferred to a 50 mL conical tube and this was used for NMR experiments.

Standard solutions of ATP, ADP, AMP and P_i were prepared in a buffer solution comprised of Bis-Tris methane (25 mM), MOPS (25 mM) and Tris-Cl (25 mM) as outlined in table 2.3. Each solution was brought to the correct pH via additions of hydrochloric acid or sodium hydroxide solution. A 540 µL sample of each solution was taken and 60 µL D_2O was added to enable signal lock. In experiments with magnesium

chloride, a 962 mM stock solution was prepared using deionised water (458 mg, 4.81 mmol, 5 mL) and 26 µL of this was added to the samples prepared as stated above.

Table 2.3: *ATP, ADP, AMP and NaH_2PO_4 solutions prepared for high-resolution NMR experiments.*

Compound	Mass (mg)	Moles (mmol)	Volume (cm^3)	Concentration (mM)	pH
ATP disodium salt	275.7	0.5	25	20	6.7
	275.7	0.5	25	20	7.7
	275.7	0.5	25	20	8.7
ADP sodium salt	213.6	0.5	25	20	6.7
	213.6	0.5	25	20	7.7
	213.6	0.5	25	20	8.7
AMP disodium salt	195.7	0.5	25	20	6.7
	195.7	0.5	25	20	7.7
	195.7	0.5	25	20	8.7
$NaH_2PO_4 \cdot 2H_2O$	78.0	0.5	25	20	6.2
	78.0	0.5	25	20	7.2
	78.0	0.5	25	20	8.2

For the high-resolution spectrum of *M. smegmatis*, *M. smegmatis* mc^2155 cells were grown as using the same conditions as for bioenergetic chamber experiments. Once cells reached mid-exponential phase (OD_{600} = 2.3), they were pelleted (tabletop swing bucket centrifuge, 4500 rpm, 5 mins, 37 ^oC). 540 µL of cells were removed and resuspended in 300 µL of supernatant and 60 µL D_2O.

2.3.2. Wide-bore NMR experiments

NMR spectra were recorded on a Bruker 400 MHz UltraShield^{TM} wide-bore spectrometer with a pre-installed micro-imaging gradient system (Bruker, Micro2., 1.5 T/m) operated using Paravision 6.0.1 (Bruker) (162 MHz for ^{31}P). Chemical shifts are reported in units of parts per million (ppm) relative to 85% orthophosphoric acid.

To determine the reference power, spectra were recorded using a single-pulse sequence (averages = 1, acquisition time = 102.4 ms, spectral width = 123.5 ppm, 2048 points) with the reference power being varied from 5 to 40 W in increments of 2.5 W. The integrals of the resulting signals were then plotted against the power using MATLAB code written by Dr Aneurin Kennerly (supervisor).

^{31}P NMR spectra of *M. smegmatis* were recorded using single-pulse sequences (reference power = 15 W, acquisition time = 102.4 ms, spectral width = 123.5 ppm, 2048 points) with some parameters being varied as outlined in table 2.4. Spectra were processed in Bruker TopSpin 3.6.1 using a line broadening factor of 3 Hz.

***Table 2.4**: NMR Parameters used in wide-bore NMR experiments performed on M. smegmatis cells.*

Experiment number	Repetition time (TR) (ms)	Averages ()	Flip angle (°)
1	1000	2000	90
2	800	2000	90
3	600	2000	90
4	400	2000	90
5	200	2000	90
6	600	1000	90
7	200	4000	90
8	200	4000	60
9	200	4000	30

2.3.3. High-resolution NMR experiments

NMR spectra were recorded on a Bruker 400 MHz UltraShield™ wide-bore spectrometer operated using Bruker TopSpin 3.6.1 (162 MHz for ^{31}P). Chemical shifts are reported in units of parts per million (ppm) relative to 85% orthophosphoric acid. All spectra were recorded using a single-pulse sequence (averages = 4096, TR = 2.5 s, acquisition time = 511.2 ms, flip angle = 30°, spectral width = 395.7 ppm, 32768 points). Spectra were processed in Bruker TopSpin 3.6.1 using a line broadening factor of 3 Hz and were then exported to Microsoft Excel.

3. VISIBLE WAVELENGTH REMISSION SPECTROSCOPY

3.1. INTRODUCTION

3.1.1. Cytochrome spectroscopy

SDH2, the supercomplex and cytochrome *bd* oxidase in mycobacteria contain prosthetic haem groups, porphyrin rings complexed to central Fe atoms (figure 3.1), which are involved in electron transport (Safarian et al., 2016; Iqbal et al., 2018; Gong et al., 2020). When a haem group is contained in a protein complex, these complexes are dubbed cytochromes.

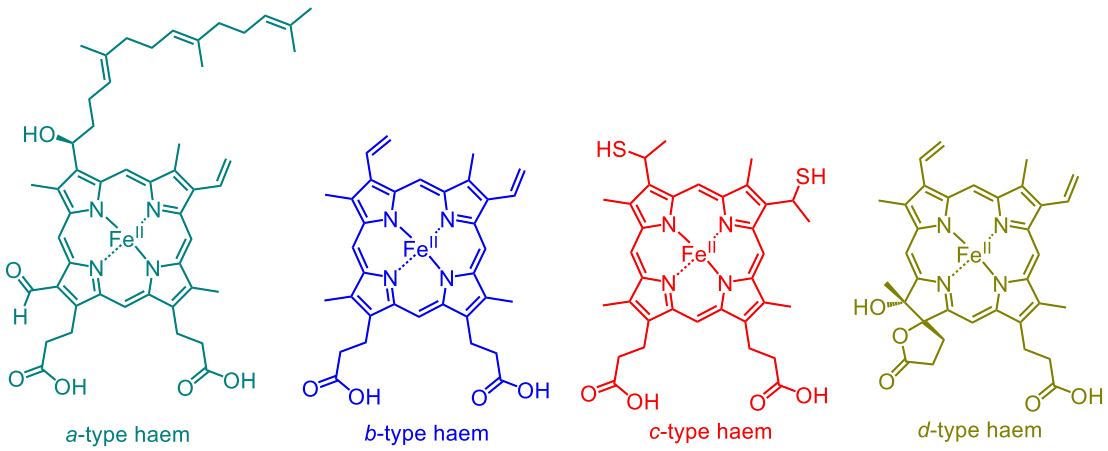

Figure 3.1*: Types of haems found in mycobacterial ETCs. In this diagram iron is shown in the +2 ferrous oxidation state but will oxidise to the +3 ferric oxidation state upon electron transfer.*

Both complex III in mitochondria and MK-cytochrome *c* oxidoreductase *bcc* in mycobacteria contain two *b*-type haems (b_L and b_H) (Nicholls and Ferguson, 2002; Iqbal et al., 2018). MK-cytochrome *c* oxidoreductase *bcc* also has two *c*-type haems (c_1 and *c*) while complex III in mitochondria has one *c*-type haem (c_1), with a second being contained in cytochrome *c*. Complex IV in mitochondria and cytochrome *c* oxidase aa_3 in mycobacteria contain two *a*-type haems. No further cytochromes exist in the mitochondrial ETC, while in mycobacteria SDH2 contains two *b*-type haems and

cytochrome *bd* oxidase contains two further *b*-type haems and a *d*-type haem (Safarian et al., 2016; Gong et al., 2020).

These cytochromes have absorbances in the UV-vis region and thus can be studied using UV-vis spectroscopy. The type of haem group present and its environment influence cytochrome absorption spectra, allowing for the identification of different cytochromes through this method. By recording spectra at multiple wavelengths and using deconvolution techniques, spectra recorded on mixtures of cytochromes can be resolved and individual components identified (Berry and Trumpower, 1987).

This technique can be applied to isolated proteins or whole cells using specialised equipment described below, enabling cytochrome concentrations to be measured (Serebrennikova, Huffman and Garcia-Rubio, 2015). Additionally, the absorption spectrum of a cytochrome depends on the oxidation state of the Fe centre (Stokes, 1864). As a result, multi-wavelength spectroscopy can be used to monitor changes in the oxidation state of cytochromes in the ETC (figure 3.2). These measurements provide a valuable insight into the state of the ETC and its response to the presence of various inhibitors/conditions.

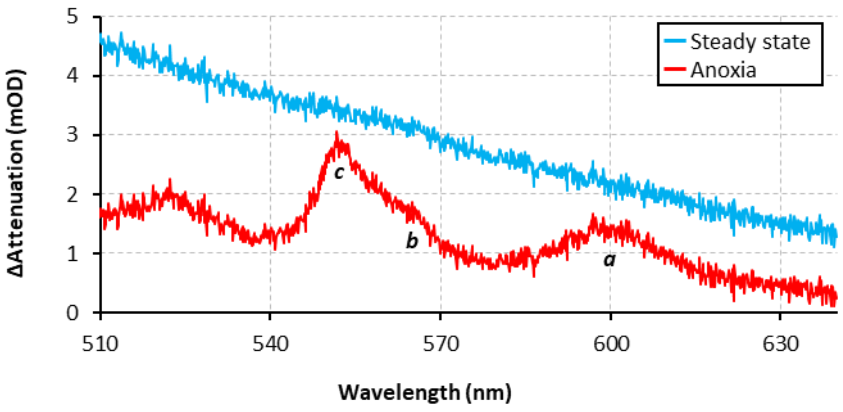

***Figure 3.2**: Remission spectra of M. smegmatis mc²155 cells recorded under steady state and anoxic conditions, with changes in attenuation (Δattenuation) being measured relative to an initial spectrum recorded on cells to reduce the impact of baseline attenuation on the spectra. Under anoxic conditions the cytochromes are*

more reduced and cytochrome peaks become visible in the spectrum, with the peaks at 600 nm, 563.5 nm and 552 nm corresponding to a, b and c cytochromes respectively.

3.1.2. The bioenergetic chamber

The bioenergetic chamber (figure 3.3) is a device that allows simultaneous monitoring of cytochrome oxidation states and oxygen consumption in live cells (Rocha and Springett, 2019). It consists of a 5 mL quartz crucible surrounded by a metal heating block into which liquid cultures can be loaded. A phosphorescent membrane with a fluorescence lifetime dependent on oxygen concentration is fitted inside the chamber and acts as an oxygen sensor. Oxygen-permeable platinum-cured silicon tubing is used to supply cultures with oxygen and the OCR of cells can be determined using the rate of oxygen delivery along with measurements of oxygen concentration in the chamber.

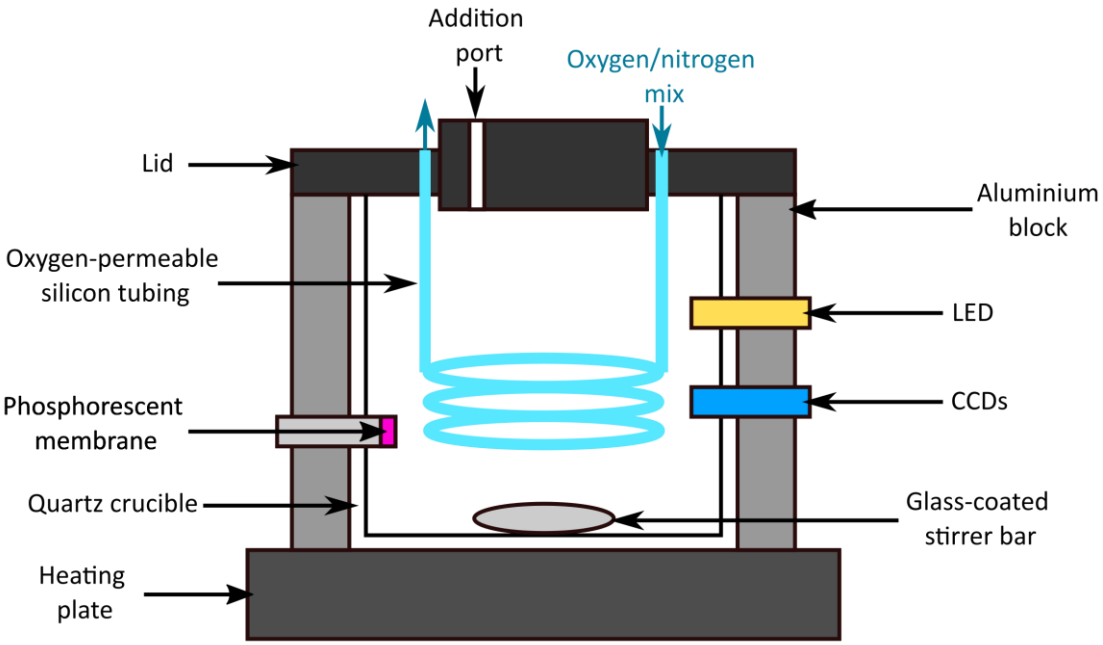

***Figure 3.3**: Basic diagram showing the structure of the bioenergetic chamber, featuring an LED light source, with spectra being recorded by the CCDs (Rocha and Springett, 2019).*

This method of measuring oxygen concentration has several advantages over the conventional Clark electrode (Ripple, Abajian and Springett, 2010). In a Clark electrode, oxygen diffuses across a semi-permeable membrane and is reduced at a

platinum electrode, while silver is oxidised at a silver/silver chloride reference electrode (Nicholls and Ferguson, 2002). The resulting current is directly proportional to the oxygen concentration in solution. Due to the need for oxygen to diffuse across the membrane, a Clark electrode has a higher threshold for oxygen detection than a phosphorescent membrane suspended directly in solution (Melnikov et al., 2022). This also results in the Clark electrode having a slower response time to changes in oxygen concentration. Furthermore, replacement of a phosphorescent membrane upon signs of degradation is less demanding than maintenance of a Clark electrode.

In addition to providing information on the OCR, the device contains CCDs that record spectra of back-scattered light from the culture in the visible light region (Rocha and Springett, 2019). These spectra enable detection of changes in the oxidation state of the cytochromes. Fitting the spectra to those obtained from isolated proteins produces traces which show changes in the oxidation state of individual cytochromes in response to metabolic inhibitors/uncouplers or changes in conditions.

The use of remission spectroscopy (back-scattered light) versus transmission spectroscopy (light passing through a solution) allows spectra to be collected from turbid cultures which are unsuitable for the latter (Rocha and Springett, 2019). The ability to collect spectra independent of cell density enables more control over the OCR of samples, ensuring the OCR is high enough that detected changes are not subject to a high margin of error.

However, use of this method does not give absolute spectra, with the amount of back-scatter being affected by factors such as cell-morphology. Instead, spectra can be accessed qualitatively to determine whether cytochrome groups have oxidised or reduced. Alternatively, if fully reduced and fully oxidised spectra are able to be collected over the course of an experiment (and the experimentalist is reasonably sure that this is the case), these can be set as reference points and the ratio of oxidised versus reduced cytochromes can be determined and plotted (Ripple, Kim and Springett, 2013).

Early data was collected using model spectra of the b_H, b_L and c_1 cytochromes from mitochondrial complex III, mitochondrial cytochrome *c* and a_{605} from mitochondrial

complex IV with the expectation they would correlate with absorbances from the mycobacterial supercomplex. Later, this approach was found to be unsuitable and instead raw difference spectra were used.

3.1.3. Aims for this chapter

The aim of this chapter is to develop a protocol for running experiments on mycobacteria in the bioenergetic chamber and apply this to understanding BDQ's mechanism. This can be broken down into the following objectives:

I. Develop a method for preparing and using *M. smegmatis* samples in the bioenergetic chamber.
II. Investigate the impact of various metabolic inhibitors and uncouplers/ionophores on *M. smegmatis* to establish a metabolic toolkit that can be used for studying the ETC in mycobacteria.
III. Use findings from objective I to develop a protocol for running experiments on BSL-2 compatible *M. tuberculosis* strains in the bioenergetic chamber.
IV. Determine the most effective means for analysing and interpreting data obtained using the bioenergetic chamber.
V. Apply the results of objectives I-IV to elucidate the mode of action of BDQ in *M. smegmatis* and *M. tuberculosis*.

3.2. OPTIMISATION OF COLLECTING DATA FROM MYCOBACTERIA IN THE BIOENERGETIC CHAMBER

3.2.1. Developing a protocol for running experiments on *M. smegmatis* in the bioenergetic chamber

Prior to this work, the bioenergetic chamber had only been used to examine the ETC in mitochondria. As a result, a method for working with mycobacteria in the chamber had to be developed before starting any work with BDQ. Interest in uncovering BDQ's mechanism stems from its role in treating TB, however due to *M. tuberculosis* being slow growing, difficult to culture and requiring stricter safety protocols, initial experiments were done in the rapidly growing mycobacterium *M. smegmatis*. It was in screenings performed with *M. smegmatis* that DARQs were first identified as

potential anti-TB compounds (Andries et al., 2005), validating it as a model organism for studying BDQ's mechanism and performing these preliminary experiments. A kanamycin-resistant strain of *M. smegmatis* (JR128) (Rock et al., 2015) was used in initial experiments as this allowed use of growth media containing kanamycin in starter cultures, therefore reducing the risk of culture contamination.

The data presented here is not fitted to mycobacterial spectra due to a lack of available reference spectra and is therefore not a perfect insight into the state of the mycobacterial ETC. Despite this, changes in cytochrome oxidation state due to anoxia/inhibitors were observed, showing the mitochondrial model used serves to make these initial measurements.

Figure 3.4 shows one of the first sets of data recorded on a culture of *M. smegmatis* using the chamber, collected by Rowan Walters (PhD student). The top graph shows the set and actual oxygen concentration in chamber, while the second shows the measured OCR. The bottom three graphs all provide information on the oxidation state of the cytochromes. As the cytochromes were not fully reduced and then oxidised over the course of the experiment, exact oxidised/reduced ratios cannot be calculated. Instead, the changes in oxidation of the cytochromes are measured in AU, with a decrease being representative of reduction and an increase indicating oxidation.

In this run, no inhibitors were added but the oxygen concentration in the chamber was set to zero for a short period. As the oxygen concentration falls to zero, all of the cytochromes, except for a_{605}, reduce as oxygen is no longer present to act as a terminal acceptor and so there is a build-up of charge on the ETC. Once oxygen is reintroduced, oxidation of the cytochromes can be observed.

Of note, is that even when the oxygen concentration in the chamber is set to 100 µM prior to anoxia, it can be seen to decrease. This indicates the length of silicon tubing used did not allow for sufficient oxygen diffusion. The length was increased from 80 mm to 130 mm, which allowed the oxygen concentration in later experiments to reach and remain fixed at 100 µM.

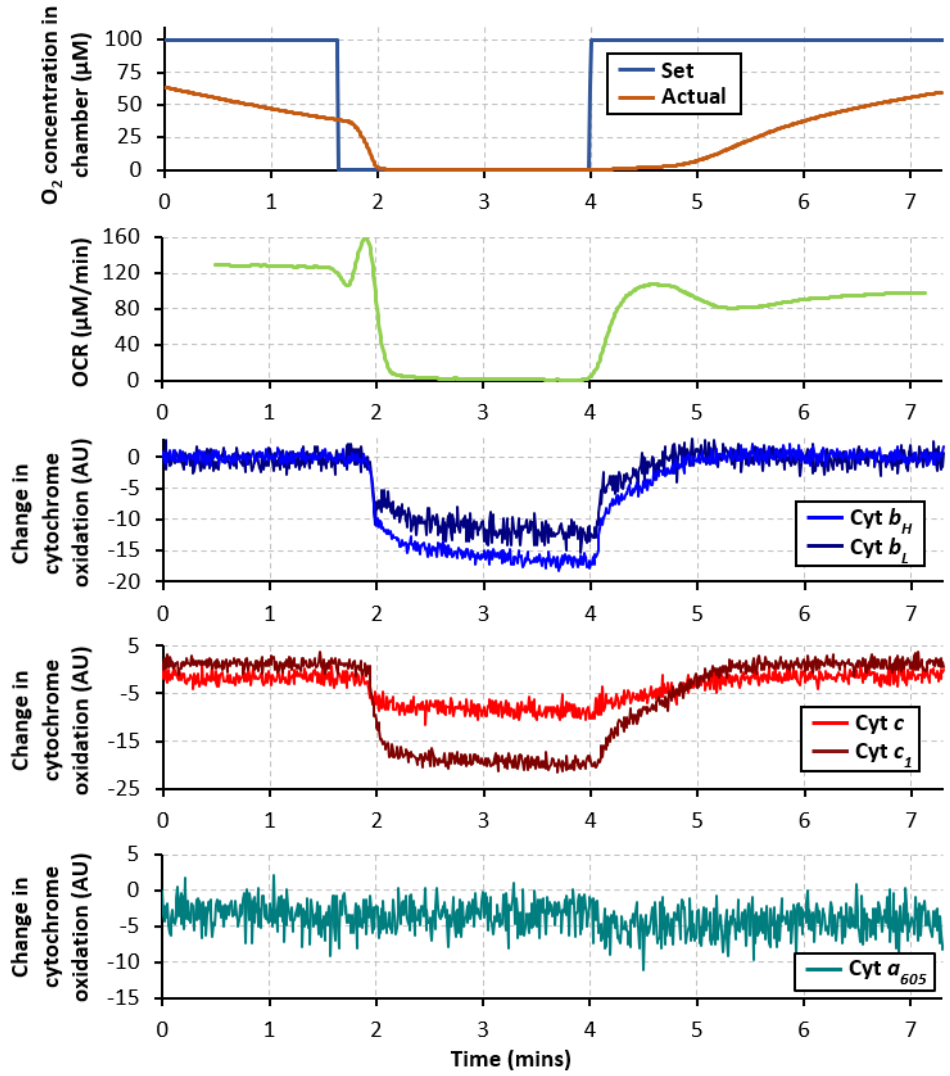

***Figure 3.4**: An example of data output from the bioenergetic chamber showing the oxygen concentration in the chamber along with changes in OCR and cytochrome oxidation states in M. smegmatis JR128 cells on taking the chamber to anoxia and then reintroducing oxygen. Cells were grown in 7H9 media with Tween 80 (0.05% v/v) and succinate (50 mM)and a sample was taken directly from culture. Data collection was performed by Rowan Walters (PhD student). Haem model: mammalian.*

Carbonyl cyanide *m*-chlorophenyl hydrazine (CCCP) was selected as the first inhibitor to use in experiments with the bioenergetic chamber, given that it has been shown to act in mycobacteria and should have a noticeable effect on cytochrome oxidation states (Jeon et al., 2019). Furthermore, the action of uncouplers should result in an

increase in cells' OCR as they try to re-establish the PMF. To find the concentration of CCCP needed in order for its effects to be observed using the device, an initial titration experiment was performed (figure 3.5).

Prior to the addition of CCCP, the oxygen concentration is increased to and held at 150 µM for a short period before being returned to 100 µM and then lowered to 0 µM for a period. This is referred to as a top-hat and allows calibration of the oxygen measurements, as well as demonstrating that cells are respiring.

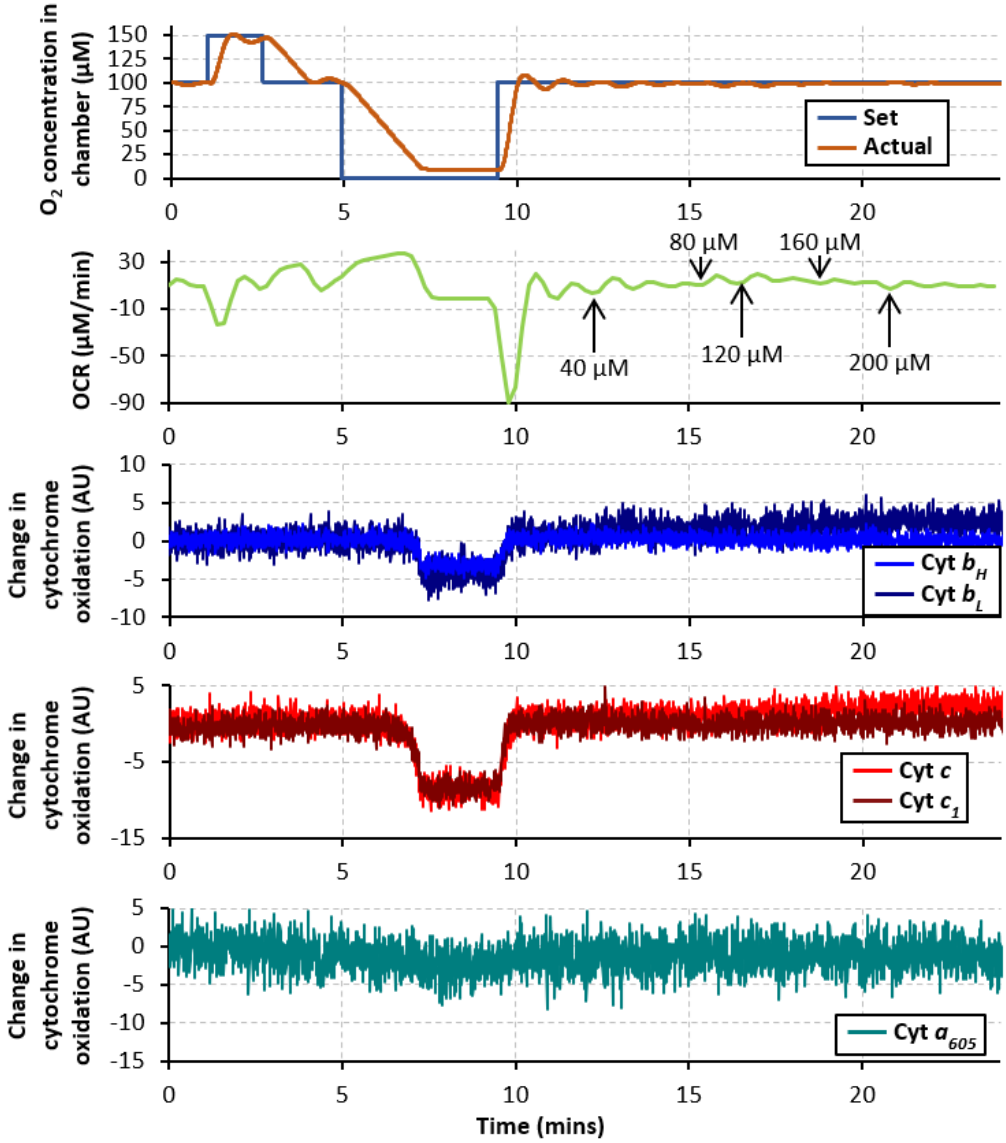

Figure 3.5: *Changes in OCR and cytochrome oxidation states in M. smegmatis JR128 cells in response to treatment with CCCP. Cells were grown in 7H9 media with Tween 80 (0.05% v/v) and succinate (50 mM) and a sample was taken directly from culture*

once an OD_{600} of 0.6 was reached. Arrows on the second panel indicate the time of CCCP additions, with the concentration given being the total concentration of CCCP in the chamber following addition. Data collection was performed collaboratively with Rowan Walters (PhD student). Haem model: mammalian.

Following the return of the oxygen concentration inside the chamber to 100 µM, 2 µL of 100 mM CCCP is added, resulting in a total concentration in the chamber of 40 µM. As the MIC of CCCP in *M. tuberculosis* was found to be 20 µM (Jeon et al., 2019), it was anticipated that an impact on cytochromes and OCR would be observed and this could be treated as a maximum in future titration experiments. However, while there is potentially a slight oxidation in the b_H cytochrome population, no other effects are observed. Even at a CCCP concentration of 120 µM where oxidation of b_H is more apparent and there appears to be slight oxidation of *c*, there is no obvious change in the OCR.

Cells in this experiment were taken directly from culture that contained the detergent Tween 80. Detergents are used when growing mycobacteria to prevent cells from clumping together, as this results in an uneven suspension and could lead to different cells receiving different levels of oxygenation. It is possible some CCCP may be dissolving in the hydrophobic phase created by the detergent, reducing the amount of CCCP reaching cells, as this would explain why such high concentrations are needed to see significant effects under these conditions. Following this experiment, the carbon source used was changed to glycerol, as prior work by Rowan Walters (PhD student) demonstrated glycerol-grown *M. smegmatis* cells contained the lowest amounts of cytochrome *bd* oxidase compared with *M. smegmatis* cells grown on other carbon sources (data not published). This is because there were concerns over cytochrome signals from cytochrome *bd* oxidase overlapping with those from the supercomplex, complicating interpretation of the data.

To test this hypothesis, experiments were conducted with cells grown using different concentrations of Tween 80, with the expectation that using a lower concentration of the detergent would result in CCCP demonstrating stronger effects on cells at lower concentrations. Additionally, in case small changes in OCR were being masked by the

chamber adjusting the oxygen concentration in the tubing in order to maintain the set concentration in the chamber, these experiments were run without running oxygen through the tubing. This was achieved by flowing 100% oxygen through the tubing prior to the experiment and allowing the oxygen concentration in the chamber to equilibrate before setting the oxygen flow to 0% and titrating in CCCP.

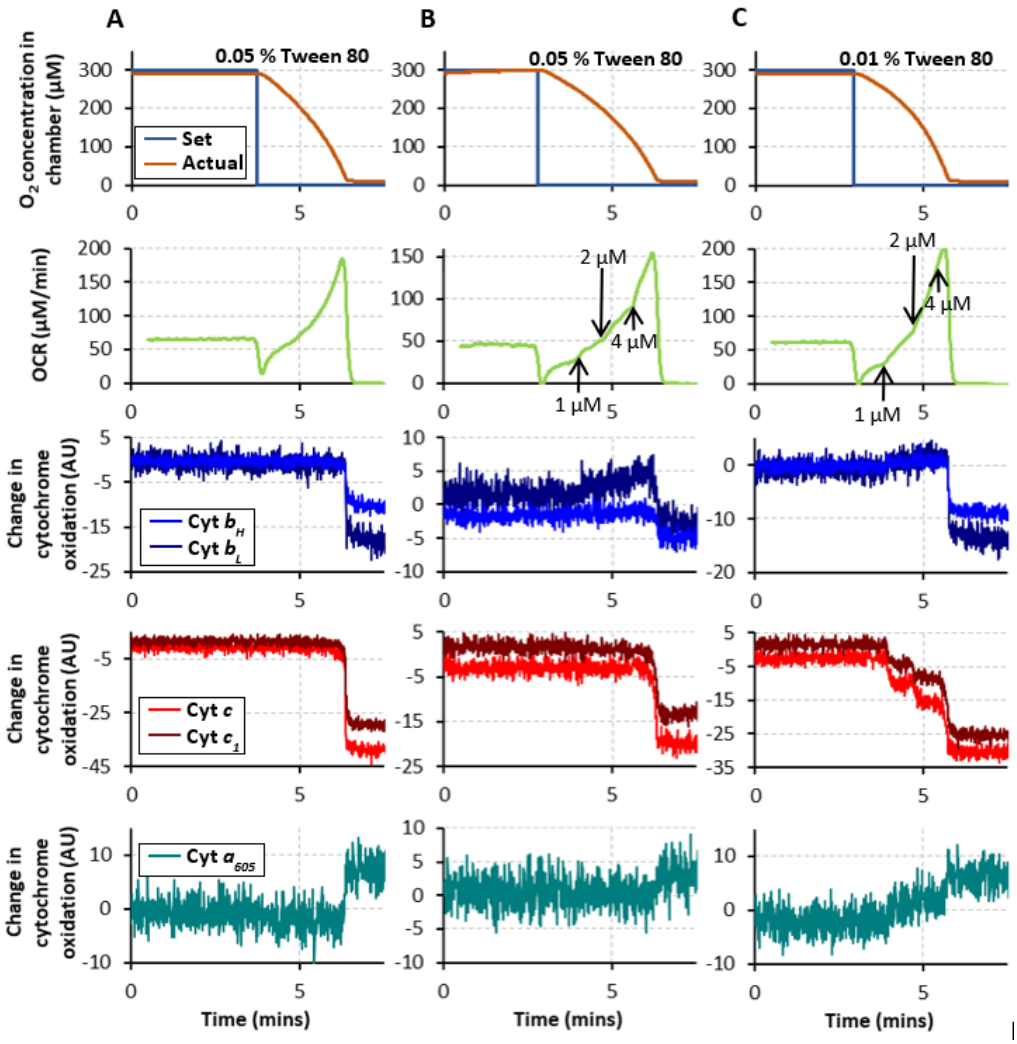

Figure 3.6: *Changes in OCR and cytochrome oxidation states in M. smegmatis JR128 cells grown in 7H9 media containing (**A** and **B**) 0.05% Tween 80 or (**C**) 0.01% Tween. Cells were grown using glycerol (50 mM) as a carbon source and a sample was taken directly from culture once an* OD_{600} *of (**A**) 2.2 (**B**) 0.7 or (**C**) 1.6 was reached. (**B** and **C**) Arrows indicate the time of CCCP additions, with the concentration given being the total concentration of CCCP in the chamber following each addition. Data collection*

was performed collaboratively with Rowan Walters (PhD student). Haem model: mammalian.

Changes in the oxidation states of all cytochromes are observed with 1 µM CCCP in cells taken from cultures containing 0.01% v/v Tween 80 (figure 3.6), while in the culture containing 0.05% v/v Tween 80, only a small change in the oxidation level of the b_L cytochrome is seen. In both cases, as well as a control in which no CCCP was added, the OCR of cells increases as they near anoxia. This may be a response of the cells to a decrease in oxygen concentration, however it could also be an artifact generated from how the OCR rate is determined when no oxygen is flowing through the tubing. Due to this, it is difficult to interpret the impact of CCCP on OCR under these conditions.

As a decrease in the amount of detergent in the sample increased the sensitivity of the cells to CCCP, this indicates that the presence of a detergent does affect cellular uptake of CCCP. Therefore, to acquire the best quality data, later experiments were done on washed cells, rather than those taken directly from a culture containing a detergent.

The method of running the chamber without flowing oxygen through the tubing is not effective for measuring changes in OCR and a limited number of additions are possible before the chamber becomes anoxic. Another experiment was performed, this time using the oxygen delivery system to maintain the oxygen concentration in the chamber at 100 µM (figure 3.7). Cells were washed and resuspended in a HEPES buffer solution, with the hope that removal of any detergent may allow for changes in OCR on addition of CCCP to be observed.

When washed cells are added to the chamber, their OCR is relatively low as a result of the majority of the carbon source being removed during the wash. 10 µL of 70% glycerol are added prior to calibration of the oxygen delivery system to ensure there is sufficient carbon source. From the end of the top-hat, the level of oxidation of all cytochromes except for a_{605} appears to gradually decrease, while for a_{605} a gradual increase in oxidation is observed. As this trend does not change with the additions of CCCP up to a total CCCP concentration of 800 nM (at which point a slight reduction in

cyt *c* can be seen corresponding with a CCCP addition), it can be concluded that this overall trend is not due to the presence of CCCP and is likely due to some sort of spectral artefact that may be unrelated to the cytochromes.

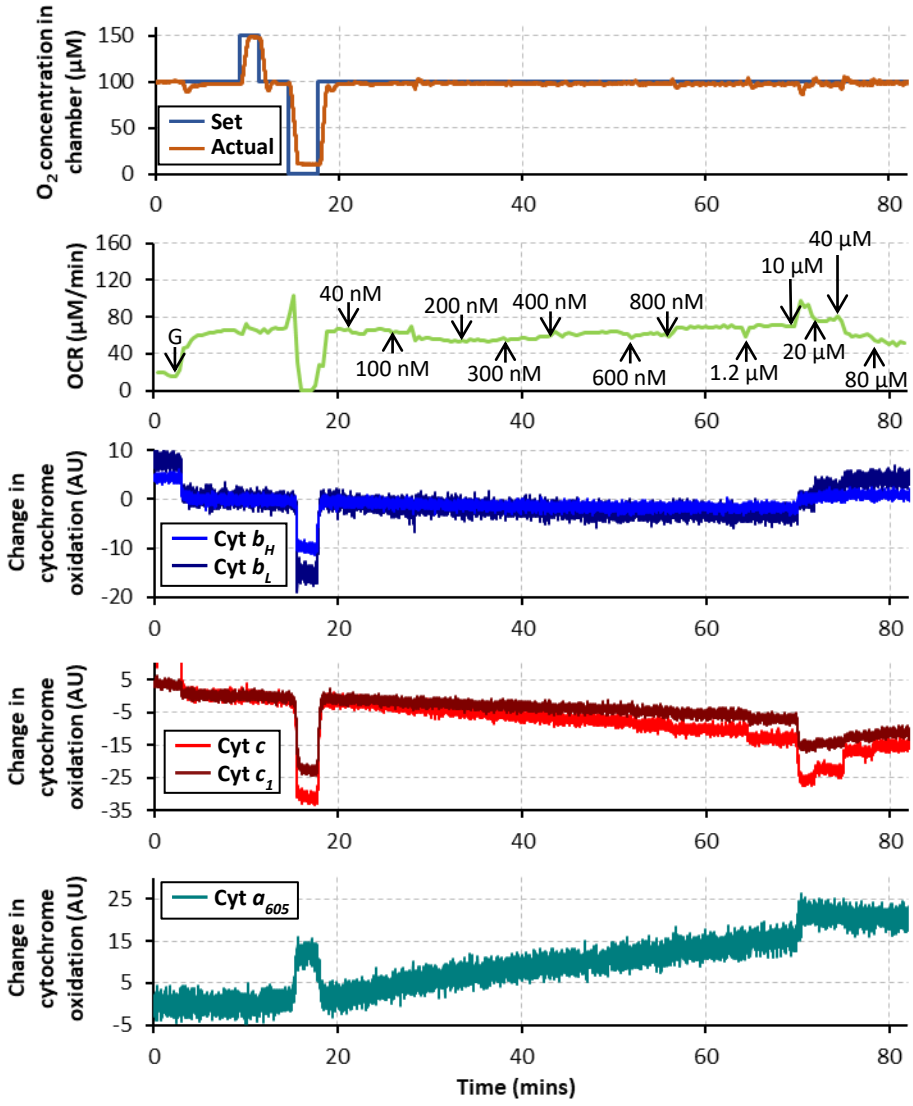

Figure 3.7: *Changes in OCR and cytochrome oxidation states in M. smegmatis JR128 cells on addition of increasing concentrations of CCCP. Cells were grown in 7H9 media with Tween 80 (0.05% v/v) and glycerol (50 mM), once an OD_{600} of 2.3 was reached, a 5 mL sample was taken, washed once and resuspended in HEPES buffer solution (20 mM HEPES, 150 mM sodium chloride, pH = 7.4). Arrows indicate the time of additions, with G representing the addition of 10 µL 70% glycerol (final concentration 19 mM) and the subsequent concentration values being the total concentration of CCCP in the*

chamber following each addition. Data collection was performed collaboratively with Rowan Walters (PhD student). Haem model: mammalian.

At a 1.2 µM concentration of CCCP, there is another slight reduction in cyt *c* and cyt c_1 but it is only at 10 µM CCCP that an impact on all of the cytochromes is observed. There is a small increase in OCR on addition of 800 nM CCCP, with a further increase occurring when the CCCP concentration is raised to 10 µM. At ≥20 µM CCCP, oxidation of *c* and c_1 is observed and the OCR decreases with each addition of CCCP. This may be a sign that at this concentration and under these conditions, CCCP affects cell viability in *M. smegmatis*.

These results demonstrate the importance of removing the detergent from samples before transferring them to the bioenergetic chamber. Having established a method for exploring the effects of specific compounds on mycobacteria using the bioenergetic chamber, experiments with other metabolic inhibitors/uncouplers were conducted (see section 3.2.2) and further revisions were made to this protocol, based on the results obtained.

Experiments with nigericin and valinomycin, which act as a proton/potassium ion exchanger and a potassium ion transporter respectively, prompted consideration of the salt included in the buffer (figure 3.8). In initial experiments, 150 mM sodium chloride was added to ensure the salinity was appropriate so no or very few potassium ions would have been present outside cells. Under these conditions an increase in OCR and reduction of the *b* cytochromes is observed with valinomycin, while nigericin appears to have no effect up to 20 µM despite having activity against *M. tuberculosis* with a minimum bactericidal concentration 90% (MBC_{90}) value of 1.25 µM (Rao et al., 2008). Swapping sodium chloride for potassium chloride did not have a significant impact on the effects seen with nigericin but did result in a notable increase in OCR in the control compared to the sodium chloride buffer (table 3.1). The reason for this increase is unclear but did bring into question the importance of the ion composition of the buffer. Additionally, there was some concern that removing the carbon source and then reintroducing it after the washing process may impact cells' metabolism, so

in future experiments the carbon source was added to the wash media at the same concentration as in cells' growth media.

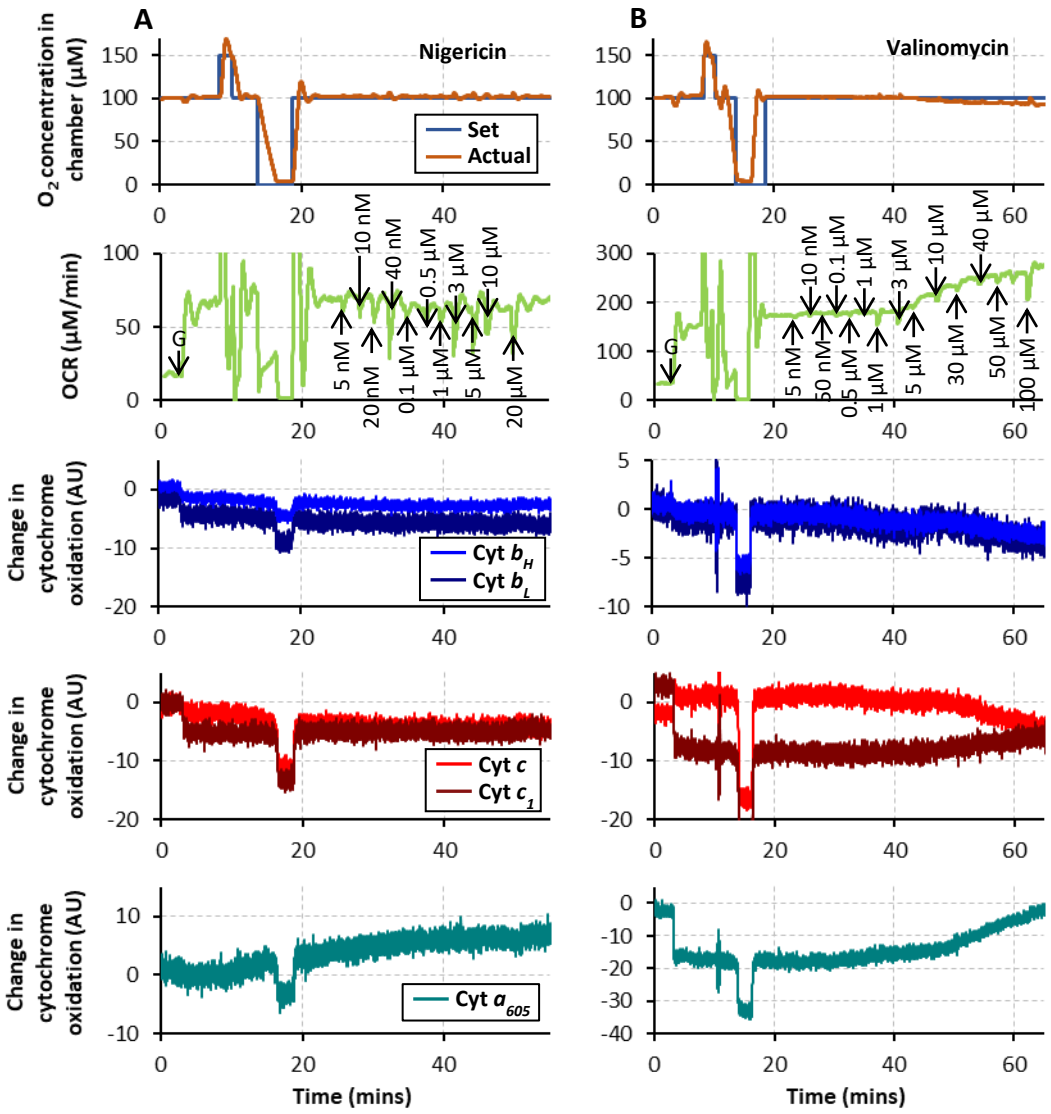

Figure 3.8: *Changes in OCR and cytochrome oxidation states in M. smegmatis JR128 cells on addition of increasing concentrations of (**A**) nigericin or (**B**) valinomycin. Cells were grown in 7H9 media with Tween 80 (0.05% v/v) and glycerol (50 mM), once an OD_{600} of (**A**) 0.9 (**B**) 1.7 was reached, a 5 mL sample was taken, washed once and resuspended in HEPES buffer solution (20 mM HEPES, 150 mM sodium chloride, pH = 7.4). Arrows indicate the time of additions, with G representing the addition of 10 µL 70% glycerol (final concentration 19 mM) and the subsequent concentration values being the total concentration of (**A**) nigericin or (**B**) valinomycin in the chamber following each addition. Haem model: mammalian.*

***Table 3.1**: Changes in the OCR of M. smegmatis JR128 measured in the bioenergetic chamber on the addition of 1) nothing, 2) 1 µM valinomycin, 3) 1 µM nigericin in 20 mM HEPES buffer (pH = 7.4) containing 150 mM sodium chloride or 150 mM potassium chloride.*

Salt in Buffer	Ionophore	Change in OCR 20 mins post addition (µM min^{-1})	Percentage change (%)
Sodium chloride	None	1	2
	Valinomycin	8	11
	Nigericin	0	0
Potassium chloride	None	8	10
	Valinomycin	10	13
	Nigericin	9	12

In an effort to place as little stress on the cells as possible prior to any drug additions, the decision was made to try resuspending them in 7H9 media, without Tween 80. The HEPES-containing resuspension buffers used prior to these tests had a pH of 7.4 while 7H9 growth media has a pH of 6.6±0.2. To check whether changes observed in the bacteria were due to a change in ion composition of the resuspension buffer or a change in pH, experiments were first run using 7H9 media with a pH of 7.4. There were concerns that the ferric ammonium citrate and copper sulfate in 7H9 may result in production of reactive oxygen species via Fenton chemistry with prolonged exposure to the bioenergetic chamber's LED. To test this, experiments looking at the change in cells' OCR over time were conducted in 7H9 with and without the inclusion of these two compounds (figure 3.9). These experiments were performed using a WT strain of *M. smegmatis* (mc^2155), to ensure the kanamycin-resistance mechanism of the JR128 strain did not impact the results.

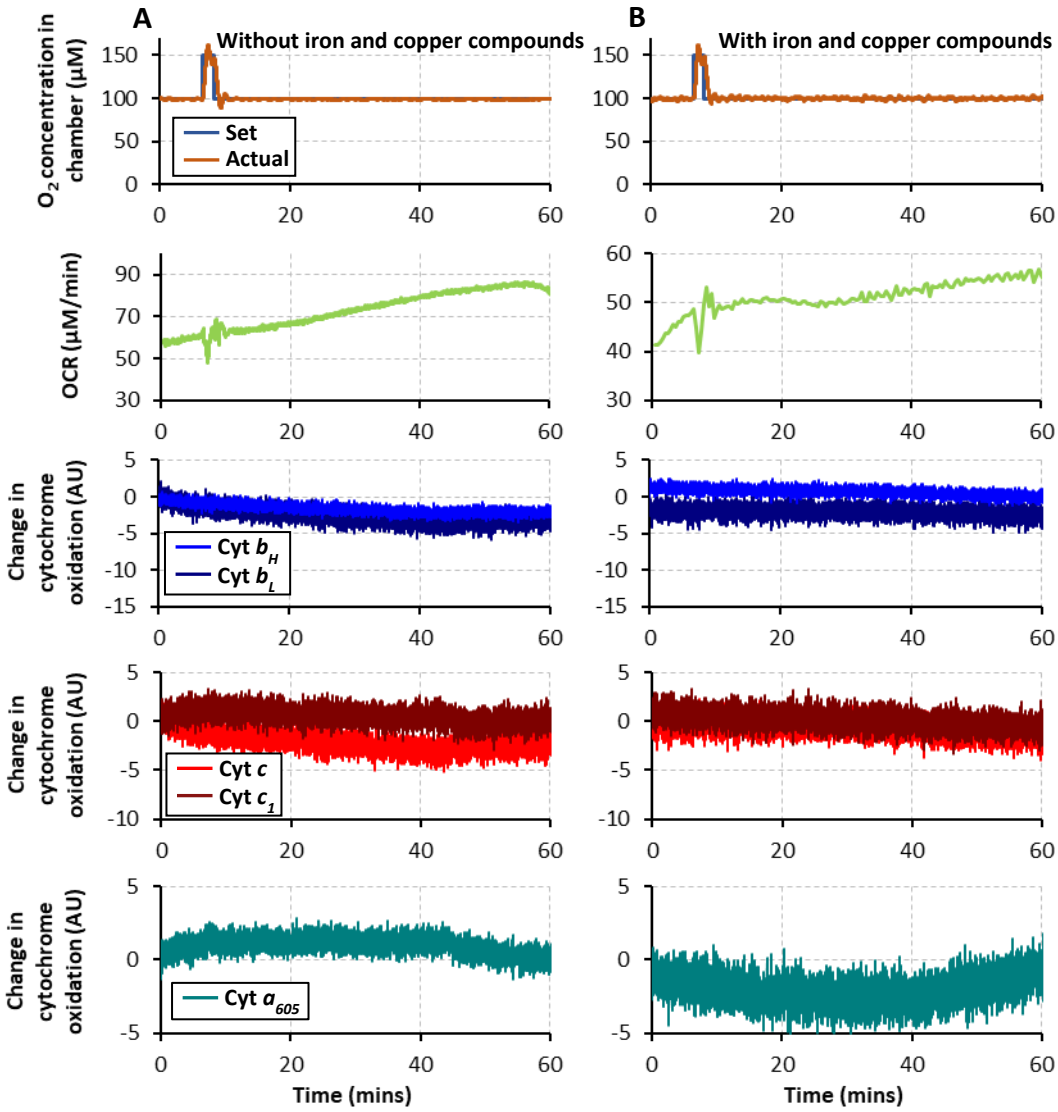

Figure 3.9: *Changes in OCR and cytochrome oxidation states in M. smegmatis mc²155 cells washed and resuspended in (**A**) 7H9 without ferric ammonium citrate and copper sulfate supplemented with 50 mM glycerol (pH = 7.4) or (**B**) 7H9 supplemented with 50 mM glycerol (pH = 7.4). Cells were grown in 7H9 media with Tween 80 (0.05% v/v) and glycerol (50 mM) and samples were taken once an OD_{600} of (**A**) 1.4 or (**B**) 1.3 was reached. Haem model: mammalian.*

Inclusion of ferric ammonium citrate and copper sulfate leads to a more stable OCR, with a 6% increase over a 20-minute period following calibration of the oxygen system, compared with a 25% increase in the absence of these compounds. There are two possible explanations for this, the first being that the greater increase in OCR without ferric ammonium citrate and copper sulfate is due to cell growth over the

course of the experiment which would indicate the compounds do have a negative impact on cells under the conditions present in the bioenergetic chamber. Alternatively, the lack of these compounds may place more stress upon cells, with the increase in oxygen consumption being a response to this.

Of these two explanations, the latter is more likely as *M. smegmatis* has a doubling time of 3-4 hours and so cell growth alone is not sufficient to account for a 25% increase in OCR over a 20-minute period. Because of this, and because a more stable OCR makes it easier to track changes due to compound addition, the decision was made to include ferric ammonium citrate and copper sulfate in the resuspension buffer in future experiments.

Experiments with 7H9 media at pH 6.6 reveal the importance of maintaining the correct pH. Under these conditions there is a drop in OCR accompanied by changes in *b* and *c* cytochrome oxidation state on addition of 1 µM nigericin (figure 3.10). It is likely that resuspending cells in a pH 7.4 media means the PMF is composed entirely of ΔΨ. The proton/potassium ion exchanging activity of nigericin is able to disrupt ΔpH but not ΔΨ, thus why no effects are observed. One of BDQ's proposed mechanisms is that it acts as a proton/potassium ion exchanger, collapsing ΔpH while maintaining ΔΨ, so it is important the conditions used in the bioenergetic chamber would allow this to be observed. A summary of how the protocol for performing bioenergetic chamber experiments with *M. smegmatis* has been optimised is included in table 3.2.

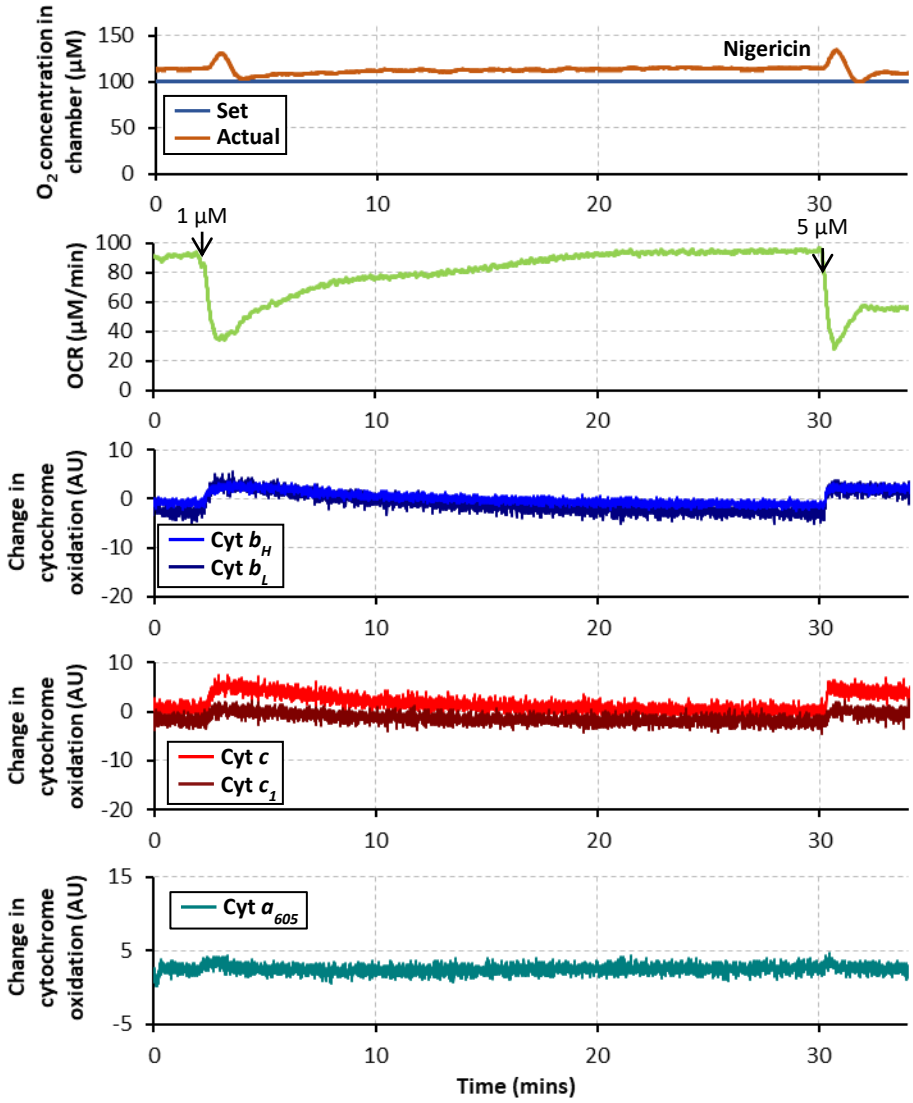

Figure 3.10: *Changes in OCR and cytochrome oxidation states in M. smegmatis mc²155 cells on addition of nigericin. Cells were grown in 7H9 media with Tween 80 (0.05% v/v) and glycerol (50 mM). Once an OD_{600} of 2.1 was reached, a 5 mL sample was taken, washed once and resuspended in 7H9 supplemented with 50 mM glycerol (pH = 6.6). Arrows indicate the time of nigericin additions, with the concentration given being the total concentration of nigericin in the chamber following addition. Haem model: mammalian.*

***Table 3.2**: Summary of the changes made to the protocol for performing experiments on M. smegmatis cells using the bioenergetic chamber in order to optimise the procedure.*

Observation	Response
Chamber unable to hold oxygen concentration at 100 µM	Increased length of tubing from 80 mm to 130 mm
High concentrations of CCCP required to see any effect on cells	Washed and resuspended cells in HEPES buffer (20 mM HEPES, 150 mM sodium chloride, pH = 7.4) to remove detergent
No effects observed on addition of nigericin	Changed salt in buffer to potassium chloride
Still no effects observed on addition of nigericin; notable increase in OCR even when no compound is added	Resuspended cells in 7H9 (at pH 7.4) excluding ferric ammonium citrate and copper sulfate and supplemented with glycerol
Notable increase in OCR even when no compound is added	Resuspended cells in 7H9 (at pH 7.4) supplemented with glycerol
OCR more stable in the absence of inhibitor/ionophore addition	Resuspended cells in 7H9 (at pH 6.6) supplemented with glycerol
Nigericin displays effects on cells at a concentration of 1 µM	No further optimisation of *M. smegmatis* protocol

3.2.2. Establishing a metabolic "toolkit" in *M. smegmatis*

In order to elucidate BDQ's mechanism, it is important to have a library of compounds with well-established modes of action to which BDQ can be compared. Furthermore, being able to selectively inhibit specific complexes in the oxidative phosphorylation system allows for a deeper probing of the impact of different drugs and could highlight targets for potential combination therapies.

As part of the preliminary work with the bioenergetic chamber, various respiratory complex inhibitors were trialled to establish whether they are active in mycobacteria, what concentration is required to see activity and under which conditions. Results from these experiments are summarised in table 3.3.

***Table 3.3**: List of uncouplers, ionophores and oxidative phosphorylation inhibitors examined for activity in M. smegmatis using the bioenergetic chamber and their observed effects on the bacteria. All samples were grown to log phase in 7H9, 50 mM glycerol and 0.05% Tween, before being washed and resuspended in the listed media/buffer. 7H9 media was at a pH of 6.6 while HEPES buffer solutions were at pH 7.4.*

Compound	Target	Resuspension media	Conc.	Observations
CCCP	Uncoupler	7H9, 50 mM Gly	1-5 µM	Increase in OCR. Oxidation of *b* cytochromes.
			25 µM	Decrease in OCR. Further oxidation of *c* cytochromes.
FCCP	Uncoupler	7H9, 50 mM Gly	1 µM	Increase in OCR. Oxidation of *b* and *c* cytochromes.

			5-25 µM	Decrease in OCR. Further oxidation of *b* and *c* cytochromes.
BAM15	Uncoupler	7H9, 50 mM Gly	1-5 µM	Increase in OCR. Oxidation of *b* cytochromes.
			25 µM	Decrease in OCR. Oxidation of *b* and *c* cytochromes.
Rotenone	NDH-1 inhibitor	7H9, 50 mM Gly	5 µM	No observable effects.
Piericidin A	NDH-1 inhibitor	7H9, 50 mM Gly	≥10 µM	Drop in OCR, likely due to off targets effects at this concentration.
TRZ	NDH-2 inhibitor	20 mM HEPES, 150 mM NaCl	180 µM	Increase in OCR. Reduction of *b* cytochromes.
			360 µM	Arrest of oxygen consumption. Slow oxidation of *b* and *c* cytochromes over 15-20 mins.

TFPZ	NDH-2 inhibitor	20 mM HEPES, 150 mM NaCl	200 µM	Increase in OCR. Reduction of *b* cytochromes.
			400 µM	Arrest of oxygen consumption. Slow oxidation of *b* and *c* cytochromes over 15-20 mins.
HQNO	NDH-2 inhibitor	20 mM HEPES, 150 mM KCl	10 µM	Increase in OCR. Oxidation of *b* cytochromes, reduction of *a* and *c* cytochromes.
			100 µM	Decrease in OCR. Further reduction of *c* cytochromes.
CFZ	NDH-2 inhibitor	7H9, 50 mM Gly	35 nM	Absorbance of CFZ obscures spectral changes of cytochromes.
CHQAD	NDH-2 inhibitor	7H9, 50 mM Gly	3.2-22.8 µM	OCR decreases as concentration increases. Slight oxidation of *b*, *c* and *a* cytochromes at highest concentration.
3NP	SDH inhibitor	7H9, 50 mM Gly	50 µM	No observable effect.

Antimycin A	*bcc* complex inhibitor	20 mM HEPES, 150 mM NaCl	6 µM	No observable effect, may not be active in mycobacteria.
Oligomycin	ATP synthase inhibitor	7H9, 50 mM Gly	10 µM	No observable effect, may not be active in mycobacteria.
DCCD	ATP synthase inhibitor	7H9, 50 mM Gly	10 µM	Slight increase in OCR. Slight reduction of *b* and *c* cytochromes.
			50 µM	Decrease in OCR, likely due to off-target effects.
Nigericin	H^+/K^+ exchanger	7H9, 50 mM Gly	1 µM	Immediate drop in OCR that recovers with time. Oxidation of *b* and *c* cytochromes and slight oxidation of *a* cytochromes.
Valinomycin	K^+ transporter	7H9, 50 mM Gly	10 µM	Increase in OCR. Reduction of *b* cytochromes.

Piericidin A and rotenone are two common inhibitors of complex I in mitochondria and both have been used in experiments on mycobacteria (Degli Esposti et al., 1994; Rao et al., 2008; Beites et al., 2019). High concentrations of Piericidin A (around 10-100 µg mL^{-1}) have been observed to inhibit growth of *M. tuberculosis* grown on Sauton's medium (Beites et al., 2019). This concentration was greatly reduced to <1 µg mL^{-1} in a strain of *M. tuberculosis,* in which genes for NDH-2 had been deleted with

a similar, although less marked, trend being observed with rotenone, indicating that both inhibitors are able to enter mycobacterial cells and inhibit NDH-1.

Results in *M. smegmatis* found rotenone displayed no activity up to a concentration of 5 μM, the maximum that could reasonably be achieved in the chamber due to rotenone's solubility. This lack of activity is likely due to NDH-1 activity being significantly lower (95%) than NDH-2 activity in *M. smegmatis* (Vilchèze et al., 2005), thus even if rotenone is able to enter cells and bind to NDH-1, there is little effect on the activity of the ETC.

A drop in OCR is observed with 10 μM Piericidin A, however this is far above the concentration that should be required to inhibit NDH-1 such that there is an equal drug-to-protein ratio. It was concluded this decrease in OCR is likely due to off-target effects.

All NDH-2 inhibitors trialled displayed activity in *M. smegmatis*. CFZ has a strong broad absorbance at 495 nm in its monoprotonated form making it unsuited for experiments with the bioenergetic chamber focused on examining cytochrome redox states. 10 μM 2-heptyl-4-quinolinol 1-oxide (HQNO) stimulates an increase in OCR, with a decrease being observed when this concentration is increased to 100 μM. Due to the solubility of HQNO, concentrations above 200 μM could not be achieved in the chamber. Trifluoperazine (TFPZ) and thioridazine (TRZ) both increase the OCR of *M. smegmatis* at concentrations ≤200 μM (figure 3.11).

Higher concentrations of TFPZ and TRZ result in complete inhibition of oxygen consumption, with the *b* and *c* cytochromes oxidising over a period of 15-25 mins following the drop in OCR. The mechanisms of these two compounds have not been investigated in detail, however they are structurally related to CFZ and so likely have a mechanism similar to that outlaid in section 1.5.3. The difference in the effects of TFPZ and TRZ at different concentrations is likely a consequence of them undergoing this redox cycling at lower concentrations, while at higher concentrations they are able to outcompete MK, resulting in oxidation of the quinone pool and consequently oxidation of the supercomplex cytochromes and arrest of oxygen consumption.

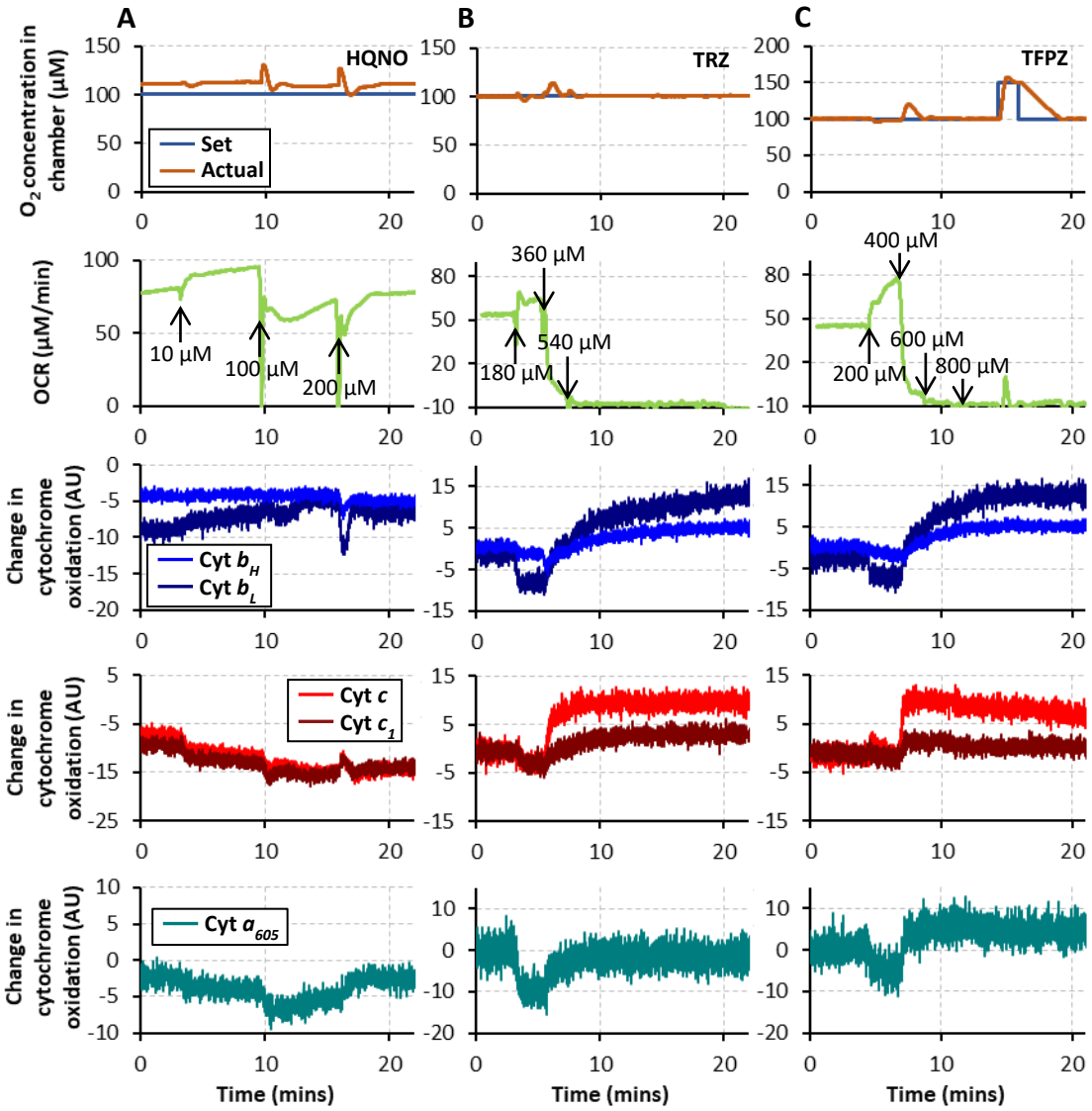

Figure 3.11: *Changes in OCR and cytochrome oxidation states in (**A**) M. smegmatis mc²155 cells in response to increasing concentrations of HQNO (**B**,**C**) M. smegmatis JR128 cells in response to increasing concentrations of (**B**) TRZ or (**B**) TFPZ. Cells were grown in 7H9 media with Tween 80 (0.05% v/v) and glycerol (50 mM), once an OD_{600} of (**A**) 2.4 (**B**) 2.0 (**C**) 2.3 was reached, a 5 mL sample was taken, washed once and resuspended in HEPES buffer solution (20 mM HEPES, pH = 7.4) with either (**A**) 150 mM KCl or (**B**,**C**) 150 mM NaCl. 10 µL of glycerol was added prior to the start of each run. Arrows represent the time of additions, with concentrations corresponding to the total concentration of the relevant inhibitor in the chamber following each addition. (**B**,**C**) Data collection was performed collaboratively with Rowan Walters (PhD student). Haem model: mammalian.*

N-(4,4-difluorocyclohexyl)-2-((4-oxo-3,4-dihydroquinazolin-2-yl)thio)acetamide (CHQAD) is a recently discovered inhibitor of NDH-2 in *M. tuberculosis* with a reported MIC of 0.4 µM (Murugesan et al., 2018). While the compound did show some activity in *M. smegmatis*, it was not able to fully arrest oxygen consumption at the maximum concentration that could be added to the chamber (figure 3.12). This suggests it does not fully inhibit NDH-2 in *M. smegmatis*.

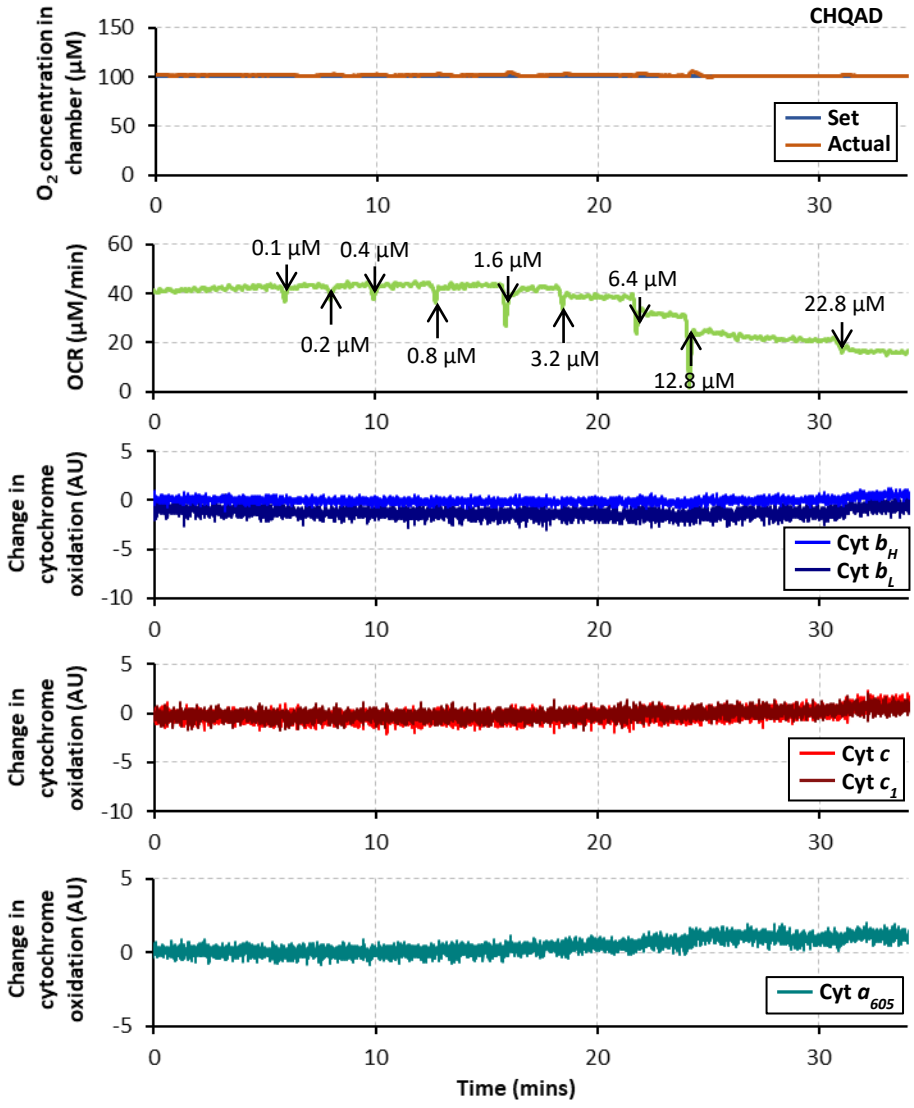

Figure 3.12: *Changes in OCR and cytochrome oxidation states in M. smegmatis mc²155 cells on addition of CHQAD. Cells were grown in 7H9 media with Tween 80 (0.05% v/v) and glycerol (50 mM). Once an OD_{600} of 1.1 was reached, a 5 mL sample was taken, washed once and resuspended in 7H9 supplemented with 50 mM glycerol (pH = 6.6). Arrows indicate the time of additions of CHQAD, with the concentration given being*

the total concentration of inhibitor in the chamber following addition. Haem model: mammalian.

3-nitropropionate (3NP) is able to act as an inhibitor of SDH and isocitrate lyase, but has been found to act predominantly as an SDH inhibitor in *M. tuberculosis* (Eoh and Rhee, 2013). Although 3NP has been shown to have detrimental effects on cell growth/viability in mycobacterial cells adapting to hypoxia, it does not display any activity in *M. smegmatis* and *M. tuberculosis* (Eoh and Rhee, 2013; Pecsi et al., 2014). No effects were observed on glycerol-grown *M. smegmatis* cells in the bioenergetic chamber, although this is likely because glycerol-grown cells will contain little SDH.

There are several known inhibitors of the *bcc* complex in *M. tuberculosis*, including Q203, with an MIC_{50} of 2.7 nM in broth, and lansoprazole sulfide, with an IC_{50} of 460 nM in broth (Pethe et al., 2013; Rybniker et al., 2015). *M. smegmatis* is insensitive to both of these compounds, indicating it is less susceptible to cytochrome *bcc* inhibition. This may explain the lack of activity observed with antimycin A, which has not previously been trialled in mycobacteria, however, this insensitivity is partially mediated by activation of cytochrome *bd* oxidase (Chauhan et al., 2022) which should be observable using the bioenergetic chamber through changes in cytochrome oxidation states. The absence of these changes with the addition of antimycin A suggest it is not active in mycobacteria, either due to an inability to enter cells or bind to mycobacterial MK-cytochrome *c* oxidoreductase *bcc*.

CCCP, carbonyl cyanide-p-trifluoromethoxyphenylhydrazone (FCCP) and N^5,N^6-Bis(2-fluorophenyl)[2,1,3]oxadiazolo[4,5-*b*]pyrazine-5,6-diamine (BAM15) are known protonophores and all display similar activity in *M. smegmatis*. At lower concentrations they stimulate an increase in the OCR, along with oxidation of the *b* cytochromes. At higher concentrations, (≥25 µM for CCCP and BAM15, ≥5 µM for FCCP) a drop in the OCR is observed on addition of the protonophore along with oxidation of the *c* cytochromes (figure 3.13). These changes are likely due to the concentration being such that cells can no longer offset the movement of protons via the protonophore by increasing the activity of proton pumping complexes in the chain, resulting in dissipation of the PMF and disruption to PMF-linked processes.

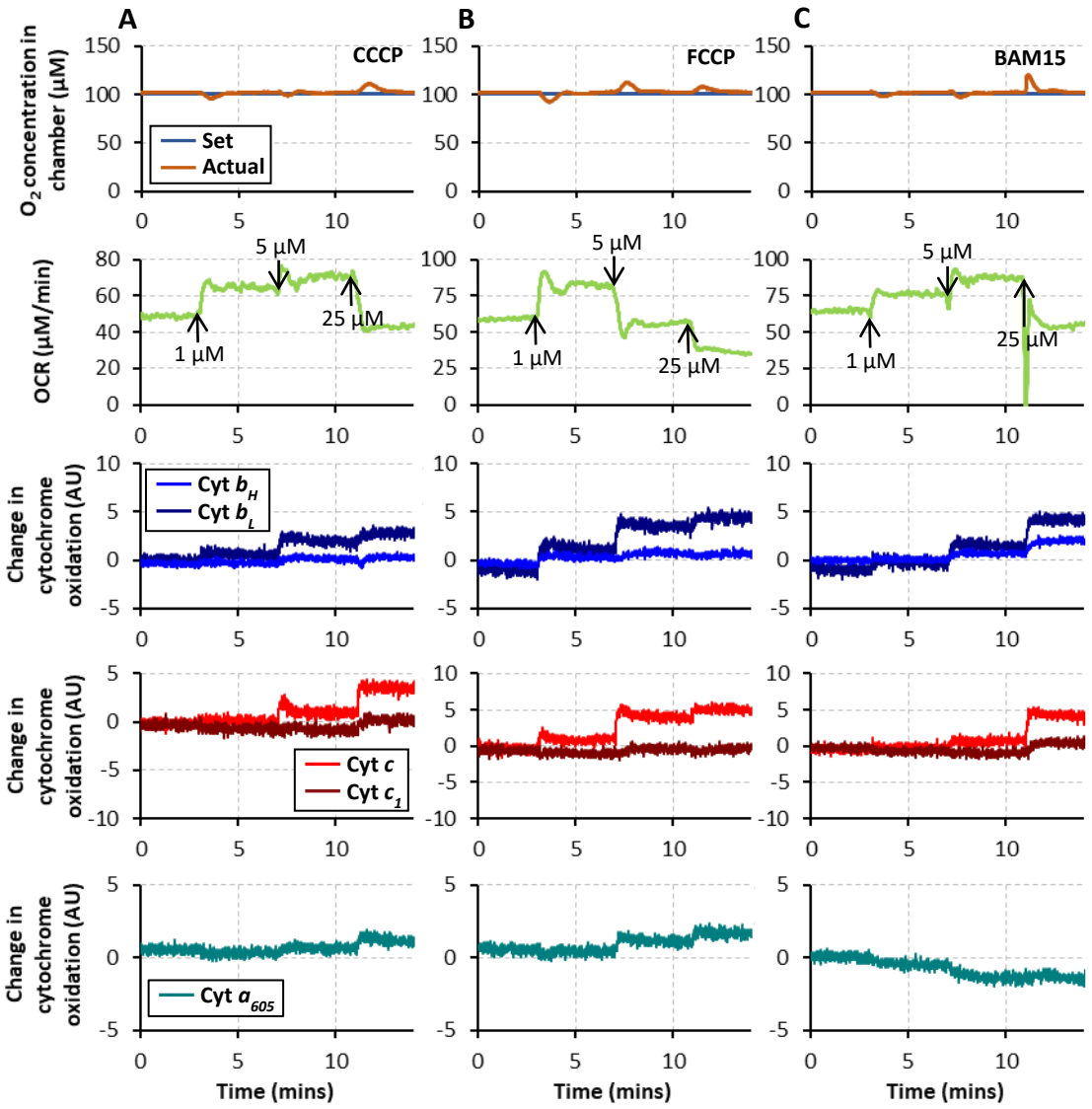

Figure 3.13: *Changes in OCR and cytochrome oxidation states in M. smegmatis mc²155 cells in response to increasing concentrations of (**A**) CCCP, (**B**) FCCP or (**C**) BAM15. Cells were grown in 7H9 media with Tween 80 (0.05% v/v) and glycerol (50 mM), and once mid-exponential phase was reached, a sample was taken, washed once and resuspended in 7H9 supplemented with 50 mM glycerol (pH = 6.6), such that the final OD_{600} was between 1.6-1.7. Arrows represent the time of additions, with concentrations corresponding to the total concentration of the relevant uncoupler in the chamber following each addition. Haem model: mammalian.*

In addition to changes in cytochrome spectra, an increase in absorbance at the far end of the spectrum (510 nm) is seen with increasing concentrations of BAM15 (figure

3.14). BAM15 has a λ_{max} of 328 nm at pH 7 (Firsov et al., 2021), so it is possible the changes observed are due to a broad absorbance of BAM15. Alternatively, BAM15 may be affecting the scattering of light, either due to it precipitating out of solution or through it impacting the morphology of cells. Therefore, while BAM15 is active in mycobacteria, it is less suitable for experiments with the bioenergetic chamber than CCCP and FCCP.

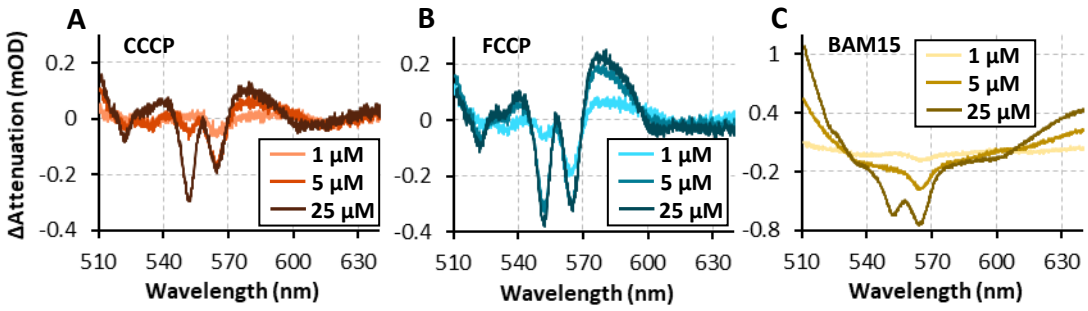

Figure 3.14: *Difference spectra recorded during the experiments shown in figure 3.13, showing the effect of increasing concentrations of (**A**) CCCP, (**B**) FCCP or (**C**) BAM15 on cytochrome oxidation in M. smegmatis mc²155 cells. Attenuation spectra were averaged over a period of 1 min.*

In addition to protonophores, the ionophores nigericin and valinomycin were tested for activity in mycobacteria. In theory, nigericin should collapse ΔpH while maintaining ΔΨ by transporting protons into the cell while transporting potassium ions out of the cell. Addition of 1 µM nigericin results in an initial drop in OCR and oxidation of the *b* and *c* cytochromes followed by a recovery to steady state conditions over a period of 15-20 mins (figure 3.15). These changes are likely due to disruption of ΔpH-linked processes which cells are then able to compensate for through increasing ΔΨ to minimise the overall change to the PMF.

Valinomycin transports potassium ions across the cell membrane, thereby disrupting ΔΨ. Addition of 10 µM stimulates an increase in OCR, consistent with an increase in the activity of complexes in the ETC to counter the uncoupled transport of cations across the membrane. Counter to the action of protonophores however, a reduction of the *b* cytochromes is observed.

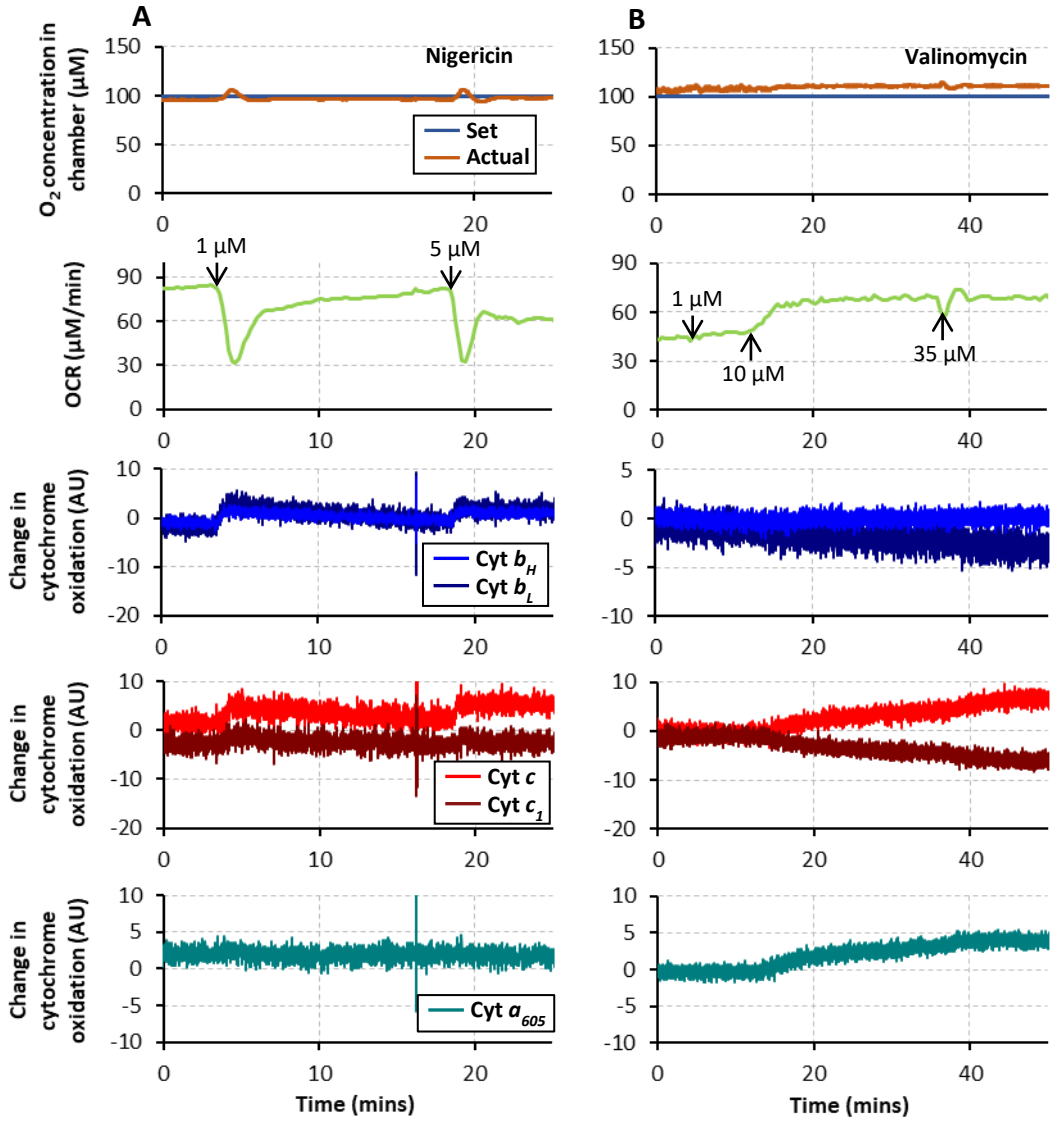

Figure 3.15: *Changes in OCR and cytochrome oxidation states in M. smegmatis mc²155 cells in response to increasing concentrations of (**A**) nigericin or (**B**) valinomycin. Cells were grown in 7H9 media with Tween 80 (0.05% v/v) and glycerol (50 mM), once an OD_{600} of (**A**) 1.9 or (**B**) 0.9 was reached, a 5 mL sample was taken, washed once and resuspended in 7H9 supplemented with 50 mM glycerol (pH = 6.6). Arrows represent the time of additions, with concentrations corresponding to the total concentration of the relevant ionophore in the chamber following each addition. Haem model: mammalian.*

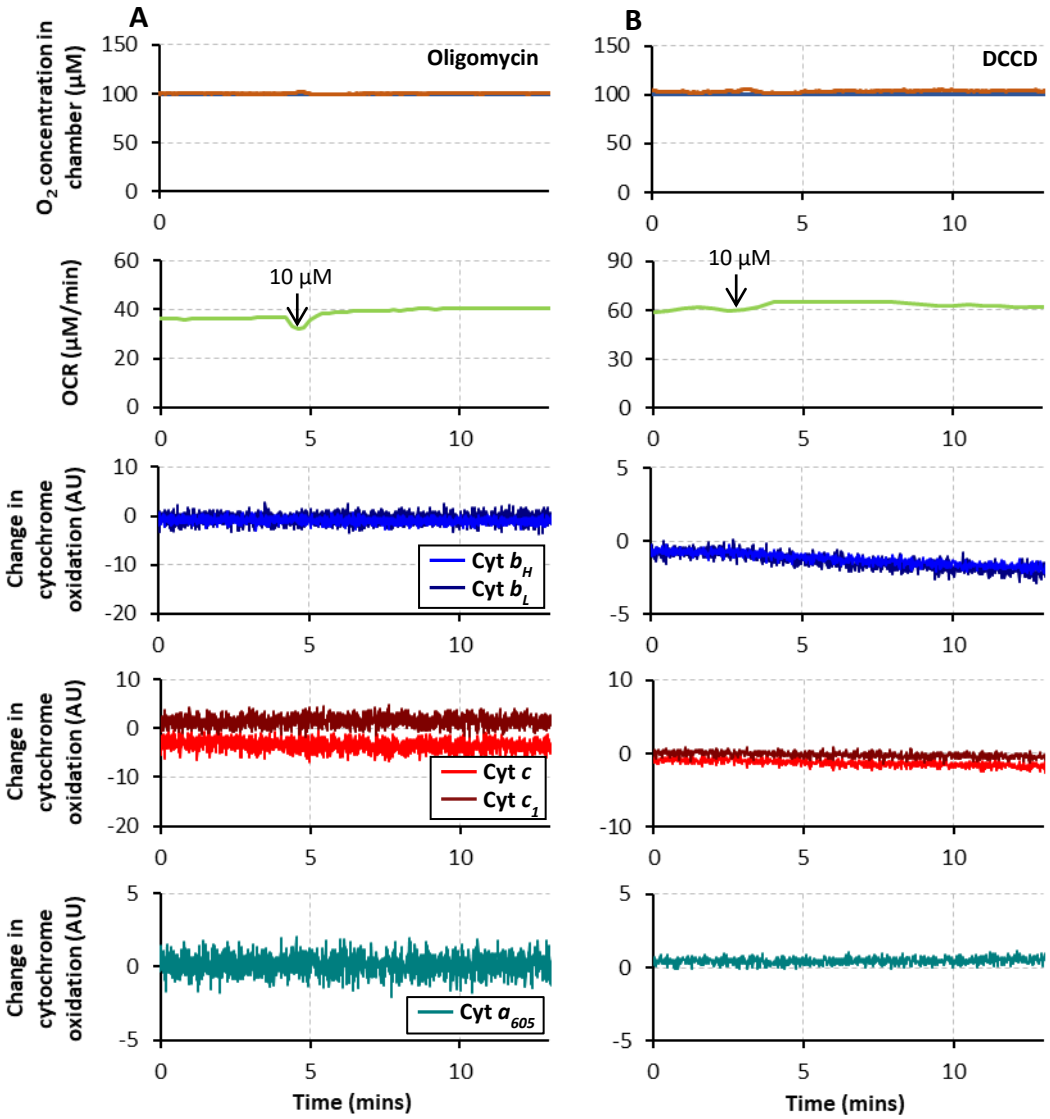

Figure 3.16: *Changes in OCR and cytochrome oxidation states in M. smegmatis mc²155 cells in response to increasing concentrations of (**A**) oligomycin or (**B**) DCCD. Cells were grown in 7H9 media with Tween 80 (0.05% v/v) and glycerol (50 mM), once an OD_{600} of (**A**) 0.7 or (**B**) 1.1 was reached, a 5 mL sample was taken, washed once and resuspended in 7H9 supplemented with 50 mM glycerol (pH = 6.6). Arrows represent the time of additions, with concentrations corresponding to the total concentration of the relevant inhibitor in the chamber following each addition. Haem model: mammalian.*

For experiments with BDQ, comparison with a known ATP synthase inhibitor is essential. Oligomycin is a well-known mitochondrial ATP synthase inhibitor but is inactive in *E.coli* (Nieuwenhuis et al., 1973) and did not display any activity in *M.*

smegmatis (figure 3.16). *N*,*N*-dicyclohexylcarboiimide (DCCD) also acts as an ATP synthase inhibitor and binds covalently to carboxyl residues, blocking the movement of protons through the enzyme (Hong and Pedersen, 2008). Addition of 10 μM DCCD to *M. smegmatis* results in a slight immediate increase in OCR along with reduction of *b* and *c* cytochromes. Higher concentrations result in a decrease in OCR, however this is likely due to off-target effects, as DCCD will react with any exposed carboxyl residues, not just those on ATP synthase.

Through these sets of experiments, there is now a catalogue of compounds active in mycobacteria that can be used in studies with BDQ and future work on mycobacterial bioenergetics. In addition, these data highlight some of the strengths of the bioenergetic chamber. By acquiring measurements in real time, the chamber can be used to investigate concentrations at which drugs begin to display effects on bacteria in a single experiment without needing to wait for cell growth. Monitoring the OCR and spectral changes in conjunction also allows verification of whether a drug is acting as expected or displaying off-target effects.

3.2.3. Growth of *M. smegmatis* strains

Initial experiments with the bioenergetic chamber were performed using a kanamycin-resistant strain of *M. smegmatis* (JR128), with kanamycin being added to the growth media of starter cultures to reduce chances of contamination. To avoid the possibility of any results with BDQ and other key drugs being impacted by the strain's kanamycin-resistance mechanism, the WT strain (mc^2155) was used for experiments performed subsequent to investigations on the effects of buffer composition.

The WT strain was observed to have a faster doubling time than JR128, which meant the previous approach of taking samples from a single 500 mL culture over the course of a day resulted in a large variation between the OD_{600} of samples. To ensure samples would be in the same growth phase across experiments, the use of smaller cultures (50 mL) set up with different starting OD_{600}s was trialled. Table 3.4 demonstrates the impact of the starting OD_{600} on the difference in time taken for cultures to reach the same OD_{600}. This method, combined with adjusting the initial sample volume taken

from cultures depending on the OD_{600}, allows for greater control over the cell densities of samples.

Table 3.4: *Growth of 50 mL cultures of M. smegmatis mc²155 (WT), set off with different volumes of starter culture and therefore at different starting OD_{600}s. Cells were grown in 7H9 media supplemented with Tween 80 (0.05% v/v) and glycerol (50 mM) in 250 mL flasks which were incubated at 37 °C with shaking.*

Time (hrs)	OD_{600} of culture 1 ()	OD_{600} of culture 2 ()	OD_{600} of culture 3()	OD_{600} of culture 4 ()
0.0	0.005	0.010	0.020	0.040
17.3	0.400	0.600	1.200	1.600
18.9	0.600	0.900	1.600	2.300
20.4	0.800	1.300	2.100	2.700
22.0	1.300	1.800	2.300	2.800
23.8	1.800	2.300	2.900	3.000
25.5	2.300	2.900	3.500	3.600

Growth of *M. smegmatis* mutant strains was a subject of interest as these strains can provide deeper insights into BDQ's mechanism. Two key strains of interest are a cytochrome *bd* oxidase knockout (Δ*cydAB*) lacking the *cydAB* genes (Lu et al., 2019) and a strain with a point mutation in the *atpE* gene that renders it resistant to BDQ via reducing its binding affinity with the c-ring ($AtpE^{D32V}$) (Koul et al., 2007). Prior to working with these strains in the bioenergetic chamber, growth measurements were taken to determine the timings required for cultures to reach a suitable OD_{600} (table 3.5).

The Δ*cydAB* strain has a slower growth rate compared to the WT strain but is otherwise similar. The $AtpE^{D32V}$ strain also displays slower growth and at an OD_{600} of

around 0.7 cells are observed clumping together even in the presence of 0.05% Tween 80. This clumping is not ideal for making measurements in the chamber as it can result in cells being unevenly oxygenated which could impact results with BDQ.

Table 3.5: *Growth of 50 mL cultures of different strains of M. smegmatis. Cells were grown in 7H9 media supplemented with Tween 80 (0.05% v/v) and glycerol (50 mM) in 250 mL flasks which were incubated at 37 °C with shaking.*

Time (hrs)	OD_{600} of WT culture ()	OD_{600} of *ΔcydAB* culture()	OD_{600} of $AtpE^{D32V}$ culture ()
0.0	0.01	0.01	0.01
16.9	0.70	0.20	0.30
19.0	1.20	0.40	0.50
21.2	2.20	0.70	0.60
23.6	3.40	1.30	1.10
25.7	4.10	1.80	1.40

In addition to these strains, growth measurements of a *M. smegmatis* mutant strain with deletion of the *qcrCAB* genes which encode the *bcc* complex (Δ*qcrCAB*) were also performed (table 3.6). Growth of this strain was notably slower than that of Δ*cydAB* and $AtpE^{D32V}$, speaking to the importance of the role of the *bcc* complex in maintaining the PMF, and therefore facilitating cell growth. As this strain is missing the cytochromes contained in the bcc complex, it is unsuitable for use with the fitting using modified mitochondrial spectra. Quantitative analysis would require reference spectra of the remaining terminal oxidase (cytochrome *bd* oxidase). Due to this, extensive experiments on this strain with BDQ were not planned but it remains a potential tool to probe the mycobacterial ETC.

Table 3.6: *Growth of a 50 mL culture of M. smegmatis ΔqcrCAB. Cells were grown in 7H9 media supplemented with Tween 80 (0.05% v/v) and glycerol (50 mM) in a 250 mL flask which was incubated at 37 ^{o}C with shaking.*

Time (hrs)	OD_{600} of Δ*qcrCAB* culture ()
0.0	0.01
21.8	0.20
24.8	0.30
25.8	0.40
28.2	0.40
45.4	4.40

In an attempt to solve the clumping issue with the $AtpE^{D32V}$ strain, it was grown up in LB supplemented with Tween 80 and glycerol, in the hopes that a richer media would limit any clumping. Cells did grow more rapidly, but clumping was still observed at OD_{600} values >1. D-arabinose has previously been shown to disperse large clumps of mycobacteria (Anton, Rougé and Daffé, 1996), so another growth in LB, this time supplemented with tyloxapol and D-arabinose was performed. Clumps were only observed once cells reached the stationary phase, however use of this media resulted in anomalous results in experiments with the bioenergetic chamber and is also not suitable for comparison with experiments done with other strains in 7H9.

To address these issues, the $AtpE^{D32V}$ strain was once again grown in 7H9 supplemented with Tween 80 and glycerol, but with the addition of 5 mM D-arabinose. Growth in this media is slower than that observed in LB and remains free of visible cell clumps up to an OD_{600} of 2 (table 3.7). These conditions were used for bioenergetic chamber experiments, with D-arabinose being included in the wash media in efforts to limit cells clumping once in the chamber.

Table 3.7: *Growth of 50 mL cultures of M. smegmatis WT and AtpE^{D32V}. Cells were grown in 7H9 media supplemented with Tween 80 (0.05% v/v), glycerol (50 mM) and D-arabinose (5 mM) in 250 mL flasks which were incubated at 37 ^{o}C with shaking.*

Time (hrs)	OD_{600} of WT culture ()	OD_{600} of AtpE^{D32V} culture ()
0.0	0.01	0.01
17.9	0.50	0.20
20.0	0.90	0.30
22.4	1.60	0.50
24.5	2.20	0.60

3.2.4. Modifying the procedure to work with BSL-2 compatible *M. tuberculosis*

M. smegmatis is a useful model organism for method development due to its fast growth time comparative to other mycobacteria and non-pathogenic nature. However, it is important to replicate key experiments with BDQ in *M. tuberculosis* to demonstrate findings in *M. smegmatis* are relevant in the pathogen. Developing a protocol for working with *M. tuberculosis* strains in the chamber also allows for future experiments further probing their biology.

The most commonly used *M. tuberculosis* strain in laboratory work is *M. tuberculosis* H37Rv, a virulent strain derived from one originally isolated from a tuberculosis patient (Chitale et al., 2022). *M. tuberculosis* H37Rv must be handled under BSL-3 conditions (Asai et al., 2020), which were not available for this project so BSL-2 compatible strains were used. BSL-2 compatible strains have the disadvantage that the mutations which render them less virulent can also impact the systems under examination (Behr et al., 1999; Liang et al., 2022). For experiments with the bioenergetic chamber and BDQ, it is important the metabolism, and in particular the

oxidative phosphorylation system, of the strain used is as close as possible to that in virulent TB strains.

Some of the most widely used BSL-2 strains in TB research are *M. bovis* BCG strains, the TB vaccine, and *M. tuberculosis* H37Ra, an attenuated strain derived from the same clinical isolate as H37Rv (Zheng et al., 2008; Liang et al., 2022). *M. bovis* strains lack 61 open-reading frames compared to *M. tuberculosis* H37Ra, and all *M. bovis* BCG strains have a region of difference 1 (RD1) deletion (Behr et al., 1999). RD1 contains several genes associated with *M. tuberculosis* virulence, including those for CFP-10 and ESAT-6, which are both important antigens (Daugelat et al., 2003; Guinn et al., 2004). BCG strains harbour additional deletions compared to *M. tuberculosis* H37Rv, with these varying between strains (Behr et al., 1999). These mutations have been acquired through random events over the course of *M. bovis* BCG being cultured throughout the past century rather than via directed means. The result is that the differences between these strains and virulent *M. tuberculosis* are not well-defined in terms of the impact on metabolism, making *M. bovis* BCG unsuited for this project.

M. tuberculosis H37Ra was generated via culturing virulent *M. tuberculosis* on solid egg media for 3-4 months (Steenken, 1935). Compared to *M. tuberculosis* H37Rv, the genome of H37Ra contains 53 insertions, 21 deletions and 198 single nucleotide variations (Zheng et al., 2008). The affected genes include several related to metabolism, however the impacts of these differences are not fully understood, making the H37Ra strain ill-suited for experiments with the bioenergetic chamber.

M. tuberculosis $mc^2$6206 is a strain derived from *M. tuberculosis* H37Rv containing deletions of genes required for leucine and pantothenate synthesis (*leuD* and *panCD*), meaning supplementation with leucine and pantothenate is required for growth (Samspon et al., 2004). While these genes are involved in metabolism, compared to *M. bovis* BCG and *M. tuberculosis* H37Ra, the differences between $mc^2$6206 and H37Rv are well-defined (Behr et al., 1999; Sampson et al., 2004; Zheng et al., 2008). Additionally, *leuD* and *panCD* are not directly involved in oxidative phosphorylation, making the $mc^2$6206 strain better suited for the purpose of studying BDQ's mechanism.

The protocol for preparing samples of *M. tuberculosis* was kept similar to that for *M. smegmatis*, save for additions to the growth and resuspension media and a longer incubation period without shaking. Catalase contains four haem groups and so OADC was excluded from the resuspension media along with Tween 80 to ensure these haem groups would not interfere with the cytochrome spectra.

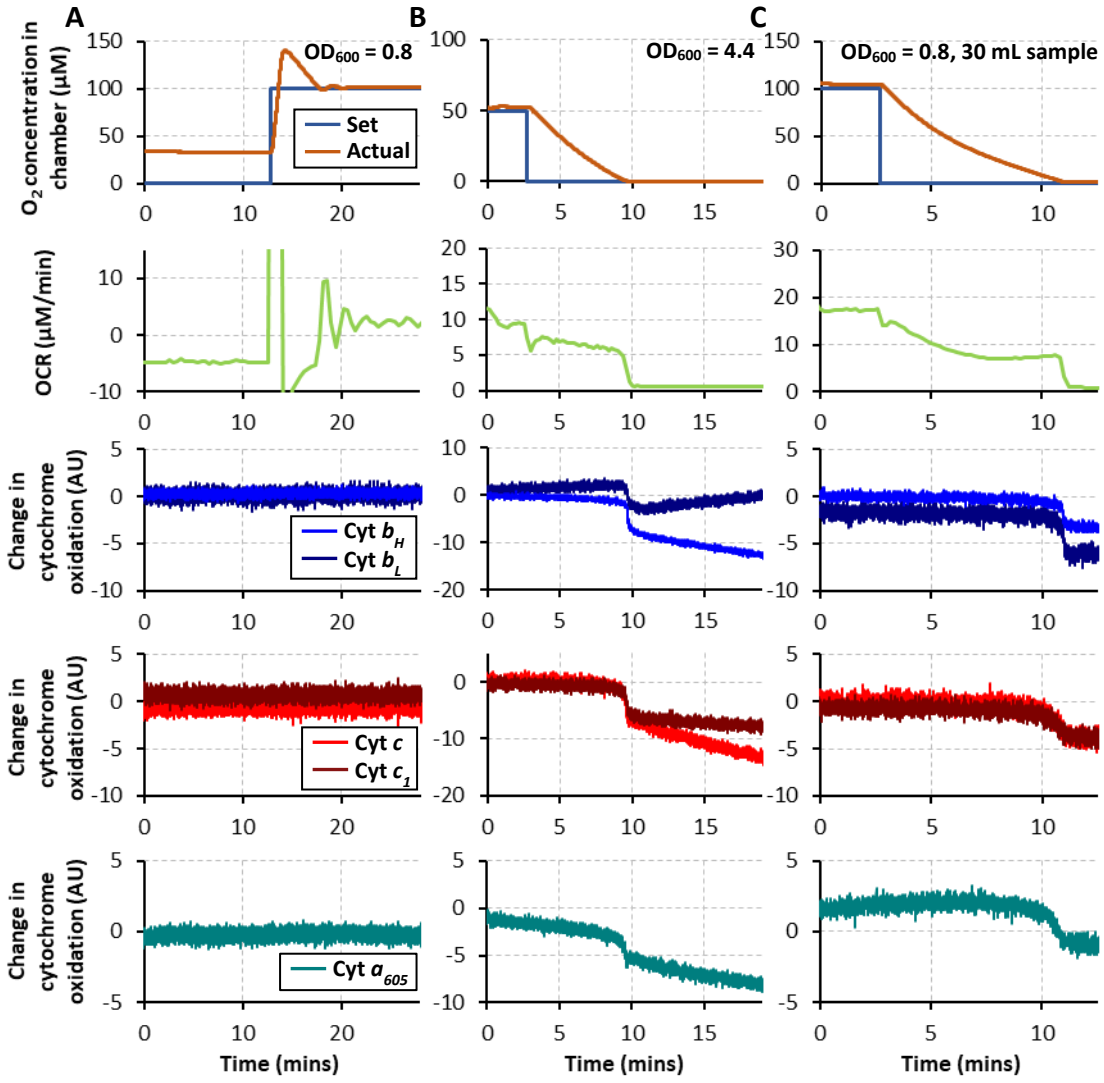

Figure 3.17: *Effects of OD_{600} and sample volume on OCR and cytochrome oxidation state traces in M. tuberculosis mc²6206. (**A**,**B**) 5 mL or (**C**) 30 mL were taken from of a culture of cells grown in 7H9 supplemented with Tween 80 (0.05% v/v), glycerol (55 mM), Middlebrook OADC (10% v/v), pantothenate (48 µg/mL) and leucine (0.5 mg/mL) once an OD_{600} of (**A**,**C**) 0.8 or (**B**) 4.4 was reached. Cells were washed and resuspended in 5 mL 7H9 supplemented with glycerol (55 mM), pantothenate (48 µg/mL) and leucine (48 µg/mL). Haem model: mammalian.*

The first sample added to the chamber had an OD_{600} of 0.8, similar to that used for some early *M. smegmatis* experiments (figure 3.17). At this OD_{600} the OCR of cells is around 4 µM/min which is too low to provide reliable information on the impact of drug addition or allow the chamber to reach anoxia for calibration.

The next sample was taken from a culture which had been incubated until an OD_{600} of 4.4 was reached. This gave an OCR between 9-13 µM/min, which is lower than any recorded for *M. smegmatis* at an OD_{600} of around 1 but is still sufficient for monitoring changes in response to compounds that target the oxidative phosphorylation system. At this OD_{600}, however, the *b* and *c* cytochrome traces appeared to split as the experiment progressed even without the addition of any inhibitors or ionophores. Examination of attenuation spectra revealed the presence of 3 peaks, located at 530 nm, 570 nm and 620 nm, that correspond to a porphyrin mixture reported to accumulate in dormant *M. smegmatis* cells (Nikitushkin et al., 2016) (figure 3.18).

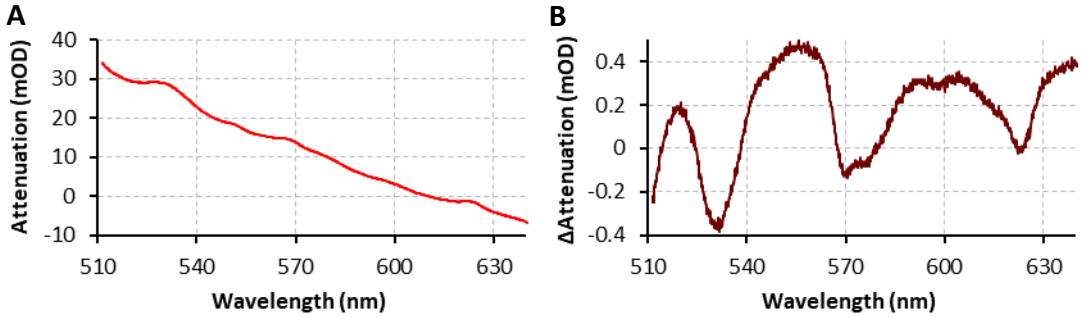

Figure 3.18: *(A) Attenuation spectrum of M. tuberculosis mc²6206 cells recorded during the experiment shown in figure 3.17B at 0.5 mins. (B) Difference spectrum produced by subtracting the spectrum in (A) from one recorded at 18 mins in the same experiment. All attenuation spectra were averaged over a period of 1 min with the reported timepoint being the centre of the averaged period.*

Subtracting a spectrum recorded at the start of the experiment from one recorded at the end reveals there is a loss of this porphyrin mixture over the course of data collection, with a decrease in attenuation observed at all 3 wavelengths. The role of this porphyrin mixture in cells has yet to be uncovered. Subsequent experiments showed the mixture is not present in an observable quantity in cells at an earlier growth phase (0.8-1.0), and so it may be produced as part of a stress response upon

the depletion of certain nutrients in the growth media. This would potentially explain why a loss of the porphyrins is seen in the bioenergetic chamber, with the reintroduction of previously depleted nutrients via the wash media resulting in a reversal of the stress response.

The presence of the porphyrin mixture is undesirable as a change in the concentration of porphyrins has the potential to obscure or distort changes in the cytochrome spectra. To solve this issue without compromising the OCR, cells were grown to an OD_{600} of 0.7-1.0 and then a 30 mL sample volume was taken. This sample was washed and resuspended in 5 mL of resuspension media to achieve a final sample $OD_{600} > 4$. This protocol generated samples with an OCR between 10-20 µM/min without any traces of the porphyrin mixture being observed in spectra (figure 3.20 C) and was used in all subsequent *M. tuberculosis* mc^26206 experiments.

Following experiments with BDQ and *M. smegmatis*, it became clear a cytochrome *bd* oxidase knockout strain of *M. tuberculosis* would be required to see if similar results could be replicated in a BSL-2 compatible strain of the pathogen. In order to ensure any differences observed with the cytochrome oxidase *bd* knockout strain were due to the absence of the enzyme in question, the knockout used must be derived from the same strain used for other experiments. A cytochrome *bd* oxidase knockout strain of mc^26206 was not available, so the decision was made to switch to using *M. tuberculosis* mc^26230. The mc^26230 strain is similar to the mc^26206 strain, having been derived from H37Rv with well-defined genetic differences: deletion of RD1 and *panCD* (Sambandamurthy et al., 2006). These genes are not directly involved in oxidative phosphorylation and a cytochrome *bd* oxidase knockout strain of mc^26230 (*M. tuberculosis* Δ*cydAB)* was readily available, making mc^26230 best suited for subsequent experiments with the bioenergetic chamber. In experiments with *M. tuberculosis* strains mc^26230 and Δ*cydAB*, the sample volume taken from culture was increase to 35 mL to further increase the OCR and intensity of the cytochrome spectra.

3.2.5. Changes in data analysis methodology

The original intention with the bioenergetic chamber was to collect reference spectra from the mycobacterial supercomplex to replace the modified mitochondrial

cytochrome fitting used in preliminary experiments. With the topic of BDQ's mechanism being so debated, it is imperative to prevent the introduction of any errors in analysis due to incorrect fitting. Additionally, by collecting these spectra and determining values for the mid-point potentials of the b_H and b_L cytochromes, it would enable the determination of ΔΨ in live cells.

Equation 3.1 demonstrates the relationship between the redox potentials of the b_L and b_H cytochromes and ΔΨ. $\Delta G^{b_L \rightarrow b_H}$ is the Gibbs free energy for electron transfer from b_L to b_H, $E_h^{b_H}$ and $E_h^{b_L}$ are the redox potentials of b_H and b_L and β is the fraction of the dielectric distance of the insulating phase between b_H and b_L (Kim, Ripple and Springett, 2012).

$$\Delta G^{b_L \rightarrow b_H} = -\left(E_h^{b_H} - E_h^{b_L}\right) + \beta \Delta \Psi \qquad \textbf{(Equation 3.1)}$$

By fully oxidising and fully reducing the *b* cytochromes in a single experiment with the bioenergetic chamber and setting these as reference points, it is therefore possible to use the chamber to observe changes in ΔΨ.

Reduction of cytochrome groups in the ETC can be achieved via anoxia and addition of the reducing agent sodium dithionite. Finding conditions to fully oxidise the supercomplex cytochromes is more challenging, though in principle can be achieved by inhibiting complexes earlier in the chain, resulting in oxidation of the MK/MKH_2 pool.

The focus of my project was originally on using NMR spectroscopy to study levels of phosphorylated metabolites in live mycobacteria, as reported in chapter 4, and applying this to the study of BDQ's mechanism. The bioenergetic chamber was set up in early 2021 after my project was started. After preliminary experiments with the bioenergetic chamber performed by Rowan Walters (PhD student) showed it could be used with mycobacteria, I also started working with the chamber as a means to study live cells. The first experiments with CCCP, as well the first titration experiments with TFPZ and TRZ, were undertaken by Rowan and myself together. The results of these studies demonstrated the power of the bioenergetic chamber, that it could be used

to study BDQ's mechanism, and that the technology was more immediately tractable that NMR.

Once our initial method of resuspending cells in a buffer solution was established, the decision was made for Rowan to focus on the biochemistry required to obtain mycobacterial reference spectra and midpoint potentials. Meanwhile, I continued performing experiments on live cells, further optimising the protocol for working with mycobacteria in the bioenergetic chamber and establishing our metabolic "toolkit", before conducting experiments with BDQ. This division of labour allowed us both to have clear and distinct aims and contributions.

Under the growth conditions used, the dominant contributor to the reduction of MK is NDH-2, thus a selection of NDH-2 inhibitors was examined as a way to oxidise the supercomplex cytochromes. Table 3.3 contains a full list of all inhibitors examined but the most promising for this purpose were TRZ and TFPZ. Addition of 360 µM of both of these compounds to *M. smegmatis* results in oxidation of the cytochromes over a period of around 15-20 mins. From the modified mitochondrial fitting, higher concentrations appeared to oxidise the cytochromes further, but examination of difference spectra revealed this was due to absorbance of the inhibitors interfering with the fit.

To test whether this may allow us to measure changes in ΔΨ, experiments were conducted with the established uncoupler CCCP, which should be able to diminish, if not collapse, ΔΨ. TFPZ was selected to oxidise the cytochromes as there were concerns over TRZ precipitating out of solution at the concentrations used.

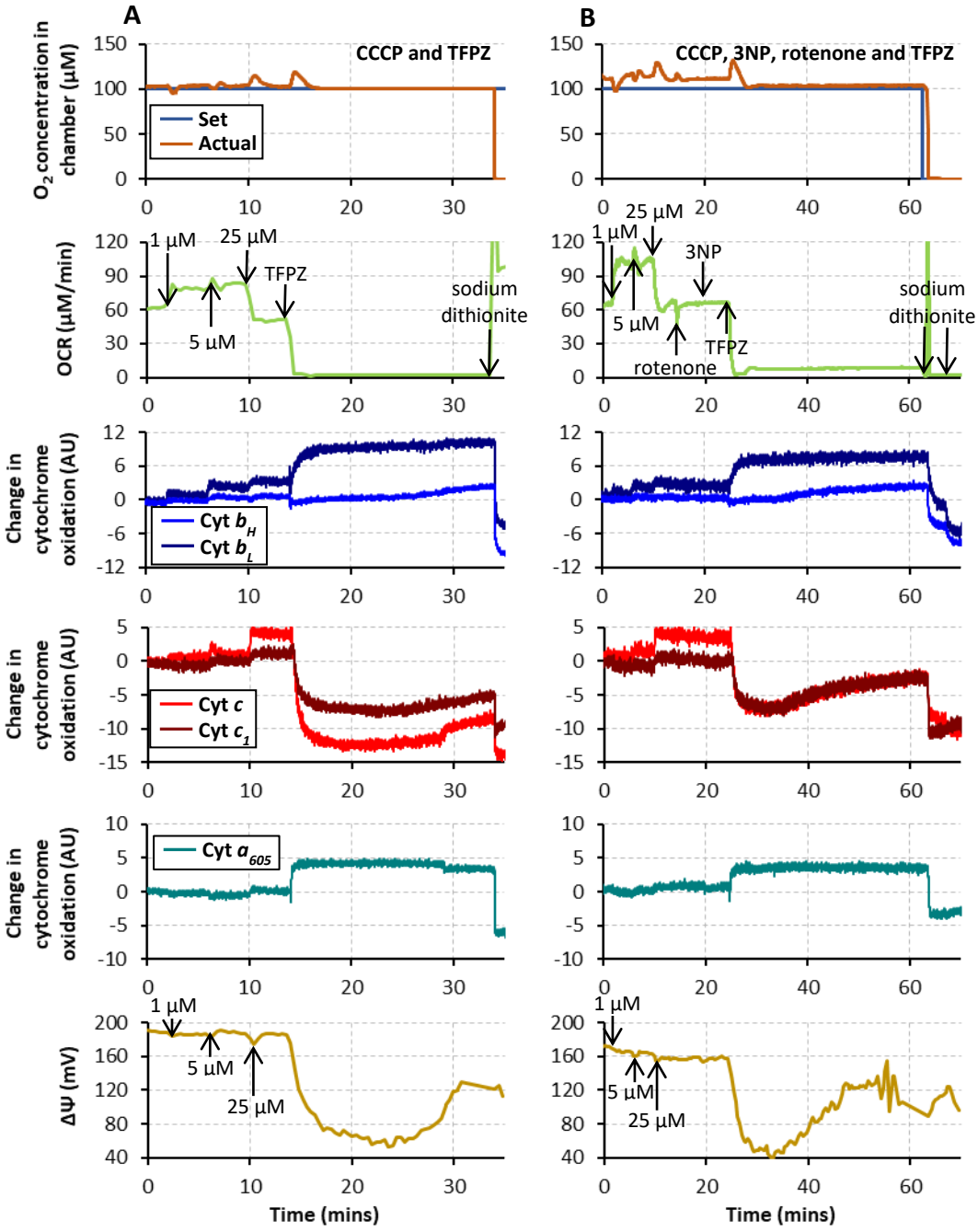

Figure 3.19: *Changes in OCR, cytochrome oxidation states and ΔΨ measurements in M. smegmatis mc²155 cells in response to increasing concentrations of CCCP using (**A**) TFPZ only or (**B**) rotenone, 3NP and TFPZ to oxidise the cytochromes to obtain an oxidised reference point for the ΔΨ calculation. Cells were grown in 7H9 media with Tween 80 (0.05% v/v) and glycerol (50 mM), and were resuspended in 7H9 supplemented with glycerol (50 mM), with the sample in (**A**) having an OD_{600} of 1.8 and the sample in (**B**) having an OD_{600} of 1.6. Arrows with concentrations represent the time of CCCP additions with the concentration corresponding to the total*

*concentration of CCCP in the chamber. Sodium dithionite solution was added until reduction of the b cytochromes was observed while the concentrations of other compounds added were as follows: (**A**,**B**) 360 µM TFPZ, (**B**) 5 µM rotenone, 50 µM 3NP.*

There is a clear increase in OCR on addition of 1 µM CCCP, along with oxidation of the cytochrome groups, indicating it displays uncoupling activity at these concentrations (figure 3.19). Little change is observed in ΔΨ as the concentration of CCCP is increased, which is unexpected even with the errors that may arise from using the modified mitochondrial fitting and mitochondrial midpoint potentials.

This led to the question of whether the cytochromes were fully oxidised on inhibition of NDH-2. NDH-1 and SDH are not expected to have a significant contribution towards to reduction of MK under the growth conditions used. No impact on the cytochromes or OCR was observed with the addition of the NDH-1 inhibitor rotenone or the SDH inhibitors 3NP and malonate in glycerol-grown cells when these inhibitors were used in isolation.

To confirm NDH-1 and SDH were not responsible for incomplete reduction of the cytochromes on inhibition of NDH-2, a CCCP titration experiment was conducted with addition of rotenone and 3NP prior to the introduction of TFPZ. Small changes in ΔΨ are observed on addition of 1 µM and 25 µM CCCP, however as these changes do not follow the same stepwise pattern as the *b* cytochrome oxidation states with each addition of CCCP, they still bring into question the accuracy of the measurements and thus the quality of the oxidised spectrum and cytochrome fitting. Additionally, similar experiments with CCCP in mitochondria show a much more dramatic decrease in ΔΨ with increasing CCCP concentration.

Developing a mycobacterial cytochrome fitting model proved challenging, with fits of the *b* cytochromes using spectra from isolated protein not matching the response that would be expected on addition of uncouplers/inhibitors to live cells. Therefore, the decision was made to analyse data using difference spectra to observe changes in cytochrome oxidation on addition of compounds that target oxidative phosphorylation rather than fitting the cytochrome peaks (figure 3.20). To ensure changes in cytochrome oxidation across difference spectra could be easily viewed,

linear regression analysis was used to subtract baseline shifts from the spectra. This method does not account for all baseline changes but repeats of experiments showed it produces consistent results with regards to whether cytochromes reduce or oxidise and is therefore suitable for this form of qualitative analysis. ΔΨ measurements cannot be attained without cytochrome fitting but it does allow for comparison of the effects of different inhibitors, uncouplers or ionophores on the mycobacterial ETC.

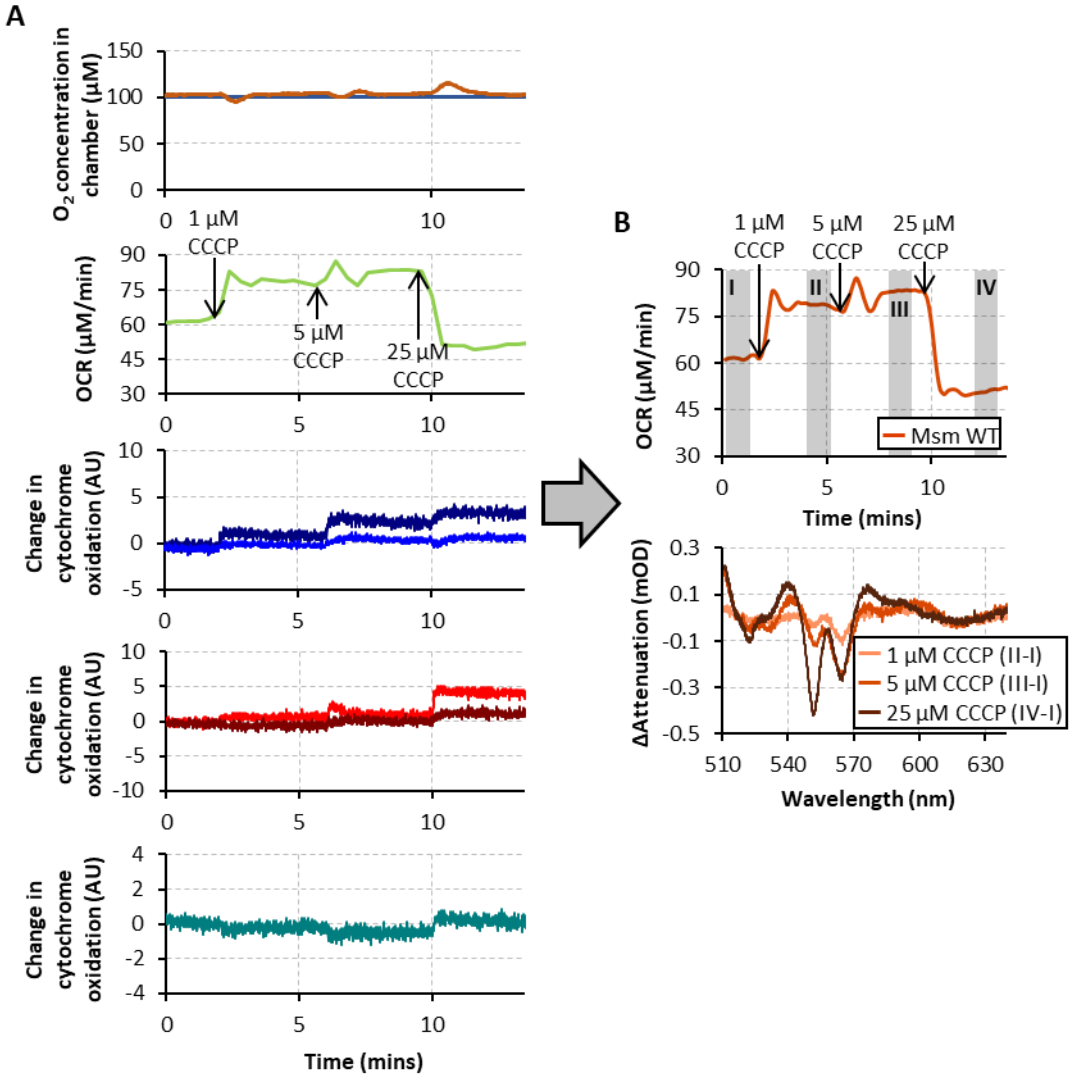

***Figure 3.20**: The change in presentation of data collected using the bioenergetic chamber after concluding it would not be possible to acquire adequate mycobacterial reference spectra for cytochrome fitting, with (**A**) being the old layout showing changes in OCR cytochrome oxidation based on fitting to mitochondrial reference spectra and (**B**) being the new layout showing changes in OCR along with difference*

*spectra. The shaded regions are the time-periods over which attenuation spectra were averaged. Linear regression analysis was used to fit a flat baseline to difference spectra which was then subtracted from the spectra to produce those shown in (**B**) The example data shown is the same as that in figure 3.19.*

3.3. INVESITGATING THE MECHANISM OF BDQ IN *M. SMEGMATIS*

3.3.1. The proposed mechanisms of BDQ

Having optimised methods for running and analysing data from the bioenergetic chamber for work with mycobacteria, they were applied to resolving the mode of action of BDQ. The proposed ideas of BDQ acting as an ATP synthase inhibitor versus an uncoupler/ionophore should have opposite effects on the cytochromes contained in the supercomplex (figure 3.21).

In the case that BDQ is acting as an ATP synthase inhibitor, this should result in an increase in ΔΨ and the resulting backpressure should reduce the activity of the supercomplex, leading to reduction of the cytochromes. Results obtained with BDQ should also be similar to those acquired with DCCD. If BDQ is instead acting as an uncoupler or ionophore then there should be some dissipation of the PMF, along with an increase in the activity of the supercomplex and oxidation of the cytochromes. These effects are expected to be larger in the case BDQ is acting as an uncoupler, and will therefore dissipate both ΔpH and ΔΨ, than if it is acting as an ionophore in which case there will only be dissipation of ΔpH. These two modes of action can also be distinguished between via comparisons with CCCP and nigericin. These experiments were first conducted in *M. smegmatis*, both due to its shorter culture time and because the lab was already in possession of *M. smegmatis* mutants that could be used to further probe BDQ's mechansim.

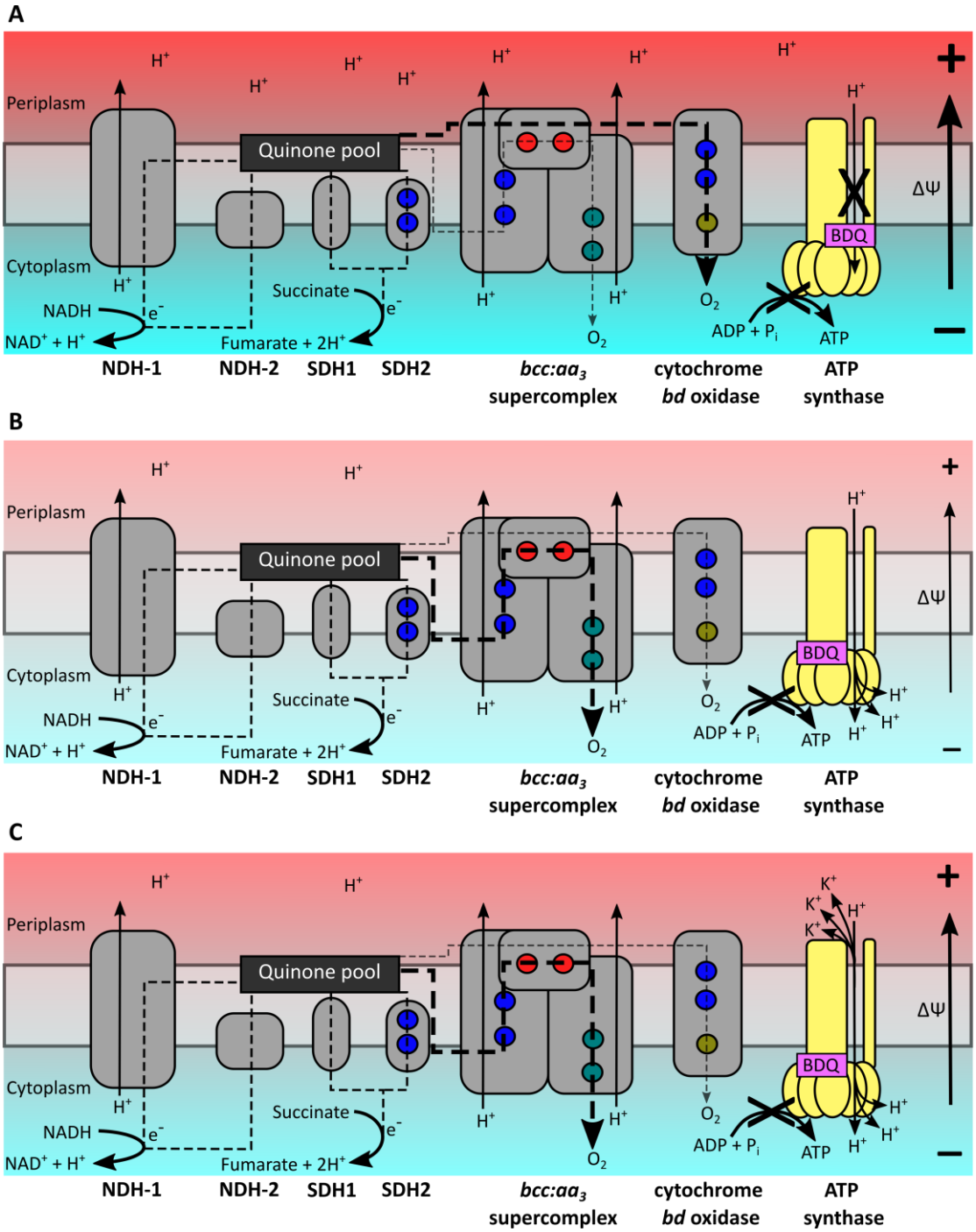

***Figure 3.21**: The proposed mechanisms of BDQ and the resulting consequences for the oxidative phosphorylation system. (**A**) BDQ acts as an ATP synthase inhibitor by preventing rotation of the c-ring and therefore blocking the proton channel. (**B**) BDQ acts an uncoupler, disrupting the action of ATP synthase and allowing protons to move freely without any ATP generation. (**C**) BDQ acts as an ionophore, allowing protons to move freely into the cytoplasm through ATP synthase without any ATP generation while potassium ions are transported in the opposite direction.*

3.3.2. Action of BDQ in *M. smegmatis*

The first step in the process of determining BDQ's mechanism in live mycobacteria is to establish BDQ's effects in *M. smegmatis* WT versus a control (figure 3.22). A BDQ concentration of 30 nM, roughly 2.4× the MIC (12.6 nM) (Andres et al., 2005), was selected as no further changes in cytochrome oxidation state or increase in OCR are observed at higher concentrations. Ethanol was chosen as the solvent for BDQ due to concerns the presence of DMSO may impact the ETC, and was therefore selected as the control.

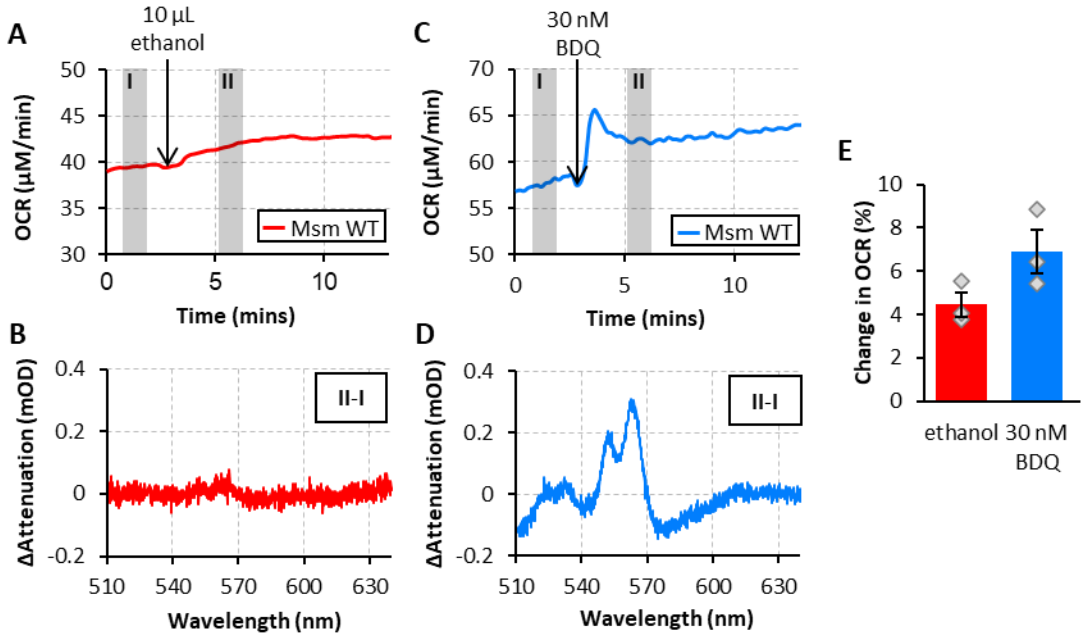

***Figure 3.22**: Changes in OCR and cytochrome oxidation state on addition of BDQ to M. smegmatis WT versus ethanol-only controls. (**A**) OCR trace showing changes on addition of 10 µL ethanol. (**B**) Difference spectra were acquired by subtracting spectra averaged over the two shaded regions in (**A**). (**C**) OCR trace showing changes on addition of 30 nM BDQ. (**D**) Difference spectrum acquired by subtracting spectra averaged over the two shaded regions in (**C**). (**E**) Mean percentage change in OCR 3 mins after the addition of ethanol or 30 nM BDQ, with the grey diamonds representing individual datapoints and the error bars showing standard error. Cells were grown in 7H9 supplemented with Tween 80 (0.05 % v/v) and glycerol (50 mM), and were resuspended in 7H9 supplemented with 50 mM glycerol. The OD_{600} of each sample was (**A**,**B**) 1.6 or (**C**,**D**) 1.4.*

On addition of BDQ to *M. smegmatis* WT there is an immediate increase in oxygen consumption along with reduction of the *b* (peak at 563.5 nm) and *c* (peak at 552 nm) cytochromes. Reduction of these cytochromes matches the predictions of BDQ acting as an ATP synthase inhibitor, however the OCR increase does not match findings with ATP synthase inhibitors in mitochondrial systems, where a decrease in OCR is observed. In the ethanol control run there is little change in cytochrome oxidation state, however there is a gradual increase in OCR. This is likely due to cell growth occurring while the sample is in the chamber.

Each experiment was repeated two more times and the direction of the change in cytochrome oxidation was found to be consistent across all repeats with only small differences in peak magnitude. There was some variation in starting OCRs between samples so to compare changes in OCR, the percentage change was determined. Although the rate of change in OCR seen with BDQ is much more rapid versus that with ethanol, comparison of the mean percentage change after 3 mins shows the increase with BDQ is only slightly larger, with some datapoints overlapping. Some of the previously reported increases in OCR on addition of BDQ were recorded in *M. tuberculosis* (Lamprecht et al., 2016), so it is possible the modest increase in *M. smegmatis* is due to a difference in the composition of ETC between the two species.

The next step in solving BDQ's mode of action is to confirm whether the changes observed in the WT are dependent on the binding of BDQ to ATP synthase. As mutations in the c-ring are associated with BDQ resistance, if any of the same changes at nanomolar concentrations are observed in *M. smegmatis* $AtpE^{D32V}$ as in the WT, then it suggests they are not related to BDQ's bacteriostatic effects. To verify the $AtpE^{D32V}$ strain has the expected mutation and properties, experiments adding increasing concentrations of BDQ to WT and $AtpE^{D32V}$ strains were performed (figure 3.23). As the point mutation in the $AtpE^{D32V}$ strain should reduce BDQ's ability to bind to the c-ring but not prevent binding entirely, it is expected any changes related to BDQ's ability to bind to ATP synthase should increase with BDQ concentration in a dose dependent manner.

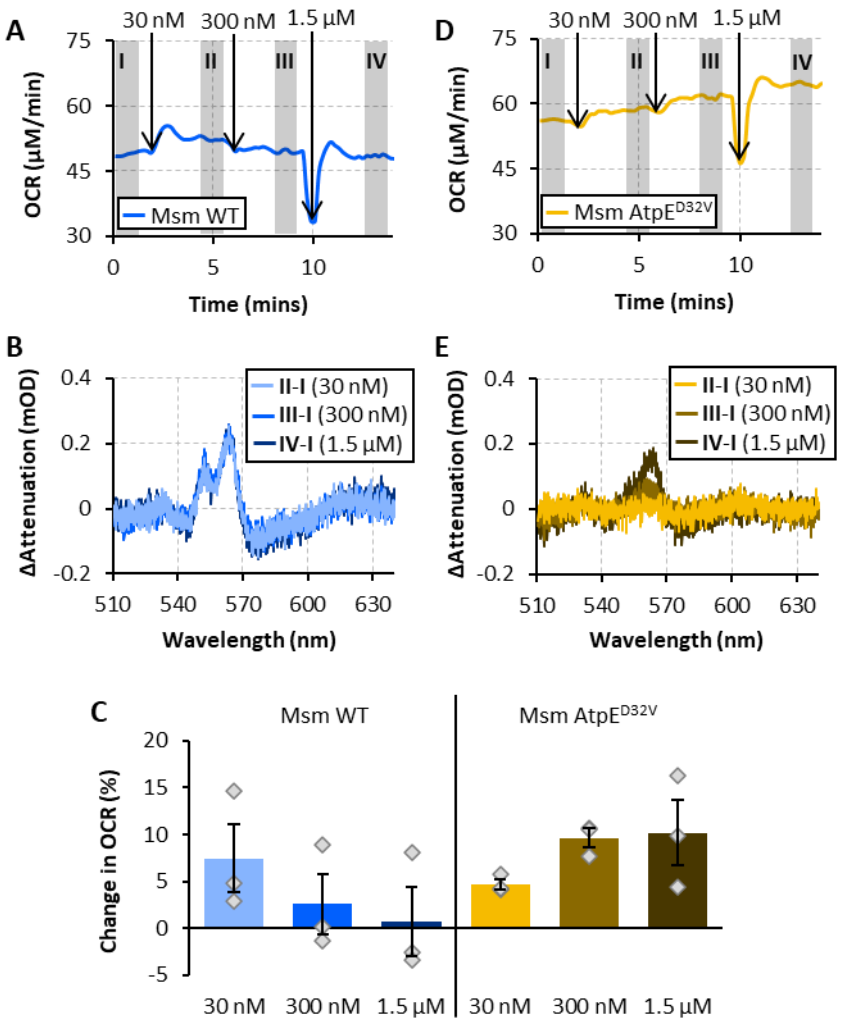

***Figure 3.23**: Changes in OCR and cytochrome oxidation state on addition of BDQ to M. smegmatis (**A**,**B**) WT and (**D**,**E**) AtpE^{D32V}. (**C**) Mean percentage change in OCR 3 mins after the addition of each concentration of BDQ relative to the OCR before any BDQ addition, with the grey diamonds representing individual datapoints and the error bars showing standard error. Difference spectra in (**B**,**E**) were acquired by subtracting spectra averaged over the labelled shaded regions in (**A**,**D**) respectively. Arrows represent the time of additions, with concentrations corresponding to the total concentration of BDQ in the chamber following each addition. Cells were grown in 7H9 media with Tween 80 (0.05% v/v) and glycerol (50 mM), and were resuspended in 7H9 supplemented with glycerol (50 mM) and D-arabinose (5 mM). The OD_{600} values of all samples were between 1.2-1.7.*

There is notable variation in the changes in OCR between repeats with the WT strain, however all three sets of data show a similar trend where a small initial increase in

OCR is observed followed by a decrease upon further additions of BDQ. As BDQ has a delayed bactericidal effect, this decrease is not likely to be due to cell death caused by BDQ. If BDQ is acting as an ATP synthase inhibitor, then it is possible the mechanism *M. smegmatis* cells use to alleviate backpressure and increase their OCR is not sufficient to cope with any further inhibition of ATP synthase on the addition of more BDQ. The same level of reduction of the cytochromes is observed at all three concentrations and this is consistent across all experiments.

In the AtpE^{D32V} strain a small increase in OCR occurs on addition of 30 nM BDQ, however this is not dissimilar to the increase seen with ethanol controls and no clear peaks are visible in the difference spectrum. As the concentration of BDQ is increased, a further increase in OCR is observed along the emergence of a *b* cytochrome peak and a small *c* cytochrome peak, showing the cytochromes are reducing. These results demonstrate that the AtpE^{D32V} strain is resistant to BDQ, but some BDQ binding does occur at higher concentrations. The reduction of the cytochromes observed in the WT is dependent on BDQ binding to ATP synthase. Conclusions about changes in OCR are harder to draw due to the small changes in the WT however the clear increase between 30 nM and 300 nM in the AtpE^{D32V} strain suggest this increase is also due to BDQ binding to the ATP synthase enzyme.

3.3.3. Comparisons with CCCP, nigericin and DCCD

To investigate the disparity between the predicted effects of an ATP inhibitor versus an uncoupler and those observed with BDQ, the data collected were compared with those obtained using compounds with clearly understood mechanisms (figure 3.24). Addition of 1-5 µM of the protonophore CCCP to *M. smegmatis* WT results in a sharp increase in OCR, with the average increase at 5 µM being over 4-fold higher than that observed with BDQ. This is accompanied by oxidation of the *b* cytochromes, demonstrating CCCP does not have the same impact on the ETC as BDQ.

Results obtained with nigericin also do not match those obtained with BDQ and further showcase that dissipation of the PMF results in oxidation of the *b* and *c* cytochromes rather than the reduction observed with BDQ. Additionally, the recovery

of OCR and cytochrome oxidation states back towards those observed under steady state conditions is unlike any effects observed with BDQ.

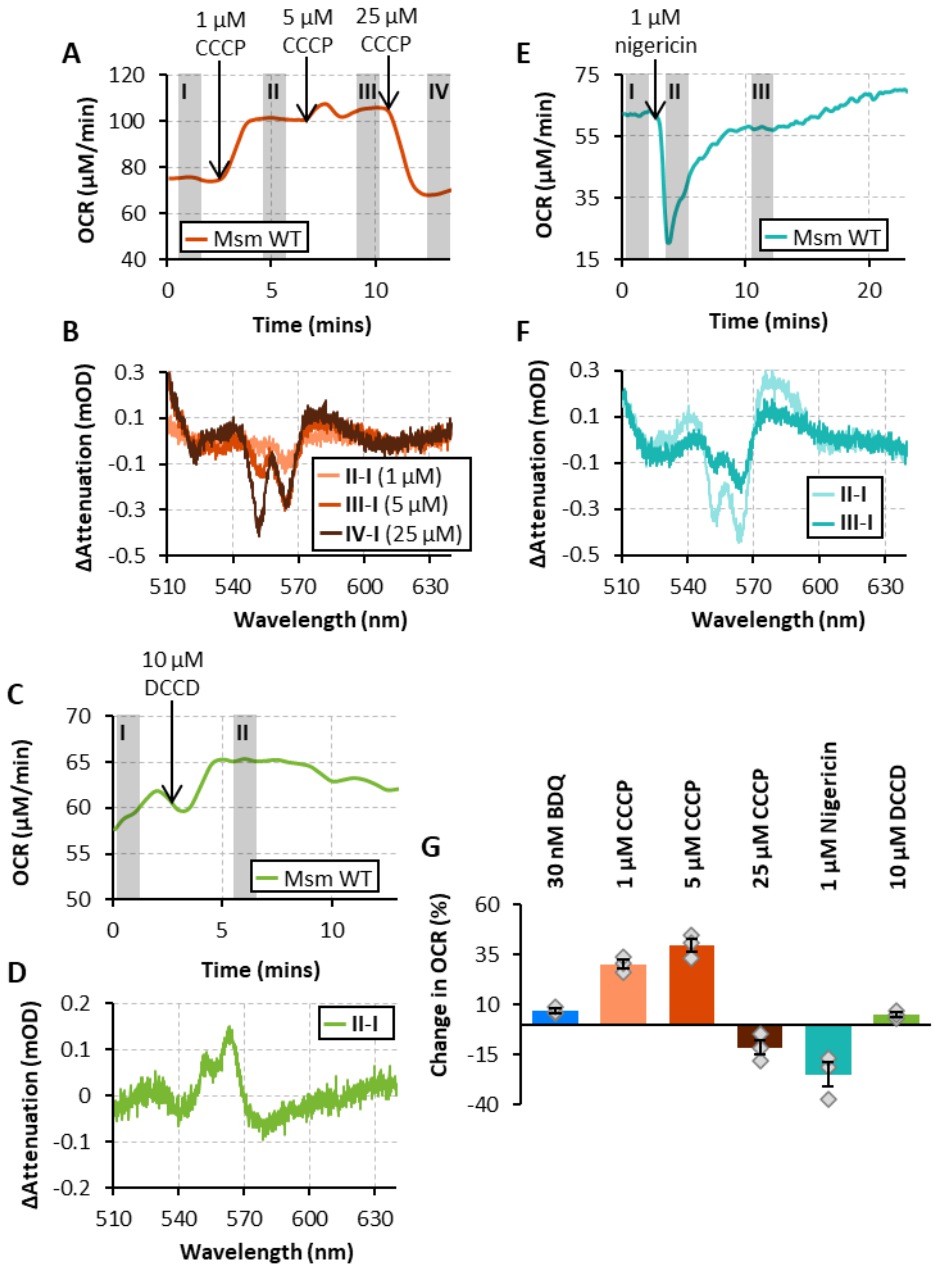

***Figure 3.24**: Changes in OCR and cytochrome oxidation state on the addition of (**A**,**B**) CCCP, (**C**,**D**) DCCD or (**E**,**F**) nigericin to M. smegmatis WT. (**G**) Mean percentage change in OCR 3 mins after the addition of each compound relative to the OCR before any additions, with the grey diamonds representing individual datapoints and the error bars showing standard error. The BDQ data shown is the same as in figure 3.25 and panels (**C**,**D**) show data from the same experiment as in figure 3.16. Difference spectra*

*in (**B**,**D**,**F**) were acquired by subtracting spectra averaged over the labelled shaded regions in (**A**,**C**,**E**) respectively. Arrows represent the time of additions, with concentrations corresponding to the total concentration of the relevant compound in the chamber following each addition. Cells were grown in 7H9 media with Tween 80 (0.05% v/v) and glycerol (50 mM), and were resuspended in 7H9 supplemented with glycerol (50 mM). The OD_{600} values of all samples were between 1.1-1.6.*

Relative to the ethanol control, there is no significant change in OCR on addition of DCCD to *M. smegmatis* WT but there is reduction of the *b* and *c* cytochromes. These effects are similar to those of BDQ and indicate BDQ is acting as a direct inhibitor of ATP synthase like DCCD. The lack of increase in OCR and smaller changes in cytochrome oxidation state can be explained by DCCD being a less specific inhibitor than BDQ. The lack of a drop in OCR on DCCD addition suggests mycobacteria do not respond to ATP synthase inhibition in the same manner as mitochondria. To conclusively prove BDQ's mode of action, this phenomenon needs to be explained.

3.3.4. BDQ and cytochrome *bd* oxidase

Of the two terminal oxidases in the mycobacterial ETC, the *bcc*:aa_3 supercomplex is proton-pumping while cytochrome *bd* oxidase is not, meaning it contributes less to the PMF. It was theorised that the OCR increase seen with BDQ may be due to cells increasing the activity of cytochrome *bd* oxidase as a means of limiting build-up of the PMF on inhibition of ATP synthase, allowing cells to maintain vital redox ratios.

To test this, the experiments performed with *M. smegmatis* WT were repeated using the cytochrome *bd* oxidase knockout strain (Δ*cydAB*) (figure 3.25). Treating this strain with BDQ results in similar cytochrome changes as those observed in WT cells, accompanied by a sharp drop in OCR that was consistent across all replicates. This supports the theory that cytochrome *bd* oxidase is responsible for the increase in OCR on addition of BDQ to WT cells and that by rerouting electrons to cytochrome *bd* oxidase, these cells are able to alleviate backpressure. Δ*cydAB* cells are not able to perform this redirection of electron flow and the resulting backpressure results in a decrease in activity of the supercomplex and thus a drop in OCR. This observation also explains why only a moderate OCR increase is observed in experiments with *M.*

smegmatis, as under the growth conditions used, there should be little cytochrome *bd* oxidase present.

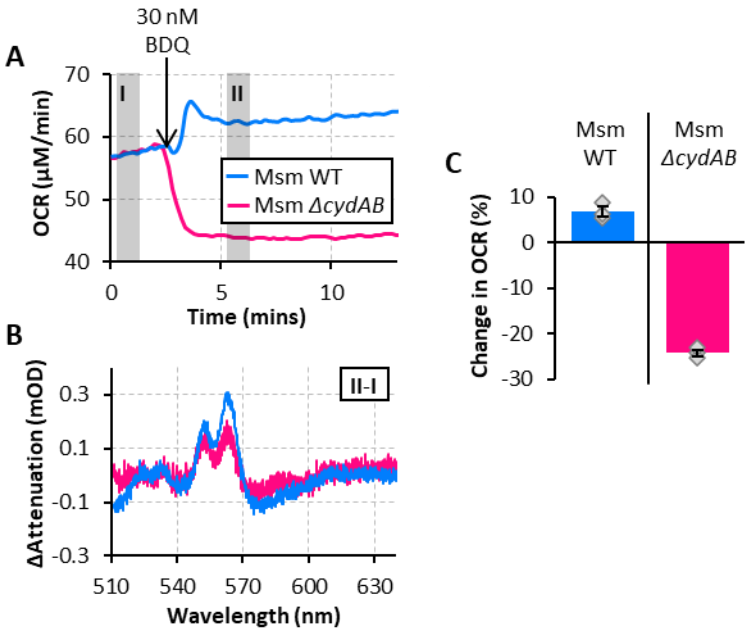

***Figure 3.25**: (**A**,**B**) Changes in OCR and cytochrome oxidation state on the addition of 30 nM BDQ to M. smegmatis WT and ΔcydAB. (**C**) Mean percentage change in OCR 3 mins after the addition of BDQ relative to the OCR before addition, with the grey diamonds representing individual datapoints and the error bars showing standard error. The WT data shown is the same as in figure 3.22 and is included for comparison purposes. Difference spectra in (**B**) were acquired by subtracting spectra averaged over the labelled shaded regions in (**A**). Arrows represent the time of BDQ addition. Cells were grown in 7H9 media with Tween 80 (0.05% v/v) and glycerol (50 mM), and were resuspended in 7H9 supplemented with glycerol (50 mM). The OD_{600} of the WT sample was 1.6 and the OD_{600} of the ΔcydAB sample was 1.3.*

Experiments looking at the impact of cytochrome *bd* oxidase on BDQ's activity have previously been performed in *M. tuberculosis*, however rather than lacking the *cydAB* genes, the cytochrome *bd* oxidase mutant generated was missing the ends of the *cydB* and *cydC* genes and all of the *cydD* gene (*cydKO*) (Arora et al., 2014). *cydDC* encodes an ABC transporter, which in *E. coli* has been theorised to have a role in cytochrome biogenesis but this has not yet been shown in mycobacteria (Aung, Berney and Cook, 2014; Shepherd, 2015). Treatment of this mutant with BDQ had the same effects as in

M. tuberculosis H37Rv, i.e. an increase in OCR was observed (Lamprecht et al., 2016). The disparity between this and the results with *M. smegmatis* Δ*cydAB* is likely due to the incomplete deletion in the *cydKO* mutant meaning there is still some cytochrome *bd* oxidase present.

To confirm these results are not due to an unusual response to uncoupling or dissipation of ΔpH in the Δ*cydAB* strain, experiments with CCCP and nigericin were repeated with this strain figure 3.26. The changes in OCR and cytochrome oxidation seen on the addition of increasing concentrations of CCCP closely match those observed in the WT. In the case of nigericin, the initial oxidation of the *b* and *c* cytochromes followed by a period of recovery to steady state conditions also matches observations made in the WT. The recovery of OCR in Δ*cydAB* cells is faster than that in WT cells (approximately 6 mins in Δ*cydAB* versus 15 mins in WT). This may be due to cells altering the levels of ion transporters in their cell membranes in response to the absence of cytochrome *bd* oxidase, allowing them to offset the effects of nigericin more rapidly than WT cells.

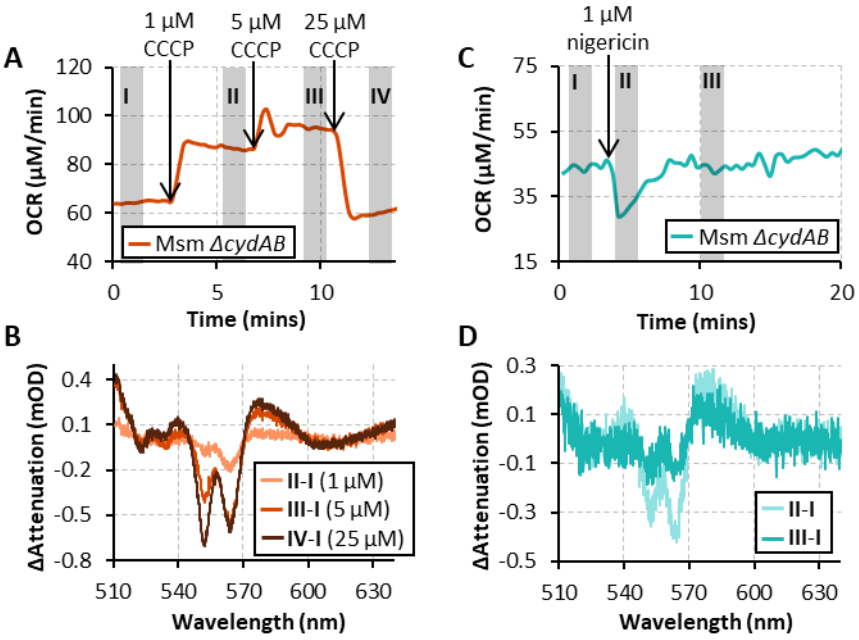

Figure 3.26*: Changes in OCR and cytochrome oxidation state on the addition of (**A**,**B**) CCCP or (**C**,**D**) nigericin to M. smegmatis* Δ*cydAB. Difference spectra in (**B**,**D**) were acquired by subtracting spectra averaged over the labelled shaded regions in (**A**,**C**) respectively. Arrows represent the time of additions, with concentrations*

*corresponding to the total concentration of the relevant compound in the chamber following each addition. Cells were grown in 7H9 media with Tween 80 (0.05% v/v) and glycerol (50 mM), and were resuspended in 7H9 supplemented with 50 mM glycerol. The OD_{600} of each sample was (**A**,**B**) 1.5 or (**C**,**D**) 1.6.*

Neither of these sets of results matches those observed with BDQ, discounting the possibility that the Δ*cydAB* simply behaves differently to the WT in response to the addition of an uncoupler or proton/potassium ionophore. This lends more evidence to BDQ acting as a direct inhibitor of ATP synthase, with cytochrome *bd* oxidase effectively acting as a relief valve to reduce the impacts of backpressure on the cell.

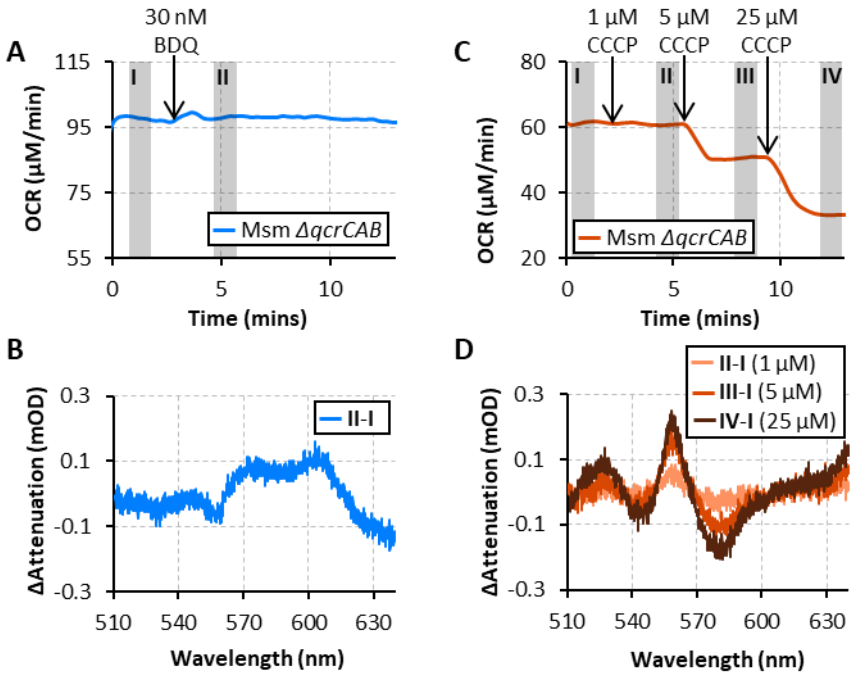

***Figure 3.27**: Changes in OCR and cytochrome oxidation state on the addition of (**A**,**B**) BDQ or (**C**,**D**) CCCP to M. smegmatis ΔqcrCAB. Difference spectra in (**B**,**D**) were acquired by subtracting spectra averaged over the labelled shaded regions in (**A**,**C**) respectively. Arrows represent the time of additions, with concentrations corresponding to the total concentration of the relevant compound in the chamber following each addition. Cells were grown in 7H9 media with Tween 80 (0.05% v/v) and glycerol (50 mM), and were resuspended in 7H9 supplemented with glycerol (50 mM). The OD_{600} of each sample was (**A**,**B**) 1.7 or (**C**,**D**) 1.6.*

To further demonstrate this, an experiment was conducted where BDQ was added to *M. smegmatis* Δ*qcrCAB* cells which lack a functioning supercomplex. The expectation was that no increase in OCR should be observed with BDQ as all electrons should already be running through cytochrome *bd* oxidase and so no rerouting to the enzyme could occur and this is indeed what was observed (figure 3.27).

For comparison Δ*qcrCAB* cells were also treated with CCCP. Unlike in WT cells, no increase in OCR occurs on addition of 1 µM CCCP. This is because the OCR increase in the WT strain is due to an increase in activity of the supercomplex as the cell attempts to counteract the effects of the uncoupler on the PMF, which cannot occur in Δ*qcrCAB* cells. The drop in OCR occurring at a lower concentration is similarly due to cells being unable to compensate for the impact of CCCP due to the lowered proton-pumping capacity of the ETC, leading to disruption of PMF-linked processes.

The cytochrome spectra in both sets of Δ*qcrCAB* experiments do not resemble those recorded with the WT, as cytochromes in the supercomplex are the main contributors to these spectra, while cytochrome *bd* oxidase cytochromes will be the main contributors in Δ*qcrCAB* experiments. Interestingly, BDQ and CCCP seem to have opposite effects on these cytochromes than those seen with cytochromes belonging to the supercomplex. When BDQ is added to Δ*qcrCAB* cells, a small dip at 558 nm is seen in the difference spectra reflecting oxidation of the *b* cytochromes contained in cytochrome *bd* oxidase. On addition of CCCP to cells, an increase in attenuation is observed at this wavelength, showing the *b* cytochromes are reducing. To better understand this phenomenon, further study and reference spectra of cytochrome *bd* oxidase are required. For the sake of studying BDQ's mechanism, these data support the conclusion of cytochrome *bd* oxidase activity being responsible for the OCR increase observed with BDQ in the WT and that BDQ and CCCP have distinctly different mechanisms.

3.4. BDQ AND *M. TUBERCULOSIS*

3.4.1. Action of BDQ in *M. tuberculosis*

In order to study BDQ's mechanism in BSL-2 compatible *M. tuberculosis*, an appropriate concentration of BDQ to use in these experiments had to be found. Using the same concentration as for *M. smegmatis* (30 nM), results in no notable change in OCR or cytochrome oxidation state (figure 3.28). This is likely because the MIC of BDQ is higher in *M. tuberculosis* versus *M. smegmatis* (54 nM compared to 12.6 nM) (Andries et al., 2005). There is a slight increase in OCR when the total concentration of BDQ in the chamber is brought up to 60 nM and peaks from the *b* and *c* cytochromes appear in the difference spectrum. These effects increase in magnitude with further additions of BDQ.

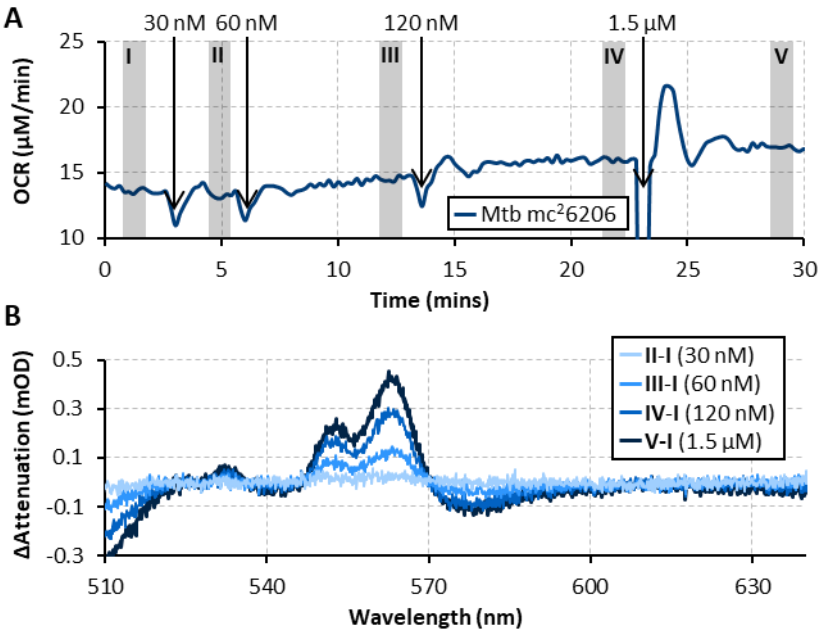

***Figure 3.28**: Changes in OCR and cytochrome oxidation state on the addition of BDQ to M. tuberculosis mc²6206. Difference spectra in (**B**) were acquired by subtracting spectra averaged over the labelled shaded regions in (**A**). Arrows represent the time of additions, with concentrations corresponding to the total concentration of the BDQ in the chamber following each addition. Cells were grown in 7H9 supplemented with Tween 80 (0.05% v/v), glycerol (55 mM), Middlebrook OADC (10% v/v), pantothenate (48 µg/mL) and leucine (0.5 mg/mL) and were washed and resuspended in growth*

media excluding Tween 80 and OADC. The OD_{600} of the sample in the chamber was 4.8.

120 nM was selected as the best concentration for future experiments as at this concentration there are clear changes in the OCR and cytochrome oxidation states. Greater effects are observed with 1.5 µM BDQ but as BDQ has been theorised to have different effects on cells at nanomolar versus micromolar concentrations (Guo et al., 2021), it was desirable to perform initial experiments using nanomolar concentrations of BDQ that are closer to the MIC before examining the impacts of micromolar concentrations of BDQ. Additionally, by selecting a concentration close to the MIC, BDQ is less likely to display off-target effects which may confuse the interpretation of results.

After this initial experiment, the switch to using *M. tuberculosis* mc^26230 was made so the results could be compared to those obtained with the available cytochrome *bd* oxidase knockout strain, *M. tuberculosis ΔcydAB.* Versus ethanol controls, addition of 120 nM BDQ to mc^26230 cells results in a gradual increase in OCR and reduction of the *b* and *c* cytochromes (figure 3.29). This is similar to the effects observed in *M. smegmatis* WT, with the prolonged response time possibly being a result of there being a lower electron flux through the ETC in the slower-growing *M. tuberculosis.*

The increase in OCR is ultimately larger in *M. tuberculosis*, which is likely due to there being a larger proportion of cytochrome *bd* oxidase in the ETC than there is in *M. smegmatis* WT under the growth conditions used. Unlike in *M. smegmatis,* a small decrease in OCR is observed with mc^26230 ethanol controls rather than an increase. This can be explained by *M. tuberculosis* cells' longer doubling time meaning there is little to no cell growth over the course of the experiment, with the decrease possibly being related to the lack of OADC in the resuspension media.

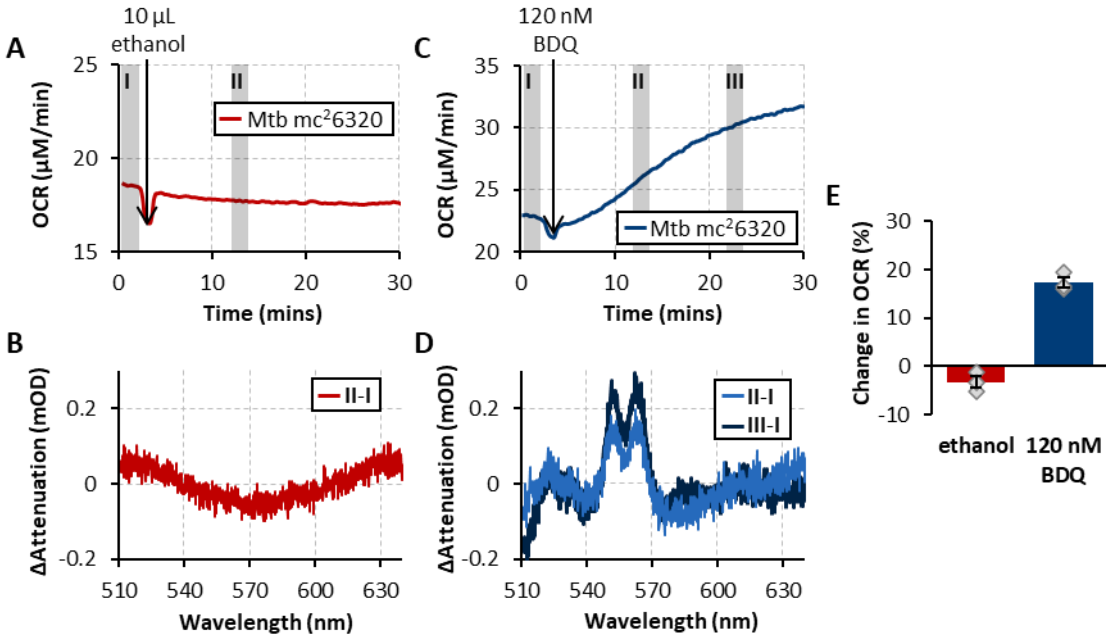

***Figure 3.29**: Changes in OCR and cytochrome oxidation state on addition of BDQ to M. tuberculosis mc²6230 versus ethanol-only controls. Difference spectra in (**B,D**) were acquired by subtracting spectra averaged over the labelled shaded regions in (**A,C**) respectively. (**E**) Mean percentage change in OCR 10 mins after the addition of ethanol or 120 nM BDQ, with the grey diamonds representing individual datapoints and the error bars showing standard error. Cells were in grown in 7H9 supplemented with Tween 80 (0.05% v/v), glycerol (55 mM), Middlebrook OADC (10% v/v) and pantothenate (48 µg/mL) and were resuspended in 7H9 supplemented with glycerol (55 mM) and pantothenate (48 µg/mL). The OD_{600} of samples in (**A,B,C,D**) was 5.6.*

Having shown BDQ displays similar effects in both species, the next stage of demonstrating BDQ's mechanism in *M. tuberculosis* is to compare its effects with those of CCCP, nigericin and DCCD (figure 3.30). Much like in *M. smegmatis* WT, CCCP and nigericin have different effects to BDQ, however there are some differences between the effects of each compound on the two species.

Early experiments with CCCP in the mc²6206 strain showed little change on the addition of 1 µM to *M. tuberculosis* cells, so only the two higher concentrations used in experiments with *M. smegmatis* were added to samples of mc²6320. The impact of CCCP on OCR in *M. tuberculosis* mc²6320 is very similar to the results obtained with

M. smegmatis WT; a sharp increase is observed with 5 µM which then drops when the concentration of CCCP is raised to 25 µM.

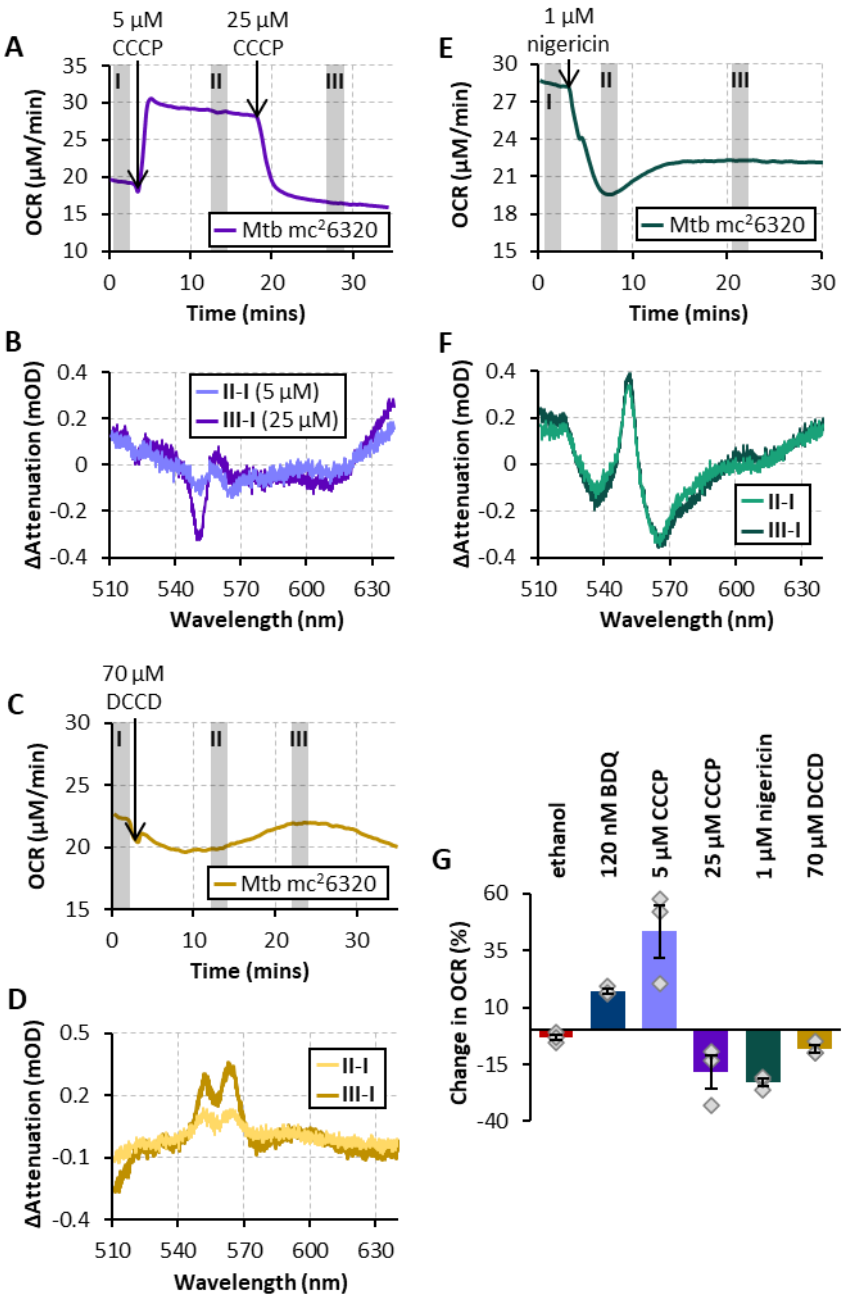

***Figure 3.30**: Changes in OCR and cytochrome oxidation state on the addition of (**A**,**B**) CCCP, (**C**,**D**) DCCD or (**E**,**F**) nigericin to M. tuberculosis mc²6320. (**G**) Mean percentage change in OCR 10 mins after the addition of each compound relative to the OCR before any additions, with the grey diamonds representing individual datapoints and the error bars showing standard error. The ethanol and BDQ data shown is the same as in figure 3.32 and is repeated here for comparison. Difference spectra in (**B**,**D**,**F**) were acquired*

*by subtracting spectra averaged over the labelled shaded regions in (**A**,**C**,**E**) respectively. Arrows represent the time of additions, with concentrations corresponding to the total concentration of the relevant compound in the chamber following each addition. Cells were in grown in 7H9 supplemented with Tween 80 (0.05% v/v), glycerol (55 mM), Middlebrook OADC (10% v/v) and pantothenate (48 µg/mL) and were resuspended in 7H9 supplemented with glycerol (55 mM) and pantothenate (48 µg/mL).The OD_{600} values of all samples were between 4.9-7.7.*

There is a notable difference in how CCCP affects cytochrome oxidation state in the two species. In *M. smegmatis* WT the *b* and *c* cytochromes oxidise at both concentrations, while in *M. tuberculosis*, the *b* cytochromes appear to reduce on addition of 5 µM CCCP while the *c* cytochromes oxidise as the CCCP concentration is increased. The reason for this difference is likely due to the ETC in each species having slightly different compositions. The changes in the *b* cytochromes in *M. tuberculosis* are more similar to those observed in *M. smegmatis ΔqcrCAB*, which may be due to higher amounts of cytochrome *bd* oxidase being present in *M. tuberculosis* mc^26320 compared to *M. smegmatis* WT.

Addition of 1 µM nigericin to *M. tuberculosis* mc^26320 leads to a rapid drop in OCR which is followed by a gradual increase before the OCR plateaus at around 80-85% of the original OCR. This incomplete recovery suggests *M. tuberculosis* is more susceptible to the effects of nigericin. Combined with the observations in *M. smegmatis WT* and *ΔcydAB*, there appears to be an inverse correlation between the amount of cytochrome *bd* oxidase in the ETC and how quickly/well cells are able offset the effects of nigericin. The precise mechanisms behind this, i.e. whether the better recovery is due to the increased activity of the supercomplex when there is little to no cytochrome *bd* oxidase or whether certain ion transporters are upregulated/downregulated depending on how much cytochrome *bd* oxidase is present, is unclear and requires further study.

There is a large difference in the changes in cytochrome oxidation state on the addition of nigericin between *M. smegmatis* and *M. tuberculosis*, with the *c* cytochromes in *M. tuberculosis* mc^26320 reducing compared to the oxidation

observed in *M. smegmatis*. Similar to the differences in cytochrome oxidation between the two species seen with CCCP, this is likely due to different proportions of enzymes being present in the membranes of the two species. Despite these differences, it is clear neither compound has the same effects as BDQ in *M. tuberculosis*.

70 µM DCCD was found to be the highest concentration that can be added to *M. tuberculosis* before a sharp drop in OCR is observed, showing off-target effects occur at higher concentrations. When 70 µM DCCD is added to *M. tuberculosis* mc^26320, there is a gradual reduction of the *b* and *c* cytochromes, similar to the effects seen with BDQ. The two compounds appear to have different effects on the OCR however, with there being a decrease in OCR after addition of DCCD, followed by an increase that peaks around 20-23 mins after addition before the OCR starts to decrease again. The increase in OCR around 20 mins is not seen in ethanol controls and is consistently observed in experiments with DCCD, showing it is a delayed effect of adding DCCD. The reasons behind this may be related to DCCD's lack of specificity as an ATP synthase inhibitor combined with lower electron flux through the ETC in *M. tuberculosis* compared to *M. smegmatis*.

Although the impact of DCCD on *M. tuberculosis* is not identical to that of BDQ, the two still demonstrate more similar effects on the oxidative phosphorylation system compared to CCCP and nigericin, giving further evidence that BDQ acts as a direct inhibitor of ATP synthase in *M. smegmatis* and *M. tuberculosis*. These results also highlight the difficulty of not having an established ATP synthase inhibitor in mycobacteria with a higher specificity than DCCD with which to compare BDQ to.

3.4.2. Effects of BDQ in *M. tuberculosis ΔcydAB*

If the OCR increase observed with BDQ in *M. tuberculosis* is due to increased activity of cytochrome *bd* oxidase, then addition of BDQ to *M. tuberculosis ΔcydAB* should have similar effects to those observed with *M. smegmatis ΔcydAB*. When 120 nM BDQ is added to *M. tuberculosis ΔcydAB*, there is the same reduction of the *b* and *c* cytochromes as is seen with the mc^26320 strain, however there is not a sharp drop in OCR (figure 3.31). Overall, a gradual increase in OCR is observed, although in one

repeat this was preceded by an initial decrease over the first 10 mins following the addition of BDQ. Despite the variation between repeats, the increase in OCR in M. *tuberculosis ΔcydAB* is consistently lower than that observed in mc^{2}6320 cells over the 30-min course of the experiment.

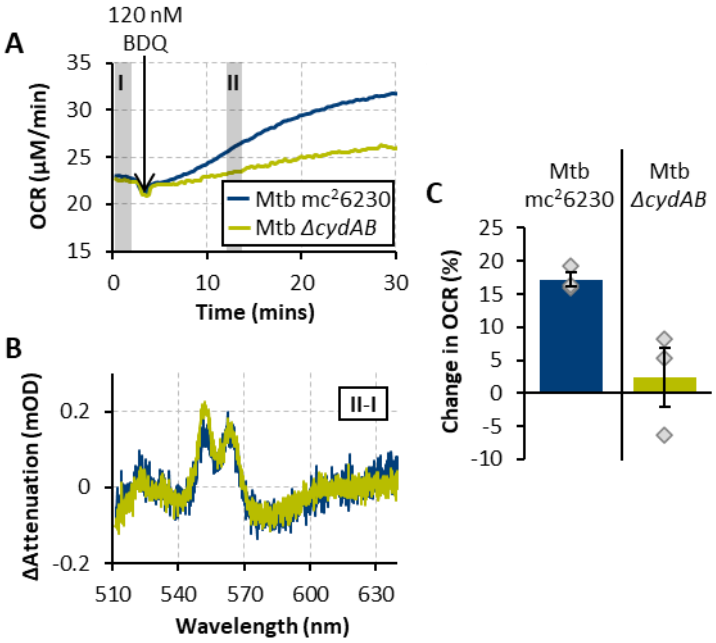

***Figure 3.31**: (**A**,**B**) Changes in OCR and cytochrome oxidation state on the addition of 120 nM BDQ to M. tuberculosis mc^{2}6230 and ΔcydAB. (**C**) Mean percentage change in OCR 10 mins after the addition of BDQ relative to the OCR before addition, with the grey diamonds representing individual datapoints and the error bars showing standard error. The mc^{2}6230 data shown is the same as in figure 3.32 and is included for comparison purposes. Difference spectra in (**B**) were acquired by subtracting spectra averaged over the labelled shaded regions in (**A**). Arrows represent the time of BDQ addition. Cells were in grown in 7H9 supplemented with Tween 80 (0.05% v/v), glycerol (55 mM), Middlebrook OADC (10% v/v) and pantothenate (48 µg/mL) and were resuspended in 7H9 supplemented with glycerol (55 mM) and pantothenate (48 µg/mL). The OD_{600} of the mc^{2}6230 sample was 5.6 and the OD_{600} of the ΔcydAB sample was 4.9.*

These results demonstrate cytochrome *bd* oxidase is partially responsible for the OCR increase observed with BDQ in mc^{2}6320 cells, however the lack of a significant

decrease demonstrates the differences in response to BDQ between *M. smegmatis* and *M. tuberculosis*. There are a couple of possible explanations for this, with one being that the lower electron flux through the *M. tuberculosis* ETC makes it less susceptible to immediate backpressure on inhibition of ATP synthase. Alternatively, *M. tuberculosis* may have other mechanisms to limit a build-up of the PMF that are not present in *M. smegmatis*, with one possibility being increased or different ion transporters.

Another possibility is that there is more NDH-1 present in *M. tuberculosis* cells compared to *M. smegmatis*, a theory that is supported by the finding that slow growing *M. bovis* BCG has a lower ratio of NDH-2 to NDH-1 activity compared to *M. smegmatis* (Vilchèze et al., 2005). If this is the case, then *M. tuberculosis* is able to further limit the impact of backpressure on the oxidative phosphorylation system by routing electrons through NDH-2 instead of NDH-1, while in *M. smegmatis* the flux through NDH-1 is already so low, routing electrons away from the complex has little effect compared with the activation of cytochrome *bd* oxidase. This theory could be tested by treating *M. tuberculosis* Δ*cydAB* cells with an NDH-1 inhibitor prior to the addition of BDQ, however this would require the NDH-1 inhibitor to have no off-target effects in *M. tuberculosis.* A double knockout strain of *M. tuberculosis* lacking the genes for NDH-1 and cytochrome *bd* oxidase could also be used to study this idea providing such a strain proved viable.

To further distinguish the activity of BDQ from CCCP and nigericin, experiments using these compounds were performed with *M. tuberculosis* Δ*cydAB*, along with DCCD (figure 3.32). Overall CCCP has similar effects in both mc^26320 and Δ*cydAB*, with there being some difference in the magnitude of the OCR changes, however as there is some variation within the results obtained with each strain, this is not indicative of a noteworthy difference between how the strains respond to uncoupling. As the difference spectra are similar in both strains, the presence of more cytochrome *bd* oxidase does not appear to be the cause of the differences between changes in spectra on CCCP addition between *M. smegmatis* and *M. tuberculosis*.

Similar to the observations made in *M. smegmatis*, deletion of the *cydAB* genes in *M. tuberculosis* appears to aid the recovery of the bacteria towards steady state conditions following the addition of nigericin. The OCR returns to that before the introduction of nigericin after a period of around 25 mins, however little change is observed in the cytochrome spectra. The sharp peak at 552 nm shows the reduction of the *c* cytochromes, although without the ability to fit spectra, it is difficult to determine whether this reduction is of a similar magnitude to that observed in mc^26320.

When DCCD is added to the *M. tuberculosis* Δ*cydAB*, changes in cytochrome oxidation are similar to those in mc^26230. The change in OCR follows a similar pattern, with an initial decrease followed by a gradual increase and subsequent decrease, however in Δ*cydAB* the peak in OCR occurs later (around 33 mins after addition versus around 23 mins in mc^26230) and is larger, with these differences being consistent across repeats. That an OCR increase is observed is not surprising given the increase seen with BDQ and DCCD's poorer selectivity for ATP synthase, with the later peak indicating some of the increase seen in mc^26230 may be due to the activation of cytochrome *bd* oxidase, The other mechanisms responsible for reducing the impact of backpressure on the system may have a slower activation period while the larger increase in OCR might be due to the components required for these mechanisms, be they ion transports or NDH-2, being upregulated in the absence of cytochrome *bd* oxidase.

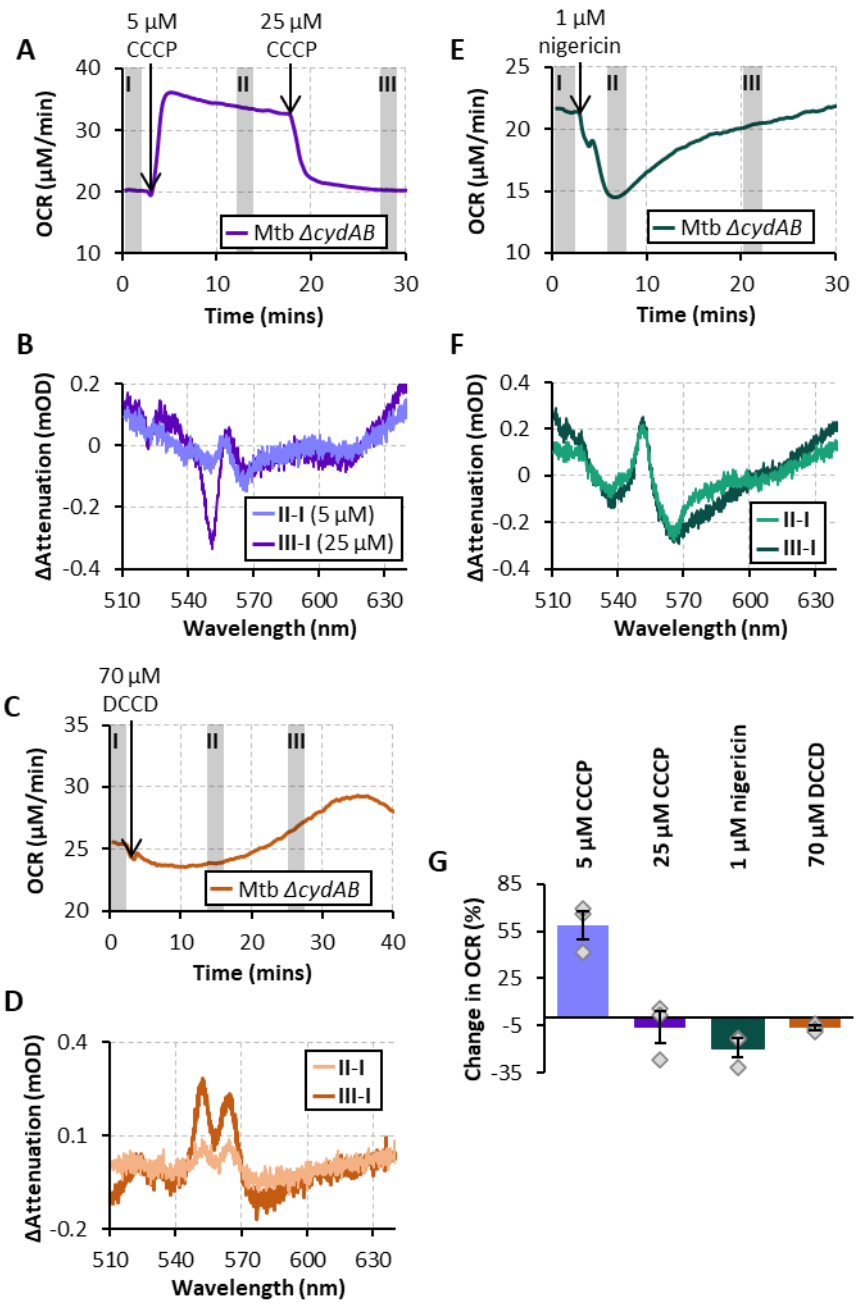

***Figure 3.32**: Changes in OCR and cytochrome oxidation state on the addition of (**A**,**B**) CCCP, (**C**,**D**) DCCD or (**E**,**F**) nigericin to M. tuberculosis ΔcydAB. (**G**) Mean percentage change in OCR 10 mins after the addition of each compound relative to the OCR before any additions, with the grey diamonds representing individual datapoint and the error bars showing standard error. Difference spectra in (**B**,**D**,**F**) were acquired by subtracting spectra averaged over the labelled shaded regions in (**A**,**C**,**E**) respectively. Arrows represent the time of additions, with concentrations corresponding to the total concentration of the relevant compound in the chamber following each addition. Cells*

were in grown in 7H9 supplemented with Tween 80 (0.05% v/v), glycerol (55 mM), Middlebrook OADC (10% v/v) and pantothenate (48 µg/mL) and were resuspended in 7H9 supplemented with glycerol (55 mM) and pantothenate (48 µg/mL). The OD_{600} values of all samples were between 4.9-5.6.

Overall, these results demonstrate that while there are differences between the responses of *M. smegmatis* and *M. tuberculosis* to compounds that affect the oxidative phosphorylation system, BDQ appears to act via the same mechanism in both, i.e. direct inhibition of ATP synthase. The reasons for the OCR increase in *M. tuberculosis* Δ*cydAB* seen with both BDQ and DCCD should be explored further to see if the mechanisms behind this increase can be inhibited to increase BDQ's killing effect.

3.5. EXPLORING WHETHER BDQ'S MECHANISM IS CONCENTRATION DEPENDENT

Having established BDQ's mechanism at nanomolar concentration, the question of whether BDQ has a different dominant mode of action at micromolar concentrations, as has been proposed in the literature (Guo et al., 2021; Courbon et al., 2023), needs to be studied. To test this, the experiments with BDQ were repeated, this time using a concentration of 10 µM, in *M. smegmatis* WT and *ΔcydAB* along with *M. tuberculosis* mc^26320 and *ΔcydAB* (figure 3.33). The cytochrome *bd* oxidase knockout strains were included as if BDQ does show protonophore activity at micromolar concentrations, then it should have similar effects to CCCP, i.e. an OCR increase should occur regardless of the presence of cytochrome *bd* oxidase, in addition to different changes in cytochrome spectra being observed. In the event BDQ acts a proton/potassium ionophore at higher concentrations, then similar effects to nigericin should be observed across all strains.

There is very little difference between the effects seen with the two concentrations in both *M. smegmatis* strains. This indicates BDQ is acting predominantly as a direct ATP synthase inhibitor at both nanomolar and micromolar concentrations.

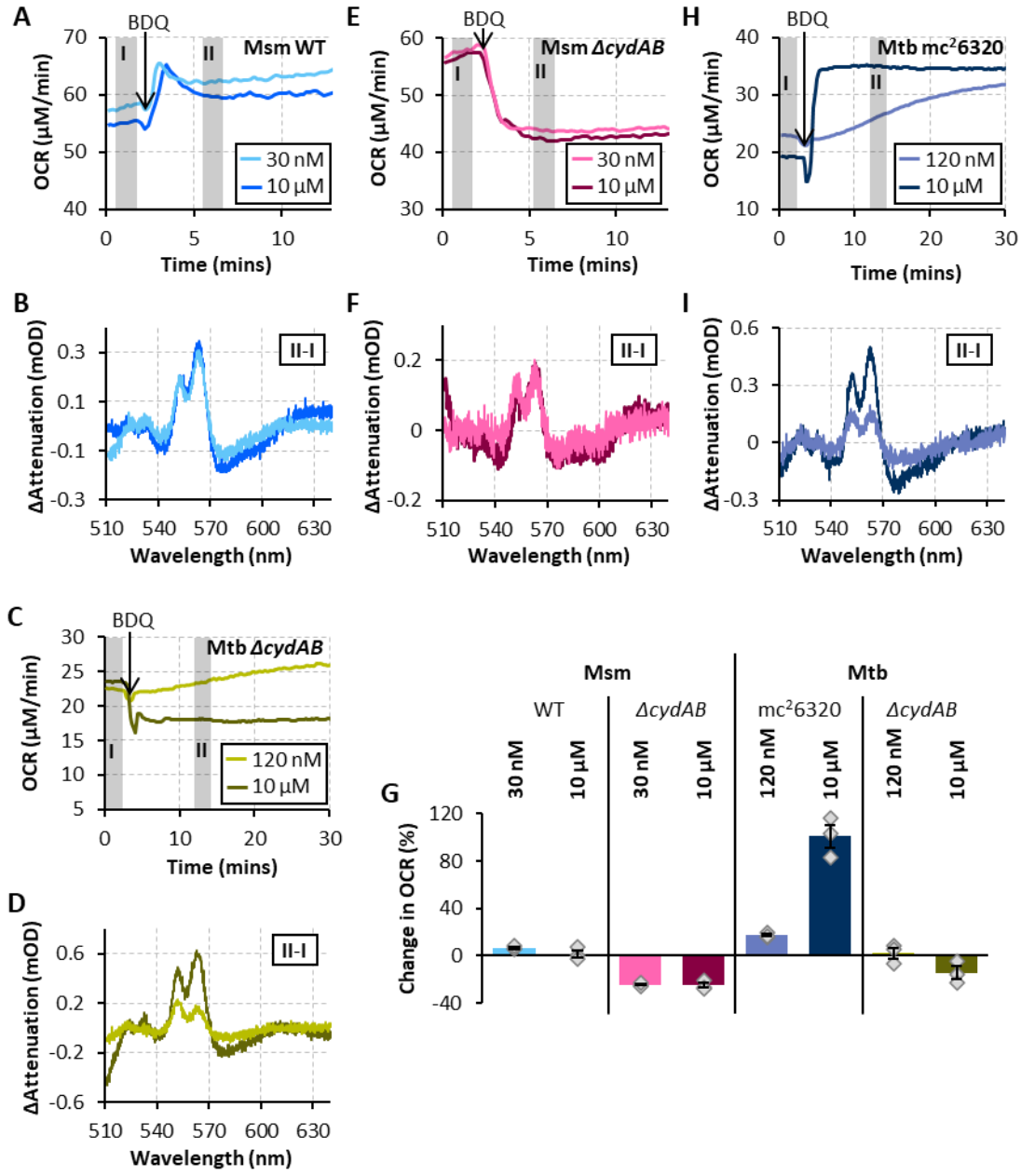

***Figure 3.33**: Changes in OCR and cytochrome oxidation state on the addition of nanomolar and micromolar amounts of BDQ to (**A**,**B**) M. smegmatis WT, (**C**,**D**) M. tuberculosis ΔcydAB, (**E**,**F**) M. smegmatis ΔcydAB and (**H**,**I**) M. tuberculosis mc²6320. (**G**) Mean percentage change in OCR 3 mins after the addition of BDQ to M. smegmatis and 10 mins after the addition of BDQ to M. tuberculosis relative to the OCR before addition, with the grey diamonds representing individual datapoints datapoint and the error bars showing standard error. The nanomolar concentration data shown is the same as in chapters 3.3 and 3.4 and is included for comparison purposes. Difference spectra in (**B**, **D**, **F**, **H**) were acquired by subtracting spectra averaged over the labelled*

*shaded regions in (**A, C, E, I**) respectively. Arrows represent the time of BDQ addition. M. smegmatis cells were grown in 7H9 supplemented with Tween 80 (0.05% v/v) and glycerol (50 mM) and were resuspended in 7H9 supplemented with glycerol (50 mM). M. tuberculosis cells were in grown in 7H9 supplemented with Tween 80 (0.05% v/v), glycerol (55 mM), Middlebrook OADC (10% v/v) and pantothenate (48 µg/mL) and were resuspended in 7H9 supplemented with glycerol (55 mM) and pantothenate (48 µg/mL).The OD_{600} of M. smegmatis samples was between 0.9-1.9 and the OD_{600} of M. tuberculosis samples was between 4.9-7.0.*

In *M. tuberculosis* mc^26230, BDQ's effects on cells occur more rapidly with 10 µM compared to the 120 nM dose, with the sharper increase in OCR being more similar to the increase seen with CCCP. However, the clear reduction of both the *b* and *c* cytochromes shows this sharper increase is not due to BDQ uncoupling the oxidative phosphorylation system. Instead, these faster changes at a higher concentration may be due to more BDQ being able to initially diffuse through the cell wall and bind to ATP synthase.

When 10 µM BDQ is added to *M. tuberculosis* Δ*cydAB*, much like in mc^26230, a more rapid reduction of the *b* and *c* cytochromes is observed. This is accompanied by a drop in OCR which is not seen at 120 nM, although the percentage decrease is still less than that in *M. smegmatis*. These results, combined with those in mc^26230, suggest cytochrome *bd* oxidase contributes significantly to the OCR increase observed in *M. tuberculosis* cells containing the enzyme on exposure to BDQ. At nanomolar concentrations, the lower respiratory rate of *M. tuberculosis* compared to *M. smegmatis* combined with less BDQ being available to immediately bind to ATP synthase means cells are not as affected by backpressure. When the concentration of BDQ is increased, complete inhibition of ATP synthase can occur immediately, and thus the activity of cytochrome *bd* oxidase is increased rapidly in response.

All of these results demonstrate BDQ's dominant mode of action is direct inhibition of ATP synthase, independent of concentration. As there is no evidence of the cytochromes oxidising when micromolar concentrations of BDQ are added to cells, if

BDQ is able to act as a protonophore or ionophore, this activity is not the major contributor to its bacteriostatic or bactericidal effects.

3.6. BDQ AND CFZ

BDQ acting as an ATP synthase inhibitor rather than an uncoupler has a number of implications for the cell. One of these is that the cytoplasm of the cell should become a more reducing environment. To further support the conclusion about BDQ's mode of action, a way to measure this effect was sought.

One potential option is using the bioenergetic chamber to monitor changes in the absorbance of the redox cycling CFZ. CFZ's strong absorbance at 495 nm in its monoprotonated form means its impact on cytochromes cannot easily be studied using the bioenergetic chamber, however it is possible to measure the absorbance of CFZ itself. CFZ loses its absorbance when reduced (Yan et al., 2011) and so it was theorised that when the environment of the cell becomes more reducing, i.e. on the addition of BDQ, a drop in the absorbance of CFZ would be observed. A further reason for using CFZ is that it has been shown to be synergistic with BDQ against *M. tuberculosis* (Cokol et al., 2017). If BDQ increases the level of CFZ reduction, and therefore the production reactive oxygen species, this provides a possible explanation for this observation and highlights redox cycling compounds as good candidates for future drug combinations with BDQ.

To test this hypothesis, experiments were run comparing the change in absorbance of CFZ over time with and without the addition of 30 nM BDQ in *M. smegmatis* WT (figure 3.34). A concentration of 750 nM CFZ was chosen to ensure the contribution of peaks due to changes in cytochrome oxidation state would be comparatively small.

Comparing the two sets of results, a smaller CFZ peak is observed in the presence of 30 nM BDQ and this appears to decrease further over time, indicating more reduction of CFZ. This observation supports the use of CFZ as a possible method for examining BDQ's effects on reductive stress in cells, however it is complicated by a possible baseline shift occurring, given the changes in attenuation at the higher wavelength

end of the spectra where CFZ should not absorb. This may be a result of CFZ precipitating out of solution and affecting the scatter of light in the chamber.

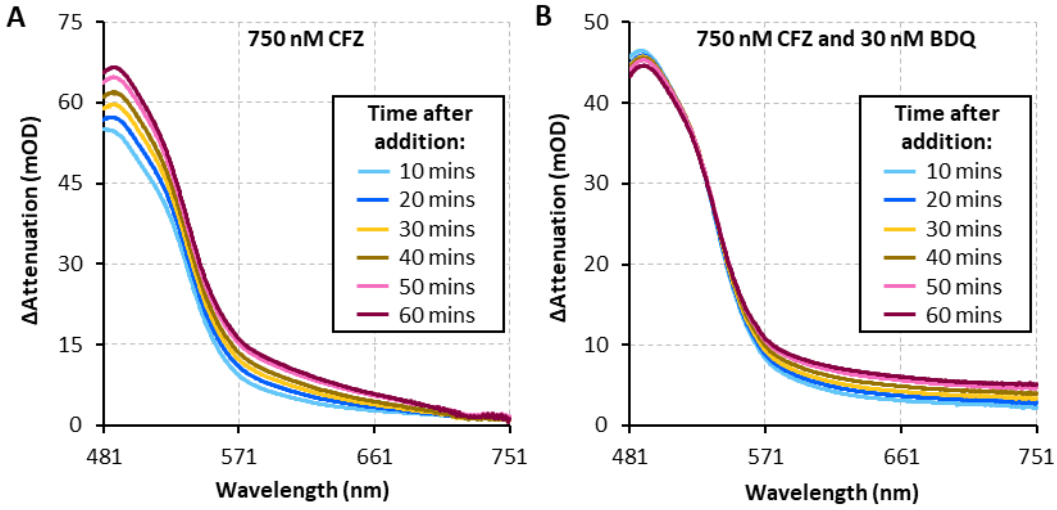

Figure 3.34: *Changes in Δattenuation over time when CFZ is added to M. smegmatis WT cells (**A**) in the absence of BDQ and (**B**) in the presence of 30 nM BDQ. Difference spectra were acquired by averaging spectra over a period of 1 min at the relevant time points and subtracting a spectrum recorded before CFZ (and BDQ) were added. M. smegmatis cells were grown in 7H9 supplemented with Tween 80 (0.05% v/v) and glycerol (50 mM) and were resuspended in 7H9 supplemented with glycerol (50 mM). The OD_{600} of each sample was (**A**) 1.6 or (**B**) 1.2.*

Another study was performed, this time using a lower concentration of CFZ to prevent possible precipitation from impacting the difference spectra (figure 3.35). As the change observed in CFZ absorbance with BDQ appears to be immediate, the procedure was also modified to compare the absorbance of CFZ with and without BDQ to the reduced conditions induced by the addition of potassium cyanide and sodium dithionite.

Unfortunately, between these sets of experiments, the bioenergetic chamber developed a fault with its wide-range CCD, meaning data could only be collected using the narrow-range CCD. The grating of the narrow-range CCD can be altered to record over a wider wavelength but only noise is recorded at any wavelength below 502 nm,

thus the chamber was no longer able to record the absorbance of CFZ at its peak wavelength.

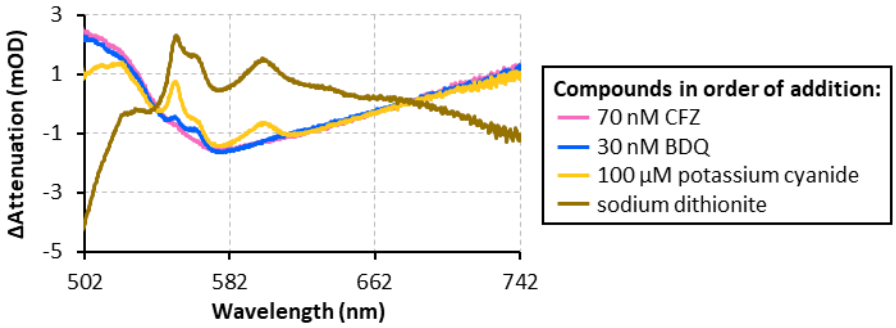

Figure 3.35: *Changes in Δattenuation on addition of CFZ to M. smegmatis WT cells, followed by additions of BDQ, potassium cyanide and sodium dithionite. Difference spectra were acquired by averaging spectra over a period of 1 min at the relevant time points and subtracting a spectrum recorded before CFZ was added. M. smegmatis cells were grown in 7H9 supplemented with Tween 80 (0.05% v/v) and glycerol (50 mM) and were resuspended in 7H9 supplemented with glycerol (50 mM). The* OD_{600} *of the sample was 1.6.*

Experiments with CFZ proceeded in *M. smegmatis* WT to see if it would still be possible to observe changes in CFZ on addition of BDQ over this more limited wavelength range. While a drop in CFZ absorbance is observed on addition of potassium cyanide and sodium dithionite, little change is seen on the addition of BDQ. This may be because the results obtained with 750 nM CFZ are affected by precipitation of the compound. Alternatively, BDQ may impact CFZ absorbance to a modest degree that is only detectable in the 480-500 nm region.

Overall, these results are inconclusive as to whether CFZ absorbance has the potential to be used as a measure of reductive stress in mycobacteria. Without replacement of the wide-range CCD or other modification to the bioenergetic chamber, it is unsuitable for investigating this matter further.

3.7. CONCLUSIONS AND FUTURE WORK

3.7.1. Strengths and weaknesses of the bioenergetic chamber

The results in this chapter demonstrate the power of the bioenergetic chamber in studying metabolism in live cells. While developing a method for using the chamber with mycobacteria was not trivial, the ability to simultaneously observe changes in OCR and cytochrome oxidation state, and then compare the effects of different compounds, has provided significant proof in understanding BDQ's mode of action in a manner not previously achieved, with these findings being summarised in section 3.7.2.

Some other strengths of the bioenergetic chamber include the ability to observe whether compounds have an immediate impact on, and are therefore active, against different species, as well as at what concentrations these effects occur. Although this does not negate the use of MIC assays, it can be used to do a preliminary evaluation of compounds targeting cellular bioenergetics and inform the range of concentrations that should be tested in a more thorough assay. Being able to view results in real-time also means experiments to determine the appropriate concentration of compounds to use usually only need to be conducted once, with subsequent amounts of the compound being added, instead of performing multiple repeats with different starting concentrations.

The potential to quantitatively measure changes in cytochrome oxidation state and $\Delta\Psi$ is another attractive feature of the device however the difficulty of acquiring the data to make these measurements means these features could not be exploited while studying BDQ's mechanism. With further research into the complexes in the ETC of *M. smegmatis*, it is possible these features will be able to be applied to this species. Ideally this would also allow further study of *M. tuberculosis*, however given the differences observed between the two species on the addition of CCCP and nigericin, reference data acquired using isolated *M. tuberculosis* complexes should be obtained and used instead for this species. Additionally, should the chamber be applied to the study of a different genus of microorganism, a new set of model spectra would need to be acquired before quantitative measurements could be made.

Another downside is the need for fully oxidised and reduced reference spectra to make these measurements. Reduction of cytochromes is possible through a combination of anoxia and reducing agents, however oxidation requires effective inhibitors of early complexes in the chain, which are not always available as evidenced in this work.

Although a single experiment in the bioenergetic chamber provides a significant insight into the bioenergetics of the cell, the time required for preparation of samples as well as of the chamber itself, makes performing repeat experiments significantly more laborious than techniques where repeats can be performed simultaneously. This, in turn, presents difficulties in terms of statistical analysis, for example, to perform t-tests to show the effects of BDQ, CCCP, Nigericin and DCCD are significant compared to ethanol controls, the control experiments would have to be acquired separately for each compound to minimise the risk of a false positive which comes from using the same set of results across comparisons. This translates to at least 12 (4 x 3 repeats) ethanol control runs which is the equivalent of around 18 hours of labour, with the potential for more if the data are variable.

The calibration system for the OCR readings is highly susceptible to user error, with the calibration varying depending upon the exact timepoint the readings are taken during the calibration procedure. Furthermore, while the phosphorescent membrane has advantages over a Clark electrode, its gradual degradation may further contribute to this issue. While this does call into question the accuracy of the exact OCR measurements, the percentage change should not be impacted and so these readings act as a useful method of comparison across experiments.

The environment of cells in the bioenergetic chamber must also be considered. In order to remove the detergent used for culture growth, the cells must undergo centrifugation and washing with fresh media without detergent. The impacts of these manipulations on bioenergetic systems are unknown, as are the effects of excluding detergent, and the OADC supplement in the case of *M. tuberculosis,* for the duration of an experiment using the bioenergetic chamber. The media used does not represent the environment of bacteria during the course of infection (Rustad et al., 2009).

Adjustments to the media may allow for better modelling relative to the conditions during infection but the chamber is unsuitable for macrophage studies as signals from cytochromes in the macrophages would interfere with those from mycobacteria. Therefore, the bioenergetic chamber cannot, at present, provide a true insight into the exact state of mycobacteria undergoing antibiotic treatment during human or animal infection.

The bioenergetic chamber is not suited to experiments longer than a few hours both due to concerns about the impact of light on cells and the lack of ability to maintain a sterile environment around the chamber which may lead to contamination of slow growing cultures like *M. tuberculosis*. It is possible to grow cultures under certain conditions and take samples to run in the chamber at set time points, however due to the lack of cytochrome fitting currently available and the aforementioned issues with OCR readings, it makes comparison between runs difficult. In this sense, experiments in the bioenergetic chamber would benefit from complementary studies performed using techniques that are better suited to long course experiments, such as NMR and metabolomics.

3.7.2. Summary of results and implications for the field

Overall, the bioenergetic chamber is an extremely useful technique for studying bioenergetic systems, however the high time cost means it is best suited to small studies which require few repeats. As such, the chamber does not present a complete solution to studying bioenergetic systems, but rather complements existing techniques.

To summarise the results of experiments with the bioenergetic chamber with regards to the mode of action of BDQ: addition of BDQ to *M. smegmatis* and BSL-2 compatible *M. tuberculosis* stimulates an increase in OCR and reduction of the *b* and *c* cytochromes contained in the supercomplex. These effects match those observed with the known ATP synthase inhibitor DCCD, but not those of established protonophore/ionophores, CCCP and nigericin. The increase in OCR is dependent on the presence of cytochrome *bd* oxidase, indicating this complex has a role in mitigating the impact of BDQ on the bacteria. Effects of BDQ at nanomolar and micromolar

concentrations are very similar, challenging the theory that BDQ has different modes of action at different concentrations (Guo et al., 2021; Courbon et al., 2023).

The data presented here provides sufficient evidence to conclude BDQ's mode of action across all concentrations is direct inhibition of ATP synthase, similar to oligomycin in mitochondria (Symersky et al., 2012). Despite BDQ's success as part of the BPaL regimen, one of its known side-effects is QT prolongation, which involves disruption of the electrical activity of the heart due to inhibition of hERG potassium channels and has raised safety concerns (Sutherland et al., 2019). As a result, second generation compounds of BDQ, namely TBAJ-587 and TBAJ-876, have already been developed and completed phase I clinical trials (Sutherland et al., 2019; Hoelscher et al., 2024). These compounds display higher MICs against *M. tuberculosis* and lower hERG channel inhibition (Sutherland et al., 2019). It has been concluded TBAJ-587 and TBAJ-876 act similarly to BDQ, however the understanding of their modes of action has been confused by the lack of clarity around BDQ's mode of action (Courbon et al., 2023). By providing clear evidence on BDQ's mode of action in a manner that was previously lacking in the field, this work lays the groundwork for further research on these upcoming compounds, particularly with regards to considering potential combination therapies.

Cytochrome *bd* oxidase is known to play a role in bacterial survival in the presence of stressors such as antibiotics (Kana et al., 2001; Boot et al., 2017). The results in this chapter highlight the role of this enzyme in the response of mycobacteria to BDQ, and offer some explanation for the observation that deletion of cytochrome *bd* oxidase in *M. tuberculosis* H37Rv shortens BDQ's killing time (Berny, Hartman and Jacobs, 2014). Cytochrome *bd* oxidase has been examined as a drug target, and while an inhibitor of the enzyme was identified, at the time of writing, no further development has taken place (Lee et al., 2021). It is the hope of the author that proof regarding the role of cytochrome *bd* oxidase in the response of mycobacteria to BDQ will renew interest in development of cytochrome *bd* oxidase inhibitors. Such compounds would likely display strong synergy with BDQ, allowing for development of a powerful new combination therapy.

In addition to providing insights on BDQ's mode of action, establishing a method for studying mycobacteria using the bioenergetic chamber enables significant future study pertaining to mycobacterial bioenergetics and the role of this system in cells' response to antibiotics. Results obtained with the chamber could be used to identify potential weaknesses following antibiotic treatment, highlighting potential future targets for drug development such that combination therapies may be intelligently designed. The chamber may also be used to study pre-existing drug combinations and their effects on the oxidative phosphorylation system, compared to single drug treatments. Furthermore, while this work focused on *M. smegmatis* and *M. tuberculosis*, this could be applied to NTM, following adjustments to the sample preparation protocol.

However, there are some remaining questions surrounding BDQ, such as how cytochrome *bd* oxidase is activated upon cells being exposed to BDQ and why deletion of this enzyme in *M. tuberculosis* has a less significant effect on changes in OCR than in *M. smegmatis*. The former will likely require further study of cytochrome *bd* oxidase's structure, while methods for studying the latter were discussed section 3.4.2. It is also worth re-examining CFZ as a means to monitor reductive stress in cells once the wide-range CCD is replaced. Additionally, how inhibition of ATP synthase ultimately results in mycobacterial cell death is currently unclear. As postulated in section 1.6.3, this may be linked to a drop in ATP levels from which the bacteria are unable to recover. Studies using ^{31}P NMR to monitor changes in ATP levels following BDQ addition to mycobacteria, alongside the rate of bacterial cell death, would provide evidence for this link.

The observed relationship between nigericin and cytochrome *bd* oxidase is also worth further study as it may provide further insights into how mycobacteria respond to changes in and regulate the PMF. This would require measuring changes in ΔpH and ΔΨ on the addition of nigericin to cells and the relationship between the observed OCR recovery and these changes with different amounts of cytochrome *bd* oxidase present. The ΔΨ measurements may be possible with the bioenergetic chamber, while ΔpH can be measured using ^{31}P NMR spectroscopy.

4. ^{31}P NMR

4.1. INTRODUCTION

4.1.1. NMR theory

NMR is a powerful analytical and diagnostic tool that allows for non-destructive and non-invasive measurements. Magnetic resonance imaging (MRI) is the mostly widely known application of magnetic resonance and has revolutionised diagnostic medicine.

An underrated purpose of NMR is its use in studying live cultures of microorganisms. NMR can provide real time data on changes in cellular metabolism on the scale of seconds to minutes. Although ^{1}H is the most common type of nucleus studied in a biological context, there are several other biologically relevant nuclei that NMR can provide data on, including but not limited to, ^{13}C, ^{15}N, ^{19}F, ^{23}Na and, most importantly for this project, ^{31}P (Grivet and Delort, 2009).

The theory behind NMR can be summarised as follows: nuclei with non-zero spin (I) have an intrinsic nuclear magnetic moment (μ). If placed in an external magnetic field (B_0), $I = \frac{1}{2}$ nuclei can align either with or against the field, resulting in two energy states, the difference between which is given by equation 4.1.

$$\Delta E = \omega \hbar \qquad \textbf{(Equation 4.1)}$$

ω is the Larmor frequency and is the product of the strength of the external magnetic field and the magnetogyric ratio of the nuclei, while ħ is Planck's constant divided by 2π.

At room temperature or below, an excess of nuclei will be in the lower energy state, i.e. they will be aligned with the external magnetic field, and thus the overall magnetisation vector, M_0, will be aligned with B_0 (figure 1). In addition, interaction of μ with B_0 generates a torque, resulting in individual nuclear magnetic moments precessing around B_0 at the Larmor frequency. At equilibrium, the nuclei are out of phase and so these motions cancel out. If the nuclei are irradiated at the Larmor

frequency via application of a radiofrequency (RF) pulse, M_0 will rotate into the xy-plane. In addition, the nuclei will start to precess in phase with each other, and so M_0 precesses around B_0 at the Larmor frequency. Precessing magnetisation induces an oscillating current in a detection coil surrounding the sample and this signal (free induction decay, FID) is recorded.

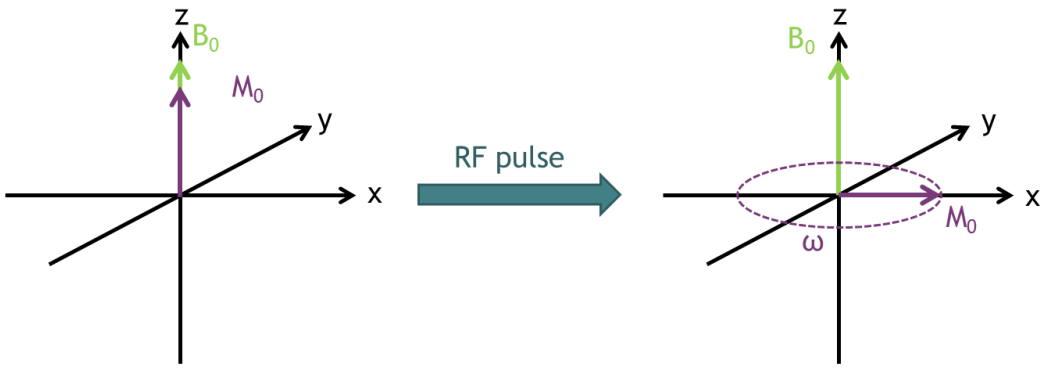

***Figure 4.1**: Illustration of magnetisation vectors in an NMR experiment, where B_0 is the applied magnetic field, ω is the Larmor frequency and M_0 is the sum of the individual magnetic moments of spin active nuclei with the same Larmor frequency or overall magnetisation vector.*

M_0 will slowly return to its equilibrium position along B_0 following application of the RF pulse, and this is known as longitudinal or T_1 relaxation. Similarly, the spins will start to dephase, reducing the xy-magnetisation and this is known as transverse or T_2 relaxation. Therefore, another RF pulse must be applied to repeat the measurement. A Fourier transform is used to convert the time domain data obtained into the frequency domain providing information on the Larmor frequencies of the nuclei in a sample.

NMR allows the identification of nuclei of the same type in different environments, as in an applied magnetic field, electrons will give rise to a small induced field, B_{ind}, aligned against B_0. The magnetic field the nuclei actually experience will be a combination of B_0 and B_{ind}, thus making the Larmor frequency of a particular nucleus dependent on the surrounding electron density. The differences in Larmor frequencies that arise due to B_{ind} fields are very small, and so the x-axis of an NMR spectrum (chemical shift, δ) is reported in terms of parts per million (ppm) of the

Larmor frequency of a set reference compound; for ^{31}P NMR this is usually 85% orthophosphoric acid.

4.1.2. Phosphorylated metabolites

There are several key components of cells that contain phosphorous and thus are of interest in *in vivo* ^{31}P NMR experiments. The area under a peak in a ^{31}P NMR spectrum is directly proportional to the concentration of the nuclei in that particular environment. Thus, NMR spectroscopy can provide information on the different phosphorous-containing compounds in a cell and their relative concentrations.

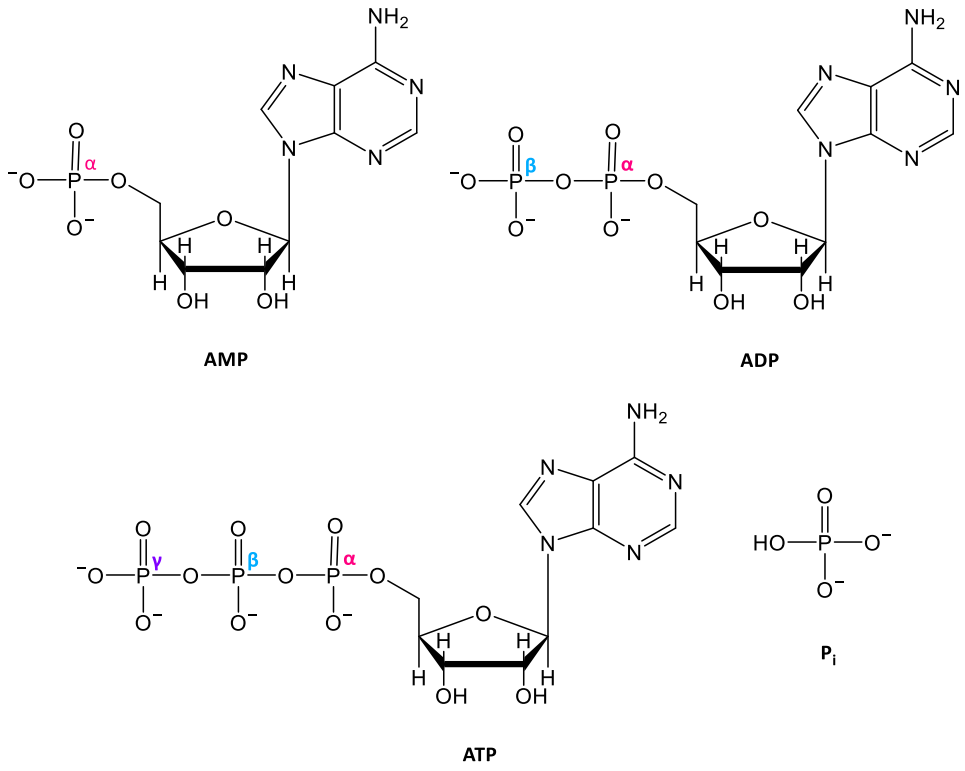

***Figure 4.2**: Structures of AMP, ADP, ATP and P_i. The protonation state of each of these molecules varies depending on pH.*

ATP, ADP and AMP along with P_i are the most crucial phosphorylated metabolites for providing information on the energetic state of a cell. In ^{31}P NMR, the signals from the α- and γ- phosphorous nuclei in ATP overlap with the α- and β- resonances of ADP, thus the β-ATP peak is the most suitable for attempting to quantify the amount of ATP (Grivet and Delort, 2009). Determining the exact concentration of ATP requires the use of an external or internal standard of known concentration. However, to roughly

monitor the changes in ATP concentration, it is simpler to compare the integrals of the β-ATP peak with the P_i peak. This ratio can provide a good indication of how the ATP concentration in cells changes over time subject to a particular stimulus.

Polyphosphates are among the other phosphorylated metabolites of interest that can provide additional information on the energetic state of cells. They are composed of multiple inorganic phosphate groups linked via phosphate-anhydride bonds and act as storage for P_i. Short chain polyphosphates can be detected via NMR providing they are solubilised (Ok-hama et al., 1986). Long chain polyphosphates cannot be detected as their T_2 relaxation times are too short (Satre, Martin and Klein, 1989).

Phospholipids are another key phosphorylated component of cells, being the main constituent of cell membranes. Phospholipids themselves appear as a very broad bump in the spectrum, making NMR spectroscopy unsuitable for direct observation of phospholipid levels. However, phosphomonoesters (PMEs), phospholipid precursors, and phosphodiesters (PDEs), phospholipid degradation products, can be clearly observed in some cells providing information on phospholipid metabolism (Daly et al., 1987; Kaplan and Cohen, 1991; Schlemmer et al., 2005).

Other phosphorous-containing compounds present at high enough concentrations inside cells are detectable by NMR, but the specific metabolites discussed are the most universally observed across *in vivo* ^{31}P NMR experiments. ^{31}P NMR can provide a unique picture of cellular energetics and metabolism in the course of a single experiment due to the simultaneous detection of these metabolites.

4.1.3. Measuring cellular pH

Aside from being used along with ATP signals to provide information on the energetics of cells, the P_i signal in ^{31}P NMR can also be used to monitor intracellular and extracellular pH (Moon and Richards, 1973; Steiert et al., 1988; Chorao et al., 2010). Protonation of P_i alters the electron density around the phosphorus nucleus which affects the magnetic field the phosphorus experiences, altering its Larmor frequency. This means P_i in different protonation states will have different chemical shifts.

Proton exchange between P_i molecules occurs at such a rate that, as opposed to seeing different peaks for different protonation states in a ^{31}P NMR spectrum, an average of the two peaks is observed, with the chemical shift dependent on the overall protonation level of all P_i in solution and, in turn, the pH. One of the pK_a values of inorganic phosphate ($H_2PO_4^- \rightleftharpoons HPO_4^{2-} + H^+$) under physiological conditions is 6.8, meaning its chemical shift is heavily dependent on pH over the pH range normally associated with biological systems (around pH 6-7.6) (Slonczewski et al., 1981; Ackerman et al., 1996).

In cases with living cells, multiple P_i resonances are often observed, with one being due to intracellular P_i (P_{iic}) and another being due to extracellular P_i (P_{iec}), due to the intracellular and extracellular environments being at different pHs. This is particularly important in the case of prokaryotes that conduct oxidative phosphorylation at their cell membranes, as this allows for the ΔpH component of the PMF to be determined via NMR, providing additional information on the energetics of the cells.

Moon and Richards performed the first experiment on intact cells in 1973, when they were able to calculate the intracellular pH of rabbit erythrocytes (Moon and Richards, 1973). Since then, it has been applied to different species of bacteria, fungi, and animal tissue to monitor changes in pH homeostasis as a result of changes in external conditions (Garlick, Radda and Seeley, 1979; Steiert et al., 1988; Lyngstad and Grasdalen, 1993; Chorao et al., 2010). Equation 4.2 is the most commonly used to determine pH from P_i chemical shift, where $\delta_{\mathrm{acid}}^{\mathrm{P_i}}$ is the chemical shift of $H_2PO_4^-$ and $\delta_{\mathrm{base}}^{\mathrm{P_i}}$ is the chemical shift of HPO_4^{2-} (Ackerman at al., 1996).

$$\mathrm{pH} = \mathrm{pK_a}^{\mathrm{P_i}} + \log\left(\frac{\Delta\delta - \delta_{\mathrm{acid}}^{\mathrm{P_i}}}{\delta_{\mathrm{base}}^{\mathrm{P_i}} - \Delta\delta}\right) \qquad \textbf{(Equation 4.2)}$$

$\Delta\delta$ is the difference between the observed chemical shift of P_i in solution and a reference ^{31}P signal that is insensitive to pH changes. This may be in the form of an external reference capillary containing a phosphorus compound with a known chemical shift that does not overlap with those of P_i or any other peaks of interest in the spectrum. Methylene diphosphonate (MDP) is a popular choice as an external reference compound, as its chemical shift (~16.4 ppm depending on the pH of the

reference solution) makes it easily distinguishable from other peaks in the spectrum (figure 4.3) (Satre, Martin and Klein, 1989; Gosset et al., 2008; Couldwell et al., 2009; Chorao et al., 2010). Use of an external reference requires consideration as to how the capillary will be incorporated into the experimental setup and magnetic field homogeneity must be maintained throughout a set of experiments.

An internal reference, either one added to or already present in the sample, is an alternative. Glycerol phosphorylcholine (GCP), which is pH-insensitive, serves as one possible example (Melvin and Shanks, 1996). pH sensitive compounds such as phenyl phosphonate (PheP) and methyl phosphonate (MeP) can also be used. Provided the compounds are taken up by cells, the chemical shift difference between them and P_i will change as a function of pH, meaning they can be employed to determine intracellular pH. If not taken up by the cells, then MeP and PheP can still act as reference compounds, but this is reliant on the pH of the sample medium being known.

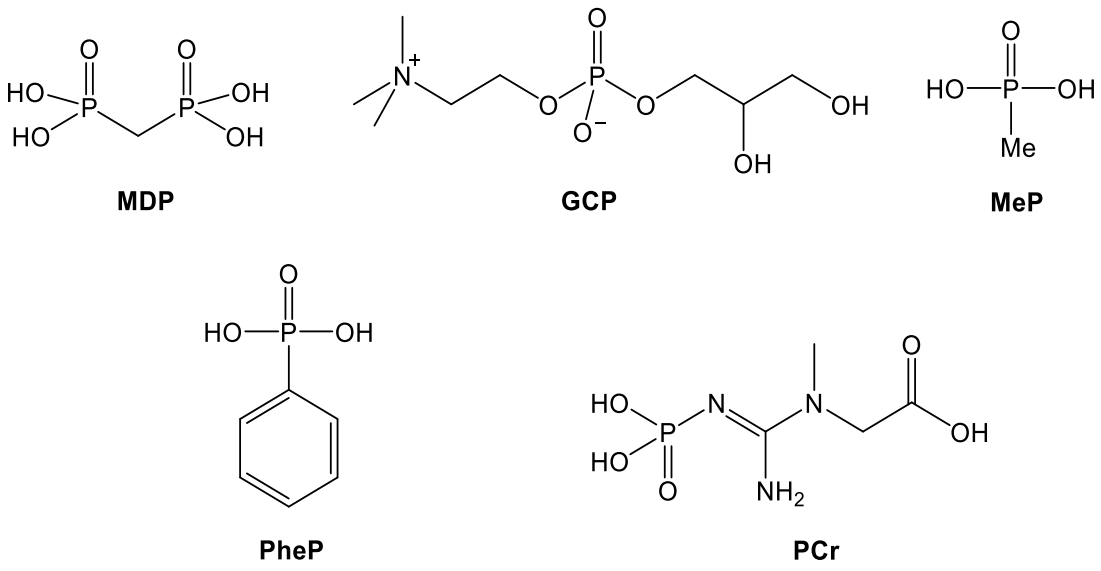

***Figure 4.3**: Structures of MDP, GCP, MeP, PheP and PCr.*

Any exogenous compound must be nontoxic and not affect the pH homeostasis of the organism under study. These requirements do not apply to biological molecules like ATP, the α-ATP peak of which is mostly pH insensitive and can be used as a reference, and phosphocreatine (PCr). PCr is a molecule capable of transferring a phosphate group to ADP to form ATP found primarily in vertebrate musculature (Feldman, 1999).

While it is a valid reference compound in some studies, its use is limited as it does not occur in all cells and, even then, is best suited for experiments done on tissues with a high level of PCr (e.g. muscle tissue) (Rata et al., 2014). ATP is a suitable reference compound for a much wider range of studies, although the peak shape of the α-ATP peak can be disrupted by signals from uridine diphosphate glucose and NAD^+ (Madden et al., 1991).

Water can be used as a chemical shift reference by obtaining a ^1H spectrum of the sample and then finding the relation between the resonance frequency of the water peak and a peak with a known identity in the ^{31}P spectrum. So far this has only been demonstrated with PCr (Rata et al., 2014). Once this relation has been found the water peak in a ^1H spectrum can be used to estimate the position of the ^{31}P species, allowing creation of a virtual peak in the ^{31}P spectrum which can then be used as a reference. Although shown to be viable, this is more involved than using a ^{31}P reference compound and no improvement in accuracy was shown over using α-ATP as a reference. Additionally, the chemical shift of water is temperature dependent, so a constant temperature must be maintained throughout experiments using this approach (Vitkin et al., 1997).

Although P_i is a convenient native pH probe, its use comes with a couple of drawbacks. Firstly, the chemical shift of P_i is pH insensitive above pH 8, making it unsuitable for monitoring the cellular response to alkaline conditions (Slonczewski et al.,1981). Secondly, in some cases P_i signals cannot be clearly distinguished as a result of signals from other compounds occurring at overlapping regions in the spectrum (Martin et al., 1987). Due to these reasons, some groups have investigated the use of alternative exogenous pH probes (Slonczewski et al., 1981; Thoma et al., 1986; Pietri et al., 2000).

Slonczewski et al. (1981) identified MeP as a potential pH probe. MeP has a pKa of 7.65 and its chemical shift was found to be pH sensitive up to and including pH 8.5, allowing the monitoring of pH homeostasis in *E. coli* under alkaline conditions. Furthermore, MeP has a significantly different chemical shift (24.90-21.05 ppm) to native phosphorus-containing compounds, making MeP resonances easy to distinguish. Because of this, MeP was used to obtain a value for the cytoplasmic pH of

the slime mould *Dictyostelium discoideum* (*D. discoideum*), after attempts to use P_i as a pH probe had proven problematic due to difficulties in correctly identifying the P_i peaks (Jentoft and Town, 1985; Martin et al., 1987; Satre, Martin and Klein, 1989).

One downside of using MeP is that its uptake by cells is variable. Intracellular MeP is only detected in *E. coli* cells if they are grown on glycerol and MeP uptake by *D. discoideum* has been recorded in some studies but not in others, however it is unclear whether this is due to a different choice of growth medium or a different strain of the amoeba being studied (Slonczewski et al., 1981; Jentoft and Town, 1985; Satre, Martin and Klein, 1989).

PheP has been proposed as an alternative pH probe and was used to measure pH in *E. coli* without the need for glycerol (Thoma et al., 1986). Unfortunately, issues with PheP uptake or toxicity have been reported for *Flavobacterium* sp. (which was later reclassified as *Sphingomonas chlorophenolica, S. chlorophenolica*) (Steiert et al., 1988; Leung et al., 1999). and *D. discoideum* respectively, (Satre, Martin and Klein, 1989) illustrating that while PheP can be used as a pH probe, much like MeP, its scope is limited.

If the P_{iic} and P_{iec} peaks are poorly separated, for example if the applied magnetic field is heterogenous, then accurate ΔpH measurements will be impossible. Therefore, a series of neutral linear and cyclic α- and β-aminophosphonates were evaluated in an effort to find more sensitive pH probes (Pietri et al., 2000). It was theorised that if the amine was the preferred protonation site, then this would lead to a more sensitive pH probe. Every aminophosphonate demonstrated a pH sensitivity 2-4 times greater than that of $P_{i.}$ One of these compounds, diethyl(2-methylpyrrolidin-2-yl)phosphonate (DEPMPH) (figure 3), was used as to obtain values for intracellular and extracellular pH in isolated rat hearts and livers (Pietri et al., 2000; Pietri et al., 2001).

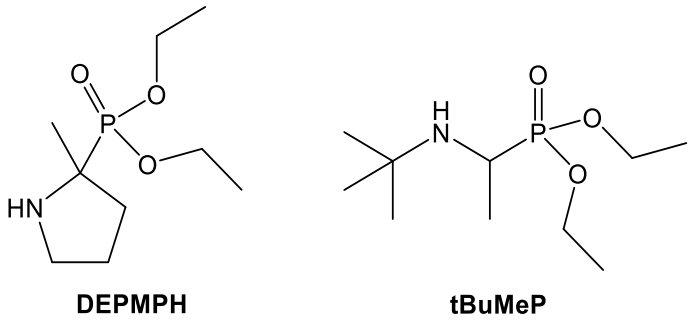

DEPMPH **tBuMeP**

Figure 4.4*: Structures of exogenous pH probes DEPMPH and tBuMeP.*

In later studies done with *D. discoideum,* DEPMPH, as well as another α-aminophosphonate probe, diethyl(1-(*tert*-butylamino)-eth-1-yl)phosphonate (tBuMeP), did not show the same toxicity issues as PheP (figure 4.4). They also allowed the determination of cytosolic and endolysomal pH, an improvement on MeP which only gave an intracellular signal assigned to the cytosolic compartment (Satre, Martin and Klein, 1989; Gosset et al., 2008). Despite the advantages of using aminophosphonate probes, the number of studies done with them are limited, likely due to the fact they are not commercially available.

^{31}P NMR is a powerful technique for measuring pH *in vivo* and can provide insights unobtainable by other methods. However, its application is nontrivial and experiments must be designed carefully to derive reliable results. While the use of intrinsic species means there is no concern over the impact of adding a compound not normally contained in growth media to the organism under study, often use of exogenous pH probes can be easier and more reliable.

4.1.4. Examples of live cell NMR studies

The ability to non-invasively monitor cellular pH in conjunction with the levels of ATP and other phosphorylated metabolites makes ^{31}P NMR a useful tool for observing cells' responses to changes in their external environment (Lohmeier-Vogel, Hahn-Hägerdal and Vogel, 1995; Chorao et al., 2010). Some examples of experiments in this area include those done on *Rhodococcus rhodochrous* OBT18 (*R. rhodochrous*), a strain of bacteria found in wastewater treatment plants (Wever et al., 1997). The ability of this strain to degrade benzothiazole pollutants led to interest in its ability to

cope with different stresses and this was investigated using ^{31}P NMR and ^{13}C NMR (Chorao et al., 2010). The ^{31}P NMR data in particular showed that following anoxia, intracellular pH and ATP levels returned to normal within 3 hours, something not previously observed in environmental bacteria.

Lohmeier-Vogel et al. (1995) investigated the effects of oxygenation on three different species of yeast metabolising glucose or xylose using a combination of ^{31}P and ^{13}C NMR (Lohmeier-Vogel, Hahn-Hägerdal and Vogel, 1995; Lohmeier-Vogel, McIntyre and Vogel, 1996). They found that while glucose metabolism in *Saccharomyces cerevisiae* (*S. cerevisiae*) and *Candida tropicalis* (*C. tropicalis*) is independent of oxygenation, this is not the case for *Pichia stipitis* (*P. stipitis*). In contrast, the rate of xylose metabolism was higher under aerobic conditions for both *P. stipitis* and *C. tropicalis*.

A combination of ^{13}C and ^{31}P NMR were also used to examine the effect of changing the substrate on growth of the bacterium *Zymomonas mobilis* (*Z. mobilis*) (De Graaf et al., 1999). Differences in *Z. mobilis* growth on fructose compared to glucose were unexplained prior to this study but use of ^{31}P NMR linked growth differences to an overall change in cellular levels of phosphorylated metabolites. Another study looked at the effects of growing the nitrogen-fixing bacteria *Bradyrhizobium japonicum* (*B. japonicum*) in a high-osmolarity medium versus a low-osmolarity medium (Pfeffer et al., 1994). *B. japonicum* produces a cyclic oligosaccharide, phosphocholine-substituted 3-1,3;1,6 cyclic glucan, which is observable via ^{31}P NMR. Through the use of this technique in conjunction with ^{13}C NMR, phosphocholine-substituted 3-1,3;1,6 cyclic glucan was implicated to play a role in adaptation of the bacteria to low-osmolarity conditions.

^{31}P NMR is also a powerful tool for investigating the effects of a specific compound, such as a pollutant, on live cells. Specifically, ^{31}P NMR can provide evidence on whether a xenobiotic acts as an uncoupler in prokaryotes (Thoma et al., 1986; Steiert et al., 1988; Lohmeier-Vogel, Ung and Turner, 2004). In a ^{31}P NMR spectrum, the collapse of ΔpH caused by an uncoupler can be observed via the convergence of the peaks assigned to P_{iic} and P_{iec} (or the equivalent peaks of an exogenous pH probe).

Uncoupling is accompanied by a drop in the β-ATP peak due to ATP being hydrolysed without reserves being replenished by oxidative phosphorylation.

^{31}P NMR has been used to observe the uncoupling activity of the biocide pentachlorophenol on *E.coli* (Thoma et al., 1986). A later study showed that while *S. chlorophenolica*, a bacterial species known to break down some chlorinated phenols, is resistant to uncoupling by pentachlorophenol, it is susceptible to the uncoupling action of a chlorinated phenol with a different substitution pattern, 3,4,5-chlorophenol (Steiert et al., 1988). Similarly, ^{31}P NMR experiments on *E. coli* investigating the toxicity action of group 16 pollutants were able to provide evidence that tellurite acts as an uncoupler, while selenite does not (Lohmeier-Vogel, Ung and Turner, 2004).

^{31}P NMR enables monitoring of cellular metabolism *in vivo* and can probe phospholipid metabolism. PME levels have been shown to be higher in tumour cells compared to healthy tissue (Sostman, Armitage and Fischer, 1984; Maris et al., 1985). ^{31}P NMR was used to identify the PMEs detected in MDA-MB-231 human breast cancer cells as phosphocholine and phosphoethanolamine, both phospholipid metabolites, and the pathways producing them (Daly et al.,1987). Later, ^{31}P NMR was also used to provide information on the pathway for synthesising phosphatidylcholine, a phospholipid formed from phosphocholine, in lymphocytes (Kaplan and Cohen, 1991).

^{31}P NMR allows the metabolism of some xenobiotics in live cells to be monitored. The main application of this is in investigating drug metabolism. Boyd et al. (1986) used ^{31}P NMR to study the conversion of cyclophosphamide, a phosphorus-containing anticancer prodrug, to its active phosphoramide mustard form in U937 human histiocytic lymphoma cells. They demonstrated that the phosphoramide mustard formed from cyclophosphamide cannot readily cross cell membranes, and therefore must be formed intracellularly. The group also obtained a rate constant for the disappearance of the phosphoramide mustard. In a similar manner, Sonawat et al. (1990) studied the metabolism of the cyclophosphamide derivative mafosfamide in P388 mice leukaemia cells. The half-life of S-2-[3-(aminopropylamino)]ethylphos

-phorothioic acid, a radioprotective agent, in mice has also been investigated using ^{31}P NMR (Knizner et al., 1986).

The number of experiments that can be conducted in this area is limited because ^{31}P NMR is only useful for monitoring phosphorus-containing drugs (or drugs with known phosphorylated metabolites). Indeed, more literature is available on studying drug metabolism *in vivo* using ^{1}H and ^{19}F NMR (Bell, Gadian and Preece, 1990). The major issue with this application of NMR spectroscopy is that a relatively high concentration of a drug is needed in order for it to be detectable via NMR (generally above 100 mM).

4.1.5. Determining exchange rates

Magnetisation transfer (MT) is a technique that allows the determination of rate constants for exchange reactions between two species. In a ^{31}P MT experiment, one of the exchanging species is selected and its signal is perturbed via inversion or saturation (i.e. continued irradiation at the Larmor frequency, eliminating the population difference between spin states). Signal perturbation is transferred to the second exchanging species by chemical exchange, and measurement of this allows quantification of the exchange rate.

The first ^{31}P MT measurements on an enzyme catalysed system (adenylate kinase) were done *in vitro* in 1977 (Brown and Ogawa, 1977). *In vivo* saturation transfer (ST) experiments were used to obtain unidirectional rate constants for the synthesis of ATP from P_i and the hydrolysis of ATP to P_i (and ADP) in *E. coli* shortly afterwards (Navon et al., 1977).

The majority of *in vivo* ^{31}P MT experiments have been done on vertebrate tissue, in which both PCr-ATP and P_i-ATP fluxes can be investigated (Befroy et al., 2012). A series of experiments on *S. cerevisiae* remain the only other notable application of ^{31}P MT to the study of microorganisms (Alger, Hollander and Shulman, 1982; Campbell, Jones and Shulman, 1985; Campbell-Burk, Jones and Shulman, 1987). The unidirectional rate for the conversion of P_i to ATP was obtained via saturation of the γ-ATP signal under aerobic and anaerobic conditions (Alger, Hollander and Shulman, 1982). The contribution from the action of mitochondrial ATPase to P_i consumption was

investigated through the addition of a mitochondrial respiratory chain inhibitor, antimycin A (Campbell-Burk, Jones and Shulman, 1987). The rate of P_i consumption observed by ST decreased appreciably and, notably, was similar to the value obtained under anaerobic conditions.

The glyceraldehyde-3-phosphate dehydrogenase/phosphoglycerate kinase (GAPDH/PGK) pathway was suspected to be responsible for the remaining P_i consumption (Alger, Hollander and Shulman, 1982). Campbell-Burk et al. (1987) used data from MT experiments with a GAPDH inhibitor, iodoacetate, to conclude that P_i consumption is the sum of contributions from mitochondrial ATPase and GAPDH/PGK, with the contribution from each pathway being dependent on growth conditions (e.g. oxygenation and substrate).

The abundance of literature on MT studies in humans and other mammals validates the technique as a non-invasive means of obtaining rate constants. Although far less work has been done on microorganisms, this particular application of ^{31}P NMR should not be ignored as it can provide further information on the bioenergetics of a cell.

4.1.6. Aims for this chapter

The original aim of this chapter was to develop a method for studying mycobacteria using ^{31}P NMR and apply this to the study of the mechanism of BDQ. When it became clear data from the bioenergetic chamber alone would be sufficient to solve BDQ's mode of action, efforts were refocused there and as such this section only describes the methods development process which was carried out via the following steps:

I. Devise a system to oxygenate and mix *M. smegmatis* cultures so that they may be sustained over the course of an NMR experiment.
II. Find an optimal set of parameters for acquiring ^{31}P NMR data from mycobacteria.
III. Acquire ^{31}P NMR reference spectra of phosphorylated metabolites so that they may be correctly identified in *M. smegmatis* spectra.

4.2. ESTABLISHING A SETUP FOR LIVE CELL NMR STUDIES

4.2.1. Examples of systems used to perform NMR studies on live cells in literature

One of the main challenges of performing NMR on cell cultures is the issue of keeping cells alive inside the magnet. In a study working with aerobic cells, a system of keeping the cells oxygenated in the NMR machine must be devised. The inability to use magnetic metals within the near vicinity of the spectrometer further complicates matters. Additionally, heterogeneity in the sample will result in peak broadening, so often a means to keep the sample stirred is also required.

The obvious solution to both of these issues is to stir the culture by bubbling air through it. However, oxygen is paramagnetic, meaning oxygen bubbles affect the homogeneity of the magnetic field which results in peak-broadening (Jentoft and Town, 1985). Navon et al. (1977) synchronised the oxygen bubbling and RF pulse, such that scans were only recorded after an oxygen bubble had finished passing through the coil. More common are systems designed with an inner and outer tube so that oxygen is bubbled above the detector, oxygenating the culture and causing liquid to flow through the inner-outer tube system, thereby mixing it; these are known as airlift systems.

Examples include one developed by Jentoft and Town (1985) used to study *D. discoideum,* which gave better signal resolution and mixing compared to simple oxygen bubbling, and one developed by Santos and Turner (1986). The Santos-Turner design has since been modified and used by several groups, likely due to oxygenation being achieved at a significantly lower O_2 bubbling rate compared with the Jentoft-Town system (15 mL min^{-1} versus 130-150 mL min^{-1}) (Kramer and Bailey, 1991; Lyngstad and Grasdalen, 1993; Melvin and Shanks, 1996).

Perfused systems, in which an oxygenated medium is cycled through the NMR tube, are another means of maintaining live cell cultures. Using a perfused system is a must if working with cells sensitive to a build-up of toxic by-products or cells that can lyse if

exposed to vigorous bubbling (Sostman, Armitage and Fischer, 1984). Changing or adding things to the medium in perfused systems is easier, facilitating long studies on the impacts of changes in external conditions. Temperature control can be achieved through heating the medium in a water bath before it is cycled through to the cells (Carvalho et al., 2019).

Perfused systems can require significantly more medium than airlift systems (depending on whether the medium is reoxygenated after being passed through the culture and recirculated). A more complicated setup is also required as pumps are needed to circulate the medium (Grivet and Delort, 2009). Cells must be prevented from cycling (usually through immobilisation in agarose gel threads/beads or alginate beads) although the method of immobilisation should not interfere with the ability of cells to extract nutrients from the medium (Lohmeier-Vogel, McIntyre and Vogel, 1996; Hesse et al., 2000; Carvalho et al., 2019).

Both airlift and perfused systems have their separate benefits, making them more suited to different types of experiment. For simple and short studies (1> day), a basic airlift system provides a straightforward solution to the task of maintaining the cells through the course of the experiment. Perfused systems are more suited to long studies (several days), particularly those focused on the effects of changes in the culture medium.

4.2.2. Air motor design

To avoid disruption of the homogeneity of the magnetic field due to stirring via bubbling, a system consisting of a mechanical stirrer powered by an air-powered motor was conceived (figure 4.5). The setup was designed to work with a Bruker 400 MHz wide-bore spectrometer. The sample is contained in a Falcon tube which screws onto another tube that runs to the top of the bore of the spectrometer. The second tube has bearings positioned throughout it to limit any potential wobbling of the rod without restricting its rotation. Rather than using bubbles to supply oxygen to the cells, oxygen-permeable platinum-cured silicon tubing is run through the Falcon tube and used to oxygenate the culture.

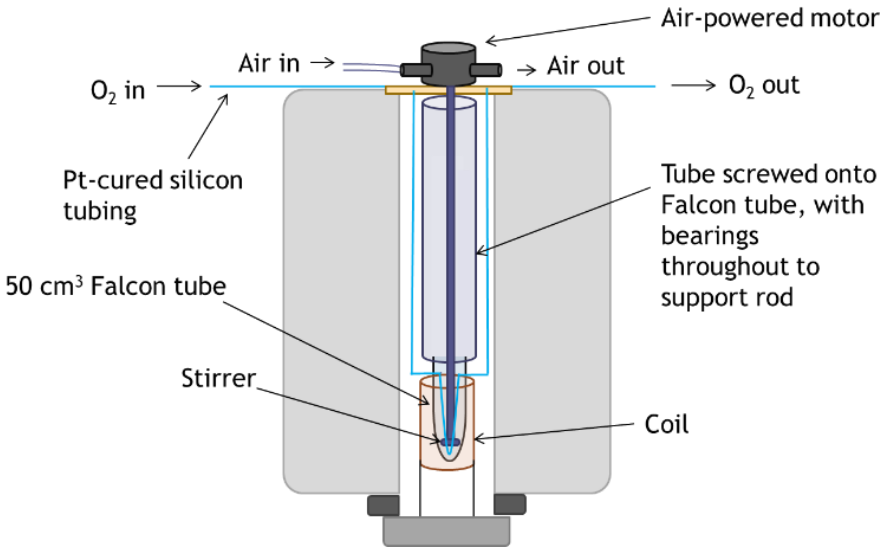

***Figure 4.5**: Diagram of air-powered motor-stirrer setup for performing NMR on live bacteria.*

Initial designs of the air-powered motor consisted solely of a rotor connected to a shaft, housing and lid. A clearance of 0.2 mm between the rotor blades and the casing was used to ensure maximum efficacy of the motor. The components were produced using a 3D printer and the ability of the design to drive mixing of a 25 cm^3 sample was tested. Hand sanitiser was selected as the sample as it has a greater viscosity than the cultures that will be used and therefore serves as a good test as to whether sufficient force can be generating using the motor.

With the 3D printed components, the rotor would only turn in the housing in the absence of the lid. Additionally, sufficient force to stir the sample was only achieved with the rotor alone. This was likely due to a lack of support to maintain the orientation of the shaft in the housing, which caused to rotor to move within the casing and come into contact with the sides, reducing the force of the rotation output. To rectify this, the motor was redesigned with the bottom of the housing designed to accommodate a bearing that fits to the shaft and should therefore prevent the rotor from moving within the casing (figure 4.6). The port for air input was also changed to one that would connect to a push fit connector which facilitates connection to the air supply.

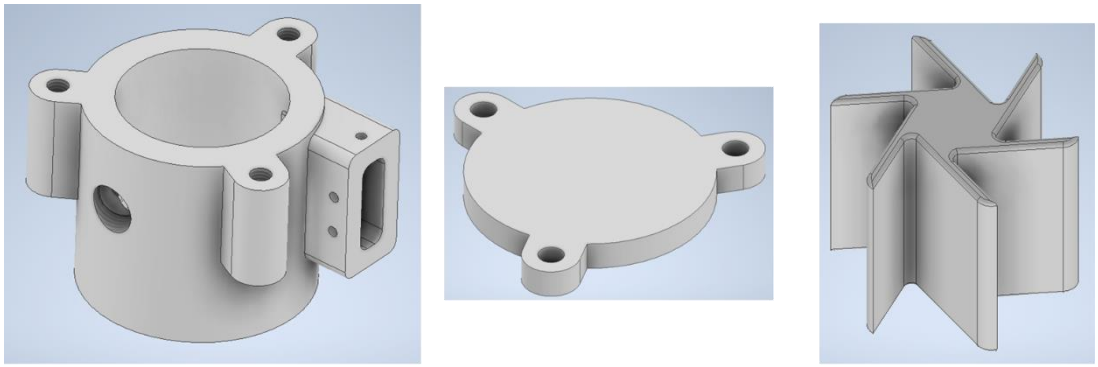

***Figure 4.6**: CAD models for the components of the redesigned air-powered motor.*

Following manufacture of these parts from hard plastic, the efficacy of the air motor was evaluated through benchtop tests with a 25 cm^3 sample of hand sanitiser, selected as its viscosity is greater than that of any culture that will be used in future experiments. The motor was able to rotate a ca. 40 cm shaft with a stirrer-bar like component at the bottom at a speed sufficient to mix the sample. This demonstrated that the motor alone is able to generate sufficient torque to mix a fluid sample without needing to include gears in the set up.

One issue, however, is that the shaft noticeably wobbled while being turned by the motor. Excess motion of the shaft, and by extension the stirrer, is undesirable as it may result in disruption of the homogeneity of the magnetic field, thereby reducing the quality of the spectra. Additionally, it has the potential to lead to mechanical wear, especially as experiments with BDQ are planned to be conducted over a period of several days.

The hope in the original design was to include a tube that would screw onto the top of the sample container and contain bearings to support the shaft and limit its motion. The practicalities of making such a tube are less simple than its conception and upon examining the dimensions of the air motor and the bore of the NMR machine, the design was redrafted (figure 4.7). By adjusting the inlet and outlet ports on the motor, it can be made to fit inside the NMR machine, just above the sample, thereby reducing the length of the shaft, and with it, any wobbling that may occur with stirring.

The reduced size means producing the components needed for this revised design would have resulted in a significant wait time. To avoid such a delay, an examination of previous setups used for *in vivo* NMR on microorganisms to look for potential alternatives was conducted.

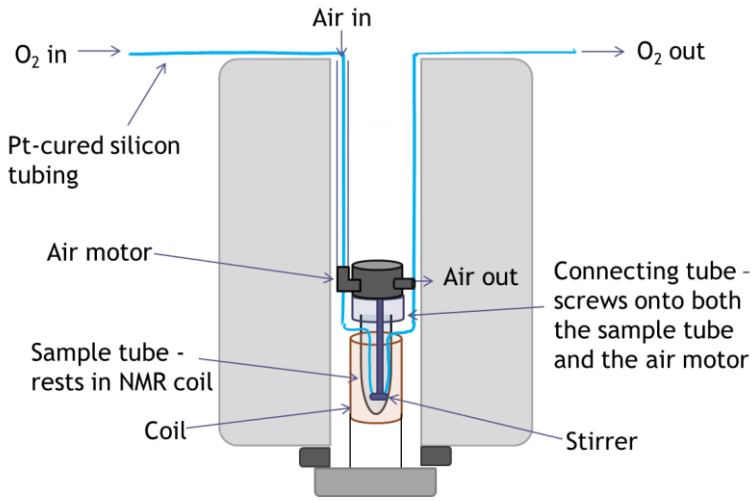

***Figure 4.7**: Diagram of redrafted air-powered motor-stirrer design for performing NMR on live bacteria.*

4.2.3. Airlift design

An airlift system published by Santos and Turner was selected as a promising base for a new live cell NMR set up (Santos and Turner, 1986). The original design features a 10 mm NMR tube with a 5 mm capillary fitted inside of it. Oxygen is introduced via air being bubbled into the inner capillary, above the part of the sample that is contained within the detection coil. As the air bubbles rise through the culture, they draw liquid up with them, thereby generating a flow and mixing the solution. The system is reasonably simple to construct and was reported to achieve high levels of oxygenation and mixing of substrates in solution.

A wide-bore NMR machine allows for a 30 mm sample tube as opposed to a 10 mm one. Having a greater sample volume inside of the coil increases the SNR for cell suspensions of the same concentration, therefore it is beneficial to capitalise upon the extra volume available. It is unclear how important the outer diameter ratio of the inner capillary and outer tube is to generating sufficient flow to mix the culture and so

the original intention was to test multiple versions of the design shown in figure 4.8. By performing mixing tests with inner capillaries of different diameters (dimension X), the optimum ratio could be found.

A 10 mm diameter inner capillary was chosen to test the proof of concept of the design. Simple plastic rings like those pictured in the diagram were made via 3D printing and the chamber was assembled with a drop of gel food colouring being placed on the bottom of the inner capillary. 40 mL of water was added, and upon the introduction of a stream of air through the air delivery tube, mixing throughout the chamber was immediately observed with the dye being fully dissolved and mixed after approximately 10 seconds of bubbling.

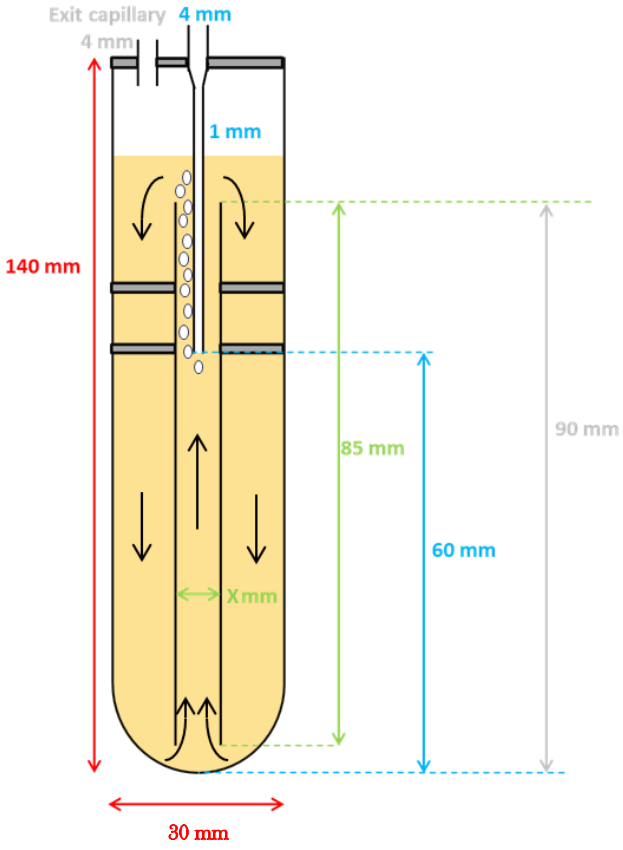

***Figure 4.8**: Diagram of an initial design for an airlift system to be used with a Bruker 400 MHz wide-bore spectrometer, where dimension X could be varied to find the inner capillary diameter to outer tube diameter ratio that achieves the best results.*

Satisfied that the system could provide adequate mixing, a culture of *M. smegmatis* WT was loaded into the chamber to see if adequate oxygen could be provided to keep

cells alive. After three hours of the chamber being incubated in a water bath at 37 ^{o}C with compressed air being bubbled through, although no growth was observed, the OCR of cells (73 μM min^{-1}), monitored using the bioenergetic chamber, was very similar to that before the culture was loaded into the chamber (76 μM min^{-1}).

This demonstrates the design is able to keep cells alive, although several issues were identified in the process. Firstly, the presence of Tween 80 in the media means that if the air flow rate is too high, the top of the culture starts to bubble up and out of the exit tube. Secondly, the simple plastic rings were designed such that ensuring the dimensions of the inside of the chamber remain the same in each experiment relies upon use of a measuring tool and the setup is liable to getting knocked out of position.

In order to solve the first issue, the decision was made to add a regulator to the air input to allow better control over the flow rate. A new design for the plastic rings was modelled using CAD software so that the air delivery tube was better supported and all the components fit together such that reassembly of the chamber after cleaning was not subject to human error in terms of positioning (figure 4.9). In order to accommodate these changes, the outer diameter of the inner capillary had to be changed from 10 mm to 15 mm. Plans to investigate the impact of altering the diameter of the inner capillary were discarded as the thickness of the plastic required to make the new rings durable meant changing the diameter of the inner tube would result in smaller holes for the liquid to pass through and would likely interfere with mixing.

Another test was done with gel food colouring using this new design and it was shown to mix effectively with an easier set up process. The new rings prevented any components from being knocked out of position and so the design was taken into the next phase of testing.

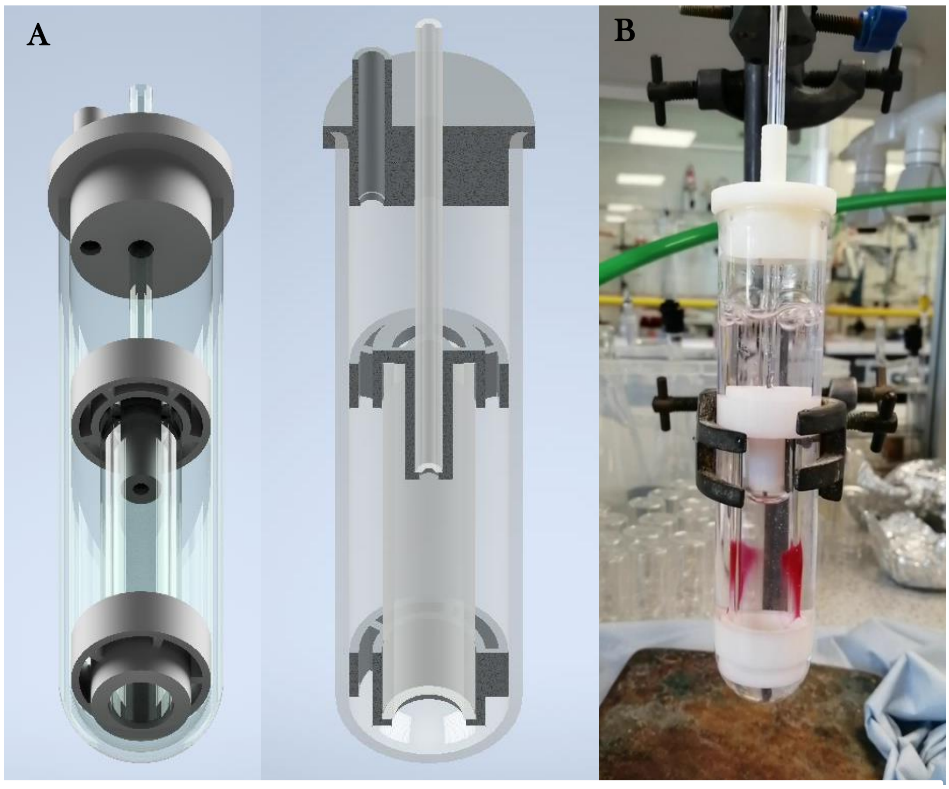

Figure 4.9: *Images of the redesigned NMR airlift chamber showing (**A**) CAD models of the structure and (**B**) the actual assembly of the chamber using a mixture of 3D printed components created from the CAD models and glassware*.

4.2.4. Verifying design is suitable for culture growth

Rather than doing another experiment with *M. smegmatis*, growth measurements of *Bacillus subtilis* (*B. subtilis*) were performed using the chamber (table 4.1). In order to show the chamber is able to oxygenate cells effectively, it is important to demonstrate it can support cell growth and *B. subtilis* has a significantly shorter doubling-time than *M. smegmatis* (20 mins versus 3-4 hrs) (Klann et al., 1998; Errington and Aart, 2020), meaning the culture can be monitored throughout growth to ensure there are no issues with the air flow rate. For initial tests, a flow of compressed air was used to oxygenate and mix the culture in the NMR chamber.

Bacterial growth is observed in the chamber over a period of 7 hrs under these conditions, showing that it can support some cell growth. When compared to a culture grown in a 250 mL conical flask placed in an incubator however, growth in the NMR chamber is slower, and appears to start to plateau around the 7-hour mark. One

explanation for this is that the bubbling rate with compressed air is not sufficient to supply cells with enough oxygen once the culture reaches a certain cell density.

Table 4.1: *Growth measurements for B. subtilis 168 grown in LB media in the NMR chamber using a flow of compressed air versus a 250 mL conical flask. All cultures were incubated at 37 ^{o}C with the 250 mL conical flask being shaken at 200 rpm.*

Time (hrs)	OD_{600} of culture in 250 mL flask ()	OD_{600} of culture in NMR chamber ()
4.3	0.4	0.4
6.3	2.0	1.4
7.5	3.0	1.6

Increasing oxygen delivery by increasing the bubbling rate further carries the risk of the bubbling being too vigorous, potentially leading to loss of culture from the air outlet tube in the lid. Therefore, the experiment was repeated with a similar bubbling rate, but this time using a 40% oxygen, 60% nitrogen mix instead of compressed air to supply the cells with more oxygen (table 4.2). Under these conditions, growth in the NMR chamber much more closely matched that in a 250 mL conical flask. This demonstrates the oxygen content in compressed air is not sufficient for maintaining cultures at an OD_{600} >1 in the airlift design. As a result, future experiments were performed using an oxygen generator, able to provide a gas flow composed of 70-80% oxygen.

Table 4.2: *Growth measurements for B. subtilis 168 grown in LB media in the NMR chamber using a flow of a 40% oxygen, 60% nitrogen mix versus a 250 mL conical flask. All cultures were incubated at 37 ^{o}C with the 250 mL conical flask being shaken at 200 rpm.*

Time (hrs)	OD_{600} of culture in 250 mL flask ()	OD_{600} of culture in NMR chamber ()
4	0.3	0.1
5.8	1.7	1.5
6.9	2.6	2.3

4.2.5. Growing *M. smegmatis* in the NMR chamber

Having shown the airlift system could support bacterial growth, attention was shifted to exploring how well it could support an *M. smegmatis* culture for potential BDQ studies. To ensure any increase in culture OD_{600} was due to *M. smegmatis* growth, air into and out of the chamber was run through microbial filters to prevent potential contamination of cultures. Additionally, all glass and silicon tubing components were autoclaved prior to use, while 3D printed components were sterilised using 70% EtOH.

Unlike *B. subtilis*, *M. smegmatis* is grown in the presence of a detergent (Tween 80) which caused cultures to foam upon bubbling air into the chamber in initial experiments. This resulted in loss of culture via the air outlet tube and so ways to minimise this effect were investigated. Mycobacteria grown in bioreactors are supplied with oxygen via a similar manner to the NMR chamber, i.e. bubbling in air, with antifoam C emulsion being added to prevent foaming. This method was trialled in the NMR chamber and it was found that adding 0.05% antifoam C emulsion to the growth media reduced the level of foaming such that air could be introduced to the chamber at a rate of 0.6 LPM without loss of culture through the outlet tube.

It was also observed that the 3D printed components swelled after being in contact with aqueous solution. As a result, they were easily damaged during disassembly of the NMR chamber and had to be replaced after a single experiment. To make the design of the chamber more sustainable, the parts were reproduced using polyether ether ketone (PEEK). PEEK is more durable and can be sterilised by autoclaving. It has also been demonstrated to be non-cytotoxic to two human cell lines, therefore making it suitable for use in biological applications (Limaye, Veschini and Coward, 2022).

Following these changes, *M. smegmatis* was left to grow in the NMR chamber overnight. Sometime during this period, the fluid level in the chamber fell to below the level of the inner tube, thus rendering the chamber unable to mix the culture properly. This drop in fluid was initially believed to be caused by evaporation due the air being bubbled through the chamber having a very low humidity. In an attempt to combat this, the air was first bubbled through a tube of deionised water before being introduced to the chamber. Although this should have increased the moisture content of air being bubbled through the chamber, significant loss of liquid overnight was still observed.

Sterile mineral oil is used to limit evaporation in tissue culture, but was found not to be suitable for use in the NMR chamber. Any level of bubbling resulted in disruption to the mineral oil layer, thereby rendering it ineffective. An alternative solution in which cultures were grown in 250 mL flasks overnight to an OD_{600} of around 0.5 and then transferred to the NMR chamber was trialled.

The logic behind this was that the fluid level in the chamber could then be observed throughout growth and the culture could be topped up with fresh growth media as required. During this process, it was noticed that there was a leak where the glass air inlet tube was inserted into the chamber lid. This is likely why such volume loss of the culture was observed when left bubbling overnight.

The lid was redesigned to have the same proportions but with O-rings incorporated in the hole for the air inlet tube and around the base of the lid to form a tight seal against all glass fittings. No leaks were observed with the new lid design and attempts to use

the chamber to grow *M. smegmatis* were restarted. The same procedure as before, wherein the culture was grown in a 250 mL flask overnight and then transferred to the NMR chamber, was used. Succinate was selected as the carbon source for this experiment as succinate grown cells have a lower oxygen consumption and so have a greater likelihood of growing in the chamber if oxygen supply is the limiting factor.

Growth measurements were acquired, showing the succinate-grown *M. smegmatis* will grow in the NMR chamber (table 4.3). Growth in the chamber is similar to that in a 250 mL conical flask, although the growth rate in the conical flask was slightly faster after an OD_{600} of around 1 was reached. The experiment was repeated using glycerol as the carbon source to match the conditions used for bioenergetic chamber experiments (table 4.4). A faster growth rate is again observed in the 250 mL conical flask, but the NMR chamber still is able to support culture growth up to an OD_{600} of 3.8.

Table 4.3: *Growth measurements for M. smegmatis WT grown in 7H9 media supplemented with Tween 80 (0.05% v/v), antifoam C emulsion (0.05% v/v) and succinate (50 mM) in the NMR chamber versus a 250 mL conical flask. All cultures were incubated at 37 ^{o}C with the 250 mL conical flask being shaken at 200 rpm.*

Time (hrs)	OD_{600} of culture in 250 mL flask ()	OD_{600} of culture in NMR chamber ()
0.0	0.5	0.6
2.1	0.9	0.9
3.6	1.5	1.2
6.6	1.9	1.7

Table 4.4: *Growth measurements for M. smegmatis WT grown in 7H9 media supplemented with Tween 80 (0.05% v/v), antifoam C emulsion (0.05% v/v) and glycerol (50 mM) in the NMR chamber versus a 250 mL conical flask. All cultures were incubated at 37 ^{o}C with the 250 mL conical flask being shaken at 200 rpm.*

Time (hrs)	OD_{600} of culture in 250 mL flask ()	OD_{600} of culture in NMR chamber ()
17.3	0.4	0.5
3.6	1.1	1.0
5.7	1.9	1.6
7.8	2.3	1.9
23.3	4.8	3.8

Having shown bacterial cultures can grow in the NMR chamber, this setup can be implemented in a wide-bore NMR machine. The effect of bubbling rate on the quality of NMR spectra obtained still needs to be investigated. This could be done by using standard solutions of phosphorylated metabolites and studying the impact of bubbling rate on peak broadness in the ^{31}P spectra acquired. Once a bubbling rate that supports sufficient cell growth and allows for the collection of high-quality spectra has been found, the NMR chamber can be used to study bioenergetics in live cells.

4.3. ^{31}P NMR ACQUISITION PARAMETERS

4.3.1. Calibrating the reference power for a 90^{o} RF pulse

The maximum signal for NMR is achieved when the overall magnetisation M_0 is rotated 90^{o} from being aligned with the z-axis into the xy-plane. This angle of rotation can be changed by altering the power of the RF pulse. In ^{1}H NMR the signal is sufficient for NMR software to calculate the power needed for a 90^{o} pulse, and subsequently the power required for other rotation angles. In ^{31}P NMR this is not the case, so the

reference power for a 90° pulse must be identified manually. To achieve this, the reference power was varied from 5 to 40 W in increments of 2.5 W and this was plotted against the integral of the resulting signal from a 25 mL sample of 0.2 M monosodium phosphate (figure 4.10).

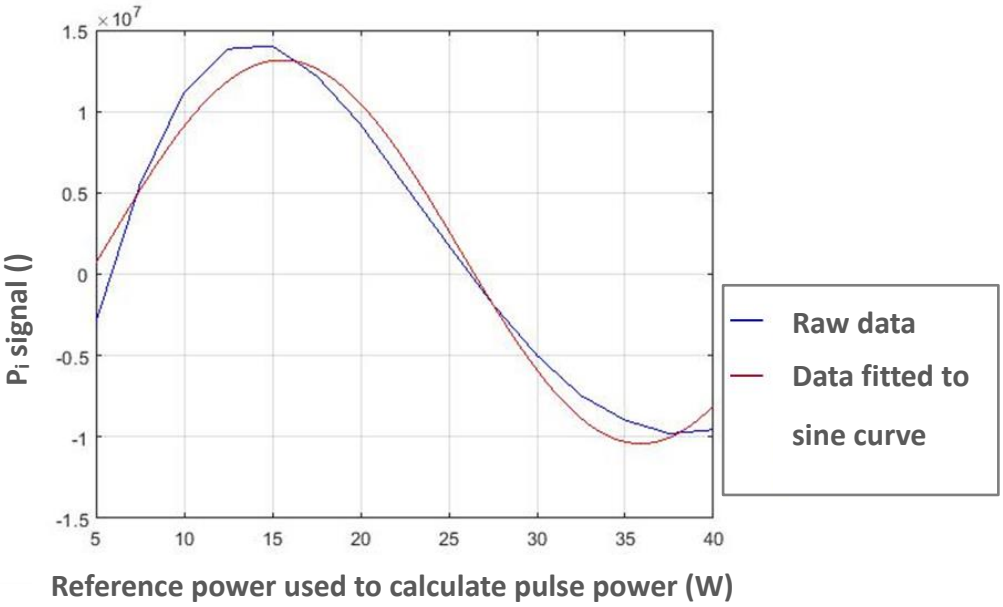

***Figure 4.10**: Effect of the reference power value input on the intensity of the P_i signal in the resulting ^{31}P NMR spectrum of a 0.2 M solution of monosodium phosphate.*

The data was fitted to a sine curve, the expected output if one considers the impact of the angle of rotation of M_0 on the degree of magnetisation in the xy-plane. The maximum signal occurred when the reference power was 15 W, therefore this is the reference power of a 90° pulse for a 25 cm^3 sample.

4.3.2. Optimising data collection

The acquisition parameters for experiments with *M. smegmatis* need to be carefully selected to provide the best quality data. To this end, a series of experiments qualitatively examining the impact of different parameters on the appearance of ^{31}P spectra of an *M. smegmatis* culture were conducted. As this work was performed prior to the full development of the NMR airlift chamber, the culture was unstirred and allowed to go anaerobic in a sealed tube for these experiments.

One of the main parameters to consider is the repetition time (TR); the time between scans. If a second RF pulse is applied before the population difference between spin states has returned to its equilibrium value, then the magnitude of the overall magnetisation vector rotated into the xy-plane will be smaller than that following application of the first pulse. This results in the signal being truncated, thus why a greater SNR is observed for longer TR values in figure 4.11. Furthermore, if different ^{31}P-containing species in a sample have different T_1 values, then a short TR can result in peak integrals being T_1 weighted.

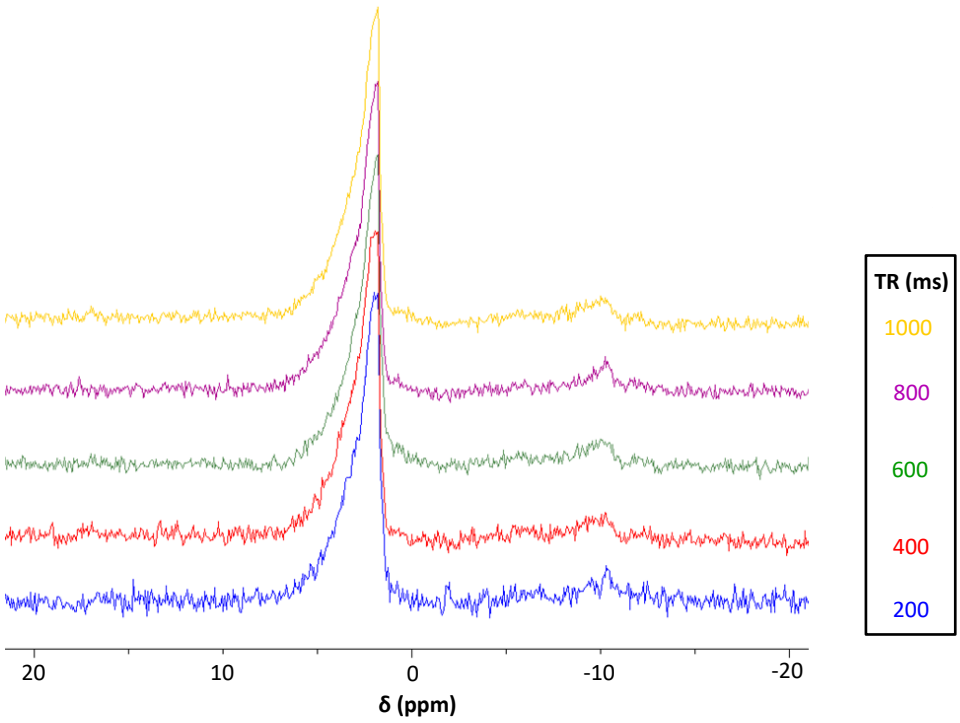

***Figure 4.11**: ^{31}P NMR spectra (162 MHz) of M. smegmatis JR128 in Tris-SO_4 buffer recorded using different TRs, 2000 averages and a flip angle of 90°. The broad peak found between 5 to 2 ppm is likely a combination of signals from AMP and P_i, while the peak at -10 ppm is due to another unidentified phosphorylated metabolite.*

It is also important to consider the effect of averaging on the SNR. While a longer TR may give a better SNR over the course of one scan, a shorter TR allows for a greater number of averages to be recorded over the same total scan time. Finding the correct balance between the TR and the number of averages was investigated through examining data from spectra recorded using different numbers of averages and different TRs but similar total scan times. Figure 4.12 shows data from three

experiments, with total scan times of 10-13 minutes. In spite of the shorter TR, the spectrum recorded using 4000 averages has a better SNR ratio compared to the other two.

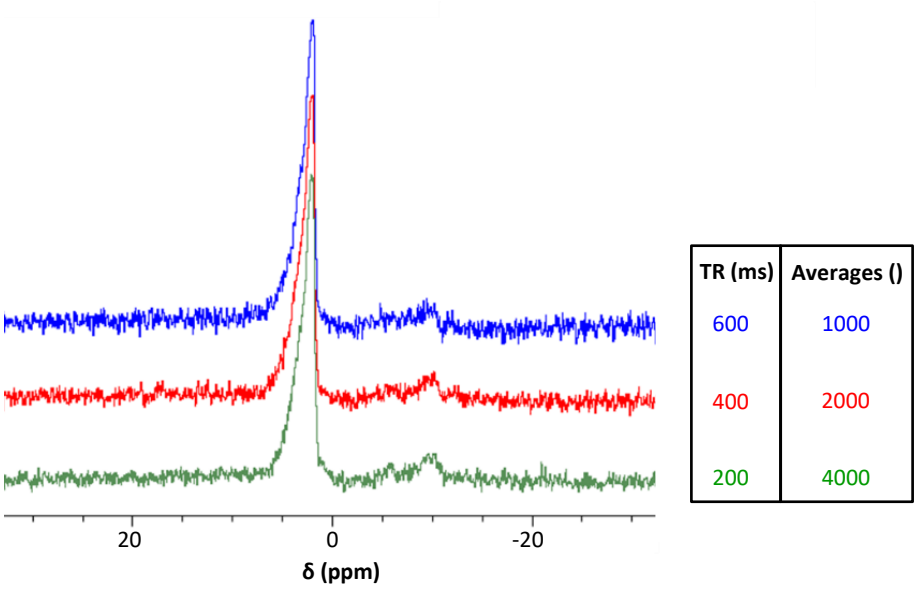

***Figure 4.12**: ^{31}P NMR spectra (162 MHz) of M. smegmatis JR128 in Tris-SO_4 buffer recorded using different TRs and numbers of averages. The flip angle for all spectra was 90°.*

There may be some T_1 weighting in the peak integrals at this lower TR which would be problematic if absolute quantification of the metabolites was required. However, comparing the ratios of the integrals of the P_i and ATP peaks between scans can still provide sufficient information on changes in cellular energetics. Providing the same scan parameters are used throughout experiments, using a shorter TR will not negatively affect the validity of the data.

Upon comparison, the acquisition parameters that give the spectrum with the best qualitative appearance are a TR value of 200 ms with 4000 averages. Once it has been shown the NMR chamber can be used to collect NMR spectra on live cells, it will need to be confirmed that these parameters are the most suited to monitoring mycobacterial metabolism in response to treatment with BDQ.

4.4. HIGH-RESOLUTION EXPERIMENTS

4.4.1. Low-resolution NMR versus high-resolution NMR

High-resolution NMR provides more detailed spectra than low-resolution NMR as it allows visualisation of *J*-coupling. *J*-coupling refers to an effect in which the signal from a spin-active nucleus is split of due to through-bond interactions with other spin-active nuclei.

To explain this briefly, consider an example of a nucleus coupled to a single other nucleus, both with $I = \frac{1}{2}$. The magnetic field experienced by the first nucleus will be impacted by whether the second nucleus is aligned with or against the applied magnetic field. As the sample being studied will contain many molecules, both possibilities will occur, resulting in the signal of the first nucleus being split into two (a pattern known as a doublet). If the first nucleus is coupled to two nuclei, there are now three possible alignments for the two nuclei with regards to the orientation of the magnetic field. In this scenario, the signal from the first nucleus is split into three peaks with a 1:2:1 ratio. Further splitting patterns follow Pascal's triangle and can be rationalised using the same logic as above. For spin-active nuclei where $I > \frac{1}{2}$, the splitting pattern does not follow the rule given above, but coupling is much more rarely observed. 3-bond coupling is the most common in ^{1}H NMR but *J*-coupling can also occur through 2 or 4 bonds.

As *J*-coupling provides insight on the number of through-bond adjacent spin-active nuclei, high-resolution NMR spectra can provide more detailed information on the structures of the substances being studied. In cases where the structure is known, this extra information makes the assignment of peaks in the spectra easier.

The wide-bore mode the NMR chamber was designed to work with is only suitable for low-resolution spectroscopy. This is because the resolution is dependent on the homogeneity of the magnetic field, with a high level of homogeneity needed for high-resolution spectra. This level of homogeneity cannot be achieved over the whole sample volume in wide-bore NMR, thus high-resolution spectra can only be obtained on smaller samples. Oxygenation of a smaller sample is more challenging, especially

as a higher density of cells would be needed to achieve the same signal strength as could be acquired with a wide-bore setup.

While less suitable for studies on live, oxygenated cultures, high-resolution NMR can be used to obtain reference spectra. During development of the NMR chamber, high-resolution NMR spectra of standard solutions of phosphorylated metabolites were collected. A spectrum of unoxygenated *M. smegmatis* cells was also acquired as further proof of concept for using NMR to study mycobacteria.

4.4.2. High-resolution ^{31}P NMR spectra of phosphorylated metabolites

Initially, the aim of these experiments was to collect spectra of phosphorylated metabolites at a concentration similar to that in the cell. A high-resolution ^{31}P NMR spectrum of ATP at a concentration of 10 µM contained only noise, likely due to the low volume of sample required for high-resolution NMR combined with the low concentration. As a much larger sample volume can be used in the wide-bore low-resolution mode, this is not cause for concern with regards to obtaining data on phosphorylated metabolite concentrations inside live cells. In order to ensure high-resolution data could be collected, the concentration of all phosphorylated metabolites studied was increased to 20 mM.

The metabolites were dissolved in a buffer solution containing 25 mM Bis-Tris methane, 25 mM MOPS and 25 mM Tris-Cl and were made up to varying pHs to demonstrate the influence of pH on the chemical shift of peaks in the spectra (figure 4.13). pH values of 6.7, 7.7 and 8.7 were selected for ATP, ADP and AMP and values of 6.2, 7.2 and 8.2 were selected for P_i, as the pKa value for monoprotonated/diprotonated forms of P_i is 6.8 (Slonczewski et al., 1981; Ackerman et al., 1996).

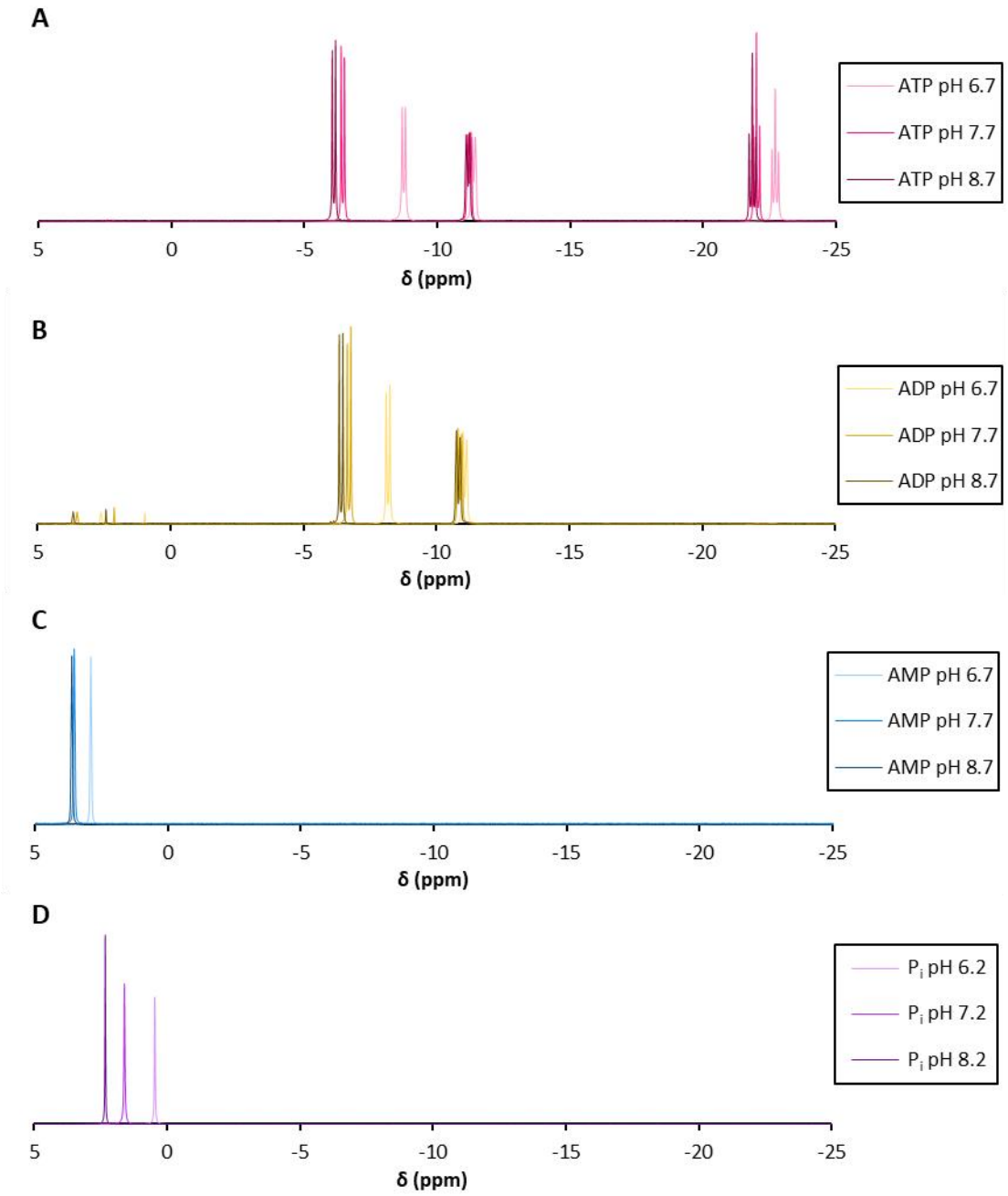

Figure 4.13: *High-resolution ^{31}P NMR spectra (162 MHz) of solutions of (**A**) ATP, (**B**) ADP, (**C**) AMP and (**D**) P_i at varying pHs.*

The splitting patterns allow assignment of the peaks, with the triplet in figure 4.13A in the -21 to -23 ppm region belonging to the β-phosphorus in ATP. This phosphorus atom couples to the α- and γ-phosphorus nuclei, resulting in three peaks in the spectra. The α- and γ-phosphorus nuclei only couple to the β-phosphorus and not each other, thus why they appear in the spectra as doublets.

The peaks in the ATP spectra shift to the right as the pH decreases, with similar trends being observed in ADP, AMP and P_i spectra. For ATP and ADP, these changes further aid the assignment of the peaks. The γ-phosphorus in ATP and the β-phosphorus in ADP are both bound to two oxygen atoms that can be protonated, while the other phosphorus atoms in these molecules are only bound to one oxygen that can be protonated. The magnetic field experienced by the γ-phosphorus in ATP and the β-phosphorus in ADP are therefore more affected by changes in pH, allowing the two to be identified. The peak due to the γ-phosphorus in ATP occurs between -6 and -9 ppm over the pH range studied, while the signal from the β-phosphorus in ADP is the doublet with a chemical shift between -5 and -8.5 ppm. This leaves the peaks around -11 to -12 ppm in the ATP spectra as being the signals from the ATP α-phosphorus nuclei, while the peaks around -11 to -12 ppm in the ADP spectra are the signals from the ADP α-phosphorus nuclei.

Several small peaks due to impurities are visible in the ADP spectra between 4 and 0.9 ppm. As these peaks are present in all samples, they are likely due to some degradation of the stock powder, with the chemical shifts being similar to those of AMP and P_i. These spectra provide a useful reference for assignment of peaks in spectra collected from cells using both high-resolution and low-resolution NMR. They also show the impact of pH on the chemical shift values of phosphorylated metabolites and how this could be capitalised upon to determine the pH inside cells.

4.4.3. High-resolution ^{31}P NMR spectra of *M. smegmatis*

On the first attempt to acquire a high-resolution spectrum of *M. smegmatis*, cells were grown to exponential phase, washed, concentrated and resuspended in phosphate free buffer in order to prevent a large signal in the spectrum from phosphate in the media. This resulted in no peaks being visible in the acquired spectrum, likely due to the removal of media and carbon source resulting in the arrest of respiration. The subsequent cell death meant levels of phosphorylated metabolites were depleted early in the 4-hour course of the experiment.

The experiment was repeated, this time without washing cells and with the addition of growth media prior to placing cells in the NMR machine (figure 4.14). The spectrum

acquired contains a large P_i peak at 1 ppm with smaller peaks visible in the 4 to 2 ppm and -6 to -12 ppm regions. The peaks in the *M. smegmatis* spectrum do not clearly match those of the isolated phosphorylated metabolite spectra. This forced consideration of the state of phosphorylated metabolites in cells versus in buffer solution.

In vivo, ATP and ADP will chelate a cation, usually magnesium as it is one of the most abundant metal cations in cells (Kleczkowski and Igamberdiev, 2021). This chelation will affect the electron density, and thus the relative strength of the magnetic field, around the phosphorus nuclei, impacting chemical shift.

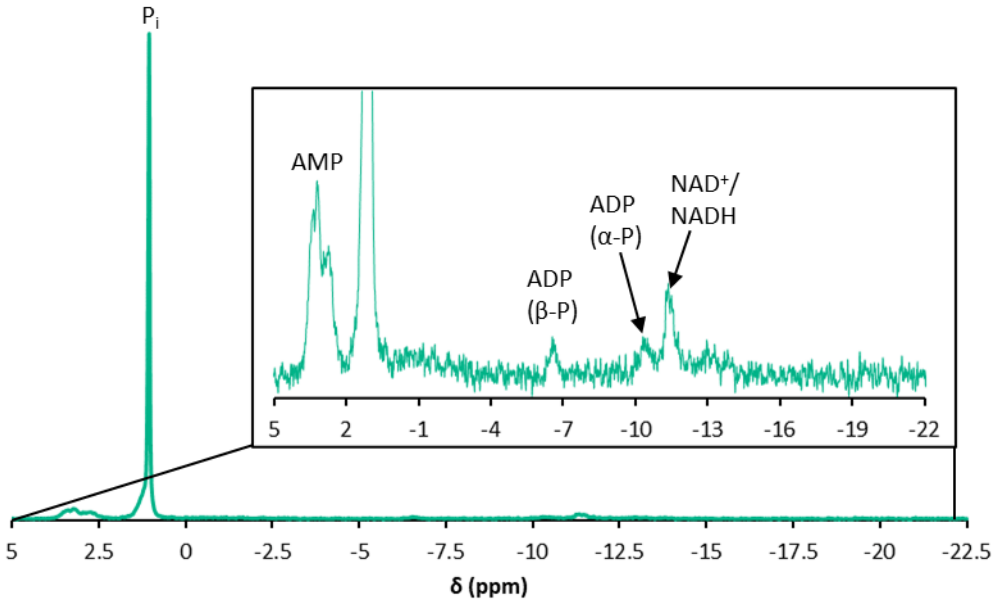

Figure 4.14: *High-resolution ^{31}P NMR spectrum (162 MHz) of M. smegmatis cells with a scaled-up section to view peaks due to phosphorylated metabolites other than P_i. The peak at -11 ppm was assigned using data from literature (Slonczewski et al., 1981). It is likely the peak from 4 to 2 ppm is due to a mixture of AMP and other phosphorylated metabolites, possibly PMEs (Satre et al., 1989).*

The isolated phosphorylated metabolite spectra were recollected with the addition of 40 mM magnesium chloride (figure 4.15). These spectra were then compared to the data collected from *M. smegmatis*. Peaks in the ADP spectrum collected at pH 6.7 with magnesium chloride added match those at -7 ppm and -10 ppm in the *M. smegmatis* spectrum. The lack of a peak at -20 ppm indicates there is little to no ATP present in

the cells. This is likely due to the lack of sufficient oxygenation preventing ATP production by oxidative phosphorylation over the course of the experiment.

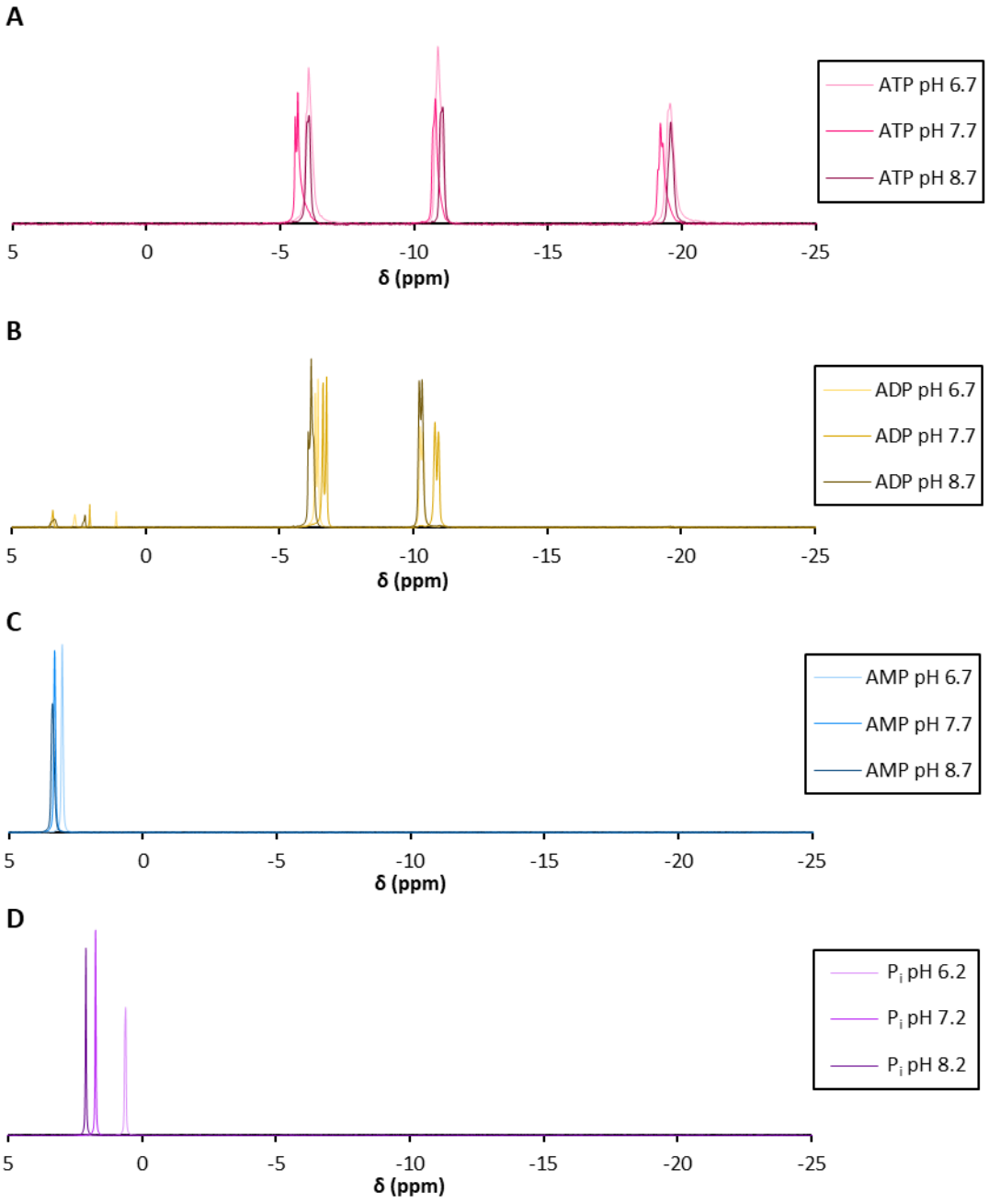

Figure 4.15: *High-resolution ^{31}P NMR spectra (162 MHz) of solutions of (**A**) ATP, (**B**) ADP, (**C**) AMP and (**D**) P_i at varying pHs, with all containing 40 mM magnesium chloride to better mimic conditions inside cells.*

The peak between 4 ppm and 2 ppm in the *M. smegmatis* spectrum is in the same region as the peak in the AMP spectrum at pH 6.7. A signal from AMP likely makes up

part of this peak but the broadness suggests signals from other phosphorylated metabolites may also be present in this region, possibly PMEs based on the chemical shift (Satre et al., 1989). The presence of overlapping signals prevents the use of NMR to quantify AMP in *M. smegmatis* cells. It is possible this could be resolved by proper identification of these metabolites, followed by recording of reference spectra and use of deconvolution techniques to determine the contribution from AMP.

While it is not possible to use high-resolution NMR to investigate antibiotic mechanisms in live cells due to the oxygenation issue, although it is possible a perfusion system may be used to allow this, these data provide a framework for future NMR studies. The high-resolution reference spectra can be used to identify peaks due to the individual phosphorus nuclei in ADP and ATP as a result of splitting patterns and changes in chemical shift with pH.

4.5. FUTURE WORK

As discussed previously, development of equipment and methods to perform NMR studies on live bacteria was originally undertaken with the intention of using the technique to aid in unravelling the mechanism of BDQ. As work with the bioenergetic chamber progressed, it became clear the visible-wavelength remission spectra and OCR measurements recorded using the chamber would be sufficient to prove and explain the immediate effects of BDQ binding to ATP synthase. The result of this is that translation of the work outlined in this chapter into performing ^{31}P NMR measurements on oxygenated cell cultures was not achieved within the time constraints of the project. However, there remains substantial potential for future work, particularly on understanding the finer details of how BDQ affects the phosphorylation potential in living cells.

Current research on the impact of BDQ on ATP levels in mycobacteria relies on quench and measure techniques, as opposed to the live cell measurements that are possible with NMR. Measurements of ATP/ADP ratios and ΔpH using NMR would provide further support for the direct ATP synthase inhibition mode of action. The NMR chamber could also be used to investigate the effects of other anti-TB drugs that target

bioenergetics. This has the potential to be expanded further to study more bacterial species.

The first step in implementing these ideas is moving onto performing NMR experiments using the NMR chamber. Prior to collecting spectra on oxygenated cells, the effect of using the airlift system to mix and oxygenate cultures on the quality of the spectra obtained must be investigated. This could be done by using a standard solution of a phosphorylated metabolite (i.e. P_i) and comparing the peak width of the signal obtained with and without bubbling air through the NMR chamber. As the air bubbles in the chamber are introduced above the sample contained within the coil, the air bubbles themselves should not impact the homogeneity of the magnetic field, but too vigorous mixing could affect the quality of the spectra. If the peaks in spectra obtained with bubbling are noticeably broader than those without, then operation of the chamber will need to be changed. Rather than using a continuous flow of air, a change could be made to the system where air is bubbled through into the chamber, turned off for the period of one NMR scan and then restarted. As NMR scan time is usually on the scale of milliseconds, this should limit disruption to the quality of the spectra while ensuring cells remain oxygenated.

Once this has been resolved, the NMR chamber can be used to record spectra of live cells. Quantification of phosphorylation ratios could be achieved by acquiring spectra of phosphorylated metabolites in buffer solution in the NMR chamber and using deconvolution techniques to separate out signal contributions from ATP, ADP and AMP. ΔpH measurements could be made via inclusion of a reference capillary containing a standard solution of MeP and comparing this to the signals from P_{iic} and P_{iec}.

Having the means to conduct NMR experiments on live cell cultures has the potential provide further insights into cells. The NMR chamber would be suitable for use in ^{31}P MT experiments, providing a means of determining the rate of ATP production in live cells. Studies on cell metabolism could be achieved with ^{13}C NMR via the use of ^{13}C-labelled carbon sources. The same methodology can also be applied to the study of other obligately aerobic bacteria of interest.

5. CONCLUSIONS

This thesis has dealt with the development of non-invasive techniques to investigate bioenergetics in live mycobacteria. Visible-wavelength remission spectroscopy is a powerful tool for observing changes in cytochrome oxidation state, especially when combined with OCR measurements as is possible with the bioenergetic chamber.

In comparison to the more established Seahorse XF Analyser, which is also used in the non-invasive study of live cells, the bioenergetic chamber allows for a deeper insight into bioenergetic processes but does not render the Seahorse XF Analyser obsolete. Both use oxygen-sensitive fluorescence to measure the OCR of cells in liquid media, with the advantages of this over using a conventional Clark electrode to measure OCRs being discussed in section 3.1.2 (Ferrick, Neilson and Beeson, 2008; Chacko et al., 2013; Rocha and Springett, 2019). Both also share the same disadvantage with regards to mycobacterial research, in that they are not suitable for use with macrophage infection models.

The Seahorse XF Analyser contains a proton sensitive fluorophore and can be used to monitor proton efflux alongside oxygen consumption (Ferrick, Neilson and Beeson, 2008; Chacko et al., 2013). The bioenergetic chamber, however, records cytochrome spectra, allowing an insight into changes in cytochrome oxidation state (Rocha and Springett, 2019). From this, if reference spectra for the organism under study are available, and it is possible to fully reduce and oxidise the cytochromes in the ETC over the course of an experiment, $\Delta\Psi$ can be determined (Kim, Ripple and Springett, 2012). Analysis of data from the bioenergetic chamber is more involved and be can be confounded by a greater number of factors, such as cell morphology and pigment production or loss, compared with the Seahorse XF Analyser (Ferrick, Neilson and Beeson, 2008; Chacko et al., 2013; Rocha and Springett, 2019). Thus, the Seahorse XF Analyser is ideal if only monitoring of OCR and/or proton efflux is required. The bioenergetic chamber is more suited to detailed studies of the oxidative phosphorylation system, especially if work on isolated proteins from the organism in question is being conducted alongside live cell experiments.

The bioenergetic chamber had previously only been used with mammalian cell cultures, and thus a protocol for working with *M. smegmatis* and *M. tuberculosis* was developed. To make physiologically relevant measurements required that mycobacteria were grown in the right conditions and the cultures suitably prepared. Inclusion of a detergent in media resulted in low susceptibility of *M. smegmatis* to the protonophore CCCP. This was likely due to CCCP dissolving into the hydrophobic phase created by the detergent and lowering the effective concentration cells were exposed to. Washing and resuspending cells in HEPES buffer solution prior to loading them into the bioenergetic chamber effectively solved this issue, however it also resulted in no effects being observed when cells were exposed to the ionophore nigericin, and in variable changes in OCR depending upon the salt included in the buffer. Resuspension in growth media without the inclusion of a detergent solved both of these issues.

The OCR of *M. tuberculosis* was found to be significantly lower than that of *M. smegmatis*, indicating the slower growth rate of *M. tuberculosis* is related to a lower respiratory rate as opposed to a less efficient system. Use of samples with a similar OD_{600} to that of *M. smegmatis* samples resulted in the OCR of *M. tuberculosis* cells being too low to be reliably measured by the bioenergetic chamber. Growth of cells to a higher OD_{600} (>1) led to the presence of a haem-containing pigment in samples, the absorbance of which overlapped with the those of the ETC cytochromes. Therefore, *M. tuberculosis* cells were concentrated during the wash and resuspension process to achieve a higher OCR.

Currently, there are a dearth of chemical effectors to modulate bioenergetic systems *in vivo*. A set of known metabolic inhibitors and protonophores/ionophores were investigated for activity against *M. smegmatis* using the bioenergetic chamber. The original hope for this work was to find an inhibitor or combination of inhibitors that could be employed to fully oxidise the cytochromes in the mycobacterial ETC. When combined with a fully reduced reference point and model mycobacterial cytochrome spectra, this could be used to quantify changes in cytochrome oxidation state as well as calculate changes in $\Delta\Psi$ (Kim, Ripple and Springett, 2012). The NDH-2 inhibitor, TFPZ, was selected as the most promising candidate to oxidise the ETC of *M. smegmatis*. Preliminary $\Delta\Psi$ measurements were made using CCCP to induce changes

in ΔΨ, however these expected changes were not observed in the ΔΨ trace produced by the bioenergetic chamber. This led to the conclusion that either incomplete oxidation of the cytochromes following treatment with TFPZ or errors in cytochrome signal fitting/midpoint potential values were responsible and would need to be rectified to allow quantitative cytochrome measurements. Due to difficulty in obtaining isolated cytochrome reference spectra, it was decided data from the bioenergetic chamber should be examined qualitatively until a method for generating accurate reference spectra is found.

Having a protocol for preparing samples of mycobacterial cells for use with the bioenergetic chamber, as well as a library of compounds that affect the oxidative phosphorylation system of the model organism *M. smegmatis*, enables many future studies on mycobacterial bioenergetics. Previous studies have relied upon the Seahorse XF Analyser/Clark electrode, working with simplified systems such as IMVs or techniques that require lysis of cells (Hards et al., 2015; Lamprecht et al., 2016; Hards et al., 2018; Wang et al., 2019; Mackenzie et al., 2020). None of these techniques have been able to elucidate the mode of action of the important antibiotic BDQ in *M. tuberculosis*, demonstrating the need for this new method of studying mycobacteria. Thus, in order to showcase the potential power of the bioenergetic chamber, the protocols developed for studying mycobacteria using the chamber were applied to the study of BDQ's mode of action.

The effects of BDQ on the mycobacterial oxidative phosphorylation system were first explored in *M. smegmatis*. When nanomolar concentrations of BDQ were added to *M. smegmatis*, reduction of the *b* and *c* cytochromes was observed alongside a slight increase in OCR. Repeating this experiment with a mutant that harboured a point mutation in the c-ring, which should render it resistant to BDQ, demonstrated these effects are reliant on BDQ being able to bind to ATP synthase. This increase in OCR on BDQ addition to *M. smegmatis* and *M. tuberculosis* has been previously reported (Hards et al., 2015; Lamprecht et al., 2016), and has been used as evidence for BDQ acting as a protonophore or ionophore (Hards et al., 2015; Hards et al., 2018). However, the observation that this is accompanied by reduction of the *b* and *c* cytochromes is novel.

Use of the bioenergetic chamber allowed comparison of changes in cytochrome oxidation and OCR on addition of BDQ versus the known ATP synthase inhibitor DCCD, as well as known protonophore/ionophores, CCCP and nigericin. BDQ's effects are most similar to those observed with DCCD, with a modest increase in OCR and reduction of the *b* and *c* cytochromes occurring on addition of either compound. Addition of CCCP and nigericin led to oxidation of the *b* and *c* cytochromes, demonstrating they operate differently from BDQ

The increase in OCR on BDQ or DCCD addition is counterintuitive to the action of direct ATP synthase inhibitors. It was hypothesised that this may be due to an increase in activity of the non-proton pumping cytochrome *bd* oxidase, which is less susceptible to backpressure resulting from ATP synthase inhibition than the supercomplex. A similar theory had previously been investigated by Lamprecht et al. (2016) using an *M. tuberculosis* knockout strain (*cydKO*), however rather than lacking the genes for cytochrome *bd* oxidase (*cydAB*), the strain used lacked the genes for an ABC transporter (Arora et al., 2014; Aung, Berney and Cook, 2014). No differences were observed when treating *cydKO* with BDQ compared with *M. tuberculosis* H37Rv so the theory was discounted (Lamprecht et al., 2016). Through experiments with a *M. smegmatis* Δ*cydAB* strain, this work was able to show the increase in OCR on BDQ addition is due to increased electron flux through cytochrome *bd* oxidase, as there is a sharp drop in the OCR of *M. smegmatis* Δ*cydAB* cells when BDQ is added.

To translate these results to the real pathogen, the action of BDQ on BSL-2 compatible strains of *M. tuberculosis* was explored ($mc^2$6206 and $mc^2$6230). BDQ has similar effects on *M. tuberculosis* as observed in *M. smegmatis* although changes in cytochrome oxidation state and OCR occur more slowly, with the increase in OCR ultimately being of a greater magnitude. This can be explained by higher amounts of cytochrome *bd* oxidase being present in the ETC. In an *M. tuberculosis* cytochrome *bd* oxidase knockout strain derived from $mc^2$6230 (*M. tuberculosis* Δ*cydAB)*, an increase in OCR is observed with nanomolar concentrations of BDQ, although it is still lower than that observed in $mc^2$6230. This may due to a difference in the utilisation of NDH-1 versus NDH-2 in *M. tuberculosis* and *M. smegmatis*. Rerouting of electrons through

the non-proton pumping NDH-2 instead of the proton-pumping NDH-1 would achieve a similar effect as routing electrons through cytochrome *bd* oxidase.

There is a proposal that BDQ acts differently when raised to micromolar concentrations (Hards et al., 2018; Guo et al., 2021), therefore experiments with *M. smegmatis* and *M. tuberculosis* were repeated at micromolar concentrations. Few differences were observed between the two concentrations, with the higher concentration in *M. tuberculosis* resulting in more rapid but similar effects in the mc^26230 strain and a decrease in OCR in the cytochrome *bd* knockout strain. This demonstrates BDQ acts predominantly as a direct inhibitor of ATP synthase regardless of concentration.

Prior to this work, the matter of whether BDQ acts as direct inhibitor of ATP synthase or as a protonophore or ionophore had not been proven (Lamprecht et al., 2016; Hards et al., 2018; Courbon et al., 2023). Due to the level of insight into live cells provided by the bioenergetic chamber, the results summarised here and discussed further in chapter 3 provide solid evidence that BDQ's mode of action is ATP synthase inhibition. Precisely how this leads to bacterial cell death is currently still unclear, but by establishing the mode of action of BDQ, the groundwork has been laid for future research in this area.

In terms of the implications of having an established mode of action for BDQ, it enables a more thorough evaluation of potential combination therapies (both with existing and future antibiotics). In addition, this knowledge allows for theories on the likely modes of action of second-generation compounds TBAJ-587 and TBAJ-876, although further experiments with the bioenergetic chamber would be needed to explicitly prove them. The finding that the increase in OCR on BDQ addition is dependent on cytochrome *bd* oxidase also highlights this complex as a potential target for future antibiotics to be used with BDQ.

While the bioenergetic chamber provides a significant insight into live cells, it does not give a complete picture of all bioenergetic processes. A thorough review of the applications of ^{31}P NMR in live cell work, a technique not yet applied to the study of mycobacteria, was conducted, with the aim of applying this knowledge to the study

of BDQ. Of particular interest in its potential use to study the effects of BDQ is the ability to monitor ATP/ADP ratios and measure changes in ΔpH. A design for a chamber that could be used to supply mycobacterial cultures with oxygen and sufficiently mix them inside an NMR machine without compromising the quality of the NMR spectra was developed based on the airlift systems found in literature. Through iterative design, this chamber was realised and its ability to sustain growth of an *M. smegmatis* culture was demonstrated.

Initial wide-bore ^{31}P NMR experiments on an unoxygenated culture of *M. smegmatis* were performed to qualitatively investigate the most suitable acquisition parameters to use with live cultures. High-resolution NMR was used to acquire a detailed ^{31}P NMR spectrum of unoxygenated *M. smegmatis* cells and signals due to phosphorylated metabolites were assigned using a mixture of reference spectra and data from literature. In order for spectra of isolated ATP, ADP and AMP to resemble the signals from cells, they must be recorded in the presence of magnesium ions, as in cells these compounds chelate magnesium. This method of investigating bioenergetics was not able to be applied to the mechanism of BDQ due to time constraints, but this remains as a future possibility using the work presented here.

The suitability of the NMR chamber for use in performing ^{31}P NMR on live mycobacteria has yet to be proven and the steps required for this are outlined in section 4.5. Once this has been established, it is possible the NMR chamber could be combined with the bioenergetic chamber to create a system that would allow simultaneous measurements of OCR, cytochrome oxidation state and changes in levels of phosphorylated metabolites. Such a system would be extremely powerful in the study of live cells, however its assembly would not be trivial due to the issue of being unable to have magnetic metals within the vicinity of the NMR machine. Fibre-optic cables could be used to allow the recording of remission spectra, with these cables running through the lid of the NMR chamber and being held in place by the upper plastic ring supporting the inner tube.

With the current design of the NMR chamber, addition of compounds to the culture within requires disassembly of the apparatus. This is not ideal if the NMR chamber is

combined with the bioenergetic chamber as it would mean data could not be recorded around the time of each addition. This could potentially be mitigated by switching to an NMR/MRI machine with a larger space for samples, as this would allow manipulation of the chamber while within the detection coil, as well as fitting a lid with a port for the addition of compounds.

Overall, the work presented here demonstrates both the power and challenges of live cell methods for studying mycobacterial bioenergetics. Use of live cells prevents concerns over the impact of lysing cells on the systems under study, however it is true neither of the methods discussed here, remission spectroscopy and ^{31}P NMR, could be used to study mycobacteria within infected cells/organisms. Despite this, the strengths of the bioenergetic chamber were demonstrated through its use to elucidate the mode of action of BDQ, something that has not been achieved in the two decades since the drug's discovery using conventional methods (Andries et al., 2005; Courbon et al., 2023). ^{31}P NMR remains a potential means of further exploring BDQ's impact on cells, as well as studying mycobacterial bioenergetics more generally.

6. REFERENCES

Abrahams, K. A., Batt, S. M., Gurcha, S. S., Veerapen, N., Bashiri, G. and Besra, G. S. (2023). DprE2 is a molecular target of the anti-tubercular nitroimidazole compounds pretomanid and delamanid. *Nature Communications*. 14 (1), 3828. Available at: doi:10.1038/s41467-023-39300-z.

Abuhammad, A. (2017). Cholesterol metabolism: a potential therapeutic target in *Mycobacteria*. *British Journal of Pharmacology*. 174 (14), 2194-2208. Available at: doi:10.1111/bph.13694.

Ackerman, J. J., Soto, G. E., Spees, W. M., Zhu, Z. and Evelhoch, J. L. (1996). The NMR chemical shift pH measurement revisited: analysis of error and modeling of a pH dependent reference. *Magnetic Resonance in Medicine.* 36 (5), 674–683. Available at: doi:10.1002/mrm.1910360505.

Adékambi, T., Ben Salah, S., Khlif, M., Raoult, D. and Drancourt, M. (2006). Survival of environmental mycobacteria in *Acanthamoeba polyphaga*. *Applied and Environmental Microbiology*. 72 (9), 5974–5981. Available at: doi:10.1128/AEM.03075-05.

Ahn, S., Jung, J., Jang, I. A., Madsen, E. L. and Park, W. (2016). Role of Glyoxylate Shunt in Oxidative Stress Response. *Journal of Biological Chemistry*. 291 (22), 11928-11938. Available at: doi:10.1074/jbc.M115.708149.

Alger, J. R., den Hollander, J. A. and Shulman, R. G. (1982). *In vivo* phosphorus-31 nuclear magnetic resonance saturation transfer studies of adenosinetriphosphatase kinetics in *Saccharomyces cerevisiae*. *Biochemistry*. 21 (12), 2957–2963. Available at: doi:10.1021/bi00541a024.

Ali, M. Z., Dutt, T. S., MacNeill, A., Walz, A., Pearce, C., Lam, H., Philp, J., Patterson, J., Henao-Tamayo, M., Lee, R. E., Liu, J., Robertson, G. T., Hickey, A. J., Meibohm, B. and Gonzalez-Juarrero, M. (2024). A modified BPaL regimen for tuberculosis treatment

replaces linezolid with inhaled spectinamides. *eLife*. 13, RP96190. Available at: doi:10.1101/2023.11.16.567434.

Alsayed, S. S. R. and Gunosewoyo, H. (2023). Tuberculosis: Pathogenesis, current treatment regimens and new drug targets. *International Journal of Molecular Sciences*. 24 (6), 5202. Available at: doi:10.3390/ijms24065202.

Andries, K., Verhasselt, P., Guillemont, J., Göhlmann, H. W. H., Neefs, J.-M., Winkler, H., Van Gestel, J., Timmerman, P., Zhu, M., Lee, E., Williams, P., de Chaffoy, D., Huitric, E., Hoffner, S., Cambau, E., Truffot-Pernot, C., Lounis, N. and Jarlier, V. (2005). A diarylquinoline drug active on the ATP synthase of *Mycobacterium tuberculosis*. *Science*. 307 (5707), 223–227. Available at: doi:10.1126/science.1106753.

Anton, V., Rougé, P. and Daffé, M. (1996). Identification of the sugars involved in mycobacterial cell aggregation. *FEMS Microbiology Letters*. 144 (2–3), 167–170. Available at: doi:10.1111/j.1574-6968.1996.tb08525.x.

Armstrong, J. A. and Hart, P. D. (1971). Response of cultured macrophages to *Mycobacterium tuberculosis*, with observations on fusion of lysosomes with phagosomes. *Journal of Experimental Medicine*. 134 (3 Pt 1), 713–740. Available at: doi:10.1084/jem.134.3.713.

Armstrong, D. T. and Parrish, N. (2021). Current updates on Mycobacterial taxonomy, 2018 to 2019. *Journal of Clinical Microbiology*. 59 (7), e0152820. Available at: doi:10.1128/JCM.01528-20.

Arora, K., Ochoa-Montaño, B., Tsang, P. S., Blundell, T. L., Dawes, S. S., Mizrahi, V., Bayliss, T., Mackenzie, C. J., Cleghorn, L. A. T., Ray, P. C., Wyatt, P. G., Uh, E., Lee, J., Barry, C. E., 3rd and Boshoff, H. I. (2014). Respiratory flexibility in response to inhibition of cytochrome C oxidase in *Mycobacterium tuberculosis*. *Antimicrobial Agents and Chemotherapy*. 58 (11), 6962–6965. Available at: doi:10.1128/AAC.03486-14.

Asai, M., Li, Y., Spiropoulos, J., Cooley, W., Everest, D., Robertson, B. D., Langford, P. R. and Newton, S. M. (2020). A novel biosafety level 2 compliant tuberculosis infection

model using a Δ *leuD* Δ *panCD* double auxotroph of *Mycobacterium tuberculosis* H37Rv and *Galleria mellonella*. *Virulence*. 11 (1), 811-824. Available at: doi:10.1080/21505594.2020.1781486.

Aubry, A., Mougari, F., Reibel, F. and Cambau, E. (2017). *Mycobacterium marinum*. *Microbiology Spectrum*. 5 (2). Available at: doi:10.1128/microbiolspec.TNMI7-0038-2016.

Aung, H. L., Berney, M. and Cook, G. M. (2014). Hypoxia-activated cytochrome bd expression in *Mycobacterium smegmatis* is cyclic AMP receptor protein dependent. *Journal of Bacteriology*. 196 (17), 3091–3097. Available at: doi:10.1128/JB.01771-14.

Avanzi, C., Del-Pozo, J., Benjak, A., Stevenson, K., Simpson, V. R., Busso, P., McLuckie, J., Loiseau, C., Lawton, C., Schoening, J., Shaw, D. J., Piton, J., Vera-Cabrera, L., Velarde-Felix, J. S., McDermott, F., Gordon, S. V., Cole, S. T. and Meredith, A. L. (2016). Red squirrels in the British Isles are infected with leprosy bacilli. *Science.* 354 (6313), 744–747. Available at: doi:10.1126/science.aah3783.

Bachmann, N. L., Salamzade, R., Manson, A. L., Whittington, R., Sintchenko, V., Earl, A. M. and Marais, B. J. (2019). Key transitions in the evolution of rapid and slow growing mycobacteria identified by comparative genomics. *Frontiers in Microbiology*. 10, 3019. Available at: doi:10.3389/fmicb.2019.03019.

Baker, O., Lee, O. Y.-C., Wu, H. H. T., Besra, G. S., Minnikin, D. E., Llewellyn, G., Williams, C. M., Maixner, F., O'Sullivan, N., Zink, A., Chamel, B., Khawam, R., Coqueugniot, E., Helmer, D., Le Mort, F., Perrin, P., Gourichon, L., Dutailly, B., Pálfi, G., Coqueugniot, H. and Dutour, O. (2015). Human tuberculosis predates domestication in ancient Syria. *Tuberculosis.* 95 Suppl 1, S4–S12. Available at: doi:10.1016/j.tube.2015.02.001.

Barberis, I., Bragazzi, N. L., Galluzzo, L. and Martini, M. (2017). The history of tuberculosis: from the first historical records to the isolation of Koch's bacillus. *Journal of Preventive Medicine and Hygiene*. 58 (1), E9–E12. Available at: https://www.ncbi.nlm.nih.gov/pmc/articles/PMC5432783/.

Befroy, D. E., Rothman, D. L., Petersen, K. F. and Shulman, G. I. (2012). ^{31}P-magnetization transfer magnetic resonance spectroscopy measurements of *in vivo* metabolism. *Diabetes*. 61 (11), 2669–2678. Available at: doi:10.2337/db12-0558.

Behr, M. A., Wilson, M. A., Gill, W. P., Salamon, H., Schoolnik, G. K., Rane, S. and Small, P. M. (1999). Comparative genomics of BCG vaccines by whole-genome DNA microarray. *Science*. 284, 1520-1523. Available at: doi:10.1126/science.284.5419.1520.

Beites, T., O'Brien, K., Tiwari, D., Engelhart, C. A., Walters, S., Andrews, J., Yang, H. J., Sutphen, M. L., Weiner, D. M., Dayao, E. K., Zimmerman, M., Prideaux, B., Desai, P. V., Masquelin, T., Via, L. E., Dartois, V., Boshoff, H. I., Barry, C. E. 3rd, Ehrt, S and Schnappinger, D. (2019). Plasticity of the *Mycobacterium tuberculosis* respiratory chain and its impact on tuberculosis drug development. *Nature Communications*. 10 (1), 4970. Available at: doi:10.1038/s41467-019-12956-2.

Bell, J. D., Gadian, D. G. and Preece, N. E. (1990). NMR studies of drug metabolism and disposition. *European Journal of Drug Metabolism and Pharmacokinetics*. 15 (2), 127–133. Available at: doi:10.1007/BF03190195.

Berney, M., Hartman, T. E. and Jacobs, W. R. (2014). A *Mycobacterium tuberculosis* Cytochrome *bd* Oxidase Mutant is Hypersensitive to Bedaquiline. *mBio*. 5 (4), e01275-14. Available at: doi:10.1128/mBio.01275-14.

Berry, E. A. and Trumpower, B. L. (1987). Simultaneous determination of hemes a, b, and c from pyridine hemochrome spectra. *Analytical Biochemistry*. 161 (1), 1–15. Available at: doi:10.1016/0003-2697(87)90643-9.

Biukovic, G., Basak, S., Manimekalai, M. S. S., Rishikesan, S., Roessle, M., Dick, T., Rao, S. P. S., Hunke, C. and Grüber, G. (2013). Variations of subunit {varepsilon} of the *Mycobacterium tuberculosis* F1Fo ATP synthase and a novel model for mechanism of action of the tuberculosis drug TMC207. *Antimicrobial Agents and Chemotherapy*. 57 (1), 168–176. Available at: doi:10.1128/AAC.01039-12.

Boot, M., Jim, K. K., Liu, T., Commandeur, S., Lu, P., Verboom, T., Lill, H., Bitter, W. and Bald, D. (2017). A fluorescence-based reporter for monitoring expression of mycobacterial cytochrome bd in response to antibacterials and during infection. *Scientific Reports*. 7 (1), 10665. Available at: doi:10.1038/s41598-017-10944-4.

Bos, K. I., Harkins, K. M., Herbig, A., Coscolla, M., Weber, N., Comas, I., Forrest, S. A., Bryant, J. M., Harris, S. R., Schuenemann, V. J., Campbell, T. J., Majander, K., Wilbur, A. K., Guichon, R. A., Wolfe Steadman, D. L., Cook, D. C., Niemann, S., Behr, M. A., Zumarraga, M., Bastida, R., Huson, D., Nieselt, K., Young, D., Parkhill, J., Buikstra, J. E., Gagneux, S., Stone, A. C. and Krause J. (2014). Pre-Columbian mycobacterial genomes reveal seals as a source of New World human tuberculosis. *Nature*. 514 (7523), 494–497. Available at: doi:10.1038/nature13591.

Boyd, V. L., Robbins, J. D., Egan, W. and Ludeman, S. M. (1986). 31P nuclear magnetic resonance spectroscopic observation of the intracellular transformations of oncostatic cyclophosphamide metabolites. *Journal of Medicinal Chemistry*. 29 (7), 1206–1210. Available at: doi:10.1021/jm00157a015.

Brites, D. and Gagneux, S. (2015). Co-evolution of *Mycobacterium tuberculosis* and Homo sapiens. *Immunological Reviews*. 264 (1), 6–24. Available at: doi:10.1111/imr.12264.

British Thoracic and Tuberculosis Association (1976). Short-course chemotherapy in pulmonary tuberculosis. *Lancet*. 308 (7995), 1102–1104. Available at: doi:10.1016/s0140-6736(76)91085-0.

Brown, T. R. and Ogawa, S. (1977). 31P nuclear magnetic resonance kinetic measurements on adenylatekinase. *Proceedings of the National Academy of Sciences of the United States of America*. 74 (9), 3627–3631. Available at: doi:10.1073/pnas.74.9.3627.

Bryant, J. M., Grogono, D. M., Rodriguez-Rincon, D., Everall, I., Brown, K. P., Moreno, P., Verma, D., Hill, E., Drijkoningen, J., Giligan, P., Esther, C. R., Noone, P.G., Giddings, O., Bell, S. C., Thomson, R., Wainwright, C. E., Coulter, C., Pandey, S., Wood, M. E., Stockwell, R. E., Ramsay, K. A., Sherrard, L. J., Kidd, T. J., Jabbour, N., Johnson, G. R.,

Knibbs, L. D., Morawska, L., Sly, P. D., Jones, A., Bilton, D., Laurenson, I., Ruddy, M., Bourke, S., Bowler, I. C., Chapman, S. J., Clayton, A., Cullen, M., Daniels, T., Dempsey, O., Denton, M., Desai, M., Drew, R. J., Edenborough, F., Evans, J., Folb, J., Humphrey, H., Isalska, B., Jensen-Fangel, S., Jönsson, B., Jones, A. M., Katzenstein, T. L., Lillebaek, T., MacGregor, G., Mayell, S., Millar, M., Modha, D., Nash, E. F., O'Brien, C., O'Brien, D., Ohri, C., Pao, C. S., Peckham, D., Perrin, F., Perry, A., Pressler, T., Prtak, L., Qvist, T., Robb, A., Rodgers, H., Schaffer, K., Shafi, N., van Ingen, J., Walshaw, M., Watson, D., West, N., Whitehouse, J., Haworth, C. S., Harris, S. R., Ordway, D. and Parkhill, J. (2016). Emergence and spread of a human-transmissible multidrug-resistant nontuberculous mycobacterium. *Science (New York, N.Y.)*. 354 (6313), 751–757. Available at: doi:10.1126/science.aaf8156.

Burkholder, P. R. and Giles, N. H., Jr (1947). Induced biochemical mutations in *Bacillus subtilis*. *American Journal of Botany*. 34 (6), 345–348. Available at: doi:10.1002/j.1537-2197.1947.tb12999.x.

Campbell, E. A., Korzheva, N., Mustaev, A., Murakami, K., Nair, S., Goldfarb, A. and Darst, S. A. (2001). Structural mechanism for rifampicin inhibition of bacterial rna polymerase. *Cell*. 104 (6), 901–912. Available at: doi:10.1016/s0092-8674(01)00286-0.

Campbell, S. L., Jones, K. A. and Shulman, R. G. (1985). In vivo 31P nuclear magnetic resonance saturation transfer measurements of phosphate exchange reactions in the yeast *Saccharomyces cerevisiae*. *FEBS Letters*. 193 (2), 189–193. Available at: doi:10.1016/0014-5793(85)80148-4.

Campbell-Burk, S. L., Jones, K. A. and Shulman, R. G. (1987). 31P NMR saturation-transfer measurements in *Saccharomyces cerevisiae*: characterization of phosphate exchange reactions by iodoacetate and antimycin A inhibition. *Biochemistry*. 26 (23), 7483–7492. Available at: doi:10.1021/bi00397a043.

Carvalho, J., Alves, S., Castro, M. M. C. A., Geraldes, C. F. G. C., Queiroz, J. A., Fonseca, C. P. and Cruz, C. (2019). Development of a bioreactor system for cytotoxic evaluation of pharmacological compounds in living cells using NMR spectroscopy. *Journal of*

Pharmacological and Toxicological Methods. 95, 70–78. Available at: doi:10.1016/j.vascn.2018.11.004.

Chacko, B. K., Kramer, P. A., Ravi, S., Johnson, M. S., Hardy, R. W., Ballinger, S. W. and Darley-Usmar, V. M. (2013). Methods for defining distinct bioenergetic profiles in platelets, lymphocytes, monocytes, and neutrophils, and the oxidative burst from human blood. *Laboratory Investigation*. 93 (6), 690–700. Available at: doi:10.1038/labinvest.2013.53.

Chaisson, R. E. and Nachega, J. B. (2010). Tuberculosis. In Warrell, D. A., Cox, T. M. and Firth, J. D. (Eds). *Oxford Textbook of Medicine Fifth Edition Volume 1*. Oxford: Oxford University Press, pp. 810-831.

Chakraborty, S. and Rhee, K. Y. (2015). Tuberculosis drug development: History and evolution of the mechanism-based paradigm. *Cold Spring Harbor Perspectives in Medicine*. 5 (8), a021147. Available at: doi:10.1101/cshperspect.a021147.

Chauhan, P., van der Meulen, S. A., Simões Caetano, J. M., Goojani, H. G., Botman, D., van Spanning, R., Lill, H. and Bald, D. (2022). Response of *Mycobacterium smegmatis* to the Cytochrome bcc Inhibitor Q203. *International Journal of Molecular Sciences*. 23 (18). Available at: doi:10.3390/ijms231810331.

Chen, K.-H., Lin, C.-Y., Su, S.-B. and Chen, K.-T. (2022). Leprosy: A review of epidemiology, clinical diagnosis, and management. *Journal of Tropical Medicine*. 2022, 8652062. Available at: doi:10.1155/2022/8652062.

Chitale, P., Lemenze, A. D., Fogarty, E. C., Shah, A., Grady, C., Odom-Mabey, A. R., Johnson, W. E., Yang, J. H., Eren, A. M., Brosch, R., Kumar, P. and Alland, D. (2022). A comprehensive update to the *Mycobacterium tuberculosis* H37Rv reference genome. *Nature Communications*. 13, 7068. Available at: doi:10.1038/s41467-022-34853-x.

Chong, S. M. S., Manimekalai, M. S. S., Sarathy, J. P., Williams, Z. C., Harold, L. K., Cook, G. M., Dick, T., Pethe, K., Bates, R.W. and Grüber, G. (2020). Antituberculosis Activity of the Antimalaria Cytochrome bcc Oxidase Inhibitor SCR0911. *ACS Infectious Diseases*. 6 (4), 725–737. Available at: doi:10.1021/acsinfecdis.9b00408.

Chorao, C., Traïkia, M., Besse-Hoggan, P., Sancelme, M., Bligny, R., Gout, E., Mailhot, G. and Delort, A.-M. (2010). *In vivo* 31P and 13C NMR investigations of *Rhodococcus rhodochrous* metabolism and behaviour during biotransformation processes. *Journal of Applied Microbiology*. 108 (5), 1733–1743. Available at: doi:10.1111/j.1365-2672.2009.04577.x.

Cokol, M., Kuru, N., Bicak, E., Larkins-Ford, J. and Aldridge, B. B. (2017). Efficient measurement and factorization of high-order drug interactions in Mycobacterium tuberculosis. *Science Advances*. 3 (10), e1701881. Available at: doi:10.1126/sciadv.1701881.

Collins, F. M. (1989). Mycobacterial disease, immunosuppression, and acquired immunodeficiency syndrome. *Clinical Microbiology Reviews*. 2 (4), 360–377. Available at: doi:10.1128/CMR.2.4.360.

Collins, A. B., Floyd, S., Gordon, S. V. and More, S. J. (2022). Prevalence of *Mycobacterium bovis* in milk on dairy cattle farms: An international systematic literature review and meta-analysis. *Tuberculosis*. 132, 102166. Available at: doi:10.1016/j.tube.2022.102166.

Comas, I., Coscollá, M., Luo, T., Borrell, S., Holt, K. E., Kato-Maeda, M., Parkhill, J., Malla, B., Berg, S., Thwaites, G., Yeboah-Manu, D., Bothamley, G., Mei, J., Wei, L., Bentley, S., Harris, S., Niemann, S., Diel, R., Aseffa, A., Gao, Q., Young, D., and Gagneux, S. (2013). Out-of-Africa migration and Neolithic coexpansion of *Mycobacterium tuberculosis* with modern humans. *Nature Genetics*. 45 (10), 1176–1182. Available at: doi:10.1038/ng.2744.

Cook, G. M., Berney, M., Gebhard, S., Heinemann, M., Cox, R. A., Danilchanka, O. and Niederweis, M. (2009). Physiology of mycobacteria. *Advances in Microbial Physiology*. 55, 81–182, 318–319. Available at: doi:10.1016/S0065-2911(09)05502-7.

Cook, G. M., Hards, K., Vilchèze, C., Hartman, T. and Berney, M. (2014). Energetics of Respiration and Oxidative Phosphorylation in Mycobacteria. *Microbiology Spectrum*. 2 (3). Available at: doi:10.1128/microbiolspec.MGM2-0015-2013.

Coscolla, M., Gagneux, S., Menardo, F., Loiseau, C., Ruiz-Rodriguez, P., Borrell, S., Otchere, I. D., Asante-Poku, A., Asare, P., Sánchez-Busó, L., Gehre, F., Sanoussi, C. N., Antonio, M., Affolabi, D., Fyfe, J., Beckert, P., Niemann, S., Alabi, A. S., Grobusch, M. P., Kobbe, R., Parkhill, J., Beisel, C., Fenner, L., Böttger, E. C., Meehan, C. J., Harris, S. R., de Jong, B. C., Yeboah-Manu, D. and Brites, D. (2021). Phylogenomics of *Mycobacterium africanum* reveals a new lineage and a complex evolutionary history. *Microbial Genomics*. 7 (2), 000477. Available at: doi:10.1099/mgen.0.000477.

Cosivi, O., Grange, J. M., Daborn, C. J., Raviglione, M. C., Fujikura, T., Cousins, D., Robinson, R. A., Huchzermeyer, H. F., de Kantor, I. and Meslin, F. X. (1998). Zoonotic tuberculosis due to *Mycobacterium bovis* in developing countries. *Emerging Infectious Diseases*. 4 (1), 59–70. Available at: doi:10.3201/eid0401.980108.

Couldwell, D. L., Dunford, R., Kruger, N.J., Lloyd, D.C., Ratcliffe, R.G. and Smith, A.M.O. (2009). Response of cytoplasmic pH to anoxia in plant tissues with altered activities of fermentation enzymes: application of methyl phosphonate as an NMR pH probe. *Annals of Botany*. 103 (2), 249–258. Available at: doi:10.1093/aob/mcn174.

Courbon, G. M., Palme, P. R., Mann, L., Richter, A., Imming, P. and Rubinstein, J. L. (2023). Mechanism of mycobacterial ATP synthase inhibition by squaramides and second generation diarylquinolines. *EMBO Journal.* 42 (15), e113687. Available at: doi:10.15252/embj.2023113687.

Cumming, B. M. and Steyn, A. J. (2015). Metabolic plasticity of central carbon metabolism protects mycobacteria. *Proceedings of the National Academy of Sciences of the United States of America.* 112 (43), 13135-13136. Available at: doi:10.1073/pnas.1518171112.

Daffé, M. and Draper, P. (1998). The envelope layers of mycobacteria with reference to their pathogenicity. *Advances in Microbial Physiology*. 39, 131–203. Available at: doi:10.1016/s0065-2911(08)60016-8.

Daly, P. F., Lyon, R. C., Faustino, P. J. and Cohen, J. S. (1987). Phospholipid metabolism in cancer cells monitored by 31P NMR spectroscopy. *Journal of Biological Chemistry*. 262 (31), 14875–14878. Available at: doi:10.1016/s0021-9258(18)48107-0.

Dam, S., Tangara, S., Hamela, C., Hattabi, T., Faïon, L., Carre, P., Antoine, R., Herledan, A., Leroux, F., Piveteau, C., Eveque, M., Flipo, M., Deprez, B., Kremer, L., Willand, N., Villemagne, B. and Hartkoorn, R. C. (2022). Tricyclic SpiroLactams kill mycobacteria in vitro and in vivo by inhibiting type II NADH dehydrogenases. *Journal of Medicinal Chemistry*. 65 (24), 16651–16664. Available at: doi:10.1021/acs.jmedchem.2c01493.

Daugelat, S., Kowall, J., Mattow, J., Bumann, D., Winter, R., Hurwitz, R. and Kaufmann S. H. E. (2003). The RD1 proteins of *Mycobacterium tuberculosis*: expression in *Mycobacterium smegmatis* and biochemical characterization. *Microbes and Infection*. 5 (12), 1082-1095. Available at: doi:10.1016/S1286-4579(03)00205-3.

Davis, N. K., Chionh, Y. H., McBee, M. E., Hia, F., Ma, D., Cui, L., Sharaf, M. L., Cai, W. M., Jumpathong, W., Levine, S. S., Alonso, S. and Dedon, P. C. (2024). Facile metabolic reprogramming distinguishes mycobacterial adaptation to hypoxia and starvation: ketosis drives starvation-induced persistence in *M. bovis* BCG. *Communications Biology.* 7, 866. Available at: doi:10.1038/s42003-024-06562-2.

de Carvalho, L. P. S., Fischer, S. M., Marrero, J., Nathan, C., Ehrt, S. and Rhee, K. Y. (2010). Metabolomics of *Mycobacterium tuberculosis* Reveals Compartmentalized Co-Catabolism of Carbon Substrates. *Chemistry & Biology*. 17 (10), 1122-1131. Available at: doi:10.1016/j.chembiol.2010.08.009.

De Graaf, A. A., Striegel, K., Wittig, R. M., Laufer, B., Schmitz, G., Wiechert, W., Sprenger, G.A. and Sahm, H. (1999). Metabolic state of *Zymomonas mobilis* in glucose-, fructose-, and xylose-fed continuous cultures as analysed by 13C- and 31P-NMR spectroscopy. *Archives of Microbiology*. 171 (6), 371–385. Available at: doi:10.1007/s002030050724.

de Jager, V. R., Dawson, R., van Niekerk, C., Hutchings, J., Kim, J., Vanker, N., van der Merwe, L., Choi, J., Nam, K. and Diacon, A.H. (2020). Telacebec (Q203), a New Antituberculosis Agent. *The New England Journal of Medicine*. 382 (13), 1280–1281. Available at: doi:10.1056/NEJMc1913327.

de Jonge, M. R., Koymans, L. H. M., Guillemont, J. E. G., Koul, A. and Andries, K. (2007). A computational model of the inhibition of *Mycobacterium tuberculosis* ATPase by a

new drug candidate R207910. *Proteins*. 67 (4), 971–980. Available at: doi:10.1002/prot.21376.

Degli Esposti, M., Ghelli, A., Ratta, M., Cortes, D. and Estornell, E. (1994). Natural substances (acetogenins) from the family Annonaceae are powerful inhibitors of mitochondrial NADH dehydrogenase (Complex I). *Biochemical Journal*. 301 (Pt 1), 161–167. Available at: doi:10.1042/bj3010161.

Delafont, V., Mougari, F., Cambau, E., Joyeux, M., Bouchon, D., Héchard, Y. and Moulin, L. (2014). First evidence of amoebae-mycobacteria association in drinking water network. *Environmental Science and Technology*. 48 (20), 11872–11882. Available at: doi:10.1021/es5036255.

Deps, P. and Collin, S. M. (2021). *Mycobacterium lepromatosis* as a Second Agent of Hansen's Disease. *Frontiers in Microbiology*. 12, 698588. Available at: doi:10.3389/fmicb.2021.698588.

Devulder, G., de Montclos, M. P. and Flandrois, J. P. (2005). A multigene approach to phylogenetic analysis using the genus Mycobacterium as a model. *International Journal of Systematic and Evolutionary Microbiology*. 55 (Pt 1), 293–302. Available at: doi:10.1099/ijs.0.63222-0.

Drage, L. A., Ecker, P. M., Orenstein, R., Phillips, P. K. and Edson, R. S. (2010). An outbreak of Mycobacterium chelonae infections in tattoos. *Journal of the American Academy of Dermatology*. 62 (3), 501–506. Available at: doi:10.1016/j.jaad.2009.03.034.

Dunn, E. A., Roxburgh, M., Larsen, L., Smith, R. A. J., McLellan, A. D., Heikal, A., Murphy, M. P. and Cook, G. M. (2014). Incorporation of triphenylphosphonium functionality improves the inhibitory properties of phenothiazine derivatives in *Mycobacterium tuberculosis*. *Bioorganic & Medicinal Chemistry*. 22 (19), 5320–5328. Available at: doi:10.1016/j.bmc.2014.07.050.

Ehlers, S. and Schaible, U. E. (2012). The granuloma in tuberculosis: dynamics of a host-pathogen collusion. *Frontiers in Immunology*. 3, 411. Available at: doi:10.3389/fimmu.2012.00411.

Eoh, H. and Rhee, K. Y. (2013). Multifunctional essentiality of succinate metabolism in adaptation to hypoxia in *Mycobacterium tuberculosis*. *Proceedings of the National Academy of Sciences of the United States of America*. 110 (16), 6554–6559. Available at: doi:10.1073/pnas.1219375110.

Errington, J. and van der Aart, L. T. (2020). Microbe Profile: *Bacillus subtilis*: model organism for cellular development, and industrial workhorse. *Microbiology*. 166 (5), 425–427. Available at: doi:10.1099/mic.0.000922.

Falkinham, J. O., 3rd (2013). Ecology of nontuberculous mycobacteria--where do human infections come from? *Seminars in Respiratory and Critical Care Medicine*. 34 (1), 95–102. Available at: doi:10.1055/s-0033-1333568.

FDA (2019). FDA approves new drug for treatment-resistant forms of tuberculosis that affects the lungs. [Online]. FDA. Last updated: 14 August 2019. Available at: https://www.fda.gov/news-events/press-announcements/fda-approves-new-drug-treatment-resistant-forms-tuberculosis-affects-lungs [Accessed 22 August 2024].

Feldman, E. B. (1999). Creatine: a dietary supplement and ergogenic aid. *Nutrition Reviews*. 57 (2), 45–50. Available at: doi:10.1111/j.1753-4887.1999.tb01777.x.

Ferebee, S. H., Doster, B. E. and Murray, F. J. (1966). Ethambutol: a substitute for para-aminosalicylic acid in regimens for pulmonary tuberculosis. *Annals of the New York Academy of Sciences*. 135 (2), 910–920. Available at: doi:10.1111/j.1749-6632.1966.tb45533.x.

Ferrick, D. A., Neilson, A. and Beeson, C. (2008). Advances in measuring cellular bioenergetics using extracellular flux. *Drug Discovery Today*. 13 (5–6), 268–274. Available at: doi:10.1016/j.drudis.2007.12.008.

Fine, A. E., Bolin, C. A., Gardiner, J. C. and Kaneene, J. B. (2011). A study of the persistence of *Mycobacterium bovis* in the environment under natural weather

conditions in Michigan, USA. *Veterinary Medicine International*. 2011, 765430. Available at: doi:10.4061/2011/765430.

Firsov, A. M., Popova, L. B., Khailova, L. S., Nazarov, P. A., Kotova, E. A. and Antonenko, Y. N. (2021). Protonophoric action of BAM15 on planar bilayers, liposomes, mitochondria, bacteria and neurons. *Bioelectrochemistry*. 137, 107673. Available at: doi:10.1016/j.bioelechem.2020.107673.

Fisher, J. F., Ganapathy, M., Edwards, B. H. and Newman, C. L. (1990). Utility of Gram's and Giemsa stains in the diagnosis of pulmonary tuberculosis. *American Review of Respiratory Disease*. 141 (2), 511–513. Available at: doi:10.1164/ajrccm/141.2.511.

Forbes, B. A., Hall, G. S., Miller, M. B., Novak, S. M., Rowlinson, M.-C., Salfinger, M., Somoskövi, A., Warshauer, D. M. and Wilson, M. L. (2018). Practical guidance for clinical microbiology laboratories: Mycobacteria. *Clinical Microbiology Reviews*. 31 (2), e00038-17. Available at: doi:10.1128/CMR.00038-17.

Formicola, V., Milanesi, Q. and Scarsini, C. (1987). Evidence of spinal tuberculosis at the beginning of the fourth millennium BC from Arene Candide cave (Liguria, Italy). *American Journal of Physical Anthropology*. 72 (1), 1–6. Available at: doi:10.1002/ajpa.1330720102.

Forrellad, M. A., Klepp, L. I., Gioffré, A., Sabio y García, J., Morbidoni, H. R., de la Paz Santangelo, M., Cataldi, A. A. and Bigi, F. (2013). Virulence factors of the *Mycobacterium tuberculosis* complex. *Virulence*. 4 (1), 3–66. Available at: doi:10.4161/viru.22329.

Futai, M. (1974). Orientation of membrane vesicles from *Escherichia coli* prepared by different procedures. *The Journal of Membrane Biology*. 15, 15-28. Available at: doi:10.1007/BF01870079.

Gagneux, S. (2018). Ecology and evolution of *Mycobacterium tuberculosis*. *Nature Reviews Microbiology*. 16 (4), 202–213. Available at: doi:10.1038/nrmicro.2018.8.

Gago, G., Diacovich, L. and Gramajo, H. (2018). Lipid metabolism and its implication in mycobacteria–host interaction. *Current Opinion in Microbiology*. 41, 36-42. Available at: doi:10.1016/j.mib.2017.11.020.

Gambhir, S., Ravina, M., Rangan, K., Dixit, M., Barai, S., Bomanji, J. and the International Atomic Energy Agency Extra-pulmonary TB Consortium (2017). Imaging in extrapulmonary tuberculosis. *International Journal of Infectious Diseases.* 56, 237–247. Available at: doi:10.1016/j.ijid.2016.11.003.

Garlick, P. B., Radda, G. K. and Seeley, P. J. (1979). Studies of acidosis in the ischaemic heart by phosphorus nuclear magnetic resonance. *Biochemical Journal*. 184 (3), 547–554. Available at: doi:10.1042/bj1840547.

Gengenbacher, M., Rao, S. P. S., Pethe, K. and Dick, T. (2010). Nutrient-starved, non-replicating *Mycobacterium tuberculosis* requires respiration, ATP synthase and isocitrate lyase for maintenance of ATP homeostasis and viability. *Microbiology*. 156 (Pt 1), 81–87. Available at: doi:10.1099/mic.0.033084-0.

Gil, E., Sweeney, N., Barrett, V., Morris-Jones, S., Miller, R. F., Johnston, V. J. and Brown, M. (2021). Bedaquiline as Treatment for Disseminated Nontuberculous *Mycobacteria* Infection in 2 Patients Co-Infected with HIV. *Emerging Infectious Diseases*. 27 (3), 944-948. Available at: doi:10.3201/eid2703.202359.

Giulieri, S., Morisod, B., Edney, T., Odman, M., Genné, D., Malinverni, R., Hammann, C., Musumeci, E., Voide, C., Greub, G., Masserey, E., Bille, J., Cavassini, M. and Jaton, K. (2011). Outbreak of *Mycobacterium haemophilum* infections after permanent makeup of the eyebrows. *Clinical Infectious Diseases.* 52 (4), 488–491. Available at: doi:10.1093/cid/ciq191.

Golden, M. P. and Vikram, H. R. (2005). Extrapulmonary Tuberculosis: An Overview. *American Family Physician*. 72 (9), 1761-1768. Avaliable at: https://www.aafp.org/pubs/afp/issues/2005/1101/p1761.html.

Goldstein, B. P. (2014). Resistance to rifampicin: a review. *The Journal of Antibiotics*. 67 (9), 625–630. Available at: doi:10.1038/ja.2014.107.

Gong, H., Gao, Y., Zhou, X., Xiao, Y., Wang, W., Tang, Y., Zhou, S., Zhang, Y., Ji, W., Yu, L., Tian, C., Lam, S. M., Shui, G., Guddat, L.W., Wong, L.-L., Wang, Q. and Rao, Z. (2020). Cryo-EM structure of trimeric *Mycobacterium smegmatis* succinate dehydrogenase with a membrane-anchor SdhF. *Nature Communications*. 11 (1), 4245. Available at: doi:10.1038/s41467-020-18011-9.

Goren, M. B., D'Arcy Hart, P., Young, M. R. and Armstrong, J. A. (1976). Prevention of phagosome-lysosome fusion in cultured macrophages by sulfatides of *Mycobacterium tuberculosis*. *Proceedings of the National Academy of Sciences of the United States of America*. 73 (7), 2510–2514. Available at: doi:10.1073/pnas.73.7.2510.

Gosset, G., Satre, M., Blaive, B., Clément, J.-L., Martin, J.-B., Culcasi, M. and Pietri, S. (2008). Investigation of subcellular acidic compartments using alpha-aminophosphonate 31P nuclear magnetic resonance probes. *Analytical Biochemistry*. 380 (2), 184–194. Available at: doi:10.1016/j.ab.2008.05.052.

Grange, J. M. and Davies, P. D. O. (2010). Disease caused by environmental mycobacteria. In Warrell D. A., Cox T. M. and Firth J. D. (Eds). *Oxford Textbook of Medicine Fifth Edition Volume 1*. Oxford: Oxford University Press, pp. 831-836.

Greenwood D., Slack R. C., Peutherer J. F. and Barer M. R. (Eds.) (2007). *Medical Microbiology: A Guide to Microbial Infections: Pathogenesis, Immunity, Laboratory Diagnosis and Control Seventeenth Edition.* Edinburgh: Churchill Livingstone.

Griffith, D. E., Girard, W. M. and Wallace, R. J., Jr (1993). Clinical features of pulmonary disease caused by rapidly growing mycobacteria. An analysis of 154 patients. *American Review of Respiratory Disease*. 147 (5), 1271–1278. Available at: doi:10.1164/ajrccm/147.5.1271.

Grivet, J.-P. and Delort, A.-M. (2009). NMR for microbiology: *in vivo* and *in situ* applications. *Progress in Nuclear Magnetic Resonance Spectroscopy*. 54 (1), 1–53. Available at: doi:10.1016/j.pnmrs.2008.02.001.

Guay, D. R. (2006). Moxifloxacin in the treatment of skin and skin structure infections. *Therapeutics and Clinical Risk Management*. 2 (4), 417–434. Available at: doi:10.2147/tcrm.2006.2.4.417.

Guillemin, I., Cambau, E. and Jarlier, V. (1995). Sequences of conserved region in the A subunit of DNA gyrase from nine species of the genus *Mycobacterium*: phylogenetic analysis and implication for intrinsic susceptibility to quinolones. *Antimicrobial Agents and Chemotherapy*. 39 (9), 2145–2149. Available at: doi:10.1128/AAC.39.9.2145.

Guinn, K. M., Hickey, M. J., Mathur, S. K., Zakel, K. L., Grotzke, J. E., Lewinsohn, D. M., Smith, S. and Sherman, D. R. (2004). Individual RD1-region genes are required for export of ESAT-6/CFP-10 and for virulence of *Mycobacterium tuberculosis. Microbiology*. 51 (2), 359-370. Available at: doi:10.1046/j.1365-2958.2003.03844.x.

Guo, H., Courbon, G. M., Bueler, S. A., Mai, J., Liu, J. and Rubinstein, J. L. (2021). Structure of mycobacterial ATP synthase bound to the tuberculosis drug bedaquiline. *Nature*. 589 (7840), 143–147. Available at: doi:10.1038/s41586-020-3004-3.

Gupta, R. S., Lo, B. and Son, J. (2018). Phylogenomics and comparative genomic studies robustly support division of the genus *Mycobacterium* into an emended genus Mycobacterium and four novel genera. *Frontiers in Microbiology*. 9, 67. Available at: doi:10.3389/fmicb.2018.00067.

Haagsma, A. C., Driessen, N. N., Hahn, M.-M., Lill, H. and Bald, D. (2010). ATP synthase in slow- and fast-growing mycobacteria is active in ATP synthesis and blocked in ATP hydrolysis direction: Role of ATP synthase in mycobacteria. *FEMS Microbiology Letters*. 313 (1), 68–74. Available at: doi:10.1111/j.1574-6968.2010.02123.x.

Haagsma, A. C., Podasca, I., Koul, A., Andries, K., Guillemont, J., Lill, H. and Bald, D. (2011). Probing the interaction of the diarylquinoline TMC207 with its target mycobacterial ATP synthase. *PLoS One*. 6 (8), e23575. Available at: doi:10.1371/journal.pone.0023575.

Hamilton, H. K., Levis, W. R., Martiniuk, F., Cabrera, A. and Wolf, J. (2008). The role of the armadillo and sooty mangabey monkey in human leprosy. *International Journal of Dermatology*. 47 (6), 545–550. Available at: doi:10.1111/j.1365-4632.2008.03722.x.

Han, X. Y., Seo, Y.-H., Sizer, K. C., Schoberle, T., May, G. S., Spencer, J. S., Li, W. and Nair, R. G. (2008). A new *Mycobacterium* species causing diffuse lepromatous leprosy. *American Journal of Clinical Pathology*. 130 (6), 856–864. Available at: doi:10.1309/AJCPP72FJZZRRVMM.

Han, X. Y., Sizer, K. C., Thompson, E. J., Kabanja, J., Li, J., Hu, P., Gómez-Valero, L. and Silva, F. J. (2009). Comparative sequence analysis of *Mycobacterium leprae* and the new leprosy-causing *Mycobacterium lepromatosis*. *Journal of Bacteriology*. 191 (19), 6067–6074. Available at: doi:10.1128/JB.00762-09.

Harden, S. A., Courbon, G. M., Liang, Y., Kim, A. S. and Rubinstein, J. L. (2024). A simple assay for inhibitors of mycobacterial oxidative phosphorylation. *Journal of Biological Chemistry*. 300 (1), 105483. Available at: doi:10.1016/j.jbc.2023.105483.

Hards, K., McMillan, D. G. G., Schurig-Briccio, L. A., Gennis, R. B., Lill, H., Bald, D. and Cook, G. M. (2018). Ionophoric effects of the antitubercular drug bedaquiline. *Proceedings of the National Academy of Sciences of the United States of America*. 115 (28), 7326–7331. Available at: doi:10.1073/pnas.1803723115.

Hards, K., Robson, J. R., Berney, M., Shaw, L., Bald, D., Koul, A., Andries, K. and Cook, G. M. (2015). Bactericidal mode of action of bedaquiline. *Journal of Antimicrobial Chemotherapy*. 70 (7), 2028–2037. Available at: doi:10.1093/jac/dkv054.

Hartkoorn, R. C., Uplekar, S. and Cole S. T. (2014). Cross-Resistance between Clofazimine and Bedaquiline through Upregulation of MmpL5 in *Mycobacterium tuberculosis*. *Antimicrobial Agents and Chemotherapy*. 58 (5), 2979-2981. Available at: doi:10.1128/aac.00037-14.

Henrichsen, J. (1972). Bacterial surface translocation: a survey and a classification. *Bacteriological Reviews*. 36 (4), 478–503. Available at: doi:10.1128/br.36.4.478-503.1972.

Hershkovitz, I., Donoghue, H. D., Minnikin, D. E., Besra, G. S., Lee, O. Y.-C., Gernaey, A. M., Galili, E., Eshed, V., Greenblatt, C. L., Lemma, E., Bar-Gal, G. K. and Spigelman, M. (2008). Detection and molecular characterization of 9,000-year-old *Mycobacterium tuberculosis* from a Neolithic settlement in the Eastern Mediterranean. *PloS One*. 3 (10), e3426. Available at: doi:10.1371/journal.pone.0003426.

Hesse, S. J., Ruijter, G. J., Dijkema, C. and Visser, J. (2000). Measurement of intracellular (compartmental) pH by 31P NMR in *Aspergillus niger*. *Journal of Biotechnology*. 77 (1), 5–15. Available at: doi:10.1016/s0168-1656(99)00203-5.

Hmama, Z., Sendide, K., Talal, A., Garcia, R., Dobos, K. and Reiner, N. E. (2004). Quantitative analysis of phagolysosome fusion in intact cells: inhibition by mycobacterial lipoarabinomannan and rescue by an 1alpha,25-dihydroxyvitamin D3-phosphoinositide 3-kinase pathway. *Journal of Cell Science*. 117 (Pt 10), 2131–2140. Available at: doi:10.1242/jcs.01072.

Hoefsloot, W., van Ingen, J., Andrejak, C., Angeby, K., Bauriaud, R., Bemer, P., Beylis, N., Boeree, M. J., Cacho, J., Chihota, V., Chimara, E., Churchyard, G., Cias, R., Daza, R., Daley, C. L., Dekhuijzen, P. N., Domingo, D., Drobniewski, F., Esteban, J., Fauville-Dufaux, M., Folkvardsen, D. B., Gibbons, N., Gómez-Mampaso, E., Gonzalez, R., Hoffmann, H., Hsueh, P. R., Indra, A., Jagielski, T., Jamieson, F., Jankovic, M., Jong, E., Keane, J., Koh, W. J., Lange, B., Leao, S., Macedo, R., Mannsåker, T., Marras, T. K., Maugein, J., Milburn, H. J., Mlinkó, T., Morcillo, N., Morimoto, K., Papaventsis, D., Palenque, E., Paez-Peña, M., Piersimoni, C., Polanová, M., Rastogi, N., Richter, E., Ruiz-Serrano, M. J., Silva, A., da Silva, M. P., Simsek, H., van Soolingen, D., Szabó, N., Thomson, R., Tórtola Fernandez, T., Tortoli, E., Totten, S. E., Tyrrell, G., Vasankari, T., Villar, M., Walkiewicz, R., Winthrop, K. L. and Wagner, D. (2013). The geographic diversity of nontuberculous mycobacteria isolated from pulmonary samples: an NTM-NET collaborative study. *European Respiratory Journal*. 42 (6), 1604–1613. Available at: doi:10.1183/09031936.00149212.

Hoelscher, M., Barros-Aguirre, D., Dara, M., Heinrich, N., Sun, E., Lange, C., Tiberi, S. and Wells, C. (2024). Candidate anti-tuberculosis medicines and regimens under

clinical evaluation. *Clinical Microbiology and Infection*. 30 (9), 1131-1138. Available at: doi:10.1016/j.cmi.2024.06.016.

Honda, J. R., Hasan, N. A., Davidson, R. M., Williams, M. D., Epperson, L. E., Reynolds, P. R., Smith, T., Iakhiaeva, E., Bankowski, M. J., Wallace, R. J., Jr, Chan, E. D., Falkinham, J. O., 3rd and Strong, M. (2016). Environmental nontuberculous mycobacteria in the Hawaiian Islands. *PLoS Neglected Tropical Diseases*. 10 (10), e0005068. Available at: doi:10.1371/journal.pntd.0005068.

Hong, H., Demangel, C., Pidot, S. J., Leadlay, P. F. and Stinear, T. (2008). Mycolactones: immunosuppressive and cytotoxic polyketides produced by aquatic mycobacteria. *Natural Product Reports*. 25 (3), 447–454. Available at: doi:10.1039/b803101k.

Hong, S. and Pedersen, P. L. (2008). ATP synthase and the actions of inhibitors utilized to study its roles in human health, disease, and other scientific areas. *Microbiology and Molecular Biology Reviews*. 72 (4), 590–641. Available at: doi:10.1128/MMBR.00016-08.

Huber, C. A., Ruf, M.-T., Pluschke, G. and Käser, M. (2008). Independent loss of immunogenic proteins in *Mycobacterium ulcerans* suggests immune evasion. *Clinical and Vaccine Immunology: CVI*. 15 (4), 598–606. Available at: doi:10.1128/CVI.00472-07.

Huitric, E., Verhasselt, P., Koul, A., Andries, K., Hoffner, S. and Andersson, D. I. (2010). Rates and mechanisms of resistance development in *Mycobacterium tuberculosis* to a novel diarylquinoline ATP synthase inhibitor. *Antimicrobial Agents and Chemotherapy*. 54 (3), 1022–1028. Available at: doi:10.1128/aac.01611-09.

Ibrahim, M., Andries, K., Lounis, N., Chauffour, A., Truffot-Pernot, C., Jarlier, V. and Veziris, N. (2006). Synergistic Activity of R207910 Combined with Pyrazinamide against Murine Tuberculosis. *Antimicrobial Agents and Chemotherapy*. 51 (3), 1011-1015. Available at: doi:10.1128/AAC.00898-06.

Indrigo, J., Hunter, R. L. and Actor, J. K. (2003). Cord factor trehalose 6,6'-dimycolate (TDM) mediates trafficking events during mycobacterial infection of murine

macrophages. *Microbiology*. 149 (Pt 8), 2049–2059. Available at: doi:10.1099/mic.0.26226-0.

Iqbal, I. K., Bajeli, S., Akela, A. K. and Kumar, A. (2018). Bioenergetics of *Mycobacterium*: An Emerging Landscape for Drug Discovery. *Pathogens*. 7 (1). Available at: doi:10.3390/pathogens7010024.

Jarlier, V. and Nikaido, H. (1994). Mycobacterial cell wall: Structure and role in natural resistance to antibiotics. *FEMS Microbiology Letters*. 123 (1–2), 11–18. Available at: doi:10.1111/j.1574-6968.1994.tb07194.x.

Jasaitis, A., Borisov, V. B., Belevich, N. P., Morgan, J. E., Konstantinov, A. A. and Verkhovsky, M. I. (2000). Electrogenic reactions of cytochrome bd. *Biochemistry*. 39 (45), 13800–13809. Available at: doi:10.1021/bi001165n.

Jentoft, J. E. and Town, C.D. (1985). Intracellular pH in *Dictyostelium discoideum*: a 31P nuclear magnetic resonance study. *Journal of Cell Biology*. 101 (3), 778–784. Available at: doi:10.1083/jcb.101.3.778.

Jeon, A. B., Ackart, D. F., Li, W., Jackson, M., Melander, R. J., Melander, C., Abramovitch, R. B., Chicco, A. J., Basaraba, R. J. and Obregón-Henao, A. (2019). 2-aminoimidazoles collapse mycobacterial proton motive force and block the electron transport chain. *Scientific Reports*. 9 (1), 1513. Available at: doi:10.1038/s41598-018-38064-7.

Johnson, C. H., Ivanisevic, J. and Siuzdak, G. (2016). Metabolomics: beyond biomarkers and towards mechanisms. *Nature Reviews Molecular Cell Biology*. 17 (7), 451–459. Available at: doi:10.1038/nrm.2016.25.

Jones, D. (2013). Tuberculosis success. *Nature Reviews Drug Discovery*. 12 (3), 175–176. Available at: doi:10.1038/nrd3957.

Kana, B. D., Weinstein, E. A., Avarbock, D., Dawes, S. S., Rubin, H. and Mizrahi, V. (2001). Characterization of the cydAB-encoded cytochrome bd oxidase from *Mycobacterium smegmatis*. *Journal of Bacteriology*. 183 (24), 7076–7086. Available at: doi:10.1128/JB.183.24.7076-7086.2001.

Kanehisa Laboratories (2024). *KEGG: Kyoto Encyclopedia of Genes and Genomes*. [Online]. Available at: https://www.genome.jp/kegg/ [Accessed 10 September 2024].

Kanehisa, M. (2019). Toward understanding the origin and evolution of cellular organisms. *Protein Science.* (11), 1947–1951. Available at: doi:10.1002/pro.3715.

Kanehisa, M., Furumichi, M., Sato, Y., Kawashima, M. and Ishiguro-Watanabe, M. (2023). KEGG for taxonomy-based analysis of pathways and genomes. *Nucleic Acids Research*. 51 (D1), D587–D592. Available at: doi:10.1093/nar/gkac963.

Kanehisa, M. and Goto, S. (2000). KEGG: kyoto encyclopedia of genes and genomes. *Nucleic Acids Research*. 28 (1), 27–30. Available at: doi:10.1093/nar/28.1.27.

Kaplan, O. and Cohen, J. S. (1991). Lymphocyte activation and phospholipid pathways. 31P magnetic resonance studies. *Journal of Biological Chemistry*. 266 (6), 3688–3694. Available at: doi:10.1016/S0021-9258(19)67849-X.

Kar, H. K. and Gupta, R. (2015). Treatment of leprosy. *Clinics in Dermatology*. 33 (1), 55–65. Available at: doi:10.1016/j.clindermatol.2014.07.007.

Kiazyk, S. and Ball, T. B. (2017). Latent tuberculosis infection: An overview. *Canada Communicable Disease Report*. 43 (3–4), 62–66. Available at: doi:10.14745/ccdr.v43i34a01.

Kim, H., Kim, S.-H., Shim, T.-S., Kim, M.-N., Bai, G.-H., Park, Y.-G., Lee, S.-H., Chae, G.-T., Cha, C.-Y., Kook, Y.-H. and Kim, B.-J. (2005). Differentiation of Mycobacterium species by analysis of the heat-shock protein 65 gene (hsp65). *International Journal of Systematic and Evolutionary Microbiology*. 55 (Pt 4), 1649–1656. Available at: doi:10.1099/ijs.0.63553-0.

Kim, C.-J., Kim, N.-H., Song, K.-H., Choe, P. G., Kim, E. S., Park, S. W., Kim, H.-B., Kim, N.-J., Kim, E.-C., Park, W. B. and Oh, M.-D. (2013). Differentiating rapid- and slow-growing mycobacteria by difference in time to growth detection in liquid media. *Diagnostic Microbiology and Infectious Disease*. 75 (1), 73–76. Available at: doi:10.1016/j.diagmicrobio.2012.09.019.

Kim, N., Ripple, M. O. and Springett, R. (2012). Measurement of the mitochondrial membrane potential and pH gradient from the redox poise of the hemes of the bc1 complex. *Biophysical Journal*. 102 (5), 1194–1203. Available at: doi:10.1016/j.bpj.2012.02.003.

Kishi, S., Saito, K., Kato, Y. and Ishikita, H. (2017). Redox potentials of ubiquinone, menaquinone, phylloquinone, and plastoquinone in aqueous solution. *Photosynthesis Research*. 134 (2), 193–200. Available at: doi:10.1007/s11120-017-0433-4.

Klann, A. G., Belanger, A. E., Abanes-De Mello, A., Lee, J. Y. and Hatfull, G. F. (1998). Characterization of the *dnaG* locus in *Mycobacterium smegmatis* reveals linkage of DNA replication and cell division. *Journal of Bacteriology*. 180 (1), 65–72. Available at: doi:10.1128/JB.180.1.65-72.1998.

Kleczkowski, L. A. and Igamberdiev, A. U. (2021). Magnesium Signaling in Plants. *International Journal of Molecular Sciences*. 22 (3). Available at: doi:10.3390/ijms22031159.

Knizner, S. A., Jacobs, A. J., Lyon, R. C. and Swenberg, C. E. (1986). In vivo dephosphorylation of WR-2721 monitored by 31P NMR spectroscopy. *The Journal of Pharmacology and Experimental Therapeutics*. 236 (1), 37–40. Available at: https://jpet.aspetjournals.org/content/236/1/37.long.

Koh, S.-J., Song, T., Kang, Y. A., Choi, J. W., Chang, K. J., Chu, C. S., Jeong, J. G., Lee, J.-Y., Song, M.-K., Sung, H.-Y., Kang, Y. H. and Yim, J.-J. (2010). An outbreak of skin and soft tissue infection caused by *Mycobacterium abscessus* following acupuncture. *Clinical Microbiology and Infection.* 16 (7), 895–901. Available at: doi:10.1111/j.1469-0691.2009.03026.x.

Kohanski, M. A., Dwyer, D. J. and Collins, J. J. (2010). How antibiotics kill bacteria: from targets to networks. *Nature Reviews Microbiology*. 8 (6), 423-425. Available at: doi:10.1038/nrmicro2333.

Koul, A., Dendouga, N., Vergauwen, K., Molenberghs, B., Vranckx, L., Willebrords, R., Ristic, Z., Lill, H., Dorange, I., Guillemont, J., Bald, D. and Andries, K. (2007).

Diarylquinolines target subunit c of mycobacterial ATP synthase. *Nature Chemical Biology*. 3 (6), 323–324. Available at: doi:10.1038/nchembio884.

Koul, A., Vranckx, L., Dendouga, N., Balemans, W., Van den Wyngaert, I., Vergauwen, K., Göhlmann, H. W. H., Willebrords, R., Poncelet, A., Guillemont, J., Bald, D. and Andries, K. (2008). Diarylquinolines are bactericidal for dormant mycobacteria as a result of disturbed ATP homeostasis. *Journal of Biological Chemistry*. 283 (37), 25273–25280. Available at: doi:10.1074/jbc.M803899200.

Koul, A., Vranckx, L., Dhar, N., Göhlmann, H. W. H., Özdemir, E., Neefs, J.-M., Schulz, M., Lu, P., Mørtz, E., McKinney, J. D., Andries, K. and Bald, D. (2014). Delayed bactericidal response of *Mycobacterium tuberculosis* to bedaquiline involves remodelling of bacterial metabolism. *Nature Communications*. 5, 3369. Available at: doi:10.1038/ncomms4369.

Kpeli, G. S. and Yeboah-Manu, D. (2019). Secondary Infection of Buruli Ulcer Lesions. In Pluschke, G. and Röltgen, K. (Eds.). *Buruli Ulcer*: *Mycobacterium Ulcerans Disease*. Cham: Springer. pp. 227–239.

Kramer, H. W. and Bailey, J. E. (1991). Mass transfer characterization of an airlift probe for oxygenating and mixing cell suspensions in an NMR spectrometer. *Biotechnology and Bioengineering*. 37 (3), 205–209. Available at: doi:10.1002/bit.260370303.

Lamprecht, D. A., Finin, P. M., Rahman, M. A., Cumming, B. M., Russell, S. L., Jonnala, S. R., Adamson, J. H. and Steyn, A. J. C. (2016). Turning the respiratory flexibility of *Mycobacterium tuberculosis* against itself. *Nature Communications*. 7, 12393. Available at: doi:10.1038/ncomms12393.

Leach, K. L., Brickner, S. J., Noe, M. C. and Miller, P. F. (2011). Linezolid, the first oxazolidinone antibacterial agent: Linezolid, antibacterial agent. *Annals of the New York Academy of Sciences*. 1222 (1), 49–54. Available at: doi:10.1111/j.1749-6632.2011.05962.x.

Lee, B. S., Hards, K., Engelhart, C. A., Hasenoehrl, E. J., Kalia, N. P., Mackenzie, J. S., Sviriaeva, E., Chong, S. M. S., Manimekalai, M. S. S., Koh, V. H., Chan, J., Xu, J., Alonso,

S., Miller, M. J., Steyn, A. J. C., Grüber, G., Schnappinger, D., Berney, M., Cook, G. M., Moraski, G. C. and Pethe, K. (2021). Dual inhibition of the terminal oxidases eradicates antibiotic-tolerant *Mycobacterium tuberculosis*. *EMBO Molecular Medicine*. 13 (1), e13207. Available at: doi:10.15252/emmm.202013207.

Lehmann, K. B. and Neumann, R. O. (1896). Atlas und Grundriss der Bakteriologie und Lehrbuch der speziellen bakteriologischen Diagnostik [Atlas and Principles of Bacteriology and Textbook of Special Bacteriologic Diagnosis]. Munich: Lehmann.

Leistikow, R. L., Morton, R. A., Bartek, I. L., Frimpong, I., Wagner, K. and Voskuil, M. I. (2010). The *Mycobacterium tuberculosis* DosR regulon assists in metabolic homeostasis and enables rapid recovery from nonrespiring dormancy. *Journal of Bacteriology*. 192 (6), 1662–1670. Available at: doi:10.1128/JB.00926-09.

Lenz, E. M. and Wilson, I. D. (2007). Analytical strategies in metabonomics. *Journal of Proteome Research*. 6 (2), 443–458. Available at: doi:10.1021/pr0605217.

Lerner, T. R., Borel, S., Gutierrez, M. G. (2015). The innate immune response in human tuberculosis. *Cellular Microbiology*. 17 (9), 1277-1285. Available at: doi: 10.1111/cmi.12480.

Leung, K. T., Campbell, S., Gan, Y., White, D. C., Lee, H. and Trevors, J. T. (1999). The role of the Sphingomonas species UG30 pentachlorophenol-4-monooxygenase in p-nitrophenol degradation. *FEMS Microbiology Letters*. 173 (1), 247–253. Available at: doi:10.1111/j.1574-6968.1999.tb13509.x.

Liang, Y. C., Berton, S., Reeks, C. and Sun, J. (2022). An *in vivo* biosafety-level-2-compatible model of *Mycobacterium tuberculosis* infection for drug susceptibility testing. *STAR Protocols*. 3 (3), 101575. Available at: doi:10.1016/j.xpro.2022.101575.

Limaye, N., Veschini, L. and Coward, T. (2022). Assessing biocompatibility and mechanical testing of 3D-printed PEEK versus milled PEEK. *Heliyon*. 8 (12), e12314. Available at: doi:10.1016/j.heliyon.2022.e12314.

Lindeboom, J. A., Bruijnesteijn van Coppenraet, L. E. S., van Soolingen, D., Prins, J. M. and Kuijper, E. J. (2011). Clinical manifestations, diagnosis, and treatment of

Mycobacterium haemophilum infections. *Clinical Microbiology Reviews*. 24 (4), 701–717. Available at: doi:10.1128/CMR.00020-11.

Lockwood, D. N. J. (2010). Leprosy (Hansen's Disease). In Warrell D. A., Cox T. M. and Firth J. D. (Eds). *Oxford Textbook of Medicine Fifth Edition Volume 1*. Oxford: Oxford University Press, pp. 836-848.

Lodhiya, T., Palande, A., Veeram, A., Larrouy-Maumus, G., Beste, D. J. V. and Mukherjee, R. (2024). ATP burst is the dominant driver of antibiotic lethality in Mycobacteria. *eLife.* 13, RP99656. Available at: doi:10.7554/eLife.99656.2.

Lohmeier-Vogel, E. M., Hahn-Hägerdal, B. and Vogel, H. J. (1995). Phosphorus-31 and carbon-13 nuclear magnetic resonance studies of glucose and xylose metabolism in *Candida tropicalis* cell suspensions. *Applied and Environmental Microbiology*. 61 (4), 1414–1419. Available at: doi:10.1128/AEM.61.4.1414-1419.1995.

Lohmeier-Vogel, E. M., McIntyre, D. D. and Vogel, H. J. (1996). Phosphorus-31 and carbon-13 nuclear magnetic resonance studies of glucose and xylose metabolism in cell suspensions and agarose-immobilized cultures of *Pichia stipitis* and *Saccharomyces cerevisiae*. *Applied and Environmental Microbiology*. 62 (8), 2832–2838. Available at: doi:10.1128/AEM.62.8.2832-2838.1996.

Lohmeier-Vogel, E. M., Ung, S. and Turner, R. J. (2004). In vivo 31P nuclear magnetic resonance investigation of tellurite toxicity in *Escherichia coli*. *Applied and Environmental Microbiology*. 70 (12), 7342–7347. Available at: doi:10.1128/AEM.70.12.7342-7347.2004.

Lounis, N., Gevers, T., Van Den Berg, J., Vranckx, L. and Andries, K. (2009). ATP Synthase Inhibition of *Mycobacterium avium* Is Not Bactericidal. *Antimicrobial Agents and Chemotherapy*. 53 (11), 4827-4929. Available at: doi:10.1128/AAC.00689-09.

Lu, X., Williams, Z., Hards, K., Tang, J., Cheung, C.-Y., Aung, H. L., Wang, B., Liu, Z., Hu, X., Lenaerts, A., Woolhiser, L., Hastings, C., Zhang, X., Wang, Z., Rhee, K., Ding, K., Zhang, T. and Cook, G. M. (2019). Pyrazolo[1,5- a]pyridine Inhibitor of the Respiratory

Cytochrome bcc Complex for the Treatment of Drug-Resistant Tuberculosis. *ACS Infectious Diseases*. 5 (2), 239–249. Available at: doi:10.1021/acsinfecdis.8b00225.

Lundgren, C. A. K., Sjöstrand, D., Biner, O., Bennett, M., Rudling, A., Johansson, A.-L., Brzezinski, P., Carlsson, J., von Ballmoos, C. and Högbom, M. (2018). Scavenging of superoxide by a membrane-bound superoxide oxidase. *Nature Chemical Biology*. 14 (8), 788–793. Available at: doi:10.1038/s41589-018-0072-x.

Luthra, S., Rominski, A. and Sander, P. (2018). The role of antibiotic-target-modifying and antibiotic-modifying enzymes in *Mycobacterium abscessus* drug resistance. *Frontiers in Microbiology*. 9, 2179. Available at: doi:10.3389/fmicb.2018.02179.

Lyngstad, M. and Grasdalen, H. (1993). A new NMR airlift bioreactor used in 31P-NMR studies of itaconic acid producing *Aspergillus terreus*. *Journal of Biochemical and Biophysical Methods*. 27 (2), 105–116. Available at: doi:10.1016/0165-022x(93)90054-r.

Mackenzie, J. S., Lamprecht, D. A., Asmal, R., Adamson, J. H., Borah, K., Beste, D. J. V., Lee, B. S., Pethe, K., Rousseau, S., Krieger, I., Sacchettini, J. C., Glasgow, J. N. and Steyn, A. J. C. (2020). Bedaquiline reprograms central metabolism to reveal glycolytic vulnerability in *Mycobacterium tuberculosis*. *Nature Communications*. 11 (1), 6092. Available at: doi:10.1038/s41467-020-19959-4.

Madden, A., Leach, M. O., Collins, D. J. and Payne, G. S. (1991). The water resonance as an alternative pH reference: relevance to in vivo 31P NMR localized spectroscopy studies. *Magnetic Resonance in Medicine.* 19 (2), 416–421. Available at: doi:10.1002/mrm.1910190232.

Manchester, K. (1984). Tuberculosis and leprosy in antiquity: an interpretation. *Medical History*. 28 (2), 162–173. Available at: doi:10.1017/s0025727300035705.

Maris, J. M., Evans, A. E., McLaughlin, A. C., D'Angio, G. J., Bolinger, L., Manos, H. and Chance, B. (1985). ^{31}P Nuclear Magnetic Resonance Spectroscopic Investigation of Human Neuroblastoma in Situ. *The New England Journal of Medicine*. 312 (23) pp.1500–1505. Available at: doi:10.1056/nejm198506063122307.

Martin, J. B., Foray, M. F., Klein, G. and Satre, M. (1987). Identification of inositol hexaphosphate in 31P-NMR spectra of *Dictyostelium discoideum* amoebae. Relevance to intracellular pH determination. *Biochimica et Biophysica Acta*. 931 (1), 16–25. Available at: doi:10.1016/0167-4889(87)90045-0.

Martínez, A., Torello, S. and Kolter, R. (1999). Sliding motility in mycobacteria. *Journal of Bacteriology*. 181 (23), 7331–7338. Available at: doi:10.1128/JB.181.23.7331-7338.1999.

Mashabela, G. T., de Wet, T. J. and Warner, D. F. (2019). *Mycobacterium tuberculosis* Metabolism. *Microbiology Spectrum*. 7 (4). Available at: doi:10.1128/microbiolspec.gpp3-0067-2019.

Matsoso, L. G., Kana, B. D., Crellin, P. K., Lea-Smith, D. J., Pelosi, A., Powell, D., Dawes, S. S., Rubin, H., Coppel, R. L. and Mizrahi, V. (2005). Function of the cytochrome bc1-aa3 branch of the respiratory network in mycobacteria and network adaptation occurring in response to its disruption. *Journal of Bacteriology*. 187 (18), 6300–6308. Available at: doi:10.1128/JB.187.18.6300-6308.2005.

Mattila, J. T., Ojo, O. O., Kepka-Lenhart, D., Marino, S., Kim, J. H., Eum, S. Y., Via, L. E., Barry, C. E., 3rd, Klein, E., Kirschner, D. E., Morris, S. M., Jr, Lin, P. L. and Flynn, J. L. (2013). Microenvironments in tuberculous granulomas are delineated by distinct populations of macrophage subsets and expression of nitric oxide synthase and arginase isoforms. *The Journal of Immunology*. 191 (2), 773–784. Available at: doi:10.4049/jimmunol.1300113.

McCaffrey, E. F., Donato, M., Keren, L., Chen, Z., Delmastro, A., Fitzpatrick, M. B., Gupta, S., Greenwald, N. F., Baranski, A., Graf, W., Kumar, R., Bosse, M., Fullaway, C. C., Ramdial, P. K., Forgó, E., Jojic, V., Van Valen, D., Mehra, S., Khader, S. A., Bendall, S. C., van de Rijn, M., Kalman, D., Kaushal, D., Hunter, R. L., Banaei, N., Steyn, A. J. C., Khatri, P. and Angelo, M. (2022). The immunoregulatory landscape of human tuberculosis granulomas. *Nature Immunology*. 23 (2), 318–329. Available at: doi:10.1038/s41590-021-01121-x.

McDermott, W., Ormond, L., Muschenheim, C., Deuschle, K., McCune, R. M., Jr and Tompsett, R. (1954). Pyrazinamide-isoniazid in tuberculosis. *American Review of Tuberculosis*. 69 (3), 319–333. Available at: doi:10.1164/art.1954.69.3.319

Meehan, C. J., Barco, R. A., Loh, Y.-H. E., Cogneau, S. and Rigouts, L. (2021). Reconstituting the genus *Mycobacterium*. *International Journal of Systematic and Evolutionary Microbiology*. 71 (9). Available at: doi:10.1099/ijsem.0.004922.

Melnikov, P. V., Alexandrovskaya, A. Y., Naumova, A. O., Arlyapov, V. A., Kamanina, O. A., Popova, N. M., Zaitsev, N. K. and Yashtulov, N. A. (2022). Optical Oxygen Sensing and Clark Electrode: Face-to-Face in a Biosensor Case Study. *Sensors*. 22 (19). Available at: doi:10.3390/s22197626.

Melvin, B. K. and Shanks, J. V. (1996). Influence of aeration on cytoplasmic pH of yeast in an NMR airlift bioreactor. *Biotechnology Progress*. 12 (2), 257–265. Available at: doi:10.1021/bp9500775.

Merritt, R. W., Walker, E. D., Small, P. L. C., Wallace, J. R., Johnson, P. D. R., Benbow, M. E. and Boakye, D. A. (2010). Ecology and transmission of Buruli ulcer disease: a systematic review. *PLoS Neglected Tropical Diseases*. 4 (12), e911. Available at: doi:10.1371/journal.pntd.0000911.

Meyers, H., Brown-Elliott, B. A., Moore, D., Curry, J., Truong, C., Zhang, Y. and Wallace, R. J., Jr (2002). An outbreak of *Mycobacterium chelonae* infection following liposuction. *Clinical Infectious Diseases.*. 34 (11), 1500–1507. Available at: doi:10.1086/340399.

Meyers, W. M., Gormus, B. J., Walsh, G. P., Baskin, G. B. and Hubbard, G. B. (1991). Naturally acquired and experimental leprosy in nonhuman primates. The *American Journal of Tropical Medicine and Hygiene*. 44 (4 Pt 2), 24–27. Available at: doi:10.4269/ajtmh.1991.44.24.

Meyers W. M. and Portaels F. (2010). Buruli Ulcer: *Mycobacterium ulcerans* infection. In Warrell D. A., Cox T. M. and Firth J. D. (Eds). *Oxford Textbook of Medicine Fifth Edition Volume 1*. Oxford: Oxford University Press, pp. 848-850.

Moon, R. B. and Richards, J. H. (1973). Determination of intracellular pH by 31P magnetic resonance. *Journal of Biological Chemistry*. 248 (20), 7276–7278. Available at: doi:10.1016/S0021-9258(19)43389-9.

Moonan, P. K. (2018). Tuberculosis—the face of struggles, the struggles we face, and the dreams that lie within. *Emerging Infectious Diseases*. 24 (3), 592–593. Available at: doi:10.3201/eid2403.170128.

Morimoto, K., Aono, A., Murase, Y., Sekizuka, T., Kurashima, A., Takaki, A., Sasaki, Y., Igarashi, Y., Chikamatsu, K., Goto, H., Yamada, H., Kuroda, M. and Mitarai, S. (2018). Prevention of aerosol isolation of nontuberculous mycobacterium from the patient's bathroom. *ERJ Open Research*. 4 (3), 00150–02017. Available at: doi:10.1183/23120541.00150-2017.

Mulkidjanian, A. Y., Dibrov, P. and Galperin, M. Y. (2008). The past and present of sodium energetics: may the sodium-motive force be with you. *Biochimica et Biophysica Acta*. 1777 (7–8), 985–992. Available at: doi:10.1016/j.bbabio.2008.04.028.

Müller, B., Dürr, S., Alonso, S., Hattendorf, J., Laisse, C. J. M., Parsons, S. D. C., van Helden, P. D. and Zinsstag, J. (2013). Zoonotic *Mycobacterium bovis*-induced tuberculosis in humans. *Emerging Infectious Diseases*. 19 (6), 899–908. Available at: doi:10.3201/eid1906.120543.

Murima, P. McKinney, J. D. and Pethe, K. (2014). Targeting bacterial central metabolism for drug development. *Chemistry & Biology.* 21 (11), 1423-1432. Available at: doi:10.1016/j.chembiol.2014.08.020.

Murugesan, D., Ray, P. C., Bayliss, T., Prosser, G. A., Harrison, J. R., Green K., Soares de Melo, C., Feng, T. S., Street, L. J., Chibale, K., Warner, D. F., Mizrahi, V., Epemolu, O., Scullion, P., Ellis, L., Riley, J., Shishikura, Y., Ferguson, L., Osuna-Cabello, M., Read, K. D., Green, S. R., Lamprecht, D. A., Finin, P. M., Steyn, A. J. C., Ioerger, T. R., Sacchettini, J., Rhee, K. Y., Arora, K., Barry, C. E. 3rd, Wyatt, P. G. and Boshoff, H. I. M. (2018). 2-Mercapto-Quinazolinones as Inhibitors of Type II NADH Dehydrogenase and *Mycobacterium tuberculosis*: Structure-Activity Relationships, Mechanism of Action

and Absorption, Distribution, Metabolism, and Excretion Characterization. *ACS Infectious Diseases*. 4 (6), 954–969. Available at: doi:10.1021/acsinfecdis.7b00275.

Muschenheim, C., Organick, A., Mccune, R. M., Jr, Batten, J., Deuschle, K., Tompsett, R. and Mcdermott, W. (1955). Pyrazinamide-isoniazid in tuberculosis. III. Observations with reduced dosage of pyrazinamide. *American Review of Tuberculosis*. 72 (6), 851–855. Available at: doi:10.1164/artpd.1955.72.6.851.

Navon, G., Ogawa, S., Shulman, R. G. and Yamane, T. (1977). High-resolution 31P nuclear magnetic resonance studies of metabolism in aerobic *Escherichia coli* cells. *Proceedings of the National Academy of Sciences of the United States of America*. 74 (3), 888–891. Available at: doi:10.1073/pnas.74.3.888.

Netikul, T., Palittapongarnpim, P., Thawornwattana, Y. and Plitphonganphim, S. (2021). Estimation of the global burden of *Mycobacterium tuberculosis* lineage 1. *Infection, Genetics and Evolution.* 91 (104802), 104802. Available at: doi:10.1016/j.meegid.2021.104802.

Ngabonziza, J. C. S., Loiseau, C., Marceau, M., Jouet, A., Menardo, F., Tzfadia, O., Antoine, R., Niyigena, E. B., Mulders, W., Fissette, K., Diels, M., Gaudin, C., Duthoy, S., Ssengooba, W., André, E., Kaswa, M. K., Habimana, Y. M., Brites, D., Affolabi, D., Mazarati, J. B., de Jong, B., C., Rigouts, L., Gagneux, S., Meehan, C. J. and Supply, P. (2020). A sister lineage of the *Mycobacterium tuberculosis* complex discovered in the African Great Lakes region. *Nature Communications*. 11, 2917. Available at: doi:10.1038/s41467-020-16626-6.

Ngo, M. D., Bartlett, S. and Ronacher, K. (2021). Diabetes-Associated Susceptibility to Tuberculosis: Contribution of Hyperglycemia vs. Dyslipidemia. *Microorganisms*. 9 (11), 2282. Available at: doi:10.3390/microorganisms9112282.

Nicholls, D. G. and Ferguson, S. J. (2002). *Bioenergetics 3*. London: Academic Press.

Nieuwenhuis, F. J., Kanner, B. I., Gutnick, D. L., Postma, P. W. and van Dam, K. (1973). Energy conservation in membranes of mutants of *Escherichia coli* defective in

oxidative phosphorylation. *Biochimica et Biophysica Acta*. 325 (1), 62–71. Available at: doi:10.1016/0005-2728(73)90151-5.

Nikitushkin, V. D., Shleeva, M. O., Zinin, A. I., Trutneva, K. A., Ostrovsky, D. N. and Kaprelyants, A. S. (2016). The main pigment of the dormant *Mycobacterium smegmatis* is porphyrin. *FEMS Microbiology Letters*. 363 (19). Available at: doi:10.1093/femsle/fnw206.

O'Reilly, L. M. and Daborn, C .J. (1995). The epidemiology of *Mycobacterium bovis* infections in animals and man: a review. *Tubercle and Lung Disease.* 76 (Suppl 1), 1–46. Available at: doi:10.1016/0962-8479(95)90591-x.

Ocepek, M., Pate, M., Zolnir-Dovc, M. and Poljak, M. (2005). Transmission of *Mycobacterium tuberculosis* from human to cattle. *Journal of Clinical Microbiology*. 43 (7), 3555–3557. Available at: doi:10.1128/JCM.43.7.3555-3557.2005.

Ok-hama, T., Siebelt, F., Furihata, K., Seto, H., Miyachi, S. and Ohmori, M. (1986). 31P-NMR studies on inorganic polyphosphates in microalgae. *Journal of Phycology*. 22 (4), 485–490. Available at: doi:10.1111/j.1529-8817.1986.tb02492.x.

Omar, S., Whitfield, M. G., Nolan, M. B., Ngom, J. T., Ismail, N., Warren, R. M. and Klopper, M. (2024). Bedaquiline for treatment of non-tuberculous mycobacteria (NTM): a systematic review and meta-analysis. *Journal of Antimicrobial Chemotherapy*. 79 (2), 211-240. Available at: doi:10.1093/jac/dkad372.

Parte A. C. (2024). *Genus Mycobacterium*. [Online]. List of Prokaryotic Names with Standing in Nomenclature. Last updated: 27 February 2024. Available at: https://lpsn.dsmz.de/genus/mycobacterium [Accessed 5 August 2024].

Parte, A. C., Sardà Carbasse, J., Meier-Kolthoff, J. P., Reimer, L. C. and Göker, M. (2020). List of Prokaryotic names with Standing in Nomenclature (LPSN) moves to the DSMZ. *International Journal of Systematic and Evolutionary Microbiology*, 70, 5607-5612. Available at: doi: 10.1099/ijsem.0.004332

Pecsi, I., Hards, K., Ekanayaka, N., Berney, M., Hartman, T., Jacobs, W. R., Jr and Cook, G. M. (2014). Essentiality of succinate dehydrogenase in *Mycobacterium smegmatis*

and its role in the generation of the membrane potential under hypoxia. *mBio*. 5 (4). Available at: doi:10.1128/mBio.01093-14.

Pereira, A. C., Ramos, B., Reis, A. C. and Cunha, M. V. (2020). Non-tuberculous mycobacteria: Molecular and physiological bases of virulence and adaptation to ecological niches. *Microorganisms*. 8 (9), 1380. Available at: doi:10.3390/microorganisms8091380.

Peters, D. H. and Clissold, S. P. (1992). Clarithromycin A Review of its Antimicrobial Activity, Pharmacokinetic Properties and Therapeutic Potential. *Drugs*. 44 (1), 117-164. Available at: doi:10.1177/106002809202600912.

Pethe, K., Bifani, P., Jang, J., Kang, S., Park, S., Ahn, S., Jiricek, J., Jung, J., Jeon, H. K., Cechetto, J., Christophe, T., Lee, H., Kempf, M., Jackson, M., Lenaerts, A. J., Pham, H., Jones, V., Seo, M. J., Kim, Y. M., Seo, M., Seo, J. J., Park, D., Ko, Y., Choi, I., Kim, R., Kim, S. Y., Lim, S., Yim, S. A., Nam, J., Kang, H., Kwon, H., Oh, C. T., Cho, Y., Jang, Y., Kim, J., Chua, A., Tan, B. H., Nanjundappa, M. B., Rao, S. P., Barnes, W. S., Wintjens, R., Walker, J. R., Alonso, S., Lee, S., Kim, J., Oh, S., Oh, T., Nehrbass, U., Han, S. J., No, Z., Lee, J., Brodin, P., Cho, S. N., Nam, K. and Kim, J. (2013). Discovery of Q203, a potent clinical candidate for the treatment of tuberculosis. *Nature Medicine*. 19 (9), 1157–1160. Available at: doi:10.1038/nm.3262.

Pfeffer, P. E., Bécard, G., Rolin, D. B., Uknalis, J., Cooke, P. and Tu, S. (1994). *In vivo* nuclear magnetic resonance study of the osmoregulation of phosphocholine-substituted beta-1,3;1,6 cyclic glucan and its associated carbon metabolism in *Bradyrhizobium japonicum* USDA 110. *Applied and Environmental Microbiology*. 60 (6), 2137–2146. Available at: doi:10.1128/AEM.60.6.2137-2146.1994.

Philley, J. V., Wallace, R. J., Benwill, J. L., Taskar, V., Brown-Elliott, A., Thakkar, F., Aksamit, T. R. and Griffith, D. E. (2015). Preliminary Results of Bedaquiline as Salvage Therapy for Patients With Nontuberculous Mycobacterial Lung Disease. *Chest*. 148 (2), 499-506. Available at: doi:10.1378/chest.14-2764.

Phyu, A. N., Aung, S. T., Palittapongarnpim, P., Htet, K. K. K., Mahasirimongkol, S., Aung, H. L., Chaiprasert, A. and Chongsuvivatwong, V. (2022). Distribution of

Mycobacterium tuberculosis Lineages and Drug Resistance in Upper Myanmar. *Tropical Medicine and Infectious Disease*. 7 (12), 448. Available at: doi:10.3390/tropicalmed7120448.

Pietri, S., Martel, S., Culcasi, M., Delmas-Beauvieux, M. C., Canioni, P. and Gallis, J. L. (2001). Use of diethyl(2-methylpyrrolidin-2-yl)phosphonate as a highly sensitive extra- and intracellular 31P NMR pH indicator in isolated organs. Direct NMR evidence of acidic compartments in the ischemic and reperfused rat liver. *Journal of Biological Chemistry*. 276 (3), 1750–1758. Available at: doi:10.1074/jbc.M008023200.

Pietri, S., Miollan, M., Martel, S., Le Moigne, F., Blaive, B. and Culcasi, M. (2000). alpha - and beta -phosphorylated amines and pyrrolidines, a new class of low toxic highly sensitive 31P NMR pH indicators. Modeling of pKa and chemical shift values as a function of substituents. *Journal of Biological Chemistry*. 275 (26), 19505–19512. Available at: doi:10.1074/jbc.M001784200.

Pin, D., Guérin-Faublée, V., Garreau, V., Breysse, F., Dumitrescu, O., Flandrois, J.-P. and Lina, G. (2014). Mycobacterium species related to *M. leprae* and *M. lepromatosis* from cows with bovine nodular thelitis. *Emerging Infectious Diseases*. 20 (12), 2111–2114. Available at: doi:10.3201/eid2012.140184.

Ploemacher, T., Faber, W. R., Menke, H., Rutten, V. and Pieters, T. (2020). Reservoirs and transmission routes of leprosy; A systematic review. *PLoS Neglected Tropical Diseases*. 14 (4), e0008276. Available at: doi:10.1371/journal.pntd.0008276.

Prammananan, T., Sander, P., Brown, B. A., Frischkorn, K., Onyi, G. O., Zhang, Y., Böttger, E. C. and Wallace, R. J., Jr (1998). A single 16S ribosomal RNA substitution is responsible for resistance to amikacin and other 2-deoxystreptamine aminoglycosides in *Mycobacterium abscessus* and *Mycobacterium chelonae*. *The Journal of Infectious Diseases*. 177 (6), 1573–1581. Available at: doi:10.1086/515328.

Preiss, L., Langer, J. D., Yildiz, Ö., Eckhardt-Strelau, L., Guillemont, J. E. G., Koul, A. and Meier, T. (2015). Structure of the mycobacterial ATP synthase Fo rotor ring in complex with the anti-TB drug bedaquiline. *Science Advances*. 1 (4), e1500106. Available at: doi:10.1126/sciadv.1500106.

Primm, T. P., Lucero, C. A. and Falkinham, J. O., 3rd (2004). Health impacts of environmental mycobacteria. *Clinical Microbiology Reviews*. 17 (1), 98–106. Available at: doi:10.1128/cmr.17.1.98-106.2004.

Rao, S. P. S., Alonso, S., Rand, L., Dick, T. and Pethe, K. (2008). The protonmotive force is required for maintaining ATP homeostasis and viability of hypoxic, nonreplicating *Mycobacterium tuberculosis*. *Proceedings of the National Academy of Sciences of the United States of America*. 105 (33), 11945–11950. Available at: doi:10.1073/pnas.0711697105.

Rata, M., Giles, S. L., deSouza, N. M., Leach, M. O. and Payne, G. S. (2014). Comparison of three reference methods for the measurement of intracellular pH using 31P MRS in healthy volunteers and patients with lymphoma. *NMR in Biomedicine*. 27 (2), 158–162. Available at: doi:10.1002/nbm.3047.

Reyrat, J-M. and Kahn, D. (2001). *Mycobacterium smegmatis:* an absurd model for tuberculosis? *Trends in Microbiology*. 9 (10), 472-473. Available at: doi:10.1016/s0966-842x(01)02168-0.

Rhee, K. Y., de Carvalho, L. P., Bryk, R., Ehrt, S., Marrero, J., Park, S. W., Schnappinger, D., Venugopal, A. and Nathan, C. (2011). Central carbon metabolism in *Mycobacterium tuberculosis*: an unexpected frontier. *Trends in Microbiology*. 19 (7), 307-314. Available at: doi:10.1016/j.tim.2011.03.008.

Riley, R. L., Mills, C. C., Nyka, W., Weinstock, N., Storey, P. B., Sultan, L.U., Riley, M. C. and Wells, W. F. (1959). Aerial dissemination of pulmonary tuberculosis a two-year study of contagion in a tuberculosis ward. *American Journal of Epidemiology*. 70 (2), 185–196. Available at: doi:10.1093/oxfordjournals.aje.a120069.

Ripple, M. O., Abajian, M. and Springett, R. (2010). Cytochrome *c* is rapidly reduced in the cytosol after mitochondrial outer membrane permeabilization. *Apoptosis*. 15 (5), 563-573. Available at: doi:10.1007/s10495-010-0455-2.

Ripple, M. O., Kim, N. and Springett, R. (2013). Mammalian complex I pumps 4 protons per 2 electrons at high and physiological proton motive force in living cells. *Journal of Biological Chemistry*. 288 (8), 5374–5380. Available at: doi:10.1074/jbc.M112.438945.

Rocha, M. and Springett, R. (2019). Measuring the functionality of the mitochondrial pumping complexes with multi-wavelength spectroscopy. *Biochimica et Biophysica Acta (BBA) - Bioenergetics*. 1860 (1), 89–101. Available at: doi:10.1016/j.bbabio.2018.11.013.

Rock, J. M., Lang, U. F., Chase, M. R., Ford, C. B., Gerrick, E. R., Gawande, R., Coscolla, M., Gagneux, S., Fortune, S. M. and Lamers, M. H. (2015). DNA replication fidelity in *Mycobacterium tuberculosis* is mediated by an ancestral prokaryotic proofreader. *Nature Genetics*. 47 (6), 677–681. Available at: doi:10.1038/ng.3269.

Rodríguez, S., Bezos, J., Romero, B., de Juan, L., Álvarez, J., Castellanos, E., Moya, N., Lozano, F., Javed, M. T., Sáez-Llorente, J. L., Liébana, E., Mateos, A., Domínguez, L., Aranaz, A. and Spanish Network on Surveillance and Monitoring of Animal Tuberculosis (2011). *Mycobacterium caprae* infection in livestock and wildlife, Spain. *Emerging Infectious Diseases*. 17 (3), 532–535. Available at: doi:10.3201/eid1703.100618.

Rogall, T., Wolters, J., Flohr, T. and Böttger, E. C. (1990). Towards a phylogeny and definition of species at the molecular level within the genus *Mycobacterium*. *International Journal of Systematic Bacteriology*. 40 (4), 323–330. Available at: doi:10.1099/00207713-40-4-323.

Runyon, E. H. (1959). Anonymous mycobacteria in pulmonary disease. *Medical Clinics of North America*. 43 (1), 273–290. Available at: doi:10.1016/s0025-7125(16)34193-1.

Rustad, T. R., Sherrid, A. M., Minch, K. J. and Sherman, D. R. (2009). Hypoxia: a window into *Mycobacterium tuberculosis* latency. *Cellular Microbiology*. 11 (8), 1151–1159. Available at: doi:10.1111/j.1462-5822.2009.01325.x.

Ruth, M. M., Sangen, J. J. N., Remmers, K., Pennings, L. J., Svensson E., Aarnoutse R. E., Zweijpfenning, S. M. H., Hoefsloot, W., Kuipers, S., Magis-Escurra, C., Wertheim, H.

F. L. and van Ingen, J. (2019). A bedaquiline/clofazimine combination regimen might add activity to the treatment of clinically relevant non-tuberculous mycobacteria. *Journal of Antimicrobial Chemotherapy.* 74 (4), 935-943. Available at: doi:10.1093/jac/dky526

Rybniker, J., Vocat, A., Sala, C., Busso, P., Pojer, F., Benjak, A. and Cole, S. T. (2015). Lansoprazole is an antituberculous prodrug targeting cytochrome bc1. *Nature Communications*. 6, 7659. Available at: doi:10.1038/ncomms8659.

Safarian, S., Rajendran, C., Müller, H., Preu, J., Langer, J. D., Ovchinnikov, S., Hirose, T., Kusumoto, T., Sakamoto, J. and Michel, H. (2016). Structure of a bd oxidase indicates similar mechanisms for membrane-integrated oxygen reductases. *Science*. 352 (6285), 583–586. Available at: doi:10.1126/science.aaf2477.

Saini, N. K., Baena, A., Ng, T. W., Venkataswamy, M. M., Kennedy, S. C., Kunnath-Velayudhan, S., Carreño, L. J., Xu, J., Chan, J., Larsen, M. H., Jacobs, W. R., Jr and Porcelli, S. A. (2016). Suppression of autophagy and antigen presentation by *Mycobacterium tuberculosis* PE_PGRS47. *Nature Microbiology*. 1 (9), 16133. Available at: doi:10.1038/nmicrobiol.2016.133.

Sambandamurthy, V. K., Derrick, S. C., Hsu, T., Chen, B., Larsen, M. H., Jalapathy, K. V., Chen, M., Kim, J., Porcelli, S. A., Chan, J., Morris, S. L. and Jacobs, W. R., Jr (2006). *Mycobacterium tuberculosis* DeltaRD1 DeltapanCD: a safe and limited replicating mutant strain that protects immunocompetent and immunocompromised mice against experimental tuberculosis. *Vaccine*. 24 (37–39), 6309–6320. Available at: doi:10.1016/j.vaccine.2006.05.097.

Sampson, S. L., Dascher, C. C., Sambandamurthy, V. K., Russell, R. G., Jacobs, W. R., Jr, Bloom, B. R. and Hondalus, M. K. (2004). Protection elicited by a double leucine and pantothenate auxotroph of *Mycobacterium tuberculosis* in guinea pigs. *Infection and Immunity*. 72 (5), 3031–3037. Available at: doi:10.1128/IAI.72.5.3031-3037.2004.

Santos, H. and Turner, D. L. (1986). Characterization of the improved sensitivity obtained using a flow method for oxygenating and mixing cell suspensions in NMR.

Journal of Magnetic Resonance . 68 (2), 345–349. Available at: doi:10.1016/0022-2364(86)90251-9.

Sassetti, C. M., Boyd, D. H. and Rubin, E. J. (2003). Genes required for mycobacterial growth defined by high density mutagenesis. *Molecular Microbiology*. 48 (1), 77–84. Available at: doi:10.1046/j.1365-2958.2003.03425.x.

Satre, M., Martin, J. B. and Klein, G. (1989). Methyl phosphonate as a 31P-NMR probe for intracellular pH measurements in *Dictyostelium amoebae*. *Biochimie*. 71 (8), 941–948. Available at: doi:10.1016/0300-9084(89)90076-x.

Sax, H., Bloemberg, G., Hasse, B., Sommerstein, R., Kohler, P., Achermann, Y., Rössle, M., Falk, V., Kuster, S. P., Böttger, E. C. and Weber, R. (2015). Prolonged outbreak of *Mycobacterium chimaera* infection after open-chest heart surgery. *Clinical Infectious Diseases.* 61 (1), 67–75. Available at: doi:10.1093/cid/civ198.

Schlemmer, H.-P. W., Sawatzki, T., Sammet, S., Dornacher, I., Bachert, P., van Kaick, G., Waldherr, R. and Seitz, H. K. (2005). Hepatic phospholipids in alcoholic liver disease assessed by proton-decoupled ^{31}P magnetic resonance spectroscopy. *Journal of Hepatology*. 42 (5), 752–759. Available at: doi:10.1016/j.jhep.2004.12.032.

Schmidt, V., Schneider, S., Schlomer, J., Krautwald-Junghanns, M.-E. and Richter, E. (2008). Transmission of tuberculosis between men and pet birds: a case report. *Avian Pathology.* 37 (6), 589–592. Available at: doi:10.1080/03079450802428901.

Schnappinger, D., Ehrt, S., Voskuil, M. I., Liu, Y., Mangan, J. A., Monahan, I. M., Dolganov, G., Efron, B., Butcher, P. D., Nathan, C. and Schoolnik, G. K. (2003). Transcriptional Adaptation of *Mycobacterium tuberculosis* within Macrophages: Insights into the Phagosomal Environment: Insights into the Phagosomal Environment. *Journal of Experimental Medicine*. 198 (5), 693–704. Available at: doi:10.1084/jem.20030846.

Segala, E., Sougakoff, W., Nevejans-Chauffour, A., Jarlier, V. and Petrella, S. (2012). New mutations in the mycobacterial ATP synthase: new insights into the binding of

the diarylquinoline TMC207 to the ATP synthase C-ring structure. *Antimicrobial Agents and Chemotherapy*. 56 (5), 2326–2334. Available at: doi:10.1128/AAC.06154-11.

Sensi, P. (1983). History of the development of rifampin. *Clinical Infectious Diseases.* 5 (Suppl 3), S402–S406. Available at: doi:10.1093/clinids/5.supplement_3.s402.

Serebrennikova, Y. M., Huffman, D. E. and Garcia-Rubio, L. H. (2015). Characterization of red blood cells with multiwavelength transmission spectroscopy. *BioMed Research International*. 2015, 382641. Available at: doi:10.1155/2015/382641.

Shen, H., Zhang, Q., Peng, L., Ma, W. and Guo, J. (2024). Cutaneous *Mycobacterium abscessus* infection following plastic surgery: Three case reports. *Clinical, Cosmetic and Investigational Dermatology*. 17, 637–647. Available at: doi:10.2147/CCID.S445175.

Shepherd, M. (2015). The CydDC ABC transporter of *Escherichia coli*: new roles for a reductant efflux pump. *Biochemical Society Transactions*. 43 (5), 908–912. Available at: doi:10.1042/BST20150098.

Slonczewski, J. L., Rosen, B. P., Alger, J. R. and Macnab, R. M. (1981). pH homeostasis in *Escherichia coli*: measurement by 31P nuclear magnetic resonance of methylphosphonate and phosphate. *Proceedings of the National Academy of Sciences of the United States of America*. 78 (10), 6271–6275. Available at: doi:10.1073/pnas.78.10.6271.

Smith, I. (2003). *Mycobacterium tuberculosis* Pathogenesis and Molecular Determinants of Virulence. *Clinical Microbiology Reviews*. 16 (3), 463-496. Available at: doi:10.1128/CMR.16.3.463-496.2003.

Snapper, S. B., Melton, R. E., Mustafa, S., Kieser, T. and Jacobs, W. R., Jr (1990). Isolation and characterization of efficient plasmid transformation mutants of *Mycobacterium smegmatis*. *Molecular Microbiology*. 4 (11), 1911–1919. Available at: doi:10.1111/j.1365-2958.1990.tb02040.x.

Somner, A. R. and Angel, J. (1981). A controlled trial of six months chemotherapy in pulmonary tuberculosis. First Report: results during chemotherapy. *British Journal of*

Diseases of the Chest. 75 (2), 141–153. Available at: doi:10.1016/0007-0971(81)90046-2.

Sonawat, H. M., Leibfritz, D., Engel, J. and Hilgard, P. (1990). Biotransformation of mafosfamide in P388 mice leukemia cells: intracellular ^{31}P-NMR studies. *Biochimica et Biophysica Acta*. 1052 (1), 36–41. Available at: doi:10.1016/0167-4889(90)90054-h.

Sostman, H. D., Armitage, I. M. and Fischer, J. J. (1984). NMR in cancer. I. High resolution spectroscopy of tumors. *Magnetic Resonance Imaging*. 2 (4), 265–278. Available at: doi:10.1016/0730-725x(84)90192-9.

Sparks, I. L., Derbyshire, K. M., Jacobs, W. R. and Morita, Y. S. (2023). *Mycobacterium smegmatis*: The Vanguard of Mycobacterial Research. *Journal of Bacteriology*. 205 (1), e0033722. Available at: doi:10.1128/jb.00337-22.

Stahl, D. A. and Urbance, J. W. (1990). The division between fast- and slow-growing species corresponds to natural relationships among the mycobacteria. *Journal of Bacteriology*. 172 (1), 116–124. Available at: doi:10.1128/jb.172.1.116-124.1990.

Stamm, L. M., Morisaki, J. H., Gao, L.-Y., Jeng, R. L., McDonald, K. L., Roth, R., Takeshita, S., Heuser, J., Welch, M. D. and Brown, E.J. (2003). *Mycobacterium marinum* escapes from phagosomes and is propelled by actin-based motility. *Journal of Experimental Medicine*. 198 (9), 1361–1368. Available at: doi:10.1084/jem.20031072.

Stead, W. W., Eisenach, K. D., Cave, M. D., Beggs, M. L., Templeton, G. L., Thoen, C. O. and Bates, J. H. (1995). When did *Mycobacterium tuberculosis* infection first occur in the New World? An important question with public health implications. *American Journal of Respiratory and Critical Care Medicine*. 151 (4), 1267–1268. Available at: doi:10.1164/ajrccm/151.4.1267.

Steenken, W. (1935). Lysis of Tubercle Bacilli in Vitro. *Proceedings of the Society for Experimental Biology and Medicine.* 33 (2), 253-255. Available at: doi:10.3181/00379727-33-8330P.

Steiert, J. G., Thoma, W. J., Ugurbil, K. and Crawford, R. L. (1988). 31P nuclear magnetic resonance studies of effects of some chlorophenols on *Escherichia coli* and a

pentachlorophenol-degrading bacterium. *Journal of Bacteriology*. 170 (10), 4954–4957. Available at: doi:10.1128/jb.170.10.4954-4957.1988.

Stincone, A., Prigione, A., Cramer, T., Wamelink, M. M., Campbell, K., Cheung, E., Olin-Sandoval, V., Grüning, N. M., Krüger, A., Tauqeer Alam, M., Keller, M. A., Breitenbach, M., Brindle, K. M., Rabinowitz, J. D. and Ralser, M. (2015). The return of metabolism: biochemistry and physiology of the pentose phosphate pathway. *Biological Reviews.* 90 (3), 927-963. Available at: doi:10.1111/brv.12140.

Stokes, G. G. (1864). VIII. On the reduction and oxidation of the colouring matter of the blood. *Proceedings of the Royal Society of London*. 13, 355–364. Available at: doi:10.1098/rspl.1863.0080.

Stover, C. K., Warrener, P., VanDevanter, D. R., Sherman, D. R., Arain, T. M., Langhorne, M. H., Anderson, S. W., Towell, J. A., Yuan, Y., McMurray, D. N., Kreiswirth, B. N., Barry, C. E. and Baker, W. R. (2000). A small-molecule nitroimidazopyran drug candidate for the treatment of tuberculosis. *Nature*. 405 (6789), 962–966. Available at: doi:10.1038/35016103.

Sutherland, H. S., Tong, A. S. T., Choi, P. J., Blaser, A., Conole, D., Franzblau, S. G., Lotlikar, M. U., Cooper, C. B., Upton, A. M., Denny, W. A. and Palmer, B. D. (2019). 3,5-Dialkoxypyridine analogues of bedaquiline are potent antituberculosis agents with minimal inhibition of the hERG channel. *Bioorganic & Medicinal Chemistry.* 27 (7), 1292–1307. Available at: doi:10.1016/j.bmc.2019.02.026.

Svensson, E. M., Murray, S., Karlsson, M. O. and Dooley, K. E. (2015) Rifampicin and rifapentine significantly reduce concentrations of bedaquiline, a new anti-TB drug. *Journal of Antimicrobial Chemotherapy.* 70 (4), 1106-1114. Available at: doi:10.1093/jac/dku504

Symersky, J., Osowski, D., Walters, D. E. and Mueller, D. M. (2012). Oligomycin frames a common drug-binding site in the ATP synthase. *Proceedings of the National Academy of Sciences of the United States of America*. 109 (35), 13961–13965. Available at: doi:10.1073/pnas.1207912109.

Tasneen, R., Betoudji, F., Tyagi, S., Li, S. Y., Williams, K., Converse, P. J., Dartois, V., Yang, T., Mendel, C. M., Mdluli, K. E. and Nuermberger E. L. (2016). Contribution of Oxazolidinones to the Efficacy of Novel Regimens Containing Bedaquiline and Pretomanid in a Mouse Model of Tuberculosis. *Antimicrobial Agents and Chemotherapy*. 60 (1), 270-277. Available at: doi:10.1128/AAC.01691-15.

TB Alliance (2024). *New Clinical Trial Examines Use of Novel Compound Telacebec in Buruli Ulcer Patients*. TB Alliance. Last updated: 21 August 2024. Available at: https://www.tballiance.org/news/new-clinical-trial-examines-use-novel-compound-telacebec-buruli-ulcer-patients [Accessed 10 September 2024].

Thoma, W. J., Steiert, J. G., Crawford, R. L. and Uğurbil, K. (1986). pH measurements by 31P NMR in bacterial suspensions using phenyl phosphonate as a probe. *Biochemical and Biophysical Research Communications*. 138 (3), 1106–1109. Available at: doi:10.1016/s0006-291x(86)80396-5.

Tortoli, E. (2012). Phylogeny of the genus *Mycobacterium*: many doubts, few certainties. *Infection, Genetics and Evolution.* 12 (4), 827–831. Available at: doi:10.1016/j.meegid.2011.05.025.

Tortoli, E., Brown-Elliott, B. A., Chalmers, J. D., Cirillo, D. M., Daley, C. L., Emler, S., Floto, R. A., Garcia, M. J., Hoefsloot, W., Koh, W. J., Lange, C., Loebinger, M., Maurer, F. P., Morimoto, K., Niemann, S., Richter, E., Turenne, C. Y., Vasireddy, R., Vasireddy, S., Wagner, D., Wallace, R. J., Jr, Wengenack, N. and van Ingen, J. (2019). Same meat, different gravy: ignore the new names of mycobacteria. *European Respiratory*. 54 (1), 1900795. Available at: doi:10.1183/13993003.00795-2019.

Traag, B. A., Driks, A., Stragier, P., Bitter, W., Broussard, G., Hatfull, G., Chu, F., Adams, K. N., Ramakrishnan, L. and Losick, R. (2010). Do mycobacteria produce endospores? *Proceedings of the National Academy of Sciences of the United States of America*. 107 (2), 878–881. Available at: doi:10.1073/pnas.0911299107.

Tran, S. L. and Cook, G. M. (2005). The F1Fo-ATP synthase of *Mycobacterium smegmatis* is essential for growth. *Journal of Bacteriology*. 187 (14), 5023–5028. Available at: doi:10.1128/JB.187.14.5023-5028.2005.

Trifiro, S., Bourgault, A. M., Lebel, F. and René, P. (1990). Ghost mycobacteria on Gram stain. *Journal of Clinical Microbiology*. 28 (1), 146–147. Available at: doi:10.1128/jcm.28.1.146-147.1990.

Tseng, Y.-T., Pan, C.-T., Yang, S.-M., Yu, S.-P. and Huang, P.-M. (2020). Recent advances and controversies in surgical intervention of nontuberculous mycobacterial lung disease: A literature review. *Journal of the Formosan Medical Association.* 119 (Suppl 1), S76–S83. Available at: doi:10.1016/j.jfma.2020.04.029.

Tufariello, J. M., Kerantzas, C. A., Vilchèze, C., Calder, R. B., Nordberg, E. K., Fischer, J. A., Hartman, T. E., Yang, E., Driscoll, T., Cole, L. E., Sebra, R., Maqbool, S. B., Wattam, A. R. and Jacobs, W. R., Jr (2015). The complete genome sequence of the emerging pathogen *Mycobacterium haemophilum* explains its unique culture requirements. *mBio*. 6 (6), e01313-15. Available at: doi:10.1128/mBio.01313-15.

Van Der Werf, T. S., Barogui, Y. T., Converse, P. J., Phillips, R. O. and Stienstra, Y. (2020). Pharmacologic management of *Mycobacterium ulcerans* infection. *Expert Review of Clinical Pharmacology*. 13 (4), 391-401. Available at: doi:0.1080/17512433.2020.1752663.

Van Gestel, J. F. E., Guillemont, J. E. G., Venet, M. G., Poignet, H. J. J., Decrane, L. F. B., Vernier, D. F. J. and Odds, F. C. (2004). *Quinoline derivatives and their use as mycobacterial inhibitors.* World Intellectual Property Organisation WO/2004/011436. 5 February 2004.

Velayati, A. A., Farnia, P., Mozafari, M., Malekshahian, D., Farahbod, A. M., Seif, S., Rahideh, S. and Mirsaeidi, M. (2015). Identification and genotyping of *Mycobacterium tuberculosis* isolated from water and soil samples of a metropolitan city. *Chest*. 147 (4), 1094–1102. Available at: doi:10.1378/chest.14-0960.

Vilchèze, C., Weisbrod, T. R., Chen, B., Kremer, L., Hazbón, M. H., Wang, F., Alland, D., Sacchettini, J. C. and Jacobs, W. R., Jr (2005). Altered NADH/NAD+ ratio mediates coresistance to isoniazid and ethionamide in mycobacteria. *Antimicrobial Agents and Chemotherapy*. 49 (2), 708–720. Available at: doi:10.1128/AAC.49.2.708-720.2005.

Vitkin, I. A., Moriarty, J. A., Peters, R. D., Kolios, M. C., Gladman, A. S., Chen, J. C., Hinks, R. S., Hunt, J. W., Wilson, B. C., Easty, A. C., Bronskill, M. J., Kucharczyk, W., Sherar, M. D. and Henkelman, R. M. (1997). Magnetic resonance imaging of temperature changes during interstitial microwave heating: a phantom study. *Medical Physics*. 24 (2), 269–277. Available at: doi:10.1118/1.598096.

Wang, X.-Y., Jia, Q.-N. and Li, J. (2023). Treatment of non-tuberculosis mycobacteria skin infections. *Frontiers in Pharmacology*. 14, 1242156. Available at: doi:10.3389/fphar.2023.1242156.

Wang, Z., Soni, V., Marriner, G., Kaneko, T., Boshoff, H. I. M., Barry, C. E., 3rd and Rhee, K. Y. (2019). Mode-of-action profiling reveals glutamine synthetase as a collateral metabolic vulnerability of *M. tuberculosis* to bedaquiline. *Proceedings of the National Academy of Sciences of the United States of America*. 116 (39), 19646–19651. Available at: doi:10.1073/pnas.1907946116.

Warman, A. J., Rito, T. S., Fisher, N. E., Moss, D. M., Berry, N. G., O'Neill, P. M., Ward, S. A. and Biagini, G. A. (2013). Antitubercular pharmacodynamics of phenothiazines. *Journal of Antimicrobial Chemotherapy*. 68 (4), 869–880. Available at: doi:10.1093/jac/dks483.

Weinstein, E. A., Yano, T., Li, L.-S., Avarbock, D., Avarbock, A., Helm, D., McColm, A. A., Duncan, K., Lonsdale, J. T. and Rubin, H. (2005). Inhibitors of type II NADH:menaquinone oxidoreductase represent a class of antitubercular drugs. *Proceedings of the National Academy of Sciences of the United States of America*. 102 (12), 4548–4553. Available at: doi:10.1073/pnas.0500469102.

Wever, H. D., Cort, S. D., Noots, I. and Verachtert, H. (1997). Isolation and characterization of *Rhodococcus rhodochrous* for the degradation of the wastewater component 2-hydroxybenzothiazole. *Applied Microbiology and Biotechnology*. 47 (4), 458–461. Available at: doi:10.1007/s002530050956.

Wi, Y. M. (2019). Treatment of extrapulmonary nontuberculous Mycobacterial diseases. *Infection and Chemotherapy*. 51 (3), 245–255. Available at: doi:10.3947/ic.2019.51.3.245.

Wiseman, B., Nitharwal, R. G., Fedotovskaya, O., Schäfer, J., Guo, H., Kuang, Q., Benlekbir, S., Sjöstrand, D., Ädelroth, P., Rubinstein, J. L., Brzezinski, P. and Högbom, M. (2018). Structure of a functional obligate complex III2IV2 respiratory supercomplex from *Mycobacterium smegmatis*. *Nature Structural and Molecular Biology*. 25 (12), 1128–1136. Available at: doi:10.1038/s41594-018-0160-3.

World Health Organisation (2023a). *Global leprosy (Hansen disease) update, 2022: new paradigm – control to elimination.* Weekly epidemiological record*,* 15 September 2023, pp. 409-430.

World Health Organisation (2023b). *Global tuberculosis report 2023* [Online]. World Health Organisation. Available at: https://www.who.int/publications/i/item/978924008
3851 [Accessed 19 August 2024].

World Health Organisation (2024a). *Tuberculosis*. [Online]. World Health Organisation. Last updated: 29 October 2024. Available at: https://www.who.int/news-room/fact-sheets/detail/tuberculosis [Accessed 27 December 2024].

World Health Organisation (2024b). *Number of suspected cases of Buruli ulcer reported.* [Online]. World Health Organisation. Last updated: 27 June 2024. https://www.who.int/data/gho/data/indicators/indicator-details/GHO/number-of-new-reported-cases-of-buruli-ulcer [Accessed 13 August 2024].

Xu, J., Koval, A. and Katanaev, V. L. (2023). Clofazimine: A journey of a drug. *Biomedicine & Pharmacotherapy*. 167, 115539. Available at: doi:10.1016/j.biopha.2023.115539.

Yano, T., Kassovska-Bratinova, S., Teh, J. S., Winkler, J., Sullivan, K., Isaacs, A., Schechter, N. M. and Rubin, H. (2011). Reduction of clofazimine by mycobacterial type 2 NADH:quinone oxidoreductase: a pathway for the generation of bactericidal levels of reactive oxygen species. *Journal of Biological Chemistry*. 286 (12), 10276–10287. Available at: doi:10.1074/jbc.M110.200501.

Yates, T. A., Khan, P. Y., Knight, G. M., Taylor, J. G., McHugh, T. D., Lipman, M., White, R. G., Cohen, T., Cobelens, F. G., Wood, R., Moore, D. A. J. and Abubakar, I. (2016). The transmission of *Mycobacterium tuberculosis* in high burden settings. *The Lancet Infectious Diseases*. 16 (2), 227–238. Available at: doi:10.1016/S1473-3099(15)00499-5.

Yip, M. J., Porter, J. L., Fyfe, J. A. M., Lavender, C. J., Portaels, F., Rhodes, M., Kator, H., Colorni, A., Jenkin, G. A. and Stinear, T. (2007). Evolution of *Mycobacterium ulcerans* and other mycolactone-producing mycobacteria from a common *Mycobacterium marinum* progenitor. *Journal of Bacteriology*. 189 (5), 2021–2029. Available at: doi:10.1128/JB.01442-06.

Yotsu, R. R., Suzuki, K., Simmonds, R. E., Bedimo, R., Ablordey, A., Yeboah-Manu, D., Phillips, R. and Asiedu, K. (2018). Buruli ulcer: A review of the current knowledge. *Current Tropical Medicine Reports*. 5 (4), 247–256. Available at: doi:10.1007/s40475-018-0166-2.

Zhang, Y., Lai, Y., Zhou, S., Ran, T., Zhang, Y., Zhao, Z., Feng, Z., Yu, L., Xu, J., Shi, K., Wang, J., Pang, Y., Li, L., Chen, H., Guddat, L. W., Gao, Y., Liu, F., Rao, Z. and Gong, H. (2024). Inhibition of *M. tuberculosis* and human ATP synthase by BDQ and TBAJ-587. *Nature*. 631 (8020), 409–414. Available at: doi:10.1038/s41586-024-07605-8.

Zhang, M., Wang, P., Li, C., Segev, O., Wang, J., Wang, X., Yue, L., Jiang, X., Sheng, Y., Levy, A., Jiang, C. and Chen, F. (2023). Comparative genomic analysis reveals differential genomic characteristics and featured genes between rapid- and slow-growing non-tuberculous mycobacteria. *Frontiers in Microbiology*. 14, 1243371. Available at: doi:10.3389/fmicb.2023.1243371.

Zhang, L., Zhao, Y., Gao, Y., Wu, L., Gao, R., Zhang, Q., Wang, Y., Wu, C., Wu, F., Gurcha, S. S., Veerapen, N., Batt, S. M., Zhao, W., Qin, L., Yang, X., Wang, M., Zhu, Y., Zhang, B., Bi, L., Zhang, X., Yang, H., Guddat, L. W., Xu, W., Wang, Q., Li, J., Besra, G. S. and Rao, Z. (2020). Structures of cell wall arabinosyltransferases with the anti-tuberculosis drug ethambutol. *Science*. 368 (6496), 1211–1219. Available at: doi:10.1126/science.aba9102.

Zheng, H., Lu, L., Wang, B., Pu, S., Zhang, X., Zhu, G., Shi, W., Zhang, L., Wang, H., Wang, S., Zhao, G. and Zhang, Y. (2008). Genetic Basis of Virulence Attenuation Revealed by Comparative Genomic Analysis of *Mycobacterium tuberculosis* Strain H37Ra *versus* H37Rv. *PLoS One.* 3 (6), e2375. Available at: doi:10.1371/journal.pone.0002375.

Zhou, X., Gao, Y., Wang, W., Yang, X., Yang, X., Liu, F., Tang, Y., Lam, S. M., Shui, G., Yu, L., Tian, C., Guddat, L. W., Wang, Q., Rao, Z. and Gong, H. (2021). Architecture of the mycobacterial succinate dehydrogenase with a membrane-embedded Rieske FeS cluster. *Proceedings of the National Academy of Sciences of the United States of America*. 118 (15), e2022308118. Available at: doi:10.1073/pnas.2022308118.

7. APPENDIX

***Table 1.A**: Complete list of bioenergetic chamber experiments conducted after the protocol of washing cells had been established.*

Exp no.	Organism	Strain	Media	Tween 80 %	Carbon source	OD_{600}	mL of culture taken	Compounds added	Concentrations	Date recorded	Buffer
1	*M. smegmatis*	JR128	7H9	0.05	Glycerol	0.91	5	Trifluoperazine (TFPZ)	20 µM to 80 µM	15/06/2021	20 mM HEPES, 150 mM NaCl
2	*M. smegmatis*	JR128	7H9	0.05	Glycerol	1.62	5	Trifluoperazine	200 µM to 800 µM	15/06/2021	20 mM HEPES, 150 mM NaCl
3	*M. smegmatis*	JR128	7H9	0.05	Glycerol	2.44	5	Trifluoperazine	200 µM to 800 µM	15/06/2021	20 mM HEPES, 150 mM NaCl
4	*M. smegmatis*	JR128	7H9	0.05	Glycerol	2.07	5	Trifluoperazine	200 µM to 800 µM	16/06/2021	20 mM HEPES, 150 mM NaCl
5	*M. smegmatis*	JR128	7H9	0.05	Glycerol	2.31	5	Thioridazine (TRZ)	180 µM to 540 µM	16/06/2021	20 mM HEPES, 150 mM NaCl
6	*M. smegmatis*	JR128	7H9	0.05	Glycerol	unrecorded	5	Thioridazine	720 µM to 1080 µM	16/06/2021	20 mM HEPES, 150 mM NaCl
7	*M. smegmatis*	JR128	7H9	0.05	Glycerol	1.24	5	Rotenone, 3NP, TRZ	1 µM, 1 mM, 360-1080 µM	01/07/2021	20 mM HEPES, 150 mM NaCl
8	*M. smegmatis*	JR128	7H9	0.05	Glycerol	2.26	5	CCCP, TPZ, 3NP	0.04-160 µM, 1080 µM, 1 mM	01/07/2021	20 mM HEPES, 150 mM NaCl
9	*M. smegmatis*	JR128	7H9	0.05	Glycerol	3.26	2.5	Rotenone, NaMal, TRZ	1 µM, 1 mM, 360-1080 µM	01/07/2021	20 mM HEPES, 150 mM NaCl
10	*M. smegmatis*	JR128	7H9	0.05	Glycerol	3.39	2.5	Rotenone, NaMal, TRZ	1 µM, 1 mM, 360-1440 µM	01/07/2021	20 mM HEPES, 150 mM NaCl
11	*M. smegmatis*	JR128	7H9	0.05	Glycerol	1.91	5	DCCD, CCCP	100-500 µM, 25 µM	16/08/2021	20 mM HEPES, 150 mM NaCl
12	*M. smegmatis*	JR128	7H9	0.05	Glycerol	2.52	5	BDQ, CCCP, TRZ	150-1500 nM, 100 µM, 720 µM	16/08/2021	20 mM HEPES, 150 mM NaCl
13	*M. smegmatis*	JR128	7H9	0.05	Glycerol	1.19	5	BDQ, CCCP, TRZ	4.5-885 nM, 10-20 µM, 360 µM	17/08/2021	20 mM HEPES, 150 mM NaCl
14	*M. smegmatis*	JR128	7H9	0.05	Glycerol	1.69	5	N/A: Glycerol only	10 µL of 70% G	17/08/2021	20 mM HEPES, 150 mM NaCl
15	*M. smegmatis*	JR128	7H9	0.05	Glycerol	2.52	5	BDQ, CCCP, TRZ	150-1500 nM, 100 µM, 720 µM	17/08/2021	20 mM HEPES, 150 mM NaCl
16	*M. smegmatis*	JR128	7H9	0.05	Glycerol	1.68	5	FCCP, TRZ	0.5-40 µM, 720 µM	07/09/2021	20 mM HEPES, 150 mM NaCl
17	*M. smegmatis*	JR128	7H9	0.05	Glycerol	2.36	5	CFZ, TRZ	0.75-30 µM, 360 µM	07/09/2021	20 mM HEPES, 150 mM NaCl
18	*M. smegmatis*	JR128	7H9	0.05	Glycerol	1.75	5	FCCP, TRZ	5 nM - 20 µM, 360 µM	08/09/2021	20 mM HEPES, 150 mM NaCl
19	*M. smegmatis*	JR128	7H9	0.05	Glycerol	2.3	5	CFZ, TRZ	0.75-273 nM, 360 µM	08/09/2021	20 mM HEPES, 150 mM NaCl
20	*M. smegmatis*	JR128	7H9	0.05	Glycerol	0.9	5	Nigericin, FCCP, TRZ	5 nM - 20 µM, 1 µM, 360 µM	09/09/2021	20 mM HEPES, 150 mM NaCl
21	*M. smegmatis*	JR128	7H9	0.05	Glycerol	1.77	5	Valinomycin, TRZ,Rotenone	5 nM - 100 µM, 360 µM, 2 µM	09/09/2021	20 mM HEPES, 150 mM NaCl
22	*M. smegmatis*	JR128	7H9	0.05	Glycerol	2.62	5	CCCP, TRZ	10 nM - 20 µM, 360 µM	09/09/2021	20 mM HEPES, 150 mM NaCl
23	*M. smegmatis*	JR128	7H9	0.05	Glycerol	1.88	5	Antimycin A, TRZ	1 - 6 µM, 40 - 360 µM	16/09/2021	20 mM HEPES, 150 mM NaCl
24	*M. smegmatis*	JR128	7H9	0.05	Glycerol	2.71	5	BDQ, TRZ	4.5 - 18 nM, 360 µM	16/09/2021	20 mM HEPES, 150 mM NaCl
25	*M. smegmatis*	JR128	7H9	0.05	Glycerol	2.18	5	Valinomycin, K2SO4,TRZ	1 µM, 500 µM, 360 µM	17/09/2021	20 mM HEPES, 150 mM NaCl
26	*M. smegmatis*	JR128	7H9	0.05	Glycerol	1.79	5	BDQ, K2SO4,TRZ	4.5 nM, 500-1000 µM, 360 µM	27/09/2021	20 mM HEPES, 150 mM NaCl
27	*M. smegmatis*	JR128	7H9	0.05	Glycerol	1.23	5	BDQ	30 nM	28/09/2021	20 mM HEPES, 150 mM NaCl
28	*M. smegmatis*	JR128	7H9	0.05	Glycerol	1.99	5	BDQ, TRZ	30 nM, 360-720 µM	28/09/2021	20 mM HEPES, 150 mM NaCl
29	*M. smegmatis*	JR128	7H9	0.05	Glycerol	1.89	5	BDQ, TRZ	30 nM, 360-720 µM	29/09/2021	20 mM HEPES, 150 mM NaCl
30	*M. smegmatis*	JR128	7H9	0.05	Glycerol	2.19	5	Nigericin, TRZ	1 µM, 360-720 µM	29/09/2021	20 mM HEPES, 150 mM NaCl
31	*M. smegmatis*	JR128	7H9	0.05	Glycerol	2.44	5	Valinomycin, TRZ	1 µM, 360-720 µM	29/09/2021	20 mM HEPES, 150 mM NaCl
32	*M. smegmatis*	JR128	7H9	0.05	Glycerol	2.49	5	Gly only	70%, 10 µL	30/09/2021	20 mM HEPES, 150 mM KCl
33	*M. smegmatis*	JR128	7H9	0.05	Glycerol	2.92	5	Nigericin, TRZ	1 µM, 360-720 µM	30/09/2021	20 mM HEPES, 150 mM KCl
34	*M. smegmatis*	JR128	7H9	0.05	Glycerol	1.1	5	BDQ, TRZ	30 nM, 360 µM	01/10/2021	20 mM HEPES, 150 mM KCl
35	*M. smegmatis*	JR128	7H9	0.05	Glycerol	1.96	5	BDQ, TRZ	30 nM, 360 µM	01/10/2021	20 mM HEPES, 150 mM KCl
36	*M. smegmatis*	JR128	7H9	0.05	Glycerol	2.43	5	Valinomycin, TRZ	1-2 µM, 360 µM	01/10/2021	20 mM HEPES, 150 mM KCl
37	*M. smegmatis*	JR128	7H9	0.05	Glycerol	3	5	Valinomycin, TRZ	10 µM, 360 µM	15/10/2021	20 mM HEPES, 150 mM NaCl
38	*M. smegmatis*	JR128	7H9	0.05	Glycerol	2.15	5	Gly and Pi solution	70% 10 µL and 25.9 mM	22/10/2021	20 mM HEPES, 150 mM KCl
39	*M. smegmatis*	JR128	7H9	0.05	Glycerol	2.5	5	Venturicidin, TRZ	2.5-10 µM, 360 µM	22/10/2021	20 mM HEPES, 150 mM KCl
40	*M. smegmatis*	JR128	7H9	0.05	Glycerol	3.15	5	Venturicidin, TRZ	10 µM, 360 µM	22/10/2021	20 mM HEPES, 150 mM NaCl
41	*M. smegmatis*	mc2155	7H9	0.05	Glycerol	2.02	5	Gly, TRZ	10 µL (70%), 360 µM	28/10/2021	20 mM HEPES, 150 mM NaCl
42	*M. smegmatis*	mc2155	7H9	0.05	Glycerol	2.66	5	BDQ, TRZ	30 nM, 360 µM	28/10/2021	20 mM HEPES, 150 mM NaCl
43	*M. smegmatis*	mc2155	7H9	0.05	Glycerol	1.38	5	TRZ	360-720 µM	29/10/2021	20 mM HEPES, 150 mM NaCl, 50 mM Gly
44	*M. smegmatis*	mc2155	7H9	0.05	Glycerol	2.22	5	BDQ, TRZ	30 nM, 360µM	29/10/2021	20 mM HEPES, 150 mM NaCl, 50 mM Gly
45	*M. smegmatis*	mc2155	7H9	0.05	Glycerol	2.51	5	BDQ, TRZ	30-1500 nM, 360 µM	29/10/2021	20 mM HEPES, 150 mM NaCl, 50 mM Gly
46	*M. smegmatis*	mc2155	7H9	0.05	Glycerol	1.36	5	Gly, TRZ	10 µL (70%), 360 µM	01/11/2021	20 mM HEPES, 150 mM KCl
47	*M. smegmatis*	mc2155	7H9	0.05	Glycerol	1.95	5	BDQ, TRZ	30 nM, 360-720 µM	01/11/2021	20 mM HEPES, 150 mM KCl
48	*M. smegmatis*	mc2155	7H9	0.05	Glycerol	2.4	5	HQNO, TRZ	10-200 µM, 360-720 µM	01/11/2021	20 mM HEPES, 150 mM KCl
49	*M. smegmatis*	mc2155	7H9	0.05	Glycerol	2.52	5	TRZ	360-720 µM	04/11/2021	20 mM HEPES, 150 mM KCl, 50 mM Gly
50	*M. smegmatis*	mc2155	7H9	0.05	Glycerol	3.04	5	BDQ, TRZ	30 nM, 360-720 µM	04/11/2021	20 mM HEPES, 150 mM KCl, 50 mM Gly

51	*M. smegmatis*	mc2155	7H9	0.05	Glycerol	3.61	5	BDQ, TRZ	30-1500 nM, 360-720 µM	04/11/2021	20 mM HEPES, 150 mM KCl, 50 mM Gly
52	*M. smegmatis*	mc2155	7H9	0.05	Glycerol	1.48	5	BDQ, TRZ	30 nM, 360-720 µM	05/11/2021	20 mM HEPES, 150 mM KCl, 50 mM Gly
53	*M. smegmatis*	mc2155	7H9	0.05	Glycerol	2.31	5	Venturicidin, TRZ	10 µM, 360 µM	05/11/2021	20 mM HEPES, 150 mM KCl, 50 mM Gly
54	*M. smegmatis*	mc2155	7H9	0.05	Glycerol	3.05	2.5	BDQ, TRZ	30 nM, 360-720 µM	05/11/2021	20 mM HEPES, 150 mM KCl, 50 mM Gly
55	*M. smegmatis*	mc2155	7H9	0.05	Glycerol	2.21	5	Venturicidin, TRZ	10 µM, 360-720 µM	19/11/2021	20 mM HEPES, 150 mM NaCl, 50 mM Gly
56	*M. smegmatis*	mc2155	7H9	0.05	Glycerol	1.82	5	DCCD, TRZ	1-100 µM, 360-720 µM	19/11/2021	20 mM HEPES, 150 mM NaCl, 50 mM Gly
57	*M. smegmatis*	mc2155	7H9	0.05	Glycerol	2.49	5	FCCP, TRZ	1-5 µM, 360-720 µM	24/11/2021	20 mM HEPES, 150 mM NaCl, 50 mM Gly
58	*M. smegmatis*	mc2155	7H9	0.05	Glycerol	2.54	5	FCCP, TRZ	1-5 µM, 360-720 µM	25/11/2021	20 mM HEPES, 150 mM KCl, 50 mM Gly
59	*M. smegmatis*	mc2155	7H9	0.05	Glycerol	2.19	5	BDQ, TRZ	30-1500 nM, 360-720 µM	26/11/2021	20 mM HEPES, 150 mM KCl, 50 mM Gly
60	*M. smegmatis*	mc2155	7H9	0.05	Glycerol	2.3	5	BDQ, TRZ	30-1500 nM, 360-720 µM	26/11/2021	20 mM HEPES, 150 mM NaCl, 50 mM Gly
61	*M. smegmatis*	mc2155	7H9	0.05	Glycerol	2.84	5	FCCP	1 µM	02/12/2021	7H9 Mimic pH = 7.40, 50 mM Gly, no Fe or Cu
62	*M. smegmatis*	mc2155	7H9	0.05	Glycerol	1.47	5	FCCP	1 µM	06/12/2021	7H9 Mimic pH = 7.40, 50 mM Gly, no Fe or Cu
63	*M. smegmatis*	mc2155	7H9	0.05	Glycerol	1.44	5	FCCP, TRZ	1-5 µM, 360-720 µM	06/12/2021	7H9 Mimic pH = 7.40, 50 mM Gly, no Fe or Cu
64	*M. smegmatis*	mc2155	7H9	0.05	Glycerol	1.58	5	BDQ, TRZ	30-1500 nM, 360-720 µM	06/12/2021	7H9 Mimic pH = 7.40, 50 mM Gly, no Fe or Cu
65	*M. smegmatis*	mc2155	7H9	0.05	Glycerol	1.81	5	Venturicidin, TRZ	10 µM, 360 µM	07/12/2021	7H9 Mimic pH = 7.40, 50 mM Gly, no Fe or Cu
66	*M. smegmatis*	mc2155	7H9	0.05	Glycerol	1.44	5	Venturicidin, TRZ	10 µM, 360-720 µM	07/12/2021	7H9 Mimic pH = 7.40, 50 mM Gly, no Fe or Cu
67	*M. smegmatis*	mc2155	7H9	0.05	Glycerol	1.44	4	DCCD, TRZ	10 µM, 360-720 µM	08/12/2021	7H9 Mimic pH = 7.40, 50 mM Gly, no Fe or Cu
68	*M. smegmatis*	mc2155	7H9	0.05	Glycerol	2.07	4	EtOH, TRZ	10 µL, 360-720 µM	08/12/2021	7H9 Mimic pH = 7.40, 50 mM Gly, no Fe or Cu
69	*M. smegmatis*	mc2155	7H9	0.05	Glycerol	1.16	5	EtOH	10 µL	18/01/2022	7H9 Mimic pH = 7.40, 50 mM Gly, no Fe or Cu
70	**N/A buffer only**						5	EtOH	10 µL	18/01/2022	7H9 Mimic pH = 7.40, 50 mM Gly, no Fe or Cu
71	*M. smegmatis*	mc2155	7H9	0.05	Glycerol	unrecorded	5	EtOH	10 µL	18/01/2022	Cells taken direct from culture
72	*M. smegmatis*	mc2155	7H9	0.05	Glycerol	unrecorded	5	EtOH	10 µL	18/01/2022	7H9 Mimic pH = 7.40, 50 mM Gly, no Fe or Cu
73	*M. smegmatis*	mc2155	7H9	0.05	Glycerol	unrecorded	5	EtOH	10 µL	18/01/2022	7H9 Mimic pH = 7.40, 50 mM Gly, no Fe or Cu
74	*M. smegmatis*	mc2155	7H9	0.05	Glycerol	1.41	5	TRZ	360-720 µM	19/01/2022	7H9 Mimic pH = 7.40, 50 mM Gly, no Fe or Cu
75	*M. smegmatis*	mc2155	7H9	0.05	Glycerol	1.1	5	DMSO, TRZ	10-20 µL, 360-720 µM	19/01/2022	7H9 Mimic pH = 7.40, 50 mM Gly, no Fe or Cu
76	*M. smegmatis*	mc2155	7H9	0.05	Glycerol	1.29	5	TRZ	360-720 µM	20/01/2022	7H9 Mimic pH = 7.40, 50 mM Gly
77	*M. smegmatis*	mc2155	7H9	0.05	Glycerol	1.34	5	TRZ	360-720 µM	20/01/2022	7H9 Mimic pH = 7.40, 50 mM Gly, no Fe or Cu
78	*M. smegmatis*	mc2155	7H9	0.05	Glycerol	1.14	5	EtOH, TRZ	10-20 µL, 360-720 µM	20/01/2022	7H9 Mimic pH = 7.40, 50 mM Gly, no Fe or Cu
79	*M. smegmatis*	mc2155	7H9	0.05	Glycerol	1	5	EtOH, TRZ	10-30 µL, 360-720 µM	24/01/2022	7H9 Mimic pH = 7.40, 50 mM Gly
80	*M. smegmatis*	mc2155	7H9	0.05	Glycerol	1.14	5	BDQ in EtOH, TRZ	30-1500 nM, 360-720 µM	24/01/2022	7H9 Mimic pH = 7.40, 50 mM Gly
81	*M. smegmatis*	mc2155	7H9	0.05	Glycerol	1.14	5	BDQ in DMSO, TRZ	30-1500 nM, 360-720 µM	24/01/2022	7H9 Mimic pH = 7.40, 50 mM Gly
82	*M. smegmatis*	mc2155	7H9	0.05	Glycerol	1.61	5	DCCD in EtOH, TRZ	10-50 µM, 360-720 µM	25/01/2022	7H9 Mimic pH = 7.40, 50 mM Gly
83	*M. smegmatis*	mc2155	7H9	0.05	Glycerol	1.51	5	DCCD in DMSO, TRZ	10-50 µM, 360-720 µM	25/01/2022	7H9 Mimic pH = 7.40, 50 mM Gly
84	*M. smegmatis*	mc2155	7H9	0.05	Glycerol	1.46	5	FCCP, TRZ	1-5 µM, 360-720 µM	25/01/2022	7H9 Mimic pH = 7.40, 50 mM Gly
85	*M. smegmatis*	mc2155	7H9	0.05	Glycerol	1.54	5	BDQ, TRZ	1.5-3 µM, 360-720 µM	28/01/2022	Cells taken direct from culture
86	*M. smegmatis*	mc2155	7H9	0.05	Glycerol	1.55	5	BDQ, TRZ	30-2400 nM, 360-720 µM	28/01/2022	Cells taken direct from culture
87	*M. smegmatis*	mc2155	7H9	0.05	Glycerol	1.27	5	FCCP, TRZ	1-5 µM, 360-720 µM	02/02/2022	7H9 Mimic pH = 6.60, 50 mM Gly
88	*M. smegmatis*	mc2155	7H9	0.05	Glycerol	1.36	5	TRZ	360-720 µM	02/02/2022	7H9 Mimic pH = 6.60, 50 mM Gly
89	*M. smegmatis*	mc2155	7H9	0.05	Glycerol	1.6	5	BDQ in EtOH, TRZ	30-1500 nM, 360-720 µM	02/02/2022	7H9 Mimic pH = 6.60, 50 mM Gly
90	*M. smegmatis*	mc2155	7H9	0.05	Glycerol	1.07	5	Venturicidin, TRZ	10 µM, 360-720 µM	03/02/2022	7H9 Mimic pH = 6.60, 50 mM Gly
91	*M. smegmatis*	mc2155	7H9	0.05	Glycerol	1.25	5	EtOH, TRZ	10-20 µL, 360-720 µM	03/02/2022	7H9 Mimic pH = 6.60, 50 mM Gly
92	*M. smegmatis*	mc2155	7H9	0.05	Glycerol	0.96	5	DCCD, TRZ	10-50 µM, 360-720 µM	03/02/2022	7H9 Mimic pH = 6.60, 50 mM Gly
93	*M. smegmatis*	mc2155	7H9	0.05	Glucose	1.41	5	TRZ	360-720 µM	07/04/2022	7H9 Mimic pH = 6.60, 50 mM Gly
94	*M. smegmatis*	mc2155	7H9	0.05	Glucose	1.42	5	FCCP, TRZ	1-5 µM, 360-720 µM	07/04/2022	7H9 Mimic pH = 6.60, 50 mM Gly
95	*M. smegmatis*	mc2155	7H9	0.05	Glucose	1.45	5	BDQ in EtOH, TRZ	30-1500 nM, 360-720 µM	07/04/2022	7H9 Mimic pH = 6.60, 50 mM Gly
96	*M. smegmatis*	mc2155	7H9	0.05	Glucose	1.31	5	DCCD, TRZ	10-50 µM, 360-720 µM	08/04/2022	7H9 Mimic pH = 6.60, 50 mM Gly
97	*M. smegmatis*	mc2155	7H9	0.05	Glucose	1.33	5	EtOH, TRZ	10-20 µL, 360-720 µM	08/04/2022	7H9 Mimic pH = 6.60, 50 mM Gly
98	*M. smegmatis*	mc2155	7H9	0.05	Glucose	1	5	Venturicidin, TRZ	10 µM, 360-720 µM	08/04/2022	7H9 Mimic pH = 6.60, 50 mM Gly
99	*M. smegmatis*	mc2155	7H9	0.05	Glycerol	1.61	5	BDQ in EtOH, TRZ	30-1500 nM, 360-720 µM	13/04/2022	7H9 (Sigma) pH = 6.60, 50 mM Gly
100	*M. smegmatis*	mc2155	7H9	0.05	Glycerol	1.09	5	BDQ in EtOH, TRZ	30-1500 nM, 360-720 µM	13/04/2022	7H9 Mimic pH = 6.60, 50 mM Gly
101	*M. smegmatis*	mc2155	7H9	0.05	Glycerol	1.12	5	FCCP, TRZ	1-5 µM, 360-720 µM	14/04/2022	7H9 (Sigma) pH = 6.60, 50 mM Gly
102	*M. smegmatis*	mc2155	7H9	0.05	Glycerol	1.04	5	DCCD, TRZ	10-50 µM, 360-720 µM	14/04/2022	7H9 (Sigma) pH = 6.60, 50 mM Gly
103	*M. smegmatis*	mc2155	7H9	0.05	Glycerol	1.03	5	TRZ	360-720 µM	14/04/2022	7H9 (Sigma) pH = 6.60, 50 mM Gly
104	*M. smegmatis*	mc2155	7H9	0.05	Glycerol	1.41	5	EtOH, TRZ	10-20 µL, 360-720 µM	22/04/2022	7H9 (Sigma) pH = 6.60, 50 mM Gly
105	*M. smegmatis*	mc2155	7H9	0.05	Glycerol	1.55	5	EtOH, TRZ	10-20 µL, 360-720 µM	22/04/2022	7H9 (Sigma) pH = 6.60, 50 mM Gly
106	*M. smegmatis*	mc2155	7H9	0.05	Glycerol	1.32	5	Venturicidin, TRZ	10 µM, 360-720 µM	29/04/2022	7H9 (Sigma) pH = 6.60, 50 mM Gly
107	*M. smegmatis*	mc2155	7H9	0.05	Glycerol	1.17	5	BAM15, TRZ	1 nM - 15 µM, 360-720 µM	29/04/2022	7H9 (Sigma) pH = 6.60, 50 mM Gly
108	*M. smegmatis*	mc2155	7H9	0.05	Glycerol	1.5	5	BAM15, TRZ	1-15 µM, 360-720 µM	05/05/2022	7H9 (Sigma) pH = 6.60, 50 mM Gly
109	*M. smegmatis*	mc2155	7H9	0.05	Glycerol	2.1	5	Nigericin, TRZ	1-5 µM, 360-720 µM	05/05/2022	7H9 (Sigma) pH = 6.60, 50 mM Gly

110	*M. smegmatis*	ΔcydABAB	7H9	0.05	Glycerol		1.4	5	BDQ in EtOH, TRZ	30-1500 nM, 360-720 µM	12/05/2022	7H9 (Sigma) pH = 6.60, 50 mM Gly
111	*M. smegmatis*	ΔcydABAB	7H9	0.05	Glycerol		1.7	5	Venturicidin, TRZ	10 µM, 360-720 µM	12/05/2022	7H9 (Sigma) pH = 6.60, 50 mM Gly
112	*M. smegmatis*	ΔcydABAB	7H9	0.05	Glycerol		1.3	5	EtOH, TRZ	10-20 µL, 360-720 µM	13/05/2022	7H9 (Sigma) pH = 6.60, 50 mM Gly
113	*M. smegmatis*	ΔcydABAB	7H9	0.05	Glycerol		1.4	5	BAM15, TRZ	10 µM, 360-720 µM	13/05/2022	7H9 (Sigma) pH = 6.60, 50 mM Gly
114	*M. smegmatis*	ΔcydABAB	7H9	0.05	Glycerol		1.1	5	BDQ in EtOH, TRZ	30-1500 nM, 360-720 µM	13/05/2022	7H9 (Sigma) pH = 6.60, 50 mM Gly
115	*M. smegmatis*	ΔcydABAB	7H9	0.05	Glycerol		1.6	5	TRZ	360-720 µM	17/05/2022	7H9 (Sigma) pH = 6.60, 50 mM Gly
116	*M. smegmatis*	ΔcydABAB	7H9	0.05	Glycerol		1.12	5	DCCD, TRZ	10-50 µM, 360-720 µM	17/05/2022	7H9 (Sigma) pH = 6.60, 50 mM Gly
117	*M. smegmatis*	ΔcydABAB	7H9	0.05	Glycerol		1.01	5	Nigericin, TRZ	1-5 µM, 360-720 µM	17/05/2022	7H9 (Sigma) pH = 6.60, 50 mM Gly
118	*M. smegmatis*	mc2155	7H9	0.05	Glycerol		0.88	5	Valinomycin, TRZ	1-30 µM, 360-720 µM	18/05/2022	7H9 (Sigma) pH = 6.60, 50 mM Gly
119	*M. smegmatis*	ΔcydABAB	7H9	0.05	Glycerol		0.74	5	DCCD, TRZ	10-50 µM, 360-720 µM	18/05/2022	7H9 (Sigma) pH = 6.60, 50 mM Gly
120	*M. smegmatis*	ΔcydABAB	7H9	0.05	Glycerol		1.16	5	Venturicidin, TRZ	10 µM, 360-720 µM	18/05/2022	7H9 (Sigma) pH = 6.60, 50 mM Gly
121	*M. smegmatis*	mc2155	LB	0.05 % Tyloxapol	D-arabinose		0.65	5	TRZ	360-720 µM	19/08/2022	LB, pH = 7.20, 5 mM D-arabinose
122	*M. smegmatis*	mc2155	LB	0.05 % Tyloxapol	D-arabinose		0.88	5	EtOH, TRZ	10-20 µL, 360-720 µM	19/08/2022	LB, pH = 7.20, 5 mM D-arabinose
123	*M. smegmatis*	mc2155	LB	0.05 % Tyloxapol	D-arabinose		1.08	5	BDQ in EtOH, TRZ	30-1500 nM, 360-720 µM	22/08/2022	LB, pH = 7.20, 5 mM D-arabinose
124	*M. smegmatis*	mc2155	LB	0.05 % Tyloxapol	D-arabinose		1.17	5	BAM15, TRZ	10 µM, 360-720 µM	22/08/2022	LB, pH = 7.20, 5 mM D-arabinose
125	*M. smegmatis*	mc2155	LB	0.05 % Tyloxapol	D-arabinose	N/A		5	BDQ in EtOH	30-1500 nM	22/08/2022	7H9 (Sigma) pH = 6.60, 50 mM Gly
126	*M. smegmatis*	AtpED32V	LB	0.05 % Tyloxapol	D-arabinose		1.32	5	BDQ in EtOH, TRZ	30-1500 nM, 360-720 µM	23/08/2022	LB, pH = 7.20, 5 mM D-arabinose
127	*M. smegmatis*	AtpED32V	LB	0.05 % Tyloxapol	D-arabinose		1.5	5	TRZ	360-720 µM	23/08/2022	LB, pH = 7.20, 5 mM D-arabinose
128	*M. smegmatis*	AtpED32V	LB	0.05 % Tyloxapol	D-arabinose		1.41	5	BAM15, TRZ	10 µM, 360-720 µM	23/08/2022	LB, pH = 7.20, 5 mM D-arabinose
129	*M. smegmatis*	mc2155	LB	0.05 % Tyloxapol	D-arabinose		1.12	5	Venturicidin, TRZ	10 µM, 360-720 µM	24/08/2022	LB, pH = 7.20, 5 mM D-arabinose
130	*M. smegmatis*	mc2155	LB	0.05 % Tyloxapol	D-arabinose		1.11	5	DCCD, TRZ	10-50 µM, 360-720 µM	24/08/2022	LB, pH = 7.20, 5 mM D-arabinose
131	*M. smegmatis*	AtpED32V	LB	0.05 % Tyloxapol	D-arabinose		1.21	5	Venturicidin, TRZ	10 µM, 360-720 µM	25/08/2022	LB, pH = 7.20, 5 mM D-arabinose
132	*M. smegmatis*	AtpED32V	LB	0.05 % Tyloxapol	D-arabinose		1.2	5	DCCD, TRZ	10-50 µM, 360-720 µM	25/08/2022	LB, pH = 7.20, 5 mM D-arabinose
133	*M. smegmatis*	mc2155	7H9	0.05	Glycerol		1.04	5	Oligomycin, TFPZ	1 µM - 20 µM, 360-720 µM	06/10/2022	7H9 (Sigma) pH = 6.60, 50 mM Gly
134	*M. smegmatis*	AtpED32V	7H9	0.05	Glycerol + D-Ara		1.1	5	EtOH, TFPZ	20 µL, 360-720 µM	07/10/2022	7H9 (Sigma) pH = 6.60, 50 mM Gly, 5 mM D-Ara
135	*M. smegmatis*	AtpED32V	7H9	0.05	Glycerol + D-Ara		1.19	5	BDQ, TFPZ	30-1500 nM, 360-720 µM	07/10/2022	7H9 (Sigma) pH = 6.60, 50 mM Gly, 5 mM D-Ara
136	*M. smegmatis*	mc2155	7H9	0.05	Glycerol		0.68	5	Oligomycin, TFPZ	10 µM, 360 µM	10/10/2022	7H9 (Sigma) pH = 6.60, 50 mM Gly
137	*M. smegmatis*	mc2155	7H9	0.05	Glycerol		0.9	5	BAM15, TFPZ	10 µM, 360 µM	10/10/2022	7H9 (Sigma) pH = 6.60, 50 mM Gly
138	*M. smegmatis*	mc2155	7H9	0.05	Glycerol		0.88	5	Piericidin A, TFPZ	1-20 µM, 360 µM	10/10/2022	7H9 (Sigma) pH = 6.60, 50 mM Gly
139	*M. smegmatis*	mc2155	7H9	0.05	Glycerol + D-Ara		0.86	5	BDQ, TFPZ	30-1500 nM, 360 µM	11/10/2022	7H9 (Sigma) pH = 6.60, 50 mM Gly, 5 mM D-Ara
140	*M. smegmatis*	AtpED32V	7H9	0.05	Glycerol + D-Ara		1.11	5	BAM15, TFPZ	10 µM, 360 µM	11/10/2022	7H9 (Sigma) pH = 6.60, 50 mM Gly, 5 mM D-Ara
141	*M. smegmatis*	AtpED32V	7H9	0.05	Glycerol + D-Ara		1.08	5	VTR, TFPZ	10 µM, 360 µM	11/10/2022	7H9 (Sigma) pH = 6.60, 50 mM Gly, 5 mM D-Ara
142	*M. smegmatis*	AtpED32V	7H9	0.05	Glycerol + D-Ara		1.29	5	DCCD, TFPZ	10-50 µM, 360 µM	11/10/2022	7H9 (Sigma) pH = 6.60, 50 mM Gly, 5 mM D-Ara
143	*M. smegmatis*	mc2155	7H9	0.05	Glycerol		1.57	4	BDQ, BAM15, TFPZ	30 nM, 1-10 µM, 360 µM	03/11/2022	7H9 (Sigma) pH = 6.60, 50 mM Gly
144	*M. smegmatis*	mc2155	7H9	0.05	Glycerol		2	4	BDQ, TFPZ	30-1500 nM, 360 µM	04/11/2022	7H9 (Sigma) pH = 6.60, 50 mM Gly
145	*M. smegmatis*	mc2155	7H9	0.05	Glycerol		1.9	5	Nigericin, TFPZ	1-5 µM, 360 µM	04/11/2022	7H9 (Sigma) pH = 6.60, 50 mM Gly
146	*M. smegmatis*	mc2155	7H9	0.05	Glycerol		3	3.3	EtOH, TFPZ	20 µL, 360-720 µM	04/11/2022	7H9 (Sigma) pH = 6.60, 50 mM Gly
147	*M. smegmatis*	mc2155	7H9	0.05	Glycerol		2.3	4	BDQ, TFPZ	30-1500 nM, 360 µM	11/11/2022	7H9 (Sigma) pH = 6.60, 50 mM Gly
148	*M. smegmatis*	mc2155	7H9	0.05	Glycerol		2.2	4	DCCD, TFPZ	10-50 µM, 360 µM	11/11/2022	7H9 (Sigma) pH = 6.60, 50 mM Gly
149	*M. smegmatis*	mc2155	7H9	0.05	Glycerol		3.2	3.3	TFPZ	360 µM	11/11/2022	7H9 (Sigma) pH = 6.60, 50 mM Gly
150	*M. smegmatis*	ΔcydABAB	7H9	0.05	Glycerol		2.1	5	BAM15, TFPZ	10 µM, 360 µM	17/11/2022	7H9 (Sigma) pH = 6.60, 50 mM Gly

151	*M. smegmatis*	ΔcydABAB	7H9		0.05	Glycerol		1.6	5	BDQ, BAM15, TFPZ	30 nM, 1-10 µM, 360 µM	17/11/2022	7H9 (Sigma) pH = 6.60, 50 mM Gly
152	*M. smegmatis*	ΔcydABAB	7H9		0.05	Glycerol		1.2	5	EtOH, TFPZ	20 µL, 360-720 µM	17/11/2022	7H9 (Sigma) pH = 6.60, 50 mM Gly
153	*M. smegmatis*	ΔcydABAB	7H9		0.05	Glycerol		1.9	5	Valinomycin, TFPZ	1-30 µM, 360-720 µM	18/11/2022	7H9 (Sigma) pH = 6.60, 50 mM Gly
154	*M. smegmatis*	ΔcydABAB	7H9		0.05	Glycerol		1.6	5	Nigericin, TFPZ	1-5 µM, 360 µM	18/11/2022	7H9 (Sigma) pH = 6.60, 50 mM Gly
155	*M. smegmatis*	ΔcydABAB	7H9		0.05	Glycerol		2.3	5	TFPZ	360 µM	18/11/2022	7H9 (Sigma) pH = 6.60, 50 mM Gly
156	*M. smegmatis*	mc2155	7H9		0.05	Glycerol		1.1	5	CHQAD	0.1-32.8 µM	18/01/2023	7H9 (Sigma) pH = 6.60, 50 mM Gly
157	*M. tuberculosis*	mc26206	7H9 + L + P + OADC		0.05	Glycerol		0.38	10	BAM15	10 µM	03/02/2023	7H9 (Sigma) pH = 6.60, 50 mM Gly, L, P
158	*M. tuberculosis*	mc26206	7H9 + L + P + OADC		0.05	Glycerol		3.18	5	TFPZ	360 µM	10/02/2023	7H9 (Sigma) pH = 6.60, 50 mM Gly, L, P
159	*M. tuberculosis*	mc26206	7H9 + L + P + OADC		0.05	Glycerol		3.18	5	BDQ	30-1500 nM	10/02/2023	7H9 (Sigma) pH = 6.60, 50 mM Gly, L, P
160	*M. tuberculosis*	mc26206	7H9 + L + P + OADC		0.05	Glycerol		4.35	5	CHQAD	0.4-2 µM	13/02/2023	7H9 (Sigma) pH = 6.60, 50 mM Gly, L, P
161	*M. tuberculosis*	mc26206	7H9 + L + P + OADC		0.05	Glycerol		4.35	5	CHQAD	2-12 µM	13/02/2023	7H9 (Sigma) pH = 6.60, 50 mM Gly, L, P
162	*M. tuberculosis*	mc26206	7H9 + L + P + OADC		0.05	Glycerol		1.11	14	CHQAD, 3NP, TFPZ	2-12 µM, 50 µM, 360 µM	20/02/2023	7H9 (Sigma) pH = 6.60, 50 mM Gly, L, P
163	*M. tuberculosis*	mc26206	7H9 + L + P + OADC		0.05	Glycerol		1.11	14	70% Gly	10 µL	20/02/2023	7H9 (Sigma) pH = 6.60, L, P
164	*M. tuberculosis*	mc26206	7H9 + L + P + OADC		0.05	Glycerol		1.11	14	70% Gly	10 µL	20/02/2023	7H9 (Sigma) pH = 6.60, L, P
165	*M. tuberculosis*	mc26206	7H9 + L + P + OADC		0.05	Glycerol		0.77	20	70% Gly, BAM15, Na2S2O4	10 µL, 10 µM	24/02/2023	7H9 (Sigma) pH = 6.60, L, P
166	*M. tuberculosis*	mc26206	7H9 + L + P + OADC		0.05	Glycerol		0.82	20	70% Gly, BAM15, Na2S2O4	10 µL, 10 µM	24/02/2023	7H9 (Sigma) pH = 6.60, L, P
167	*M. tuberculosis*	mc26206	7H9 + L + P + OADC		0.05	Glycerol		1.78	20	70% Gly, BDQ	10 µL, 30-1480 nM	27/02/2023	7H9 (Sigma) pH = 6.60, L, P
168	*M. tuberculosis*	mc26206	7H9 + L + P + OADC		0.05	Glycerol		0.77	30	BDQ, TFPZ	30-1500 nM, 360-720 µM	10/03/2023	7H9 (Sigma) pH = 6.60, L, P, 0.4% Gly
169	*M. tuberculosis*	mc26206	7H9 + L + P + OADC		0.05	Glycerol		0.77	30	BAM15, TFPZ	1-20 µM, 360-720 µM	10/03/2023	7H9 (Sigma) pH = 6.60, L, P, 0.4% Gly
170	*M. tuberculosis*	mc26206	7H9 + L + P + OADC		0.05	Glycerol		0.7	30	Nigericin, TFPZ	1-5 µM, 360 µM	16/03/2023	7H9 (Sigma) pH = 6.60, L, P, 0.4% Gly
171	*M. tuberculosis*	mc26206	7H9 + L + P + OADC		0.05	Glycerol		0.88	30	DCCD, TFPZ	10-50 µM, 360 µM	17/03/2023	7H9 (Sigma) pH = 6.60, L, P, 0.4% Gly
172	*M. tuberculosis*	mc26206	7H9 + L + P + OADC		0.05	Glycerol		0.68	30	EtOH, TFPZ	10-20 µL, 360 µM	24/03/2023	7H9 (Sigma) pH = 6.60, L, P, 0.4% Gly
173	*M. smegmatis*	ΔcydABAB	7H9		0.05	Glycerol		1.2	5	BDQ, TFPZ	30-1500 nM, 360 µM	28/03/2023	7H9 (Sigma) pH = 6.60, 50 mM Gly
174	*M. smegmatis*	ΔcydABAB	7H9		0.05	Glycerol		1	5	BAM15, TFPZ	10 µM, 360 µM	28/03/2023	7H9 (Sigma) pH = 6.60, 50 mM Gly
175	*M. smegmatis*	ΔcydABAB	7H9		0.05	Glycerol		1.5	5	EtOH, TFPZ	10-20 µL, 360 µM	28/03/2023	7H9 (Sigma) pH = 6.60, 50 mM Gly
176	*M. smegmatis*	ΔcydABAB	7H9		0.05	Glycerol		0.8	5	DCCD, TFPZ	10-50 µM, 360 µM	29/03/2023	7H9 (Sigma) pH = 6.60, 50 mM Gly
177	*M. smegmatis*	ΔcydABAB	7H9		0.05	Glycerol		1.2	5	Nigericin, TFPZ	1-5 µM, 360 µM	29/03/2023	7H9 (Sigma) pH = 6.60, 50 mM Gly
178	*M. smegmatis*	mc2155	7H9		0.05	Glycerol		1.9	5	BDQ, TFPZ	30-1500 nM, 360 µM	14/04/2023	7H9 (Sigma) pH = 6.60, 50 mM Gly
179	*M. smegmatis*	mc2155	7H9		0.05	Glycerol		2.5	5	BDQ, TFPZ	30-1500 nM, 360 µM	14/04/2023	7H9 (Sigma) pH = 6.60, 50 mM Gly
180	*M. smegmatis*	mc2155	7H9		0.05	Glycerol		1.5	5	BDQ, TFPZ	30-1500 nM, 360 µM	18/04/2023	7H9 (Sigma) pH = 6.60, 50 mM Gly, 6.5 mM K2SO4
181	*M. smegmatis*	mc2155	7H9		0.05	Glycerol		1	5	EtOH, TFPZ	10-20 µL, 360 µM	18/04/2023	7H9 (Sigma) pH = 6.60, 50 mM Gly, 6.5 mM K2SO4
182	*M. smegmatis*	mc2155	7H9		0.05	Glycerol		1.6	5	Nigericin, TFPZ	1-5 µM, 360 µM	18/04/2023	7H9 (Sigma) pH = 6.60, 50 mM Gly, 6.5 mM K2SO4
183	*M. smegmatis*	mc2155	7H9		0.05	Glycerol		1.8	5	BDQ, TFPZ	30-1500 nM, 360 µM	21/04/2023	7H9 (Sigma) pH = 6.60, 50 mM Gly, 16.5 mM K2SO4
184	*M. smegmatis*	mc2155	7H9		0.05	Glycerol		2.2	4	EtOH, TFPZ	10-20 µL, 360 µM	21/04/2023	7H9 (Sigma) pH = 6.60, 50 mM Gly, 16.5 mM K2SO4
185	*M. smegmatis*	mc2155	7H9		0.05	Glycerol		2.1	5	Nigericin, TFPZ	1-5 µM, 360 µM	21/04/2023	7H9 (Sigma) pH = 6.60, 50 mM Gly, 16.5 mM K2SO4
186	*M. tuberculosis*	mc26206	7H9 + L + P + OADC		0.05	Glycerol		0.65	30	Valinomycin, TFPZ	10-60 µM, 360 µM	25/04/2023	7H9 (Sigma) pH = 6.60, L, P, 0.4% Gly
187	*M. smegmatis*	mc2155	7H9		0.05	Glycerol		1.3	5	BDQ, TFPZ	30-1500 nM, 360 µM	26/04/2023	7H9 (Sigma) pH = 6.60, 50 mM Gly, 36.5 mM K2SO4
188	*M. smegmatis*	mc2155	7H9		0.05	Glycerol		1.3	5	Nigericin, TFPZ	1-5 µM, 360 µM	26/04/2023	7H9 (Sigma) pH = 6.60, 50 mM Gly, 36.5 mM K2SO4
189	*M. smegmatis*	mc2155	7H9		0.05	Glycerol		1.9	4	BDQ, K2SO4, TFPZ	1500 nM, 2-16 mM,360 µM	09/05/2023	7H9 (Sigma) pH = 6.60, 50 mM Gly
190	*M. smegmatis*	mc2155	7H9		0.05	Glycerol		1.9	4	BDQ, Na2SO4, Nigericin, TFPZ	1500 nM, 4-32 mM, 1 µM, 360 µ	09/05/2023	7H9 (Sigma) pH = 6.60, 50 mM Gly
191	*M. smegmatis*	mc2155	7H9		0.05	Glycerol		1.1	5	Na2SO4, Nigericin,TFPZ	4-32 mM, 1 µM, 360 µM	09/05/2023	7H9 (Sigma) pH = 6.60, 50 mM Gly
192	*M. smegmatis*	mc2155	7H9		0.05	Glycerol	N/A		5	BDQ, Nigericin,TFPZ	30 nM, 1 µM, 360 µM	09/05/2023	7H9 (Sigma) pH = 6.60, 50 mM Gly
193	*M. tuberculosis*	mc26206	7H9 + L + P + OADC		0.05	Glycerol		0.62	80	TFPZ	360-720 µM	10/05/2023	7H9 (Sigma) pH = 6.60, L, P, 0.4% Gly
194	*M. smegmatis*	mc2155	7H9		0.05	Glycerol		1.3	5	BDQ, BAM15,TFPZ	1.5 µM, 10 µM, 360 µM	12/05/2023	7H9 (Sigma) pH = 6.60, 50 mM Gly
195	*M. smegmatis*	mc2155	7H9		0.05	Glycerol		1.4	5	BDQ, K2SO4, TFPZ	1500 nM, 2-16 mM,360 µM	12/05/2023	7H9 (Sigma) pH = 6.60, 50 mM Gly
196	*M. smegmatis*	mc2155	7H9		0.05	Glycerol		1.9	4	BDQ in DMSO, TFPZ	10 µM, 384 µM	27/05/2023	7H9 (Sigma) pH = 6.60, 50 mM Gly
197	*M. smegmatis*	ΔcydABAB	7H9		0.05	Glycerol		0.6	10	BDQ in DMSO, TFPZ	10 µM, 360 µM	27/05/2023	7H9 (Sigma) pH = 6.60, 50 mM Gly
198	*M. smegmatis*	ΔcydABAB	7H9		0.05	Glycerol		0.8	5	BDQ, TFPZ	1.5 µM, 360 µM	27/05/2023	7H9 (Sigma) pH = 6.60, 50 mM Gly
199	*M. tuberculosis*	mc26206	7H9 + L + P + OADC		0.05	Glycerol		0.84	30	BDQ, BAM15, TFPZ	120 nM, 5-20 µM, 360-720 µM	31/05/2023	7H9 (Sigma) pH = 6.60, L, P, 0.4% Gly
200	*M. tuberculosis*	mc26206	7H9 + L + P + OADC		0.05	Glycerol		0.84	30	BDQ in DMSO, TFPZ	10 µM, 360 µM	31/05/2023	7H9 (Sigma) pH = 6.60, L, P, 0.4% Gly

201	*M. smegmatis*	AtpED32V	7H9	0.05	Glycerol + D-Ara	1.8	4	BDQ, TFPZ	30-1500 nM, 360 µM	01/06/2023	7H9 (Sigma) pH = 6.60, 50 mM Gly, 5 mM D-Ara
202	*M. smegmatis*	AtpED32V	7H9	0.05	Glycerol + D-Ara	2.3	3	BDQ, TFPZ	30-1500 nM, 360 µM	01/06/2023	7H9 (Sigma) pH = 6.60, 50 mM Gly, 5 mM D-Ara
203	*M. smegmatis*	mc2155	7H9	0.05	Glycerol	1.8	4	BDQ, TFPZ, Na2S2O4	30-1500 nM, 360 µM	07/06/2023	7H9 (Sigma) pH = 6.60, 50 mM Gly
204	*M. smegmatis*	ΔcydABAB	7H9	0.05	Glycerol	0.9	5	BDQ, TFPZ, Na2S2O4	30-1500 nM, 360 µM	07/06/2023	7H9 (Sigma) pH = 6.60, 50 mM Gly
205	*M. smegmatis*	ΔcydABAB	7H9	0.05	Glycerol	1.3	5	BDQ, TFPZ, Na2S2O4	30-1500 nM, 360 µM	07/06/2023	7H9 (Sigma) pH = 6.60, 50 mM Gly
206	*M. smegmatis*	ΔcydABAB	7H9	0.05	Glycerol	1.1	5	FCCP, TFPZ, Na2S2O4	1-31 µM, 360 µM	13/06/2023	7H9 (Sigma) pH = 6.60, 50 mM Gly
207	*M. smegmatis*	ΔcydABAB	7H9	0.05	Glycerol	0.9	5	CCCP, TFPZ, Na2S2O4	1-31 µM, 360-720 µM	13/06/2023	7H9 (Sigma) pH = 6.60, 50 mM Gly
208	*M. smegmatis*	ΔcydABAB	7H9	0.05	Glycerol	1.5	5	CCCP, TFPZ, Na2S2O4	1-25 µM, 360 µM	13/06/2023	7H9 (Sigma) pH = 6.60, 50 mM Gly
209	*M. smegmatis*	mc2155	7H9	0.05	Glycerol	3.4	4	TRZ	360 µM	22/06/2023	7H9 (Sigma) pH = 6.60, 50 mM Gly
210	*M. smegmatis*	mc2155	7H9	0.05	Glycerol	2.2	4	CCCP, TFPZ, Na2S2O4	1-25 µM, 360 µM	22/06/2023	7H9 (Sigma) pH = 6.60, 50 mM Gly
211	*M. smegmatis*	mc2155	7H9	0.05	Glycerol	3	3	FCCP, TFPZ, Na2S2O4	1-25 µM, 360 µM	22/06/2023	7H9 (Sigma) pH = 6.60, 50 mM Gly
212	*M. smegmatis*	mc2155	7H9	0.05	Glycerol	2.6	3	CCCP, TRZ, Na2S2O4	1-25 µM, 360 µM	27/06/2023	7H9 (Sigma) pH = 6.60, 50 mM Gly
213	*M. smegmatis*	mc2155	7H9	0.05	Glycerol	2.4	3.5	FCCP, TRZ, Na2S2O4	1-25 µM, 360 µM	27/06/2023	7H9 (Sigma) pH = 6.60, 50 mM Gly
214	*M. smegmatis*	mc2155	7H9	0.05	Glycerol	1.8	4.5	BAM15, TRZ, Na2S2O4	1-25 µM, 360 µM	27/06/2023	7H9 (Sigma) pH = 6.60, 50 mM Gly
215	*M. smegmatis*	ΔcydABAB	7H9	0.05	Glycerol	2.5	3.25	CCCP, TRZ, Na2S2O4	1-25 µM, 360 µM	29/06/2023	7H9 (Sigma) pH = 6.60, 50 mM Gly
216	*M. smegmatis*	ΔcydABAB	7H9	0.05	Glycerol	1.9	4.25	FCCP, TRZ, Na2S2O4	1-25 µM, 360 µM	29/06/2023	7H9 (Sigma) pH = 6.60, 50 mM Gly
217	*M. smegmatis*	ΔcydABAB	7H9	0.05	Glycerol	2.7	3	BDQ, CCCP, TRZ, Na2S2O4	30 nM, 1-5 µM, 360 µM	29/06/2023	7H9 (Sigma) pH = 6.60, 50 mM Gly
218	*M. smegmatis*	mc2155	7H9	0.05	Glycerol	3.8	2.5	TRZ, Na2S2O4	360 µM	11/07/2023	7H9 (Sigma) pH = 6.60, 50 mM Gly
219	*M. smegmatis*	mc2155	7H9	0.05	Glycerol	4.3	2	TRZ, Na2S2O4	360 µM	11/07/2023	7H9 (Sigma) pH = 6.60, 50 mM Gly
220	*M. smegmatis*	mc2155	7H9 + 14 nM BDQ	0.05	Glycerol	3.3	2.5	TRZ, Na2S2O4	360 µM	11/07/2023	7H9 (Sigma) pH = 6.60, 50 mM Gly
221	*M. smegmatis*	mc2155	7H9	0.05	Glycerol	6.3	1.25	TRZ, Na2S2O4	360 µM	12/07/2023	7H9 (Sigma) pH = 6.60, 50 mM Gly
222	*M. smegmatis*	mc2155	7H9 + 14 nM BDQ	0.05	Glycerol	5.2	1.5	TRZ, Na2S2O4	360 µM	12/07/2023	7H9 (Sigma) pH = 6.60, 50 mM Gly
223	*M. smegmatis*	ΔqcrB	7H9	0.05	Glycerol	2.8	3	BDQ, TRZ, Na2S2O4	30-1500 nM, 360 µM	18/07/2023	7H9 (Sigma) pH = 6.60, 50 mM Gly
224	*M. smegmatis*	ΔqcrB	7H9	0.05	Glycerol	3.6	2.25	CCCP, TRZ, Na2S2O4	1-25 µM, 360 µM	18/07/2023	7H9 (Sigma) pH = 6.60, 50 mM Gly
225	*M. smegmatis*	mc2155	7H9	0.05	Glycerol	1.6	5	TRZ, Na2S2O4	360 µM	08/08/2023	7H9 (Sigma) pH = 6.60, 50 mM Gly
226	*M. smegmatis*	mc2155	7H9	0.05	Glycerol	1.5	5	Valinomycin, Nigericin, TRZ, Na2S2O4	10 µM, 1 µM, 360 µM	08/08/2023	7H9 (Sigma) pH = 6.60, 50 mM Gly
227	*M. smegmatis*	mc2155	7H9	0.05	Glycerol	1.1	5	CFZ, BDQ	750 nM, 30 nM	08/08/2023	7H9 (Sigma) pH = 6.60, 50 mM Gly
228	*M. smegmatis*	mc2155	7H9	0.05	Glycerol	3	2.5	TRZ, Na2S2O4	360 µM	08/08/2023	7H9 (Sigma) pH = 6.60, 50 mM Gly
229	*M. smegmatis*	mc2155	7H9 + 30 nM BDQ	0.05	Glycerol	1.4	5	TRZ, Na2S2O4	360 µM	08/08/2023	7H9 (Sigma) pH = 6.60, 50 mM Gly, 30 nM BDQ
230	*M. smegmatis*	mc2155	7H9	0.05	Glycerol	6.6	1.25	TRZ, Na2S2O4	360 µM	09/08/2023	7H9 (Sigma) pH = 6.60, 50 mM Gly
231	*M. smegmatis*	mc2155	7H9 + 30 nM BDQ	0.05	Glycerol	4.6	1.67	TRZ, Na2S2O4	360 µM	09/08/2023	7H9 (Sigma) pH = 6.60, 50 mM Gly, 30 nM BDQ
232	*M. smegmatis*	mc2155	7H9	0.05	Glycerol	2	4	CFZ	750 nM	15/08/2023	7H9 (Sigma) pH = 6.60, 50 mM Gly
233	*M. smegmatis*	mc2155	7H9	0.05	Glycerol	2.6	2.5	CFZ, (20 minute wait) BDQ	750 nM, 30 nM	15/08/2023	7H9 (Sigma) pH = 6.60, 50 mM Gly
234	*M. smegmatis*	mc2155	7H9	0.05	Glycerol	1.2	5	CFZ, BDQ	750 nM, 30 nM	15/08/2023	7H9 (Sigma) pH = 6.60, 50 mM Gly
235	*M. smegmatis*	mc2155	7H9	0.05	Glycerol	2	4	CCCP, TRZ, Na2S2O4	1-25 µM, 360 µM	15/08/2023	7H9 (Sigma) pH = 6.60, 50 mM Gly
236	*M. smegmatis*	mc2155	7H9	0.05	Glycerol	2	4	CFZ	750 nM	22/08/2023	7H9 (Sigma) pH = 6.60, 50 mM Gly
237	*M. smegmatis*	mc2155	7H9	0.05	Glycerol	1.9	4	CFZ, KCN	750 nM, 200 µM	22/08/2023	7H9 (Sigma) pH = 6.60, 50 mM Gly
238	*M. smegmatis*	mc2155	7H9	0.05	Glycerol	2.9	2.5	CFZ, BDQ, KCN	750 nM, 30 nM, 100 µM	22/08/2023	7H9 (Sigma) pH = 6.60, 50 mM Gly
239	*M. smegmatis*	mc2155	7H9	0.05	Glycerol	1.9	4	Nigericin	1 µM	23/08/2023	7H9 (Sigma) pH = 6.60, 50 mM Gly
240	*M. smegmatis*	mc2155	7H9	0.05	Glycerol	1.6	5	DCCD	5-10 µM	23/08/2023	7H9 (Sigma) pH = 6.60, 50 mM Gly
241	*M. smegmatis*	mc2155	7H9	0.05	Glycerol	1.1	5	DCCD	10 µM	23/08/2023	7H9 (Sigma) pH = 6.60, 50 mM Gly
242	*M. smegmatis*	mc2155	7H9	0.05	Glycerol	1.5	5	DCCD	10 µM	23/08/2023	7H9 (Sigma) pH = 6.60, 50 mM Gly
243	*M. smegmatis*	AtpED32V	7H9	0.05	Glycerol + D-Ara	1.2	5	BDQ	30 nM	31/08/2023	7H9 (Sigma) pH = 6.60, 50 mM Gly, 5 mM D-Ara
244	*M. smegmatis*	AtpED32V	7H9	0.05	Glycerol + D-Ara	1.3	5	BDQ	30 nM	31/08/2023	7H9 (Sigma) pH = 6.60, 50 mM Gly, 5 mM D-Ara
245	*M. smegmatis*	mc2155	7H9	0.05	Glycerol	2.3	3.5	EtOH	5 µL	31/08/2023	7H9 (Sigma) pH = 6.60, 50 mM Gly
246	*M. tuberculosis*	mc26206	7H9 + L + P + OADC	0.05	Glycerol	0.81	30	EtOH	5 µL	04/09/2023	7H9 (Sigma) pH = 6.60, L, P, 0.4% Gly
247	*M. tuberculosis*	mc26206	7H9 + L + P + OADC	0.05	Glycerol	0.81	30	EtOH	5 µL	04/09/2023	7H9 (Sigma) pH = 6.60, L, P, 0.4% Gly
248	*M. tuberculosis*	mc26206	7H9 + L + P + OADC	0.05	Glycerol	0.81	30	BDQ	10 µM	04/09/2023	7H9 (Sigma) pH = 6.60, L, P, 0.4% Gly
249	*M. tuberculosis*	mc26206	7H9 + L + P + OADC	0.05	Glycerol	0.98	30	BDQ	120 nM	05/09/2023	7H9 (Sigma) pH = 6.60, L, P, 0.4% Gly
250	*M. tuberculosis*	mc26206	7H9 + L + P + OADC	0.05	Glycerol	0.98	30	BDQ	120 nM	05/09/2023	7H9 (Sigma) pH = 6.60, L, P, 0.4% Gly
251	*M. tuberculosis*	mc26206	7H9 + L + P + OADC	0.05	Glycerol	0.98	30	CCCP	5-25 µM	05/09/2023	7H9 (Sigma) pH = 6.60, L, P, 0.4% Gly

252	*M. tuberculosis*	mc26206	7H9 + L + P + OADC	0.05	Glycerol	0.98	30	BDQ	10 µM	05/09/2023	7H9 (Sigma) pH = 6.60, L, P, 0.4% Gly
253	*M. smegmatis*	mc2155	7H9	0.05	Glycerol	1.7	5	BDQ	10 µM	07/09/2023	7H9 (Sigma) pH = 6.60, 50 mM Gly
254	*M. smegmatis*	ΔcydABAB	7H9	0.05	Glycerol	1.9	5	BDQ	10 µM	07/09/2023	7H9 (Sigma) pH = 6.60, 50 mM Gly
255	*M. smegmatis*	ΔcydABAB	7H9	0.05	Glycerol	2.3	4	BDQ	10 µM	07/09/2023	7H9 (Sigma) pH = 6.60, 50 mM Gly
256	*M. smegmatis*	mc2155	7H9	0.05	Glycerol	1.6	5	EtOH	5 µL	08/09/2023	7H9 (Sigma) pH = 6.60, 50 mM Gly
257	*M. smegmatis*	mc2155	7H9	0.05	Glycerol	1.7	5	EtOH	5 µL	08/09/2023	7H9 (Sigma) pH = 6.60, 50 mM Gly
258	*M. smegmatis*	mc2155	7H9	0.05	Glycerol	2.7	3	BDQ	10 µM	08/09/2023	7H9 (Sigma) pH = 6.60, 50 mM Gly
259	*M. smegmatis*	ΔcydABAB	7H9	0.05	Glycerol	1.7	5	BDQ	10 µM	08/09/2023	7H9 (Sigma) pH = 6.60, 50 mM Gly
260	*M. tuberculosis*	mc26206	7H9 + L + P + OADC	0.05	Glycerol	0.99	30	BDQ	120 nM	11/09/2023	7H9 (Sigma) pH = 6.60, L, P, 0.4% Gly
261	*M. tuberculosis*	mc26206	7H9 + L + P + OADC	0.05	Glycerol	0.99	30	CCCP	5-25 µM	11/09/2023	7H9 (Sigma) pH = 6.60, L, P, 0.4% Gly
262	*M. tuberculosis*	mc26206	7H9 + L + P + OADC	0.05	Glycerol	0.99	30	CCCP	5-25 µM	11/09/2023	7H9 (Sigma) pH = 6.60, L, P, 0.4% Gly
263	*M. tuberculosis*	mc26206	7H9 + L + P + OADC	0.05	Glycerol	0.99	30	BDQ	10 µM	11/09/2023	7H9 (Sigma) pH = 6.60, L, P, 0.4% Gly
264	*M. smegmatis*	mc2155	7H9	0.05	Glycerol	1.1	7.5	CFZ, BDQ, KCN	35 nM, 30 nM, 100 µM	17/11/2023	7H9 (Sigma) pH = 6.60, 50 mM Gly
265	*M. smegmatis*	mc2155	7H9	0.05	Glycerol	1.6	5	CFZ, BDQ, KCN	70 nM, 30 nM, 100 µM	17/11/2023	7H9 (Sigma) pH = 6.60, 50 mM Gly
266	*M. smegmatis*	ΔcydABAB	7H9	0.05	Glycerol	2.3	3.5	CFZ, BDQ, KCN	70 nM, 30 nM, 100-200 µM	17/11/2023	7H9 (Sigma) pH = 6.60, 50 mM Gly
267	*M. smegmatis*	ΔcydABAB	7H9	0.05	Glycerol	2.9	3	CFZ, KCN, BDQ	70 nM, 100 µM, 30 nM	17/11/2023	7H9 (Sigma) pH = 6.60, 50 mM Gly
268	*M. smegmatis*	mc2155	7H9	0.05	Glycerol	1.6	5	BDQ	30 nM	21/11/2023	7H9 (Sigma) pH = 6.60, 50 mM Gly
269	*M. smegmatis*	mc2155	7H9	0.05	Glycerol	1.6	5	CFZ, KCN, BDQ	70 nM, 100 µM, 30 nM	21/11/2023	7H9 (Sigma) pH = 6.60, 50 mM Gly
270	*M. smegmatis*	ΔcydABAB	7H9	0.05	Glycerol	0.8	10	BDQ, KCN	30 nM, 100 µM	21/11/2023	7H9 (Sigma) pH = 6.60, 50 mM Gly
271	*M. smegmatis*	mc2155	7H9	0.05	Glycerol	0.8	10	CCCP, rotenone, 3NP, TFPZ, Na2S2O4	1-25 µM, 5 µM, 50 µM, 360 µM	21/11/2023	7H9 (Sigma) pH = 6.60, 50 mM Gly
272	*M. tuberculosis*	ΔcydAB	7H9 + P + OADC	0.05	Glycerol	0.4	35	EtOH	5 µL	23/01/2024	7H9 (Sigma) pH = 6.60, P, 0.4% Gly
273	*M. tuberculosis*	ΔcydAB	7H9 + P + OADC	0.05	Glycerol	0.8	35	BDQ	120 nM	24/01/2024	7H9 (Sigma) pH = 6.60, P, 0.4% Gly
274	*M. tuberculosis*	ΔcydAB	7H9 + P + OADC	0.05	Glycerol	0.8	35	BDQ	10 µM	24/01/2024	7H9 (Sigma) pH = 6.60, P, 0.4% Gly
275	*M. tuberculosis*	ΔcydAB	7H9 + P + OADC	0.05	Glycerol	0.7	35	BDQ	10 µM	25/01/2024	7H9 (Sigma) pH = 6.60, P, 0.4% Gly
276	*M. tuberculosis*	ΔcydAB	7H9 + P + OADC	0.05	Glycerol	0.7	35	BDQ	120 nM	25/01/2024	7H9 (Sigma) pH = 6.60, P, 0.4% Gly
277	*M. tuberculosis*	ΔcydAB	7H9 + P + OADC	0.05	Glycerol	0.7	35	BDQ	120 nM	25/01/2024	7H9 (Sigma) pH = 6.60, P, 0.4% Gly
278	*M. tuberculosis*	ΔcydAB	7H9 + P + OADC	0.05	Glycerol	0.9	35	BDQ	10 µM	01/02/2024	7H9 (Sigma) pH = 6.60, P, 0.4% Gly
279	*M. tuberculosis*	mc26230	7H9 + P + OADC	0.05	Glycerol	0.6	35	BDQ	10 µM	01/02/2024	7H9 (Sigma) pH = 6.60, P, 0.4% Gly
280	*M. tuberculosis*	mc26230	7H9 + P + OADC	0.05	Glycerol	0.8	35	BDQ	10 µM	01/02/2024	7H9 (Sigma) pH = 6.60, P, 0.4% Gly
281	*M. tuberculosis*	mc26230	7H9 + P + OADC	0.05	Glycerol	0.8	35	BDQ	10 µM	05/02/2024	7H9 (Sigma) pH = 6.60, P, 0.4% Gly
282	*M. tuberculosis*	mc26230	7H9 + P + OADC	0.05	Glycerol	0.8	35	BDQ	120 nM	05/02/2024	7H9 (Sigma) pH = 6.60, P, 0.4% Gly
283	*M. tuberculosis*	mc26230	7H9 + P + OADC	0.05	Glycerol	0.8	35	BDQ	120 nM	05/02/2024	7H9 (Sigma) pH = 6.60, P, 0.4% Gly
284	*M. tuberculosis*	mc26230	7H9 + P + OADC	0.05	Glycerol	1	35	BDQ	120 nM	08/02/2024	7H9 (Sigma) pH = 6.60, P, 0.4% Gly
285	*M. tuberculosis*	mc26230	7H9 + P + OADC	0.05	Glycerol	1	35	BDQ	120 nM	08/02/2024	7H9 (Sigma) pH = 6.60, P, 0.4% Gly
286	*M. tuberculosis*	ΔcydAB	7H9 + P + OADC	0.05	Glycerol	1.3	35	EtOH	5 µL	08/02/2024	7H9 (Sigma) pH = 6.60, P, 0.4% Gly
287	*M. tuberculosis*	mc26230	7H9 + P + OADC	0.05	Glycerol	0.5	35	EtOH	5 µL	09/02/2024	7H9 (Sigma) pH = 6.60, P, 0.4% Gly
288	*M. tuberculosis*	mc26230	7H9 + P + OADC	0.05	Glycerol	0.8	35	EtOH	5 µL	12/02/2024	7H9 (Sigma) pH = 6.60, P, 0.4% Gly
289	*M. tuberculosis*	mc26230	7H9 + P + OADC	0.05	Glycerol	0.8	35	BDQ	10 µM	12/02/2024	7H9 (Sigma) pH = 6.60, P, 0.4% Gly
290	*M. tuberculosis*	mc26230	7H9 + P + OADC	0.05	Glycerol	0.8	35	EtOH	5 µL	12/02/2024	7H9 (Sigma) pH = 6.60, P, 0.4% Gly
291	*M. tuberculosis*	ΔcydAB	7H9 + P + OADC	0.05	Glycerol	0.7	35	EtOH	5 µL	13/02/2024	7H9 (Sigma) pH = 6.60, P, 0.4% Gly
292	*M. tuberculosis*	ΔcydAB	7H9 + P + OADC	0.05	Glycerol	0.7	35	BDQ	120 nM	13/02/2024	7H9 (Sigma) pH = 6.60, P, 0.4% Gly
293	*M. tuberculosis*	ΔcydAB	7H9 + P + OADC	0.05	Glycerol	0.7	35	BDQ	10 µM	13/02/2024	7H9 (Sigma) pH = 6.60, P, 0.4% Gly
294	*M. tuberculosis*	mc26230	7H9 + P + OADC	0.05	Glycerol	0.8	35	CCCP	5-25 µM	19/02/2024	7H9 (Sigma) pH = 6.60, P, 0.4% Gly
295	*M. tuberculosis*	mc26230	7H9 + P + OADC	0.05	Glycerol	0.8	35	EtOH	5 µL	19/02/2024	7H9 (Sigma) pH = 6.60, P, 0.4% Gly
296	*M. tuberculosis*	mc26230	7H9 + P + OADC	0.05	Glycerol	0.8	35	CCCP	5-25 µM	19/02/2024	7H9 (Sigma) pH = 6.60, P, 0.4% Gly
297	*M. tuberculosis*	ΔcydAB	7H9 + P + OADC	0.05	Glycerol	0.7	35	BDQ	120 nM	20/02/2024	7H9 (Sigma) pH = 6.60, P, 0.4% Gly
298	*M. tuberculosis*	ΔcydAB	7H9 + P + OADC	0.05	Glycerol	0.7	35	EtOH	5 µL	20/02/2024	7H9 (Sigma) pH = 6.60, P, 0.4% Gly
299	*M. tuberculosis*	ΔcydAB	7H9 + P + OADC	0.05	Glycerol	0.7	35	CCCP	5-25 µM	20/02/2024	7H9 (Sigma) pH = 6.60, P, 0.4% Gly
300	*M. tuberculosis*	mc26230	7H9 + P + OADC	0.05	Glycerol	0.7	35	CCCP	5-25 µM	26/02/2024	7H9 (Sigma) pH = 6.60, P, 0.4% Gly
301	*M. tuberculosis*	mc26230	7H9 + P + OADC	0.05	Glycerol	0.7	35	DCCD	10-70 µM	26/02/2024	7H9 (Sigma) pH = 6.60, P, 0.4% Gly
302	*M. tuberculosis*	mc26230	7H9 + P + OADC	0.05	Glycerol	0.7	35	DCCD	70 µM	26/02/2024	7H9 (Sigma) pH = 6.60, P, 0.4% Gly
303	*M. tuberculosis*	ΔcydAB	7H9 + P + OADC	0.05	Glycerol	0.7	35	CCCP	5-25 µM	01/03/2024	7H9 (Sigma) pH = 6.60, P, 0.4% Gly
304	*M. tuberculosis*	ΔcydAB	7H9 + P + OADC	0.05	Glycerol	0.7	35	Nigericin	1 µM	01/03/2024	7H9 (Sigma) pH = 6.60, P, 0.4% Gly
305	*M. tuberculosis*	ΔcydAB	7H9 + P + OADC	0.05	Glycerol	0.7	35	CCCP	5-25 µM	01/03/2024	7H9 (Sigma) pH = 6.60, P, 0.4% Gly
306	*M. tuberculosis*	mc26230	7H9 + P + OADC	0.05	Glycerol	0.9	35	Nigericin	1 µM	04/03/2024	7H9 (Sigma) pH = 6.60, P, 0.4% Gly
307	*M. tuberculosis*	mc26230	7H9 + P + OADC	0.05	Glycerol	0.9	35	DCCD	70 µM	04/03/2024	7H9 (Sigma) pH = 6.60, P, 0.4% Gly
308	*M. tuberculosis*	mc26230	7H9 + P + OADC	0.05	Glycerol	0.9	35	DCCD	70 µM	04/03/2024	7H9 (Sigma) pH = 6.60, P, 0.4% Gly
309	*M. tuberculosis*	ΔcydAB	7H9 + P + OADC	0.05	Glycerol	0.8	35	DCCD	70 µM	05/03/2024	7H9 (Sigma) pH = 6.60, P, 0.4% Gly

310	*M. tuberculosis*	ΔcydAB	7H9 + P + OADC	0.05	Glycerol	0.8	35	DCCD	70 µM	05/03/2024 7H9 (Sigma) pH = 6.60, P, 0.4% Gly
311	*M. tuberculosis*	ΔcydAB	7H9 + P + OADC	0.05	Glycerol	0.8	35	DCCD	70-140 µM	05/03/2024 7H9 (Sigma) pH = 6.60, P, 0.4% Gly
312	*M. tuberculosis*	ΔcydAB	7H9 + P + OADC	0.05	Glycerol	0.7	35	Nigericin	1 µM	06/03/2024 7H9 (Sigma) pH = 6.60, P, 0.4% Gly
313	*M. tuberculosis*	ΔcydAB	7H9 + P + OADC	0.05	Glycerol	0.7	35	Nigericin	1 µM	06/03/2024 7H9 (Sigma) pH = 6.60, P, 0.4% Gly
314	*M. tuberculosis*	ΔcydAB	7H9 + P + OADC	0.05	Glycerol	0.7	35	BDQ	10 µM	06/03/2024 7H9 (Sigma) pH = 6.60, P, 0.4% Gly
315	*M. tuberculosis*	mc26230	7H9 + P + OADC	0.05	Glycerol	1.1	35	Nigericin	1 µM	11/03/2024 7H9 (Sigma) pH = 6.60, P, 0.4% Gly
316	*M. tuberculosis*	mc26230	7H9 + P + OADC	0.05	Glycerol	1.1	35	Nigericin	1 µM	11/03/2024 7H9 (Sigma) pH = 6.60, P, 0.4% Gly
317	*M. tuberculosis*	mc26230	7H9 + P + OADC	0.05	Glycerol	1.1	35	DCCD	70-140 µM	11/03/2024 7H9 (Sigma) pH = 6.60, P, 0.4% Gly
318	*M. smegmatis*	AtpED32V	7H9	0.05	Glycerol + D-Ara	1.7	5	BDQ	30 nM, 300 nM, 1.5 µM	20/05/2024 7H9 (Sigma) pH = 6.60, 50 mM Gly, 5 mM D-Ara
319	*M. smegmatis*	AtpED32V	7H9	0.05	Glycerol + D-Ara	1.2	5	BDQ	30 nM, 300 nM, 1.5 µM	20/05/2024 7H9 (Sigma) pH = 6.60, 50 mM Gly, 5 mM D-Ara
320	*M. smegmatis*	AtpED32V	7H9	0.05	Glycerol + D-Ara	1.5	4	BDQ	30 nM, 300 nM, 1.5 µM	20/05/2024 7H9 (Sigma) pH = 6.60, 50 mM Gly, 5 mM D-Ara
321	*M. smegmatis*	AtpED32V	7H9	0.05	Glycerol + D-Ara	1.8	3.5	BDQ	30 nM, 300 nM, 1.5 µM	20/05/2024 7H9 (Sigma) pH = 6.60, 50 mM Gly, 5 mM D-Ara
322	*M. smegmatis*	mc2155	7H9	0.05	Glycerol + D-Ara	1	7	BDQ	30 nM, 300 nM, 1.5 µM	21/05/2024 7H9 (Sigma) pH = 6.60, 50 mM Gly, 5 mM D-Ara
323	*M. smegmatis*	mc2155	7H9	0.05	Glycerol + D-Ara	2.3	3	BDQ	30 nM, 300 nM, 1.5 µM	21/05/2024 7H9 (Sigma) pH = 6.60, 50 mM Gly, 5 mM D-Ara
324	*M. smegmatis*	mc2155	7H9	0.05	Glycerol + D-Ara	2.4	3.5	BDQ	30 nM, 300 nM, 1.5 µM	21/05/2024 7H9 (Sigma) pH = 6.60, 50 mM Gly, 5 mM D-Ara
325	*M. smegmatis*	mc2155	7H9	0.05	Glycerol	0.9	7	Nigericin	1 µM	21/05/2024 7H9 (Sigma) pH = 6.60, 50 mM Gly